ELECTROCHEMICAL APPROACHES FOR WATER TREATMENT: METAL SEPARATION AND ASSOCIATED INDUSTRIAL CONTAMINANT REMOVAL

ELECTROCHEMICAL APPROACHES FOR WATER TREATMENT: METAL SEPARATION AND ASSOCIATED INDUSTRIAL CONTAMINANT REMOVAL

By Mohamed Elganzoury, B.Eng., M.S.

A Thesis Submitted to the School of Graduate Studies in Partial Fulfilment of the Requirements for the Degree Doctor of Philosophy

McMaster University © Copyright by Mohamed Elganzoury, August 2022

DOCTOR OF PHILOSOPHY (2022)

Chemical Engineering, McMaster University

1280 Main St W, Hamilton, Ontario L8S 4L7

TITLE: Electrochemical Approaches for Water Treatment: Metal Separation and Associated Industrial Contaminant Removal using Electrochemical Oxidation-In-situ Coagulation Process and Closed-loop Adsorption-Electrodesorption Cycles

AUTHOR: Mohamed Elganzoury

B.Eng. (Cairo University, Egypt)

M.S. (Cairo University, Egypt)

SUPERVISOR: Dr. Charles-François de Lannoy

NUMBER OF PAGES: xxvi , 211

Lay abstract

With rapid industrial development, industrial wastewaters are heavily contaminated with hazardous pollutants and valuable resources. As a result, there are social and economic needs for efficient industrial wastewater treatment to remove harmful contaminants and to extract useful compounds. Metals of particular interest in industrial wastewaters are organized into two categories, toxic metals (e.g., arsenic, zinc, nickel, mercury, and cadmium) and precious metals (e.g., gold, silver, platinum, and palladium). An effective metal separation from industrial waste solutions is a major goal for the sustainable development of industrial processes. Conventional metal removal technologies have intensive chemical consumption producing secondary pollution. Here, we introduce two novel environmental approaches for metal removal with minimal chemical consumption. The first approach replaces chemical coagulants with electrochemically generated in-situ coagulants for toxic metal removal from industrial wastewater. The second approach introduces a closed loop continuous process for adsorption and electro-desorption of toxic and precious metals from aqueous solutions using carbon nano tubes (CNTs) sorbents. The closed-loop continuous regenerative process enables the use of highly effective CNT sorbents for metal removal from waste solutions. The desorption process is based on electrochemical regeneration of CNTs from metals, which avoids the need for acids or other solvents to regenerate the CNT sorbents.

Abstract

Since the industrial revolution of the 18th century, rapid growth occurred in the energy, electronic, fertilizers, pesticides, detergents, pharmaceutical, mining and paper industries, among others. Consequently, wastewaters produced from these various industries is highly contaminated with hazardous pollutants including toxic metals and organic contaminants as well as useful resources such as phosphates and precious metals. It is necessary to remove hazardous pollutants from industrial wastewater to meet the environmental disposal regulations or to enable safe recycling of the treated wastewater in other applications. It is also economically beneficial to separate the valuable resources from the industrial waste solutions. Several technologies have been employed for metal and other contaminants (e.g., organics and minerals) removal from industrial wastewater including chemical precipitation, coagulation and flocculation, membrane separation, ion exchange, adsorption, chemical oxidation, and biodegradation. Chemical precipitation, coagulation and flocculation, and chemical oxidation processes have a high chemical consumption. Adsorption and ion exchange do not require a high chemical consumption while separating pollutants from wastewater, nevertheless acids and chemical reagents are required for the regeneration of sorbents and ion exchange resins for their reuse in subsequent processes. Membrane technologies suffer from membrane fouling and scaling, which require the use of chemical reagents and antiscalants to mitigate these problems. The use of bacteria in biodegradation is a common alternative in many wastewater, but this process requires a toxic-free environment, which is rarely the case in industrial wastewaters due to the presence of toxic metals in most of the industrial effluents. As such, this process is not

appropriate for most industrial separations, requiring additional unit operations to remove toxic metals before the biodegradation processes which causes higher operational and capital cost.

The objective of this thesis is to substitute metal and associated contaminants conventional removal methods with novel electrochemical approaches to decrease the chemical consumption, lower the environmental impact, extract precious metals and to decrease the overall unit operations during industrial wastewater treatment.

In the first part of the thesis, using chemical coagulants was substituted by electrochemically induced in-situ coagulants to remove toxic metals from mixed industrial wastewater. The newly introduced technique utilized the presence of iron in the waste solution and converted it into iron hydroxide coagulants through the reaction of iron with the hydroxyl groups generated via water electrolysis at a stainless-steel cathode. The generated coagulants interacted with the toxic metals (i.e., arsenic, cadmium, lead, nickel, copper, chromium) in the wastewater and separated them from the solution. To decrease the overall unit operations of the mixed industrial wastewater treatment, the associated organic pollutants in the waste solution were simultaneously degraded. A dimensionally stable anode (DSA) was used to oxidize the organic contaminants in the solution simultaneously with the metal coagulation occurring at the cathode. The electrochemical oxidation-in-situ coagulation (ECO-IC) process resulted in a treated solution with a substantially lower heavy metal content, lower organic content, greater effective diameter of the suspended particles, and distinct phases that can be separated for further treatment.

In the second part of the thesis, a closed-loop continuous cycle for metal adsorption and electrodesorption using CNT sorbents was invented. In this process, 1) metals are adsorbed onto

the surface of CNTs, 2) the metal-saturated CNTs are filtered onto a microfiltration (MF) membrane to form a temporary membrane electrode, 3) the CNT-coated membrane is used as an anode in an electrochemical cell, 4) an applied electric potential desorbs the metals from the CNT-membrane, and 5) the CNTs are separated from the membrane to be reused as adsorbents in a closed-loop process. The closed-loop regenerative cycle allowed recycling the effective but expensive CNT sorbents in subsequent adsorption-electrodesorption cycles. The electrochemical regeneration of CNTs eliminated the need for using acids and chemical reagents for CNTs regeneration. The proposed technique was successfully employed for adsorption and electrodesorption of copper (a model toxic metal) from aqueous solutions and gold (a model precious metal) from acidic chloride solutions mimicking e-waste leachate. The results of this study demonstrate a chemical-free method for metal removal that achieves removal at rates comparable to conventional chemical methods and adsorbent regeneration as high as that achieved with chemical methods.

In the third part of the thesis, limitations and sources of error during electrochemical water treatment were identified to be taken into consideration by future researchers. In the first phase of this research, sources of error arising in batch electrochemical cells were illustrated. Batch electrochemical experiments are considered the baseline for testing porous electrodes and electrochemical membranes (ECMs) in water treatment applications (including metal separation and contaminant removal) before being used in continuous processes. It was identified that electrochemical dissolution of metal fasteners holding porous conductive membranes in batch electrochemical cells occur, even when keeping the metal fasteners outside the electrolyte solution. This phenomenon can confound water treatment experimental results in batch cells.

The reason for this phenomenon was investigated and a simple solution to prevent it was proposed. In the second phase of this research, limitations on using metal feed spacers as electrodes during gypsum solution (secondary pollutants produced during metal removal from mining wastewater) RO filtration was identified. Using electro-assisted filtration has a lower environmental impact than using antiscalants for preventing gypsum scale formation on RO membranes. Nevertheless, using metal feed spacer electrodes for this purpose was not effective due to low generation of hydrogen gas and the spacers' anodic electro dissolution. Inert electrodes to electro dissolution (i.e., CNTs coated polypropylene feed spacers) are proposed as an effective and economic option for electro-assisted filtration of gypsum solutions.

Acknowledgements

First, I would like to thank God the most merciful, the most generous, the creator of all things, the ruler of the universe, who has no partner or son, and who help his worshipers when they need him.

A huge thank to my supervisor Prof. Charles de Lannoy. Charles, you are a very clever scientist and an excellent supervisor having a lot of innovative ideas and passion for discovery. This work could not have been completed without your wisdom, insight, support, and supervision. I appreciate that you helped me to develop my research, analytical thinking, time management, and academic writing skills. During my 4 years here, you represented an excellent example for honesty in conducting academic and industrial research, you were always motivating us to show our research in a clear way without hiding any negative results, you were always caring about the quality not the quantity. I also respect all your effort in the water treatment projects for the indigenous community, this really inspires me to be helpful to my community in the future. You should also know that you are my role model for the manger or the leader, I really admire how you balanced being a kind human being together with keeping the work going efficiently and smoothly. I am very thankful for your support in the tough times, I will always remember that chat we had at 3:00 am in the weekend when I was feeling disappointed about some of my results, I am thankful for all this support. I met a lot of challenges during my PhD especially during the COVID time, and it could not have been possible for me to reach this point without your continuous support. You will always have all my respect and love Dr. de Lannoy.

I would also like to sincerely thank my committee members, Dr. Raja Ghosh from The Chemical Engineering Department and Dr. Igor Zhitomirsky from The Materials Science Department for

their invaluable insight, advice, and suggestions throughout my research and for providing valuable feedback all along the way. Their constructive criticisms, clever interpretations, insightful recommendations, and out-of-the-box questions have enabled me to think beyond my field, deepen my conceptual understanding, improve my research quality, and helped me to become a better researcher.

I would like to sincerely thank all the help I received from the Department of Chemical Engineering staff, Kristina Trollip, Linda Ellis, Doug Keller, Mike Clarke, Tim Stephens. A big thank to you Michelle Whalen for always being very helpful and supportive from the first day of my journey here. Paul Gatt, thanks a lot sir for being here, I appreciate all your help and support in designing my experiments during my PhD, this work could not have been completed without your help, support, and cleverness.

Many thanks to you Nan Zhang, my twin in this journey. We started the PhD at the same time and now finishing in the same month. I was very lucky to accompany you in this journey. I think it would have taken me 1 more year to continue my PhD if you were not here. You were always my first resort when I feel bad and stressed about my research, and you never failed to re-motivate me to continue. I am very thankful for your continuous support Dr. Nan.

I am very thankful to my friend Yichen Wu, thank you Yichen for always being generous in giving support and advice during these years. Thank you also for always motivating the Lab members to collaborate and work together. I would like to also thank Amin Halali, my night lab mate, thanks a lot Amin for all your help and support you provided me since the first day here. Many thanks to Dr. Hyejin Lee and Dr. Saloumeh Ghasemian for always being kind, nice and supportive. Many

thanks to Cassandra Chidiac for being very nice and welcoming to us when we joined the lab. Abdelrahman Awad, thanks a lot for always being helpful during my last two semesters, you always allowed me to use the lab tools and postponed your work to help me. Many thanks to my beloved lab teammates, Erik, Scott, Hannah, Nathan, Maria, Colin, Melissa, Alex, and Dan. It was my pleasure working in the same lab with you. Huge thanks to my undergraduate students Jasmine, Tina, and Mohamed Farahan. Many thanks to my colleagues in the Chemical Engineering Department Wajedi, Nina, Claudia, Nelly, Matt Campea, Jinlei Li and Hongfeng Zhang.

I would like to sincerely thank my best friend in Hamilton, Maysara Ghaith. Thanks a lot Maysara for all your support in the good and tough times. Thank you so much for all the nice meals you fed me with. The hard moments during this PhD could not have been passed if you were not here. I am very happy that I have a nice and supportive friend like you.

I would like to thank my close and beloved friend here in Hamilton, Mohmed El-sefy, Ahmed Yosri, Mahmoud Madany, Gamal El-deeb, Amed Tarek, Yassien Yassien, Ahmed Abdellatif, Ahmed Shawky, Ayman Farid, Mohamed Hammuda and Mohamed Gamal for all the help and support, and the nice time we spent here together. I would also like to thank my childhood friend Ahmed Farag for all his help and support during my whole life. Thanks Ahmed for all your support, help and nice times, and more thanks for the support in the tough times.

I would like to thank the staffs and technicians at Biointerfaces Institutes (BI), Canadian Center for Electron Microscopy (CCEM) for their assistance on sample analyses, especially Dr. Zeynel Bayindir and Marcia Reid. I acknowledge staffs and students from Prof. Robert Pelton Lab, Prof.

Todd Hoare Lab and Prof. David Latulippe Lab, for equipment training and usage. I also would like to acknowledge Natural Sciences and Engineering Research Council of Canada (NSERC) for their financial support. A huge thank you to my industrial collaborators Hatch Ltd., P.W. Customs Fabrications, and Pall Water.

A huge thank to my MSc supervisor, Prof. Nageh Allam. Thank you Dr. Nageh for all your support and help during my research journey in Egypt. Thanks for supporting us with your experience, equipment, and resources to do cutting-edge academic research. I appreciate that you paved our road and enabled us to travel to great universities to continue our research journeys. It would not be possible for me to come to McMaster university and finish a PhD without your initial help.

Last but not least, I would like to thank my family, my mother Amal Hafez, my brother Mostafa and my sweetie sister Sara for all their help and support during my whole life. Mom you are the best mother ever, I appreciate all the effort you did for us after my father death. You did us everything, and any good thing we will achieve is because of you. Sara you are very kind and supportive and I love you so much, thanks for all your support. Thanks, Mostafa, for all your help and support and for taking care of the family in my absence.

Finally, I would like to dedicate this thesis to the memory of my Dad Ahmed Elganzoury, the greatest father ever. Any good thing I achieved in my life is because of the morals and values you taught me.

Table of Contents

List of Figures

Chapter 1

Chapter 2

Chapter 3

Chapter 4

List of Tables

List of Abbreviations and Symbols

AAS	Atomic Absorption Spectroscopy
AC	activated carbon
AMD	acid mine drainage
NH_2-MWCNTs	amide functionalised multiwall carbon nanotubes
BDD	boron-doped diamond
BECC	batch electrochemical cell
BET	Brunauer-Emmet-Teller
BI	Biointerfaces Institute
BOD	Biological Oxygen Demand
BSOPD	bis(salicylaldehyde) ortho-phenylenediamine
BVP4C	boundary value problem fourth order method
CB	conduction band
CCEM	Canadian Centre for Electron Microscopy
CDI	capacitive deionization
CE	counter electrode
CNF	carbon nanofiber
CNT	carbon nanotube
COD	Chemical Oxygen Demand
COOH-MWCNTs	carboxylic functionalised multiwall carbon nanotubes
CSTR	continuous stirred-tank reactor

CV	Cyclic Voltammetry
CVD	Chemical Vapor Deposition
DDTC	diethyldithiocarbamate
DI	deionized
DLS	Dynamic Light Scattering
DSA	dimensionally stable anode
DWCNT	double wall carbon nanotube
EC	electrochemical
ECF	electrocoagulation/ electroflotation
ECM	electrochemical membrane
ECO	electrochemical oxidation
ECOG	electrocoagulation
ECOIG	electrochemical oxidation-in-situ coagulation
ED	electrodeposition
EDTA	ethylenediaminetetraacetic acid
EDX	Energy dispersive X-ray spectroscopy
EF	electroflotation
ES	electrosorption
GC-MS	Gas Chromatography-Mass Spectrometry
IC	Ion Chromatography
ICP-OES	Inductively Coupled Plasma-Optical Emission Microscopy
ICP-MS	Inductively Coupled Plasma-Mass Spectroscopy

ID	inner diameter
LSV	Linear sweep voltammetry
MAC	Maximum Acceptable Concentration
MEUF	micellar enhanced ultrafiltration
MF	microfiltration
MMO	mixed metal oxide
MO	methyl orange
MPB	modified Poisson-Boltzmann
MS	Mass Spectroscopy
MWCNT	multiwall carbon nanotube
NSERC	Natural Sciences and Engineering Research Council of Canada
OD	outer diameter
OER	oxygen evolution reaction
PAC	polyaluminium chloride
PAM	polyacrylamide
PES	polyethersulfone
PEUF	polymer enhanced ultrafiltration
PP	polypropylene
P-MWCNTs	pristine multiwall carbon nanotubes
PVDF	polyvinylidene fluoride
RE	reference electrode
RO	reverse osmosis

SEM	Scanning Electron Microscopy
SHE	Standard Hydrogen Electrode
SI	Supporting Info
SOWC	Southern Ontario Water Consortium
SSA	specific surface area
SW/DWCNTs	single-walled/double-walled carbon nanotubes
TOC	total organic carbon
UF	ultrafiltration
UV	ultraviolet
VB	valance band
VIS	visible
WE	working electrode
XPS	X-ray photoelectron spectroscopy

Declaration of Academic Achievement

This Ph.D. dissertation is organized in a "sandwich style" based on published, submitted, and prepared for submission articles described as follows:

Chapter 2: MA Ganzoury, S Ghasemian, N Zhang, M Yagar, CF De Lannoy. Mixed metal oxide anodes used for the electrochemical degradation of a real mixed industrial wastewater. Chemosphere, 2022, 286, 131600. https://doi.org/10.1016/j.chemosphere.2021.131600.

Chapter 3: MA Ganzoury, C Chidiac, J Kurtz, CF de Lannoy. CNT-sorbents for heavy metals: Electrochemical regeneration and closed-loop recycling. J. Hazard. Mater, 2020, 393. https://doi.org/10.1016/j.jhazmat.2020.122432.

Chapter 4: MA Ganzoury, Christina M. Hanna, N Zhang, Y Wu, CF De Lannoy. Gold Adsorption from Acidic Solutions using Functionalized CNT-Sorbents and their Electrochemical Regeneration in Neutral Solutions. Pending submission to Chemical Engineering Journal.

Chapter 5: MA Ganzoury, Y Wu, CF de Lannoy. Electrolyte Ion Migration through Electrochemical Membranes: Potential Source of Error in Batch Electrochemical Cells. Submitted to The Canadian Journal of Chemical Engineering.

Chapter 6: MA Ganzoury, CF de Lannoy. Limitations on using Metal Feed Spacers Electrodes in Electro-assisted RO Filtration.

Mohamed Elganzoury developed the methodology, conducted the investigation and formal analyses, and wrote the original manuscripts under direct supervision of Dr. Charles-François de Lannoy, who was also responsible for funding acquisition, project planning and paper reviewing. Nan Zhang, Yichen Wu, Cassandra Chidiac, Jasmine Kurtz and Christina Hanna helped with some experiments and data analyses. Dr. Saloumeh Ghasemian and Matt Yagar contributed their

expertise and participated in some editing for some paper chapters. All the coauthors have critically reviewed the manuscripts and provided valuable insights for possible improvements.

Chapter 1

Introduction

1.1 Industrial Wastewater Pollution

With the rapid growth in industrial activities, industrial wastewater problem is escalating as it is heavily contaminated with a broad spectrum of hazardous pollutants [1]. These pollutants include organics, pesticides, microplastics, dioxins, metals, and pathogenic organisms [2–4]. Discharging industrial wastewater directly to the environment into the aquatic ecosystems or soils will severely impact livelihood, fisheries and food chains [5]. On the other hand, disposing industrial wastewater to the municipal wastewater treatment facilities has to comply with strict discharge regulations to avoid fines [6,7]. Thus, an end-of-pipe treatment is required at the plant before industrial wastewater is released to the environment or to municipal facilities [8,9]. Moreover, the efficient treatment of wastewater will enable their internal recycling in industrial applications such as mining and paper industries [6,10]. Useful resources such as phosphates and precious metals can also be extracted by proper industrial wastewater treatment [11,12]. To this end, efficient industrial wastewater treatment has become a major goal for the sustainable development of industrial processes.

Among the pollutants in industrial wastewaters, toxic metals represent a severe hazard for humans, animals, and aquatic life [13]. Toxic metals of particular concern include arsenic, zinc, copper, cadmium, chromium, lead and mercury [14]. These metals are carcinogenic, non-biodegradable and tend to accumulate in living organisms [15]. Therefore, toxic metals present in wastewaters are one of the most serious environmental problems nowadays and their efficient removal is considered an environmental priority [13–15]. On the other hand, precious metals are also present in industrial wastewaters especially that generated from electronic and mining industries [16–18]. Precious metals in industrial wastewater include gold, silver, platinum,

palladium and rhodium [19]. These precious metals have a high value as they can be used for jewelry, electronics, catalysis, and hydrogen storage [20]. Thus, there is an economic need to effectively remove precious metals from industrial wastewaters.

1.2 Metal Contaminated Industrial Wastewaters

Metal contaminated wastewaters are generated from various industries as far ranging as electro plating, battery technology, petrochemicals, pesticides, mining, and electronic industries [13,21]. Among the different categories of metal-contaminated industrial wastewaters, four types are widely spread. First, mixed industrial wastewater generated from oil and gas, and petrochemicals industries which is rich in toxic metals and organic contaminants, and this type needs several stage unit operations to effectively remove the toxic metals and the associated organics [22–24]. Second, electroplating wastewater generated from surface plating operations which is rich in various types of toxic and precious metals used for plating including brass, nickel, zinc, silver, copper, lead, platinum, chromium and gold [25,26]. Third, acid mine drainage produced from the mining industries which is rich in toxic and precious metals, and sulfuric acid produced from the reaction of oxygen and water with the sulfates dissolving from the mined rocks [27,28]. Fourth, wastewater generated from electronic waste acidic leaching which is rich in precious metals (i.e., gold, silver, platinum and palladium) dissolved mainly from the printed circuit boards (PCBs) in the electronic devices [29–31].

1.3 Conventional Removal Technologies

1.3.1 Conventional Metals Removal Technologies

There is a present environmental and economic need for removing toxic and precious metals from the industrial wastewaters. Several technologies are being used for metal removal from wastewater including chemical precipitation, ion exchange, membrane filtration, coagulation and flocculation, flotation, and adsorption [21,32]. In this section, the advantages and drawbacks of the most conventional metal removal technologies will be discussed.

Chemical Precipitation

Chemical precipitation is the most widely used metal removal technique in industry because it is easily operated and does not need high capital cost [33]. In the precipitation process, chemicals react with the metals ions in the wastewater to form insoluble precipitates which are then removed from the solution via filtration or sedimentation [34]. Hydroxide precipitation and sulfide precipitation are the most conventional metal precipitation processes [32]. In the hydroxide precipitation process, hydroxides (conventionally lime (calcium hydroxide)) are added to the wastewater and precipitate metals as metal hydroxides. Nevertheless, hydroxide precipitation generates a large sludge volume causing dewatering and disposal problems [21]. In the sulfide precipitation process, sulfides (e.g., iron sulfide or calcium sulfide) are added to the wastewater and precipitate metals as metal sulfides. The sulfide precipitation process produces a sludge with better thickening and dewatering characteristics in comparison with the hydroxide precipitation process [35]. However, metal contaminated wastewaters are often acidic, and the addition of sulfides will favor the production of toxic hydrogen sulfide gas causing an environmental hazard [21,32]. Besides the specific drawback for each chemical precipitation method, metal removal using chemical precipitation methods consumes a large amount of

chemicals and are not efficient for removing metals with low concentrations (below 5 ppm) because the soluble fraction and very fine particles are challenging to precipitate [21,36].

Coagulation and Flocculation

Coagulation and flocculation are widely used for metal removal from wastewater [37–40]. In the coagulation process, coagulants are used to remove particulates and impurities by neutralizing their charges which allow their attachment into larger particles by hydrophobic interactions [41,42]. The most widely used coagulants for metal removal are alumina, iron hydroxides and iron sulfates [32,41]. In the flocculation process, high molecular weight polymers are used for clumping the contaminants together to form micro flocs which can be easily removed from the wastewater [43]. Polyaluminium chloride (PAC) , polyacrylamide (PAM) and polyferric sulfate are widely used flocculants for metal removal from wastewater [44]. After the coagulation or the flocculation processes, the aggregated particles are removed by floatation or filtration or sedimentation [45,46]. The coagulation and flocculation processes have a low capital cost and are simple in operation. Nevertheless, they have the same drawbacks as the chemical precipitation process; high chemical consumption and incomplete metal removal [21,38].

Flotation

Flotation process are also used for metal removal from wastewaters [47,48]. Air is bubbled into the solution, and the suspended metals attach to the air micro bubbles and float to the water surface to be removed as sludge [49]. The advantages of this technology are the absence of chemicals consumption and the low operating cost. While the major drawback of the floatation process is the high initial cost [13,21]. Floatation usually follows the coagulation/flocculation

processes to separate the formed aggregates in these processes by floating them to the surface, as shown in Figure 1.1 [45,50].

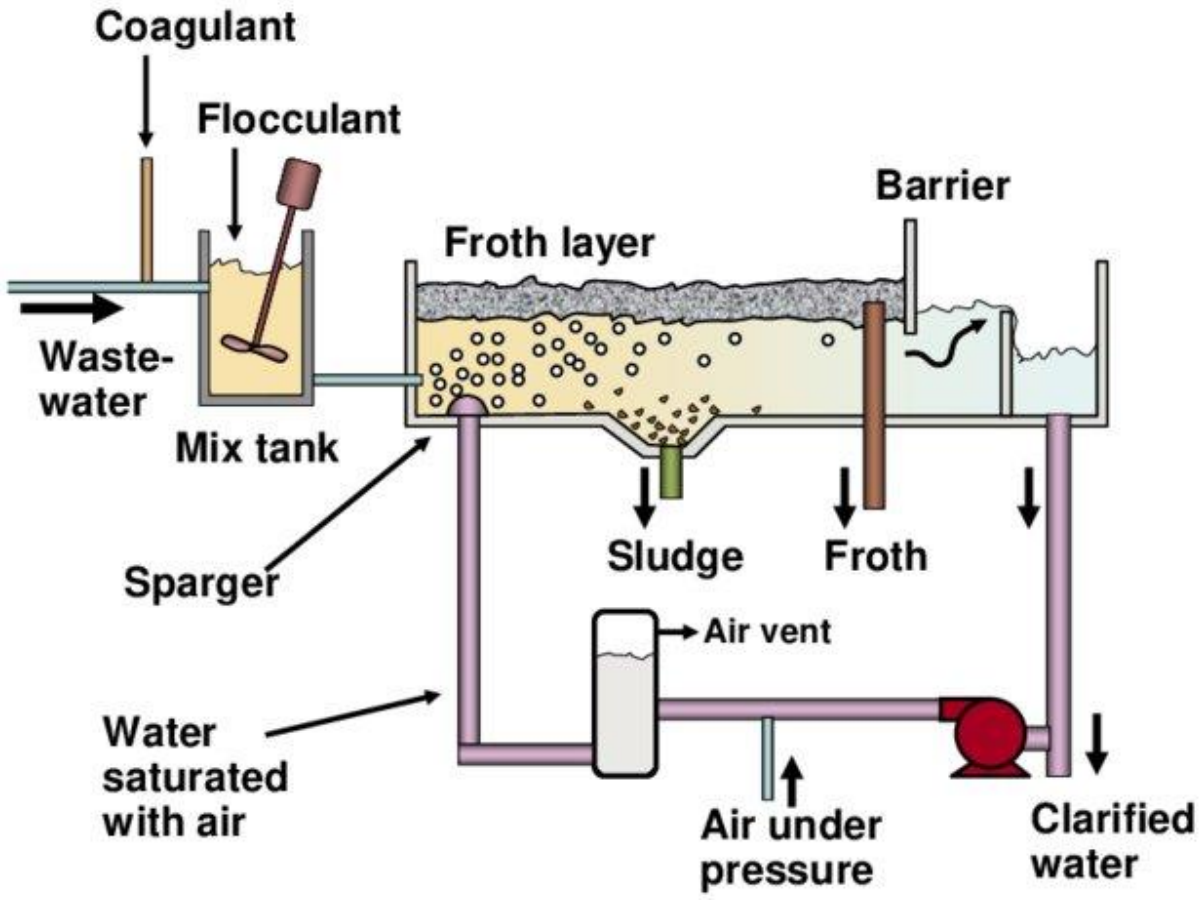

Figure 1. 1: Schematic diagram for an air flotation treatment process following a coagulation-flocculation process [50]

Ion Exchange

Ion exchange processes are widely used for metal removal from industrial wastewater due to their high removal efficiency and fast kinetics [32,51,52]. The metal contaminated wastewater is forced through a column containing ion-exchange resins. The resins are fabricated from cross-linked polymers functionalized with chemical groups, most commonly sulfonic acid (SO_3H) or

carboxylic acid (COOH) groups [21,51]. The metal cations in the wastewater are exchanged with hydrogen ions in the functional groups resulting in metal separation from the waste solution [21,34]. While the ion exchange process has a high metal removal efficiency, it is an expensive process and it is not effective in treating highly contaminated wastewaters (e.g., oily wastewater) as the resins are easily fouled [34]. Moreover, the spent ion-exchange resins are conventionally regenerated by chemical reagents causing secondary pollution that needs to be treated [53].

Membrane Filtration

Membrane filtration technology has been used for metal removal from wastewater as it has a lot of advantages such as ease of operation and low space requirement [54–57]. The membranes utilized for metal removal include ultrafiltration (UF), nanofiltration (NF) and reverse osmosis (RO) membranes [34,38]. UF membranes have a pore size much greater than the size of hydrated metal ions [54]. Therefore, polymer or surfactants are added to form polymer or micelles-metal complexes with a size big enough to be retained by UF membrane [56,58]. These processes are known as micellar enhanced UF (MEUF) or polymer enhanced UF (PEUF), and they consume large amounts of chemicals [57,59]. Since the active layers of RO membranes are very dense, RO membranes have a high retention efficiency for nearly every type of metal [54]. But taking into consideration the high operating pressure (20-30 bar), the high energy requirements (3-6 KWh), the high propensity of RO membranes to foul in mixed wastewaters, the delicate nature of these membranes, and the difficulty in cleaning RO membranes, RO processes are not favored for metal removal from wastewater [21,54]. NF processes are intermediate processes between UF and RO. NF membranes have a pore size (1-10 nm) smaller than that of UF membranes, and require a lower operating pressure than RO membranes [54,60,61]. NF membranes have a selective thin

skin that together with the small pore size are sufficient for metal retention [54,55]. Therefore, NF is preferred over UF or RO for metal removal in large scale applications. Nevertheless, the main drawback for the NF is surface and internal fouling especially when treating metal contaminated wastewater that is rich with associated contaminants (e.g., organics, colloids, surfactants) that deposit on the membrane surface causing pore blockage and a subsequent decline in permeate flux [38].

Adsorption

Adsorption is currently considered as an efficient and economic method for metal removal from industrial wastewater. The adsorption process is flexible in design, easily operated, and has a low chemical consumption [62]. Adsorption is a reversible process, several adsorbents can be regenerated to be reused in subsequent adsorption cycles [63]. Various adsorbents were used for metal removal including zeolites [64], clay minerals (e.g., kaolinites, bentonites, and mica) [62], biomaterials (e.g., algae [65]; fungi [66]; crab, seed and egg shells [67–69]; potato, citrus and banana peels [30,70,71]; and sawdust [72]) , MOFs [73], COFs [74], and carbonaceous materials (e.g., graphene [75], activated carbon (AC) [76] and carbon nanotubes (CNTs) [77]). Among the different classes of adsorbents, nanomaterials have orders of magnitude greater adsorption capacity than other sorbents due to their high surface area to volume ratio and high reactivity [62,78]. Specifically, CNTs have been recently recognized as excellent sorbents for several metals (e.g., gold [31], copper [79], zinc [80], arsenic [81] , nickel [82], mercury [83], cadmium [84], and silver [85]) due to their high specific surface area, porosity, and mechanical and chemical stability [86]. CNTs can also be functionalized with different chemical moieties which increase their adsorption capacity and allow for selective metal adsorption from mixed

solutions [87,88]. However, CNTs have a relatively higher cost in comparison with other sorbents [76]. Besides the high-cost drawback of CNTs, the major problem of the different classes of sorbents (including CNTs) is the high acidic chemical consumption usually needed for sorbent regeneration from metals, which causes a secondary pollution [80,89].

1.3.2 Conventional Associated Organics Degradation Technologies

Metal rich industrial wastewaters are usually contaminated with associated organics including organic dyes, organic acids, hydrocarbons (e.g., alkanes, alkenes, alkynes, and aromatic hydrocarbons), phenols and amines [90,91]. Some of these organic pollutants are toxic such as alkenes and phenolic compounds, and others (e.g., organic dyes) transform into toxic metabolites through the hydrolysis/oxidation processes occurring in wastewater [92,93]. Organic pollutants degradation is required for safe disposal or recycling of the industrial wastewaters. There are several conventional methods such as biodegradation, chemical oxidation, and photocatalysis.

Biodegradation

Biodegradation is a conventional method for organic pollutant removal from industrial wastewater [94,95]. Biodegradation is based on the ability of certain microorganisms to degrade organic contaminants in wastewater. Microorganisms that have been used for organics degradation include cyanobacteria, halophilic bacteria , archaea, and fungi [96–98]. In comparison with other physical and chemical methods for organics degradation, biodegradation is less expensive [96]. Nevertheless, the organic biodegradation effectiveness significantly decreases in metal rich wastewater due to the metal toxic effect on the microorganisms [99,100].

Chemical Oxidation

Chemical oxidation of the organic pollutants into less toxic products is a widely used technique for organic contaminant degradation from industrial wastewater [98]. Among the different chemical oxidation techniques, ozonation and Fenton oxidation are conventionally used for organic pollutant degradation [101,102]. In the ozonation process, O_2 reacts with dissociated O atom to form ozone (O_3) which is then bubbled into the wastewater [98,103]. At alkaline pH, ozone undergoes interactions to produce highly reactive species such as the hydroxyl radicals ($OH^{\bullet}$) and superoxides ($O_2^{\bullet -}$) which can mineralize organic contaminants [104]. At acidic and neutral pH, the oxidative radical production is much lower, and the organics degradation is done with the ozone itself [105]. The drawbacks for the ozonation process include the chemical consumption to obtain the alkaline pH and the high capital cost for ozone production [101]. In the Fenton process, hydrogen peroxide (H_2O_2) reacts with iron ions (Fe^{2+}) in the presence of strong acid to produce the highly oxidative hydroxyl radicals ($OH^{\bullet}$) which can degrade the organic contaminants in solution [106]. The optimum pH for the Fenton reaction lies in the range between 2-3.5 to avoid iron catalysts deactivation through precipitation in the form of ferric hydroxides [102]. Therefore, an extra acidic consumption will be required to degrade the organic pollutants via the Fenton process in neutral or alkaline industrial wastewaters. Moreover, there are extra costs and risks related to the provision, transportation, and storage of H_2O_2. Another drawback for the Fenton process is the difficulty of recycling the spent catalysts from the treated solution [98].

Photocatalysis

Photocatalysis is considered an environmentally friendly technique for organic pollutant degradation with a minimal chemical consumption [91]. The process involves irradiating

semiconductors with visible/UV light when they are in contact with the water and oxygen in the waste solution. Upon irradiating the semiconductor with an energy greater than its band gap energy, the valance band (VB) electrons (e^-) are excited and transfer to the conduction band (CB) leaving positive holes (h^+) in the VB [107]. Water molecules react with h^+ to produce hydroxyl radicals ($OH^\bullet$), while adsorbed oxygen molecules in the solution react with e^- to generate superoxide radicals ($O_2^{\bullet -}$), as shown in Figure 1.2 [38,108]. These radicals as aforementioned are capable of organic contaminant degradation in the wastewaters. The most widely used semiconductors for wastewater degradation are titanium dioxide (TiO_2) photocatalysts due to their photostability and strong oxidizing power [109]. Nevertheless, the organics degradation efficiency using semiconductors (including TiO_2) is always limited by the high e^-/h^+ recombination rate [98]. Several approaches have been researched to decrease the e^-/h^+ recombination rate including doping the photocatalysts with metal or non-metal ions and depositing nanoparticles on the photocatalyst surface, but these approaches complicate the photocatalyst fabrication process [110]. Another drawback for the photocatalysis degradation is the absence of concentrated sunlight most of the year in several countries which necessitates the use of UV excitation sources, increasing the overall capital cost [108].

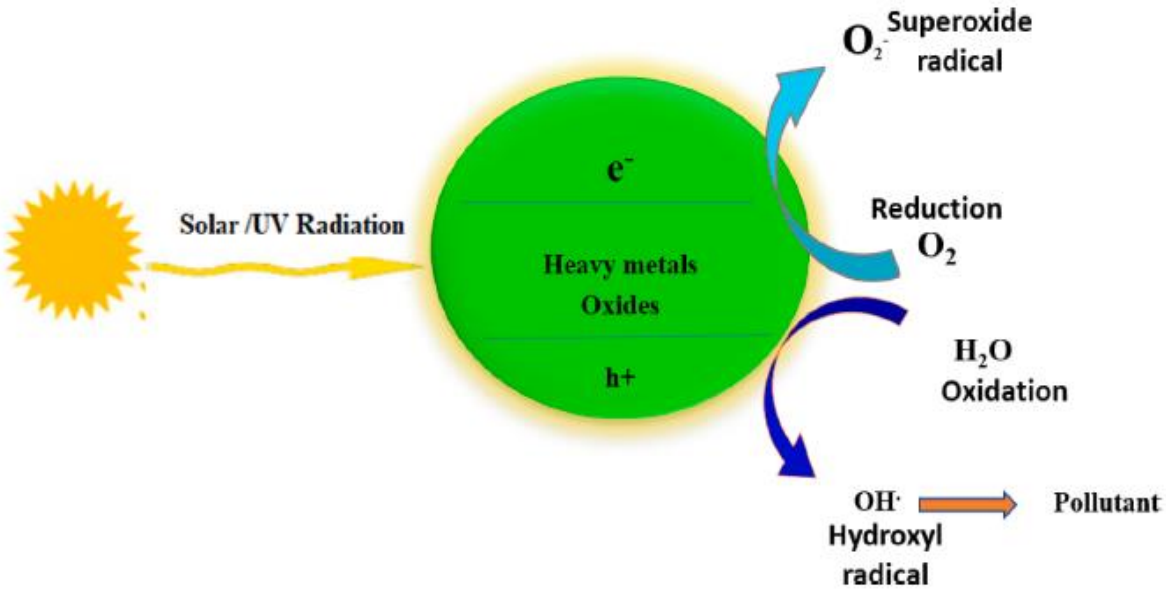

Figure 1. 2: Photocatalysis mechanism for pollutant degradation [38]

1.4 Electrochemical Water Treatment

With the stringent environmental regulations in the last two decades, electrochemical (EC) technologies have regained a great importance to be used in industrial wastewater treatment because it requires a minimal chemical consumption in comparison with other conventional processes as chemical precipitation, coagulation, flocculation, chemical and Fenton oxidation [7,111]. EC processes are also less complicated than biotreatment processes as they do not require living organisms that need nutrition and non-toxic environments [112]. EC processes can be built in continuous systems and have fast water treatment kinetics which save time and operational costs [113].

1.4.1 Electrochemical Technologies for Metal Removal

Electrochemical Deposition

Electrochemical deposition (ED), which is commonly known as electroplating, is one of the oldest EC metal removal technologies introduced by Luigi Brugnatelli in 1805 [114]. An external source of electricity is used to apply an electric current through an electrochemical cell which uses the wastewater required to be treated as an electrolyte. The metal cations in the wastewater are attracted to the negatively charged cathode by the action of electrostatic forces, and are subsequently reduced to form a metallic layer on the cathode surface [115]. ED process is used for the removal of precious metals (e.g., Au, Ag, Pt) as well as non-precious metals (e.g., Cu, Zn , Ni) from industrial wastewater [116,117]. The advantages of the ED process are the absence of any generated sludge, and the high metal selectivity gained through applying electric potentials corresponding to the reduction potentials of the selected metals to be removed [118]. Nevertheless, the metal removal efficiency of this process is limited by the electrode surface area and highly porous electrodes requirements. Another drawback is the formation of spongy or loose deposits and dendrites on the cathode surface [114]. Also, in a highly contaminated metal wastewater especially with organic pollutants, competing cathodic reactions with the metal reduction reactions will occur decreasing the metal removal efficiency [118].

Electrosorption

Electrosorption (ES) is a novel EC process for metal removal from water and wastewater [119,120]. The process is a combination of metal electrosorption and electrodesorption processes [121]. The mechanism of ES process resembles that of capacitive deionization (CDI) technology. Upon applying electric potential, the metal cations are electrically attracted to the porous cathode and temporarily stored by forming an electrical double layer inside the porous

electrode without chemical reactions. After the metal is electrically adsorbed to the electrode, the treated water solution is released from the system. The following step is to revert the electric field such that the metal ions are released from the electrode by action of electrostatic repulsion in a draw solution (as shown in Figure 1.3) [122,123]. ES electrodes are usually fabricated from carbonaceous materials such as CNTs, activated carbon (AC) and graphene aerogels owing to the their high electrical conductivity and large specific surface area [124–126]. In contrast to the ED process, metals should not be deposited on the electrode surface in the ES process to avoid decreasing the available surface area of the electrode. Thus, the applied electric potential should be maintained lower than the reduction potentials of the metals to be treated from the wastewater [127]. While the ES technique has a high metal removal efficiency, the process has a low metal selectivity and requires the fabrication of highly porous electrodes [114]. Moreover, metal solutions must be convected inside the porous electrodes to allow for metal electrosorption on the electrode surface, which requires more pumping power and engineering design considerations.

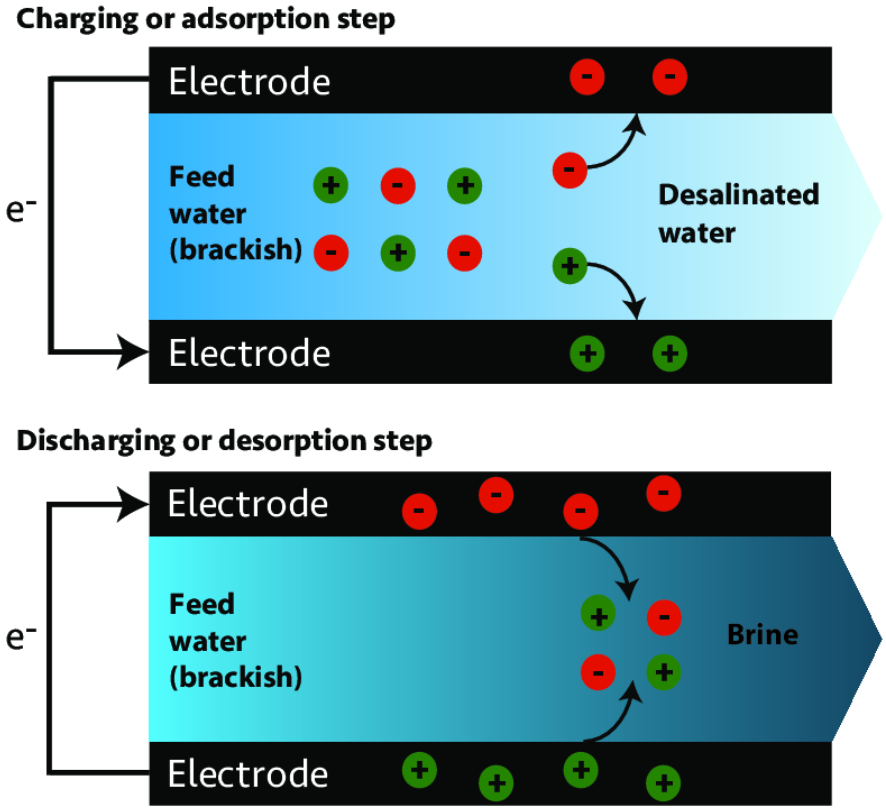

Figure 1. 3 : Schematic diagram illustrating electrosorption-electrodesorption process [128]

Electrocoagulation

Electrocoagulation (ECOG) is a widely used process for metal removal from industrial wastewater [129–131]. The process was first proposed in 1889 for sewage wastewater treatment in London [38]. In this process, a sacrificial metal anode is electrochemically dissolved through applying an electric field and produces metal hydroxides upon dissolution in solution. The generated metal hydroxides act as coagulants that can remove metals from the wastewater [132,133]. The most widely used materials for electrocoagulation anodes are iron and aluminum as they are inexpensive materials and generate strong coagulating agents (i.e., iron hydroxides and aluminum hydroxides) for metal removal [134]. The produced coagulants destabilize the

suspended metal ions in the solution allowing their aggregation in larger particles which can be easily precipitated and removed by filtration or sedimentation [135]. The electrocoagulation process has a minimal chemical consumption and produce less sludge in comparison with the chemical coagulation process [136]. Nevertheless, the sacrificial electrodes need to be monitored regularly as they dissolve in the solution which necessitates their frequent replacement resulting in plant downtime and additional operational costs in the form of replaced electrodes [137].

Electroflotation

Electroflotation (EF) is another EC process used for metal removal from wastewater [138]. In this process an electric potential enough for water electrolysis (1.23 V) is applied to produce tiny bubbles of hydrogen at the cathode and oxygen at the anode. The gas bubbles produced float the metal ions and bring them up to the water surface [114]. The EF is conventionally combined with electrocoagulation process, and this combined process is known as the electrocoagulation/ electroflotation (ECF) process [139]. Where, the generated metal-coagulants aggregates produced from the electrocoagulation process are floated to the liquid surface by the action of hydrogen and oxygen gases produced from the water electrolysis, as shown in Figure 1.4.

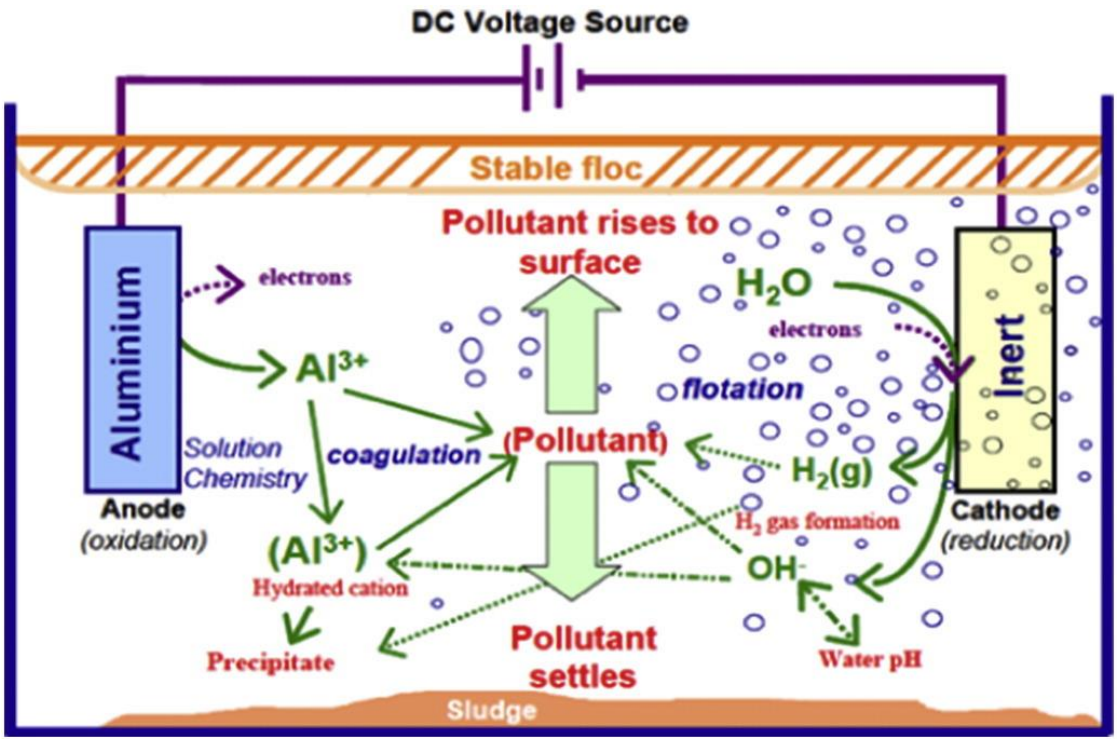

Figure 1. 4: Schematic diagram illustrating the ECF process using aluminium anode [140]

1.4.2 Electrochemical Technologies for Organics Degradation

Electrochemical Oxidation

Electrochemical oxidation (ECO) is recognized as a very promising technology for organic pollutant degradation in wastewater [7]. Anodic oxidation of organic contaminants can be carried out in different ways including the direct and indirect oxidation methods [113]. In the direct oxidation process, organic molecules are adsorbed to the anode and are electrochemically oxidized by losing electrons directly to the anode without any intermediate oxidizing agent, as shown in Figure 1.5. The direct oxidation of organic compounds usually requires a lower electric potential than that required for water electrolysis [113]. Nevertheless, this process has a low organic degradation efficiency because the anode is rapidly fouled by the deposited organic

matter, which is commonly known as the electrode poisoning effect [7]. To avoid the poisoning effect, the applied potential should be increased to the water electrolysis potential to generate superoxide and hydroxyl radicals in the solution that can oxidize the organic compounds, which is known as the indirect electrochemical oxidation technique [112,113]. The efficiency of organic indirect oxidation by superoxide and hydroxyl radicals would differ according to the anode materials. Using active anodes (i.e., dimensionally stable anodes (DSA)) fabricated from materials with low oxygen evolution overpotentials (e.g., platinum, iridium dioxide (IrO_2) and ruthenium dioxide (RuO_2)), partial degradation of the organic pollutant will occur, as some of the applied potential is scavenged by the production of oxygen gas [141,142]. While using non-active anodes fabricated from materials with higher oxygen evolution overpotentials (e.g., boron-doped diamond (BDD), lead dioxide (PbO_2) and tin dioxide (TnO_2)), a higher organic mineralization (conversion of organics into CO_2 and inorganic ions) efficiency is achieved [143,144]. Active anodes are commercially available and have high electrochemical stability in comparison with non-active anodes which have high cost and film stability problems [145]. In the presence of chloride salts in solution, active chlorine species (i.e., chlorine (Cl_2), hypochlorous acid (HClO) and hypochlorite (ClO^-)) are produced via the anodic oxidation of chloride ions [7]. Active chlorine species have high oxidizing power and can rapidly degrade the organic pollutants [142]. Interestingly, active anodes have a good electrochemical activity for generating active chlorine in contrast to non-active anodes which do not favor the production of active chlorine as their high anodic potential promotes the conversion of Cl^- into chlorate (ClO_3^-) and perchlorate (ClO_4^-) which are not strong oxidizing agents [7,146]. Thus, when choosing the electrode materials for use in

an ECO process one should identify the materials' overpotential towards various electrochemically generated products considering the chemical composition of the wastewater.

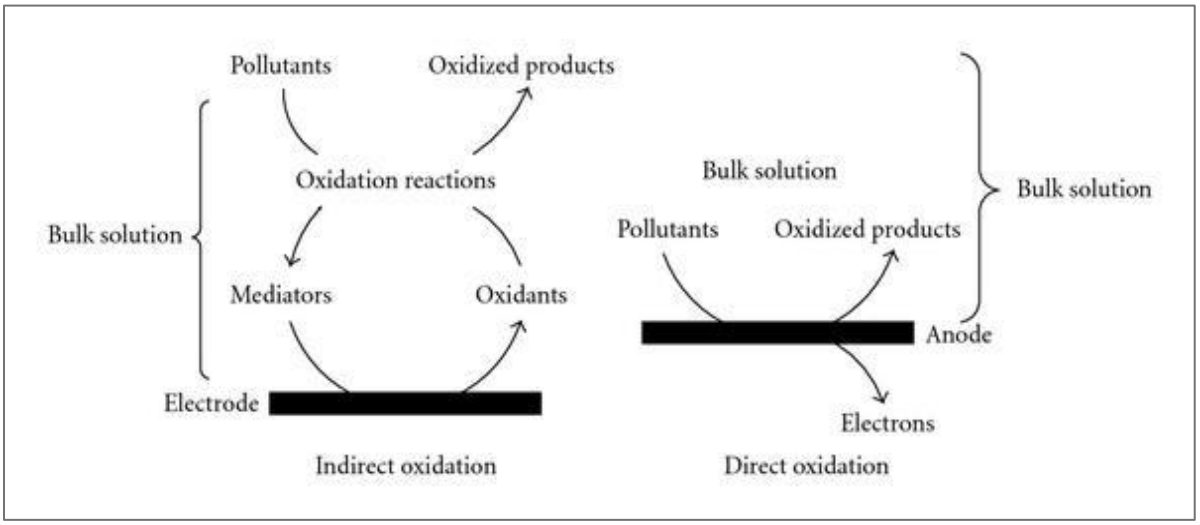

Figure 1. 5: Scheme illustrating the indirect (left) and direct (right) electrochemical oxidation processes [147]

Electro-Fenton oxidation

Electro-Fenton oxidation of organic contaminants, unlike the classical Fenton oxidation process, can mitigate the problems associated with supplying, transporting, and storing toxic H_2O_2. In this process, oxygen or air is fed to a carbonaceous cathode to electrochemically generate H_2O_2. Iron salt is supplied to the solution to react with H_2O_2 to generate hydroxyl radicals, which have high organics degradation efficiency [112]. While the electro-Fenton process eliminates the H_2O_2 addition to the treated solution, it still requires acidic conditions (pH between 2-3.5) to avoid iron hydroxide precipitation [148]. Consequently, this process is only suitable for treating acidic wastewaters similar to the classical Fenton process.

Electro-photocatalysis

Despite having the highest organic degradation efficiency, non-active anodes (e.g., BDD anodes) are expensive and have stability problems. DSA, in contrast, have high electrochemical stability and are less expensive [145]. Nevertheless, DSA have a lower organic degradation efficiency due to their limited generation of highly reactive oxidants especially in the absence of chloride salts in the treated wastewater [7,112]. Recent studies have shown that the integration of photocatalysis and electrocatalysis can overcome this limitation. Where irradiating the DSA anodes with UV light has enhanced the generation of highly reactive oxidants in solution [149,150]. Moreover, in the presence of chloride salts, UV irradiation of DSA anodes increased the generation of active chlorine species which enables higher organics degradation efficiency [151]. However, research is still ongoing to eliminate the engineering design and energy cost problems when coupling electrocatalysis and photocatalysis processes.

1.5 Objective and Thesis Structure

The objective of this research is to develop and quantitatively assess novel environmentally friendly electrochemical approaches as alternatives to conventional methods for removing metals and associated contaminants from industrial wastewaters. Specifically, the research in this thesis aims to decrease chemical consumption, lower the environmental impact, and to decrease the overall number of unit operations, while also extracting value from waste in the form of precious metal extraction. The research in this thesis was divided into three phases. In phase 1 (Chapter 2), the research goal was treating real mixed industrial wastewaters rich in toxic metals with a chemical-free technology. Conventionally, chemical precipitation or coagulation techniques are used for metal removal from mixed industrial wastewaters [33,38,39]. Nevertheless, these processes have high chemical consumption causing secondary pollution

[21,38]. Another valid alternative is using the electro-coagulation (ECOG) technology for metal removal from the wastewater. However, the ECOG process uses sacrificial electrodes which require regular monitoring and replacement resulting in an additional operational and capital cost [137]. In this research an in-situ ECOG process was used for metal removal from the waste solution without chemical consumption and without using sacrificial electrodes. The high iron concentration in the mixed industrial wastewater was used to generate iron hydroxide coagulants in-situ through the reaction of dissolved iron in solution with the hydroxide ions generated from water electrolysis at the cathode. Simultaneously with the metal removal process using the electrochemically generated coagulant at the cathode, dimensionally stable anodes (DSA) were used to electrochemically degrade the associated organic contaminants in the solution. This research introduced an electrochemical oxidation-in-situ coagulation (ECOIG) process which has the potential for both metal removal and associated organic removal and degradation from industrial mixed wastewaters using minimal unit operations and without the need for additional chemicals .

In phase 2 of the research, the goal was solving an environmental problem using novel CNT sorbents. CNT sorbents are one of the most effective sorbents for toxic and precious metal removal from wastewaters due to their high specific surface area, chemical and thermal stabilities, and excellent mechanical properties [86]. CNTs can also be functionalized with different chemical moieties which increase their adsorption capacity and allow for selective metal adsorption from mixed solutions [87,88]. Nevertheless, CNT sorbents are conventionally generated using acidic solutions causing a high chemical consumption and secondary pollution problems [80,89]. In this project, CNTs were generated using electric fields to minimize the

chemical consumption and lower the environmental impact. This research project was divided into two parts. The first part (Chapter 3) invented a closed-loop process for adsorption and electrodesorption of toxic metals from aqueous solutions using CNTs. The closed-loop regenerative cycle allowed recycling the effective but expensive CNT sorbents in subsequent adsorption-electrodesorption cycles. The electrochemical regeneration of CNTs eliminated the use of acids and chemical reagents for CNT regeneration. The second part of this project (Chapter 4) was extending the adsorption-electrodesorption technique to effectively extract precious metal (i.e., gold) from acidic solutions (mimicking e-waste leachate) and elute the adsorbed gold into neutral solutions.

In phase 3 of this research, potential sources of error and limitations that can occur during electrochemical water treatment were investigated. Part 1 of this research (Chapter 5) identified the source of errors occurring in batch electrochemical cells (BECC). Lab-scale experiments in BECCs are the baseline for developing electrochemical membranes (ECMs) and porous electrodes that are widely used for metal and organic removal from waste solutions [152–154]. Electrochemical dissolution of metal fasteners used to hold porous conductive membranes in BECCs was observed, despite keeping the fasteners outside the electrolyte solution. The electrolyte ions migrated through the porous membranes by the action of capillary forces forming a closed electrochemical circuit with the metal fasteners. This unexpected leaching can lead to misleading results for the electrochemical water treatment experiments using porous electrodes and ECMs in BECCs. A simple solution for the problem was proposed; separating the metal fasteners from the porous membrane electrodes by graphite sheets to open the electrochemical circuit. In part 2 of this research (Chapter 6), electro-assisted RO filtration of

calcium sulfate solutions was investigated. Calcium sulfate is a secondary pollutant produced during the metal-rich mining wastewater treatment [155,156]. Calcium sulfates are then deposited as gypsum scale during the RO filtration of the treated solution, causing a low permeate flux and possible damage for the RO membranes [157,158]. Using antiscalants for gypsum mitigation during RO filtration led to a high chemical consumption causing environmental problems. Using electrochemical technologies for gypsum mitigation can reduce the environmental impacts caused by antiscalants. In this study, conventional polymeric membrane spacers were replaced with electrically conductive metal spacers and an electrical potential was applied to these spacers to investigate mineral scaling mitigation on the RO membranes. Applying electric potentials on metal spacers showed limitations on gypsum scale mitigation due to the electrochemical dissolution of metal spacers. Inert electrodes to electro dissolution (i.e., CNTs coated polypropylene feed spacers) are proposed as an effective and economic choice for electro-assisted filtration of gypsum solutions.

This thesis introduced two novel environmental electrochemical approaches for metal separation with minimal chemical consumption and unit operations. It also demonstrated potential sources of error and limitations that can occur during electrochemical water treatment. The main contributions of the thesis and future perspectives to foster next step research are summarized in Chapter 7.

1.6 References

[1] G. Mao, Y. Han, X. Liu, J. Crittenden, N. Huang, U.M. Ahmad, Technology status and trends of industrial wastewater treatment: A patent analysis, Chemosphere. 288 (2022) 132483. doi:10.1016/j.chemosphere.2021.132483.

[2] M. Ahmed, M.O. Mavukkandy, A. Giwa, M. Elektorowicz, E. Katsou, O. Khelifi, V. Naddeo,

S.W. Hasan, Recent developments in hazardous pollutants removal from wastewater and water reuse within a circular economy, Npj Clean Water. 5 (2022) 1–25. doi:10.1038/s41545-022-00154-5.
[3] S. Sharma, S. Basu, Fabrication of centimeter-sized Sb2S3/SiO2 monolithic mimosa pudica nanoflowers for remediation of hazardous pollutants from industrial wastewater, J. Clean. Prod. 280 (2021) 124525. doi:10.1016/j.jclepro.2020.124525.
[4] B. Guieysse, Z.N. Norvill, Sequential chemical-biological processes for the treatment of industrial wastewaters: Review of recent progresses and critical assessment, J. Hazard. Mater. 267 (2014) 142–152. doi:10.1016/j.jhazmat.2013.12.016.
[5] C. He, C.P. Harden, Y. Liu, Comparison of water resources management between China and the United States, Geogr. Sustain. 1 (2020) 98–108. doi:10.1016/j.geosus.2020.04.002.
[6] UNESCO, The United Nations World Water Development Report 2017. Wastewater: The Untapped Resource., 2017.
[7] Y. Feng, L. Yang, J. Liu, B.E. Logan, Electrochemical technologies for wastewater treatment and resource reclamation, Environ. Sci. Water Res. Technol. 2 (2016) 800–831. doi:10.1039/c5ew00289c.
[8] G. Mao, H. Hu, X. Liu, J. Crittenden, N. Huang, A bibliometric analysis of industrial wastewater treatments from 1998 to 2019, Environ. Pollut. 275 (2021) 115785. doi:10.1016/j.envpol.2020.115785.
[9] A. Popat, P. V. Nidheesh, T.S. Anantha Singh, M. Suresh Kumar, Mixed industrial wastewater treatment by combined electrochemical advanced oxidation and biological processes, Chemosphere. 237 (2019) 124419. doi:10.1016/j.chemosphere.2019.124419.
[10] D. Fatta-Kassinos, D.D. Dionysiou, K. Kümmerer, Wastewater Reuse and Current Challenges, Springer, 2016. http://link.springer.com/10.1007/978-3-319-23892-0.
[11] D. Dutta, S. Arya, S. Kumar, Industrial wastewater treatment: Current trends, bottlenecks, and best practices, Chemosphere. 285 (2021) 131245. doi:10.1016/j.chemosphere.2021.131245.
[12] J.W. Choi, M.H. Song, J.K. Bediako, Y.S. Yun, Sequential recovery of gold and copper from bioleached wastewater using ion exchange resins, Environ. Pollut. 266 (2020). doi:10.1016/j.envpol.2020.115167.
[13] Ihsanullah, A. Abbas, A.M. Al-Amer, T. Laoui, M.J. Al-Marri, M.S. Nasser, M. Khraisheh, M.A. Atieh, Heavy metal removal from aqueous solution by advanced carbon nanotubes: Critical review of adsorption applications, Sep. Purif. Technol. 157 (2016) 141–161. doi:10.1016/j.seppur.2015.11.039.
[14] A.E. Burakov, E. V. Galunin, I. V. Burakova, A.E. Kucherova, S. Agarwal, A.G. Tkachev, V.K. Gupta, Adsorption of heavy metals on conventional and nanostructured materials for wastewater treatment purposes: A review, Ecotoxicol. Environ. Saf. 148 (2018) 702–712. doi:10.1016/j.ecoenv.2017.11.034.
[15] V.K. Gupta, O. Moradi, I. Tyagi, S. Agarwal, H. Sadegh, R. Shahryari-Ghoshekandi, A.S.H. Makhlouf, M. Goodarzi, A. Garshasbi, Study on the removal of heavy metal ions from industry waste by carbon nanotubes: Effect of the surface modification: A review, Crit. Rev. Environ. Sci. Technol. 46 (2016) 93–118. doi:10.1080/10643389.2015.1061874.
[16] M.E.H. Ahamed, X.Y. Mbianda, A.F. Mulaba-Bafubiandi, L. Marjanovic, Selective

extraction of gold(III) from metal chloride mixtures using ethylenediamine N-(2-(1-imidazolyl)ethyl) chitosan ion-imprinted polymer, Hydrometallurgy. 140 (2013) 1–13. doi:10.1016/j.hydromet.2013.08.004.
[17] R. Chand, T. Watari, K. Inoue, H. Kawakita, H.N. Luitel, D. Parajuli, T. Torikai, M. Yada, Selective adsorption of precious metals from hydrochloric acid solutions using porous carbon prepared from barley straw and rice husk, Miner. Eng. 22 (2009) 1277–1282. doi:10.1016/j.mineng.2009.07.007.
[18] K. Fujiwara, A. Ramesh, T. Maki, H. Hasegawa, K. Ueda, Adsorption of platinum (IV), palladium (II) and gold (III) from aqueous solutions onto l-lysine modified crosslinked chitosan resin, J. Hazard. Mater. 146 (2007) 39–50. doi:10.1016/j.jhazmat.2006.11.049.
[19] W. Wei, C.W. Cho, S. Kim, M.H. Song, J.K. Bediako, Y.S. Yun, Selective recovery of Au(III), Pt(IV), and Pd(II) from aqueous solutions by liquid-liquid extraction using ionic liquid Aliquat-336, J. Mol. Liq. 216 (2016) 18–24. doi:10.1016/j.molliq.2016.01.016.
[20] C.R. Lim, J.W. Choi, Y.S. Yun, C.W. Cho, Selection of low-toxic and highly efficient ionic liquids for the separation of palladium and platinum in acidic solution, and prediction of the metal affinity of ionic liquids, Sep. Purif. Technol. 258 (2021). doi:10.1016/j.seppur.2020.118019.
[21] F. Fu, Q. Wang, Removal of heavy metal ions from wastewaters: A review, J. Environ. Manage. 92 (2011) 407–418. doi:10.1016/j.jenvman.2010.11.011.
[22] F.A. Nasr, H.S. Doma, H.S. Abdel-Halim, S.A. El-Shafai, Chemical industry wastewater treatment, Environmentalist. 27 (2007) 275–286. doi:10.1007/s10669-007-9004-0.
[23] L.G. Torres, J. Jaimes, P. Mijaylova, E. Ramírez, B. Jiménez, Coagulation-flocculation pretreatment of high-load chemical-pharmaceutical industry wastewater: Mixing aspects, Water Sci. Technol. 36 (1997) 255–262. doi:10.1016/S0273-1223(97)00395-8.
[24] A. Asatekin, A.M. Mayes, Oil industry wastewater treatment with fouling resistant membranes containing amphiphilic comb copolymers, Environ. Sci. Technol. 43 (2009) 4487–4492. doi:10.1021/es803677k.
[25] E. De Beni, W. Giurlani, L. Fabbri, R. Emanuele, S. Santini, C. Sarti, T. Martellini, E. Piciollo, A. Cincinelli, M. Innocenti, Graphene-based nanomaterials in the electroplating industry: A suitable choice for heavy metal removal from wastewater, Chemosphere. 292 (2022) 133448. doi:10.1016/j.chemosphere.2021.133448.
[26] M.T. Bankole, A.S. Abdulkareem, I.A. Mohammed, S.S. Ochigbo, J.O. Tijani, O.K. Abubakre, W.D. Roos, Selected Heavy Metals Removal From Electroplating Wastewater by Purified and Polyhydroxylbutyrate Functionalized Carbon Nanotubes Adsorbents, Sci. Rep. 9 (2019) 1–19. doi:10.1038/s41598-018-37899-4.
[27] D.C. Buzzi, L.S. Viegas, M.A.S. Rodrigues, A.M. Bernardes, J.A.S. Tenório, Water recovery from acid mine drainage by electrodialysis, Miner. Eng. 40 (2013) 82–89. doi:10.1016/j.mineng.2012.08.005.
[28] A.O. Aguiar, L.H. Andrade, B.C. Ricci, W.L. Pires, G.A. Miranda, M.C.S. Amaral, Gold acid mine drainage treatment by membrane separation processes: An evaluation of the main operational conditions, Sep. Purif. Technol. 170 (2016) 360–369. doi:10.1016/j.seppur.2016.07.003.
[29] H. Salimi, Extraction and Recovery of Gold from both Primary and Secondary Sources by Employing A Simultaneous Leaching and Solvent Extraction Technique and Gold Leaching

In Acidified Organic Solvents, University of Saskatchewan, 2017.
[30] J.K. Bediako, J.W. Choi, M.H. Song, Y. Zhao, S. Lin, A.K. Sarkar, C.W. Cho, Y.S. Yun, Recovery of gold via adsorption-incineration techniques using banana peel and its derivatives: Selectivity and mechanisms, Waste Manag. 113 (2020) 225–235. doi:10.1016/j.wasman.2020.05.053.
[31] S.K. Pang, K.C. Yung, Prerequisites for achieving gold adsorption by multiwalled carbon nanotubes in gold recovery, Chem. Eng. Sci. 107 (2014) 58–65. doi:10.1016/j.ces.2013.11.026.
[32] C.F. Carolin, P.S. Kumar, A. Saravanan, G.J. Joshiba, M. Naushad, Efficient techniques for the removal of toxic heavy metals from aquatic environment: A review, J. Environ. Chem. Eng. 5 (2017) 2782–2799. doi:10.1016/j.jece.2017.05.029.
[33] K. Tanong, L.H. Tran, G. Mercier, J.F. Blais, Recovery of Zn (II), Mn (II), Cd (II) and Ni (II) from the unsorted spent batteries using solvent extraction, electrodeposition and precipitation methods, J. Clean. Prod. 148 (2017) 233–244. doi:10.1016/j.jclepro.2017.01.158.
[34] M.A. Barakat, New trends in removing heavy metals from industrial wastewater, Arab. J. Chem. 4 (2011) 361–377. doi:10.1016/j.arabjc.2010.07.019.
[35] J.L. Huisman, G. Schouten, C. Schultz, Biologically produced sulphide for purification of process streams, effluent treatment and recovery of metals in the metal and mining industry, Hydrometallurgy. 83 (2006) 106–113. doi:10.1016/j.hydromet.2006.03.017.
[36] Woodard & Curran. Inc, Industrial Waste Treatment Handbook, 2005. doi:10.1016/s0304-3894(01)00391-0.
[37] Q. Chang, G. Wang, Study on the macromolecular coagulant PEX which traps heavy metals, Chem. Eng. Sci. 62 (2007) 4636–4643. doi:10.1016/j.ces.2007.05.002.
[38] T.A. Saleh, M. Mustaqeem, M. Khaled, Water treatment technologies in removing heavy metal ions from wastewater: A review, Environ. Nanotechnology, Monit. Manag. 17 (2022) 100617. doi:10.1016/j.enmm.2021.100617.
[39] A.G. El Samrani, B.S. Lartiges, F. Villiéras, Chemical coagulation of combined sewer overflow: Heavy metal removal and treatment optimization, Water Res. 42 (2008) 951–960. doi:10.1016/j.watres.2007.09.009.
[40] J. Duan, Q. Lu, R. Chen, Y. Duan, L. Wang, L. Gao, S. Pan, Synthesis of a novel flocculant on the basis of crosslinked Konjac glucomannan-graft-polyacrylamide-co-sodium xanthate and its application in removal of Cu2+ ion, Carbohydr. Polym. 80 (2010) 436–441. doi:10.1016/j.carbpol.2009.11.046.
[41] F. Akbal, S. Camci, Comparison of electrocoagulation and chemical coagulation for heavy metal removal, Chem. Eng. Technol. 33 (2010) 1655–1664. doi:10.1002/ceat.201000091.
[42] D. Ghernaout, Brownian Motion and Coagulation Process, Am. J. Environ. Prot. 4 (2015) 1. doi:10.11648/j.ajeps.s.2015040501.11.
[43] M.H. Mohamed Noor, S. Wong, N. Ngadi, I. Mohammed Inuwa, L.A. Opotu, Assessing the effectiveness of magnetic nanoparticles coagulation/flocculation in water treatment: a systematic literature review, Int. J. Environ. Sci. Technol. (2021). doi:10.1007/s13762-021-03369-0.
[44] Q. Chang, M. Zhang, J. Wang, Removal of Cu2+ and turbidity from wastewater by mercaptoacetyl chitosan, J. Hazard. Mater. 169 (2009) 621–625.

doi:10.1016/j.jhazmat.2009.03.144.
[45] G. Pooja, P.S. Kumar, S. Indraganti, Recent advancements in the removal/recovery of toxic metals from aquatic system using flotation techniques, Chemosphere. 287 (2022) 132231. doi:10.1016/j.chemosphere.2021.132231.
[46] N.P. Hankins, N. Lu, N. Hilal, Enhanced removal of heavy metal ions bound to humic acid by polyelectrolyte flocculation, Sep. Purif. Technol. 51 (2006) 48–56. doi:10.1016/j.seppur.2005.12.022.
[47] H. Polat, D. Erdogan, Heavy metal removal from waste waters by ion flotation, J. Hazard. Mater. 148 (2007) 267–273. doi:10.1016/j.jhazmat.2007.02.013.
[48] H. Al-Zoubi, K.A. Ibrahim, K.A. Abu-Sbeih, Removal of heavy metals from wastewater by economical polymeric collectors using dissolved air flotation process, J. Water Process Eng. 8 (2015) 19–27. doi:10.1016/j.jwpe.2015.08.002.
[49] E.A. Deliyanni, G.Z. Kyzas, K.A. Matis, Various flotation techniques for metal ions removal, J. Mol. Liq. 225 (2017) 260–264. doi:10.1016/j.molliq.2016.11.069.
[50] M. Hubbe, J. Metts, D. Hermosilla, M. Blanco, L. Yerushalmi, F. Haghighat, P. Lindholm-Lehto, Z. Khodaparast, M. Kamali, A. Elliott, Wastewater treatment and reclamation: A review of pulp and paper industry practices and opportunities, Bioresources. 11 (2016) 7953–8091.
[51] A. Bashir, L.A. Malik, S. Ahad, T. Manzoor, M.A. Bhat, G.N. Dar, A.H. Pandith, Removal of heavy metal ions from aqueous system by ion-exchange and biosorption methods, Environ. Chem. Lett. 17 (2019) 729–754. doi:10.1007/s10311-018-00828-y.
[52] F.B. Liang, Y.L. Song, C.P. Huang, Y.X. Li, B.H. Chen, Synthesis of novel lignin-based ion-exchange resin and its utilization in heavy metals removal, Ind. Eng. Chem. Res. 52 (2013) 1267–1274. doi:10.1021/ie301863e.
[53] Z. Wang, Y. Feng, X. Hao, W. Huang, X. Feng, A novel potential-responsive ion exchange film system for heavy metal removal, J. Mater. Chem. A. 2 (2014) 10263–10272. doi:10.1039/c4ta00782d.
[54] N. Abdullah, N. Yusof, W.J. Lau, J. Jaafar, A.F. Ismail, Recent trends of heavy metal removal from water/wastewater by membrane technologies, J. Ind. Eng. Chem. 76 (2019) 17–38. doi:10.1016/j.jiec.2019.03.029.
[55] R. Castro-Muñoz, L.L. González-Melgoza, O. García-Depraect, Ongoing progress on novel nanocomposite membranes for the separation of heavy metals from contaminated water, Chemosphere. 270 (2021). doi:10.1016/j.chemosphere.2020.129421.
[56] M.A. Barakat, E. Schmidt, Polymer-enhanced ultrafiltration process for heavy metals removal from industrial wastewater, Desalination. 256 (2010) 90–93. doi:10.1016/j.desal.2010.02.008.
[57] J. Landaburu-Aguirre, E. Pongrácz, P. Perämäki, R.L. Keiski, Micellar-enhanced ultrafiltration for the removal of cadmium and zinc: Use of response surface methodology to improve understanding of process performance and optimisation, J. Hazard. Mater. 180 (2010) 524–534. doi:10.1016/j.jhazmat.2010.04.066.
[58] F. Ferella, M. Prisciandaro, I. De Michelis, F. Veglio', Removal of heavy metals by surfactant-enhanced ultrafiltration from wastewaters, Desalination. 207 (2007) 125–133. doi:10.1016/j.desal.2006.07.007.
[59] R. Molinari, T. Poerio, P. Argurio, Selective separation of copper(II) and nickel(II) from

aqueous media using the complexation-ultrafiltration process, Chemosphere. 70 (2008) 341–348. doi:10.1016/j.chemosphere.2007.07.041.
[60] M. Muthukrishnan, B.K. Guha, Effect of pH on rejection of hexavalent chromium by nanofiltration, Desalination. 219 (2008) 171–178. doi:10.1016/j.desal.2007.04.054.
[61] Z.V.P. Murthy, L.B. Chaudhari, Application of nanofiltration for the rejection of nickel ions from aqueous solutions and estimation of membrane transport parameters, J. Hazard. Mater. 160 (2008) 70–77. doi:10.1016/j.jhazmat.2008.02.085.
[62] A.E. Burakov, E. V. Galunin, I. V. Burakova, A.E. Kucherova, S. Agarwal, A.G. Tkachev, V.K. Gupta, Adsorption of heavy metals on conventional and nanostructured materials for wastewater treatment purposes: A review, Ecotoxicol. Environ. Saf. 148 (2018) 702–712. doi:10.1016/j.ecoenv.2017.11.034.
[63] I. Ali, New generation adsorbents for water treatment, Chem. Rev. 112 (2012) 5073–5091. doi:10.1021/cr300133d.
[64] E. Erdem, N. Karapinar, R. Donat, The removal of heavy metal cations by natural zeolites, J. Colloid Interface Sci. 280 (2004) 309–314. doi:10.1016/j.jcis.2004.08.028.
[65] K. Yin, Q. Wang, M. Lv, L. Chen, Microorganism remediation strategies towards heavy metals, Chem. Eng. J. 360 (2019) 1553–1563. doi:10.1016/j.cej.2018.10.226.
[66] D. Gola, P. Dey, A. Bhattacharya, A. Mishra, A. Malik, M. Namburath, S.Z. Ahammad, Multiple heavy metal removal using an entomopathogenic fungi Beauveria bassiana, Bioresour. Technol. 218 (2016) 388–396. doi:10.1016/j.biortech.2016.06.096.
[67] P.X. Pinto, S.R. Al-Abed, D.J. Reisman, Biosorption of heavy metals from mining influenced water onto chitin products, Chem. Eng. J. 166 (2011) 1002–1009. doi:10.1016/j.cej.2010.11.091.
[68] O.S. Amuda, F.E. Adelowo, M.O. Ologunde, Kinetics and equilibrium studies of adsorption of chromium(VI) ion from industrial wastewater using Chrysophyllum albidum (Sapotaceae) seed shells, Colloids Surfaces B Biointerfaces. 68 (2009) 184–192. doi:10.1016/j.colsurfb.2008.10.002.
[69] H.J. PARK, S.W. JEONG, J.K. YANG, B.G. KIM, S.M. LEE, Removal of heavy metals using waste eggshell, J. Environ. Sci. 19 (2007) 1436–1441. doi:10.1016/S1001-0742(07)60234-4.
[70] S. Schiewer, S.B. Patil, Modeling the effect of pH on biosorption of heavy metals by citrus peels, J. Hazard. Mater. 157 (2008) 8–17. doi:10.1016/j.jhazmat.2007.12.076.
[71] T. Aman, A.A. Kazi, M.U. Sabri, Q. Bano, Potato peels as solid waste for the removal of heavy metal copper(II) from waste water/industrial effluent, Colloids Surfaces B Biointerfaces. 63 (2008) 116–121. doi:10.1016/j.colsurfb.2007.11.013.
[72] A. Ahmad, M. Rafatullah, O. Sulaiman, M.H. Ibrahim, Y.Y. Chii, B.M. Siddique, Removal of Cu(II) and Pb(II) ions from aqueous solutions by adsorption on sawdust of Meranti wood, Desalination. 247 (2009) 636–646. doi:10.1016/j.desal.2009.01.007.
[73] S.W. Lv, J.M. Liu, C.Y. Li, N. Zhao, Z.H. Wang, S. Wang, A novel and universal metal-organic frameworks sensing platform for selective detection and efficient removal of heavy metal ions, Chem. Eng. J. 375 (2019) 122111. doi:10.1016/j.cej.2019.122111.
[74] N. Huang, L. Zhai, H. Xu, D. Jiang, Stable Covalent Organic Frameworks for Exceptional Mercury Removal from Aqueous Solutions, J. Am. Chem. Soc. 139 (2017) 2428–2434. doi:10.1021/jacs.6b12328.

[75] M. Pan, C. Shan, X. Zhang, Y. Zhang, C. Zhu, G. Gao, B. Pan, Environmentally Friendly in Situ Regeneration of Graphene Aerogel as a Model Conductive Adsorbent, Environ. Sci. Technol. 52 (2018) 739–746. doi:10.1021/acs.est.7b02795.
[76] C. Lu, C. Liu, G.P. Rao, Comparisons of sorbent cost for the removal of Ni2+ from aqueous solution by carbon nanotubes and granular activated carbon, J. Hazard. Mater. 151 (2008) 239–246. doi:10.1016/j.jhazmat.2007.05.078.
[77] S. Mallakpour, E. Khadem, Carbon Nanotubes for Heavy Metals Removal, Elsevier Inc., 2019. doi:10.1016/b978-0-12-814132-8.00009-5.
[78] C. Santhosh, V. Velmurugan, G. Jacob, S.K. Jeong, A.N. Grace, A. Bhatnagar, Role of nanomaterials in water treatment applications: A review, Chem. Eng. J. 306 (2016) 1116–1137. doi:10.1016/j.cej.2016.08.053.
[79] A.B. Dichiara, M.R. Webber, W.R. Gorman, R.E. Rogers, Removal of Copper Ions from Aqueous Solutions via Adsorption on Carbon Nanocomposites, ACS Appl. Mater. Interfaces. 7 (2015) 15674–15680. doi:10.1021/acsami.5b04974.
[80] C. Lu, H. Chiu, C. Liu, Removal of zinc(II) from aqueous solution by purified carbon nanotubes: Kinetics and equilibrium studies, Ind. Eng. Chem. Res. 45 (2006) 2850–2855. doi:10.1021/ie051206h.
[81] M.K. AlOmar, M.A. Alsaadi, M. Hayyan, S. Akib, M.A. Hashim, Functionalization of CNTs surface with phosphonuim based deep eutectic solvents for arsenic removal from water, Appl. Surf. Sci. 389 (2016) 216–226. doi:10.1016/j.apsusc.2016.07.079.
[82] M.I. Kandah, J.L. Meunier, Removal of nickel ions from water by multi-walled carbon nanotubes, J. Hazard. Mater. 146 (2007) 283–288. doi:10.1016/j.jhazmat.2006.12.019.
[83] M.K. AlOmar, M.A. Alsaadi, T.M. Jassam, S. Akib, M. Ali Hashim, Novel deep eutectic solvent-functionalized carbon nanotubes adsorbent for mercury removal from water, J. Colloid Interface Sci. 497 (2017) 413–421. doi:10.1016/j.jcis.2017.03.014.
[84] Y.-H. Li, Z. Luan, Z. Di, Y. Zhu, C. Xu, D. Wu, B. Wei, J. Ding, Competitive adsorption of Pb , Cu and Cd ions from aqueous solutions by multiwalled carbon nanotubes, Carbon N. Y. 41 (2003) 2787–2792. doi:10.1016/s0008-6223(03)00392-0.
[85] W. Nitayaphat, T. Jintakosol, Removal of silver (I) from aqueous solutions by chitosan/carbon nanotube nanocomposite beads, Adv. Mater. Res. 893 (2014) 166–169. doi:10.4028/www.scientific.net/AMR.893.166.
[86] Y. Ge, Z. Li, D. Xiao, P. Xiong, N. Ye, Sulfonated multi-walled carbon nanotubes for the removal of copper (II) from aqueous solutions, J. Ind. Eng. Chem. 20 (2014) 1765–1771. doi:10.1016/j.jiec.2013.08.030.
[87] V.K. Gupta, S. Agarwal, A.K. Bharti, H. Sadegh, Adsorption mechanism of functionalized multi-walled carbon nanotubes for advanced Cu (II) removal, J. Mol. Liq. 230 (2017) 667–673. doi:10.1016/j.molliq.2017.01.083.
[88] H.A. Shaheen, H.M. Marwani, E.M. Soliman, Selective adsorption of gold ions from complex system using oxidized multi-walled carbon nanotubes, J. Mol. Liq. 212 (2015) 480–486. doi:10.1016/j.molliq.2015.09.040.
[89] H.J. Wang, A.L. Zhou, F. Peng, H. Yu, L.F. Chen, Adsorption characteristic of acidified carbon nanotubes for heavy metal Pb(II) in aqueous solution, Mater. Sci. Eng. A. 466 (2007) 201–206. doi:10.1016/j.msea.2007.02.097.
[90] L.C. Castillo-Carvajal, J.L. Sanz-Martín, B.E. Barragán-Huerta, Biodegradation of organic

pollutants in saline wastewater by halophilic microorganisms: A review, Environ. Sci. Pollut. Res. 21 (2014) 9578–9588. doi:10.1007/s11356-014-3036-z.
[91] Y. Li, H. Jiang, X. Wang, X. Hong, B. Liang, Recent advances in bismuth oxyhalide photocatalysts for degradation of organic pollutants in wastewater, RSC Adv. 11 (2021) 26855–26875. doi:10.1039/d1ra05796k.
[92] X.Y. Zhang, A.A. Elfarra, Potential roles of myeloperoxidase and hypochlorous acid in metabolism and toxicity of alkene hydrocarbons and drug molecules containing olefinic moieties, Expert Opin. Drug Metab. Toxicol. 13 (2017) 513–524. doi:10.1080/17425255.2017.1271413.
[93] W. Raza, J. Lee, N. Raza, Y. Luo, K.H. Kim, J. Yang, Removal of phenolic compounds from industrial waste water based on membrane-based technologies, J. Ind. Eng. Chem. 71 (2019) 1–18. doi:10.1016/j.jiec.2018.11.024.
[94] I.M. Bulai, E. Venturino, Biodegradation of organic pollutants in a water body, J. Math. Chem. 54 (2016) 1387–1403. doi:10.1007/s10910-016-0603-1.
[95] D.H. Pieper, V.A.P. Martins Dos Santos, P.N. Golyshin, Genomic and mechanistic insights into the biodegradation of organic pollutants, Curr. Opin. Biotechnol. 15 (2004) 215–224. doi:10.1016/j.copbio.2004.03.008.
[96] T. Kuritz, C.P. Wolk, Use of filamentous cyanobacteria for biodegradation of organic pollutants, Appl. Environ. Microbiol. 61 (1995) 234–238. doi:10.1128/aem.61.1.234-238.1995.
[97] S. Le Borgne, D. Paniagua, R. Vazquez-Duhalt, Biodegradation of organic pollutants by halophilic bacteria and archaea, J. Mol. Microbiol. Biotechnol. 15 (2008) 74–92. doi:10.1159/000121323.
[98] H.K. Paumo, S. Dalhatou, L.M. Katata-Seru, B.P. Kamdem, J.O. Tijani, V. Vishwanathan, A. Kane, I. Bahadur, TiO2 assisted photocatalysts for degradation of emerging organic pollutants in water and wastewater, J. Mol. Liq. 331 (2021) 115458. doi:10.1016/j.molliq.2021.115458.
[99] R.M. Sterritt, J.N. Lester, Interactions of heavy metals with bacteria, Sci. Total Environ. 14 (1980) 5–17.
[100] T.R. Sandrin, R.M. Maier, Impact of metals on the biodegradation of organic pollutants, Environ. Health Perspect. 111 (2003) 1093–1101. doi:10.1289/ehp.5840.
[101] M.J. Quero-Pastor, M.C. Garrido-Perez, A. Acevedo, J.M. Quiroga, Ozonation of ibuprofen: A degradation and toxicity study, Sci. Total Environ. 466–467 (2014) 957–964. doi:10.1016/j.scitotenv.2013.07.067.
[102] M. hui Zhang, H. Dong, L. Zhao, D. xi Wang, D. Meng, A review on Fenton process for organic wastewater treatment based on optimization perspective, Sci. Total Environ. 670 (2019) 110–121. doi:10.1016/j.scitotenv.2019.03.180.
[103] D. Gardoni, A. Vailati, R. Canziani, Decay of Ozone in Water: A Review, Ozone Sci. Eng. 34 (2012) 233–242. doi:10.1080/01919512.2012.686354.
[104] Q. Wu, H. Shi, C.D. Adams, T. Timmons, Y. Ma, Oxidative removal of selected endocrine-disruptors and pharmaceuticals in drinking water treatment systems, and identification of degradation products of triclosan, Sci. Total Environ. 439 (2012) 18–25. doi:10.1016/j.scitotenv.2012.08.090.
[105] M. Muthukumar, D. Sargunamani, N. Selvakumar, J. Venkata Rao, Optimisation of ozone

treatment for colour and COD removal of acid dye effluent using central composite design experiment, Dye. Pigment. 63 (2004) 127–134. doi:10.1016/j.dyepig.2004.02.003.
[106] E. Neyens, J. Baeyens, A review of classic Fenton's peroxidation as an advanced oxidation technique, J. Hazard. Mater. 98 (2003) 33–50. doi:10.1016/S0304-3894(02)00282-0.
[107] A. Malathi, J. Madhavan, M. Ashokkumar, P. Arunachalam, A review on BiVO4 photocatalyst: Activity enhancement methods for solar photocatalytic applications, Appl. Catal. A Gen. 555 (2018) 47–74. doi:10.1016/j.apcata.2018.02.010.
[108] F. Han, V.S.R. Kambala, M. Srinivasan, D. Rajarathnam, R. Naidu, Tailored titanium dioxide photocatalysts for the degradation of organic dyes in wastewater treatment: A review, Appl. Catal. A Gen. 359 (2009) 25–40. doi:10.1016/j.apcata.2009.02.043.
[109] M.R.D. Khaki, M.S. Shafeeyan, A.A.A. Raman, W.M.A.W. Daud, Application of doped photocatalysts for organic pollutant degradation - A review, J. Environ. Manage. 198 (2017) 78–94. doi:10.1016/j.jenvman.2017.04.099.
[110] S. Dong, J. Feng, M. Fan, Y. Pi, L. Hu, X. Han, M. Liu, J. Sun, J. Sun, Recent developments in heterogeneous photocatalytic water treatment using visible light-responsive photocatalysts: A review, RSC Adv. 5 (2015) 14610–14630. doi:10.1039/c4ra13734e.
[111] G. Chen, Electrochemical technologies in wastewater treatment, Sep. Purif. Technol. 38 (2004) 11–41. doi:10.1016/j.seppur.2003.10.006.
[112] F.C. Moreira, R.A.R. Boaventura, E. Brillas, V.J.P. Vilar, Electrochemical advanced oxidation processes: A review on their application to synthetic and real wastewaters, Appl. Catal. B Environ. 202 (2017) 217–261. doi:10.1016/j.apcatb.2016.08.037.
[113] M. Panizza, G. Cerisola, Direct and mediated anodic oxidation of organic pollutants, Chem. Rev. 109 (2009) 6541–6569. doi:10.1021/cr9001319.
[114] H.I. Maarof, W.M.A.W. Daud, M.K.D. Aroua, Recent trends in removal and recovery of heavy metals from wastewater by electrochemical technologies, Rev. Chem. Eng. 33 (2017) 359–386. doi:10.1515/revce-2016-0021.
[115] M. Spitzer, R. Bertazzoli, Selective electrochemical recovery of gold and silver from cyanide aqueous effluents using titanium and vitreous carbon cathodes, Hydrometallurgy. 74 (2004) 233–242. doi:10.1016/j.hydromet.2004.05.001.
[116] J.L. Arredondo, F.F. Rivera, J.L. Nava, Silver recovery from an effluent generated by plating industry using a rotating cylinder electrode (RCE), Electrochim. Acta. 147 (2014) 337–342. doi:10.1016/j.electacta.2014.09.127.
[117] S. Chellammal, S. Raghu, P. Kalaiselvi, G. Subramanian, Electrolytic recovery of dilute copper from a mixed industrial effluent of high strength COD, J. Hazard. Mater. 180 (2010) 91–97. doi:10.1016/j.jhazmat.2010.03.103.
[118] J. Paul Chen, L.L. Lim, Recovery of precious metals by an electrochemical deposition method, Chemosphere. 60 (2005) 1384–1392. doi:10.1016/j.chemosphere.2005.02.001.
[119] M. Dai, L. Xia, S. Song, C. Peng, J.R. Rangel-Mendez, R. Cruz-Gaona, Electrosorption of As(III) in aqueous solutions with activated carbon as the electrode, Appl. Surf. Sci. 434 (2018) 816–821. doi:10.1016/j.apsusc.2017.10.238.
[120] M. Ziati, S. Hazourli, Experimental investigation of activated carbon prepared from date stones adsorbent electrode for electrosorption of lead from aqueous solution, Microchem. J. 146 (2019) 164–169. doi:10.1016/j.microc.2018.12.041.
[121] C. Hu, F. Liu, H. Lan, H. Liu, J. Qu, Preparation of a manganese dioxide/carbon fiber

electrode for electrosorptive removal of copper ions from water, J. Colloid Interface Sci. 446 (2015) 380–386. doi:10.1016/j.jcis.2014.12.051.
[122] X. Gu, Y. Yang, Y. Hu, M. Hu, C. Wang, Fabrication of graphene-based xerogels for removal of heavy metal ions and capacitive deionization, ACS Sustain. Chem. Eng. 3 (2015) 1056–1065. doi:10.1021/acssuschemeng.5b00193.
[123] L. Liu, X. Guo, R. Tallon, X. Huang, J. Chen, Highly porous N-doped graphene nanosheets for rapid removal of heavy metals from water by capacitive deionization, Chem. Commun. 53 (2017) 881–884. doi:10.1039/c6cc08515f.
[124] E.J. Bain, J.M. Calo, R. Spitz-Steinberg, J. Kirchner, J. Axén, Electrosorption/electrodesorption of arsenic on a granular activated carbon in the presence of other heavy metals, Energy and Fuels. 24 (2010) 3415–3421. doi:10.1021/ef901542q.
[125] Y. Wei, L. Xu, K. Yang, Y. Wang, Z. Wang, Y. Kong, H. Xue, Electrosorption of Toxic Heavy Metal Ions by Mono S- or N-Doped and S, N-Codoped 3D Graphene Aerogels, J. Electrochem. Soc. 164 (2017) E17–E22. doi:10.1149/2.1301702jes.
[126] H. Wang, C. Na, Binder-free carbon nanotube electrode for electrochemical removal of chromium, ACS Appl. Mater. Interfaces. 6 (2014) 20309–20316. doi:10.1021/am505838r.
[127] M.E. Suss, S. Porada, X. Sun, P.M. Biesheuvel, J. Yoon, V. Presser, Water desalination via capacitive deionization: What is it and what can we expect from it?, Energy Environ. Sci. 8 (2015) 2296–2319. doi:10.1039/c5ee00519a.
[128] J.E. Dykstra, Desalination with porous electrodes mechanisms of ion transport and adsorption, Wageningen University, 2018. doi:10.18174/443551.
[129] K. Thella, B. Verma, V.C. Srivastava, K.K. Srivastava, Electrocoagulation study for the removal of arsenic and chromium from aqueous solution, J. Environ. Sci. Heal. - Part A Toxic/Hazardous Subst. Environ. Eng. 43 (2008) 554–562. doi:10.1080/10934520701796630.
[130] X. Zhao, B. Zhang, H. Liu, J. Qu, Removal of arsenite by simultaneous electro-oxidation and electro-coagulation process, J. Hazard. Mater. 184 (2010) 472–476. doi:10.1016/j.jhazmat.2010.08.058.
[131] I. Kabdaşli, T. Arslan, T. Ölmez-Hanci, I. Arslan-Alaton, O. Tünay, Complexing agent and heavy metal removals from metal plating effluent by electrocoagulation with stainless steel electrodes, J. Hazard. Mater. 165 (2009) 838–845. doi:10.1016/j.jhazmat.2008.10.065.
[132] A. Shafaei, M. Rezayee, M. Arami, M. Nikazar, Removal of Mn2+ ions from synthetic wastewater by electrocoagulation process, Desalination. 260 (2010) 23–28. doi:10.1016/j.desal.2010.05.006.
[133] É. Fekete, B. Lengyel, T. Cserfalvi, T. Pajkossy, Electrocoagulation: An electrochemical process for water clarification, J. Electrochem. Sci. Eng. 6 (2016) 57–65. doi:10.5599/jese.218.
[134] F. Prieto-García, J. Callejas-Hernández, J. Prieto-Méndez, Y. Marmolejo-Santillán, Electrocoagulation of whey acids: Anode and cathode materials, electroactive area and polarization curves, J. Electrochem. Sci. Eng. 7 (2017) 89–101. doi:10.5599/jese.381.
[135] P.R. Kumar, S. Chaudhari, K.C. Khilar, S.P. Mahajan, Removal of arsenic from water by electrocoagulation, Chemosphere. 55 (2004) 1245–1252.

doi:10.1016/j.chemosphere.2003.12.025.
[136] H.J. Mansoorian, A.H. Mahvi, A.J. Jafari, Removal of lead and zinc from battery industry wastewater using electrocoagulation process: Influence of direct and alternating current by using iron and stainless steel rod electrodes, Sep. Purif. Technol. 135 (2014) 165–175. doi:10.1016/j.seppur.2014.08.012.
[137] M.Y. Mollah, R. Schennach, J. Parga, D.L. Cocke, Electrocoagulation(EC)-Science and applications, J. Hazard. Mater. 84 (2001) 29–41. doi:10.2166/wst.2020.199.
[138] A. Khelifa, S. Moulay, A.W. Naceur, Treatment of metal finishing effluents by the electroflotation technique, Desalination. 181 (2005) 27–33. doi:10.1016/j.desal.2005.01.011.
[139] E. Mohora, S. Rončević, B.Ž. Dalmacija, J. Agbaba, M. Watson, E. Karlović, M. Dalmacija, Removal of natural organic matter and arsenic from water by electrocoagulation/flotation continuous flow reactor, J. Hazard. Mater. 235–236 (2012) 257–264. doi:10.1016/j.jhazmat.2012.07.056.
[140] J.N. Hakizimana, B. Gourich, M. Chafi, Y. Stiriba, C. Vial, P. Drogui, J. Naja, Electrocoagulation process in water treatment: A review of electrocoagulation modeling approaches, Desalination. 404 (2017) 1–21. doi:10.1016/j.desal.2016.10.011.
[141] E. Brillas, C.A. Martínez-Huitle, Decontamination of wastewaters containing synthetic organic dyes by electrochemical methods. An updated review, Appl. Catal. B Environ. 166–167 (2015) 603–643. doi:10.1016/j.apcatb.2014.11.016.
[142] E. Isarain-Chávez, M.D. Baró, E. Rossinyol, U. Morales-Ortiz, J. Sort, E. Brillas, E. Pellicer, Comparative electrochemical oxidation of methyl orange azo dye using Ti/Ir-Pb, Ti/Ir-Sn, Ti/Ru-Pb, Ti/Pt-Pd and Ti/RuO2 anodes, Electrochim. Acta. 244 (2017) 199–208. doi:10.1016/j.electacta.2017.05.101.
[143] A.N. Subba Rao, V.T. Venkatarangaiah, Metal oxide-coated anodes in wastewater treatment, Environ. Sci. Pollut. Res. 21 (2014) 3197–3217. doi:10.1007/s11356-013-2313-6.
[144] M. Rueffer, D. Bejan, N.J. Bunce, Graphite: An active or an inactive anode?, Electrochim. Acta. 56 (2011) 2246–2253. doi:10.1016/j.electacta.2010.11.071.
[145] F.L. Souza, J.M. Aquino, D.W. Miwa, M.A. Rodrigo, A.J. Motheo, Photo-assisted electrochemical degradation of dimethyl phthalate ester on a DSA electrode, J. Environ. Chem. Eng. 2 (2014) 811–818. doi:10.5935/0103-5053.20140007.
[146] M. Zhou, H. Särkkä, M. Sillanpää, A comparative experimental study on methyl orange degradation by electrochemical oxidation on BDD and MMO electrodes, Sep. Purif. Technol. 78 (2011) 290–297. doi:10.1016/j.seppur.2011.02.013.
[147] Q. Zhou, W. Li, T. Hua, Removal of organic matter from landfill leachate by advanced oxidation processes: A review, Int. J. Chem. Eng. (2010) 1–10. doi:10.1155/2010/270532.
[148] D. Gümüş, F. Akbal, Comparison of Fenton and electro-Fenton processes for oxidation of phenol, Process Saf. Environ. Prot. 103 (2016) 252–258. doi:10.1016/j.psep.2016.07.008.
[149] R. Pelegrini, P. Peralta-Zamora, A.R. De Andrade, J. Reyes, N. Durán, Electrochemically assisted photocatalytic degradation of reactive dyes, Appl. Catal. B Environ. 22 (1999) 83–90. doi:10.1016/S0926-3373(99)00037-5.
[150] G. Li, M. Zhu, J. Chen, Y. Li, X. Zhang, Production and contribution of hydroxyl radicals between the DSA anode and water interface, J. Environ. Sci. 23 (2011) 744–748.

doi:10.1016/S1001-0742(10)60470-6.
[151] Y. Feng, D.W. Smith, J.R. Bolton, Photolysis of aqueous free chlorine species (HOCl and OCl-) with 254 nm ultraviolet light, J. Environ. Eng. Sci. 6 (2007) 277–284. doi:10.1139/S06-052.
[152] W. Duan, G. Chen, C. Chen, R. Sanghvi, A. Iddya, S. Walker, H. Liu, A. Ronen, D. Jassby, Electrochemical removal of hexavalent chromium using electrically conducting carbon nanotube/polymer composite ultrafiltration membranes, J. Memb. Sci. 531 (2017) 160–171. doi:10.1016/j.memsci.2017.02.050.
[153] H.J. Lee, N. Zhang, M.A. Ganzoury, Y. Wu, C.F. De Lannoy, Simultaneous Dechlorination and Advanced Oxidation Using Electrically Conductive Carbon Nanotube Membranes, ACS Appl. Mater. Interfaces. 13 (2021) 34084–34092. doi:10.1021/acsami.1c06137.
[154] M.A. Halali, M. Larocque, C.F. de Lannoy, Investigating the stability of electrically conductive membranes, J. Memb. Sci. 627 (2021) 119181. doi:10.1016/j.memsci.2021.119181.
[155] D. Feng, C. Aldrich, H. Tan, Treatment of acid mine water by use of heavy metal precipitation and ion exchange, Miner. Eng. 13 (2000) 623–642. doi:10.1016/S0892-6875(00)00045-5.
[156] S. Heviánková, I. Bestová, M. Kyncl, The application of wood ash as a reagent in acid mine drainage treatment, Miner. Eng. 56 (2014) 109–111. doi:10.1016/j.mineng.2013.10.032.
[157] Y.A. Le Gouelleec, M. Elimelech, Control of calcium sulfate (gypsum) scale in nanofiltration of saline agricultural drainage water, Environ. Eng. Sci. 19 (2002) 387–397. doi:10.1089/109287502320963382.
[158] A. Matin, F. Rahman, H.Z. Shafi, S.M. Zubair, Scaling of reverse osmosis membranes used in water desalination: Phenomena, impact, and control; future directions, Desalination. 455 (2019) 135–157. doi:10.1016/j.desal.2018.12.009.

Chapter 2

Mixed Metal Oxide Anodes Used for the Electrochemical Degradation of a Real Mixed Industrial Wastewater

Reprinted from MA Ganzoury, S Ghasemian, N Zhang, M Yagar, CF De Lannoy. Mixed metal oxide anodes used for the electrochemical degradation of a real mixed industrial wastewater. Chemosphere, 2022, 286, 131600. Copyright (2022), with permission from Elsevier.

2.1 Abstract

Mixed industrial wastewaters are often highly contaminated with heavy metals and organic pollutants. Treating these mixed wastewaters requires many stagewise unit operations. Our work investigates using an electrochemical oxidation-in-situ coagulation (ECO-IC) process as a pre-treatment step toward the efficient treatment of real mixed industrial wastewater rich with heavy metals and organic contaminants. The process degraded organic contaminants in the wastewater via anodic electrochemical oxidation. Simultaneously, heavy metals were precipitated in the solution by coagulants (iron hydroxides) formed in-situ by cathode-generated hydroxyl ions reacting with the significant amounts of dissolved iron in the wastewater. IrO_2-RuO_2 mixed metal oxide anodes were identified as the best electrodes for organic compound degradation demonstrating 97% degradation of methyl orange (MO) as a model compound within 15 min. These anodes were used to treat real industrial wastewater produced from the industrial cleaning of train tanker cars transporting industrial solvents. The electrochemical treatment experiments resulted in a treated solution with a lower heavy metal content, achieving 96% reduction in Fe and 30% reduction in As content. Only moderate decreases in organic content were observed up to a maximum of 13% reduction in total organic carbon after 1 h of treatment. Electrochemical treatment of the mixed industrial wastewater produced greater effective diameter of the suspended particles and distinct sediment, liquid, and suspended foam phases that could be easily separated for further treatment. ECO-IC shows promise as an efficient and chemical-free method to coagulate heavy metals in real industrial wastewaters and could be an effective pre-treatment in their separation.

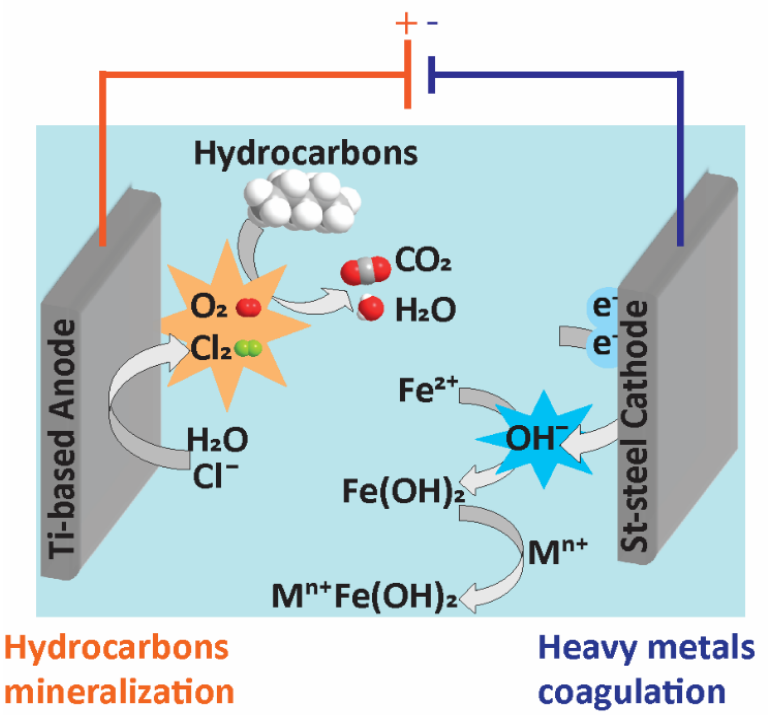

2.2 Introduction

Pollutants produced by heavy industry, specifically the chemical and oil and gas industries, produce heavily contaminated wastewaters containing both organics and heavy metals [1–3]. These mixed industrial wastewaters represent an environmental hazard and must meet stringent quality limits before they can be accepted by municipal wastewater treatment facilities [4,5]. For example, Ontario has an Industrial Discharge Limit to sewer treatment plants for Total Suspended Solids (350 ppm), Biological Oxygen Demand (300 ppm), iron (50 ppm), manganese (5 ppm), phenolic compounds (1 ppm) and arsenic (1 ppm) [6–9]. Thus, effective treatment of mixed industrial wastewaters is needed [10,11]. The major challenge for treating these wastewaters is the high cost required to meet the environmental regulations as these wastewaters can not be treated directly by municipal processes [4,12].

Several treatment technologies have been scaled for treating industrial wastewater; these can be broadly categorized as biological, chemical and physical treatment methods [5,13]. Biological methods include aerobic and anaerobic digestion, which are effective for treating wastewater containing a high BOD/COD ratio, however, the efficiency of these methods decreases as the BOD/COD ratio decreases [14]. Moreover, if the wastewater is contaminated with heavy metals, biological treatment will often not be effective because heavy metals are not biodegradable and are toxic to many bacteria [12,15]. When heavy metals are present, biological treatment of wastewater should be preceded by chemical methods such as alkaline precipitation [12,16]. While effective, chemical precipitation is limited to reducing aqueous heavy metal concentrations to approximately 5 ppm because very fine particles and the soluble fraction of heavy metals are challenging to precipitate [12,17]. These concentrations are often higher than acceptable environmental disposal levels. For example, according to Ontario Industrial Discharge Limit several heavy metals are regulated including zinc (3 ppm), lead (2 ppm), nickel (2 ppm) and arsenic (1 ppm), which are representative of discharge limits across North America [6–9,18]. As such, chemical precipitation is often followed by a physical method, such as sand filtration, to remove heavy metals from the solution to meet environmentally regulated limits [12]. Conventionally, several technologies operated as separate unit operations are needed when treating mixed industrial wastewater and each additional unit operation incurs additional cost to safe disposal.

Electrochemistry has recently been used in several environmental applications such as drinking water and wastewater treatment, membrane fouling detection, and soil remediation [19–22]. Electrochemical methods as compared with conventional methods require fewer or no

chemicals, can be single-stage operations reducing operational complexity, can be more energy-efficient technologies and produce less sludge [19,20,23,24]. For wastewater treatment, several electrochemical methods can be used for pollutant removal. For heavy metal removal from wastewater, electrochemical methods that have been evaluated in the literature include electrodeposition, electrocoagulation and electro-sorption techniques [19,25]. Electrocoagulation is considered an efficient process that can achieve nearly complete removal of heavy metals from aquatic solutions [26–28]. In this process, a sacrificial anode made from an inexpensive material (e.g. iron or aluminium) is electrochemically dissolved through the application of an electric potential. As the metal ions dissolve, they produce metal hydroxides, which are strong coagulating agents for the removal of heavy metals from solution [29–31]. For organic molecule removal from wastewater, electrochemical oxidation (ECO) as well as Fenton reactions have been demonstrated [13,20]. ECO is a widely used process for removing organic compounds from industrial wastewaters [32–34]. ECO degrades organic compounds by generating oxidizing species in water such as hydroxyl radicals and/or active chlorine at the anode surface. These electrochemically produced radicals oxidatively degrade organic compounds [32,35–37].

Wastewater produced from mining, oil and gas, and the chemical industry often contains large amounts of iron as well as other heavy metals [12]. Another common source of mixed industrial wastewater comes from the large volumes of hot water used to steam-clean the inside of train tanker cars that carry various oil and gas products including solvents [38,39]. This wastewater often contains high concentrations of iron, which likely comes from the walls of storage tanks or from tanker cars with degraded linings. Fortunately, the presence of iron can make wastewater

easier to treat. Ferrous iron (Fe^{2+}) is soluble in water but ferric iron (Fe^{3+}) is insoluble in water. Ferrous iron can be easily oxidized in the presence of oxygen to form ferric oxide which then reacts with water to form ferric hydroxide [12,40]. Nearly all heavy metals such as zinc, cadmium and lead are sparingly soluble in water, thus they will tend to adsorb on solid particulates, especially those with a high number of negative charges. Iron hydroxides are known to be effective coagulating agents for heavy metals due to their high oxidation states [12]. Therefore, wastewater containing a significant amount of iron can be treated through aeration which can lead to coagulation and sedimentation [12].

Several studies have investigated the electrochemical treatment of model wastewater solutions synthesized in laboratory [26,28,33,37,41–45]. However, studies on treatment of real mixed industrial wastewaters contaminated with metals and organics are rare. In this study, (1) we investigated the electrochemical treatment of real industrial wastewaters with high concentrations of heavy metals and organics (i.e., concentrations greater than the regulatory environmental disposal limits in Ontario, Canada), and (2) we proposed and demonstrated the use of an electrochemical oxidation-in-situ coagulation (ECO-IC) process to treat this highly contaminated wastewater. We aimed to treat a mixed industrial wastewater collected from Sarnia in Southwestern Ontario, Canada. This industrial wastewater was the product of steam-cleaning the inside of train tanker cars carrying various industrial products including those from the oil and gas, oil sands and other petrochemical industries. We hypothesized that electrochemical oxidation would have the dual effect of oxidatively degrading organic compounds with the wastewater while also providing sufficient aeration to produce iron hydroxide coagulants to aid in the removal of sparingly soluble heavy metals. We aimed to

explore removing the organic compounds as well as the heavy metals in a single unit operation. Our goal was to degrade organic compounds in the solution through anodic ECO while using (1) hydroxyl ions produced at the cathode by water electrolysis and (2) significant amounts of dissolved iron in the wastewater to produce in-situ coagulants (iron hydroxides) to precipitate the heavy metals. In this study, we evaluated three titanium-based metal oxide anodes for ECO widely researched for the electrochemical degradation of organic contaminants in wastewater. We compared the efficiency of mixed metal oxide (MMO) titanium-based electrodes with different combinations of transition metals oxides (IrO_2 and RuO_2) for their ability to degrade organic compounds to identify the metal oxide combination with (1) the best organic degradation efficiency and (2) the highest rate of degradation. A model organic compound, methyl orange (MO), was used to evaluate the performance of these titanium-based electrodes. Afterwards, we examined the proposed ECO-IC process for real mixed industrial wastewater while determining its efficiency in removing organics and heavy metals from the solution. The wastewater was analyzed for its organic and heavy metal composition. A quantification of the complex mixture before and after treatment provided an indication of how the electrochemical process changed the wastewater composition. We also studied the effect of the electrochemical process on the size of the suspended particles in the wastewater and we compared the effect of using different electrode geometries on the degradation efficiency of organic compounds in the wastewater.

2.3 Materials and methods

2.3.1 Materials

Three types of flat titanium-based electrodes (surface area of 56 cm^2), 1) titanium coated with IrO_2, RuO_2 and TiO_2, 2) titanium coated with RuO_2 and TiO_2 and 3) titanium coated with IrO_2 and

RuO_2, and one curved electrode (surface area of 84 cm^2) made of titanium coated with IrO_2 and RuO_2 were purchased from Shaanxi Elade New Material Technology China. Graphite and stainless-steel electrodes (surface area of 56 cm^2) were purchased from McMaster-Carr Canada. Methyl Orange (MO) and sodium chloride (NaCl) were purchased from Sigma Alderich Canada. Sodium sulfate (Na_2SO_4) was purchased from Fisher Scientific Canada. Mixed industrial wastewater samples were provided by our industrial partner, P.W. Custom Fabrications, from a mixed industrial wastewater collection tank in Southwestern Ontario.

2.3.2 Electrochemical degradation experiments

Electrochemical degradation experiments were performed in an aqueous solution containing a model organic contaminant (50 ppm MO with 0.1 M Na_2SO_4 and 0.01 M NaCl). 400 ml of this solution was used as an electrolyte in a three-electrode electrochemical cylindrical cell with an inner diameter of 8 cm. The electrolyte solution was stirred at 300 RPM to ensure uniform mixing during the electrochemical degradation experiments. Within this cell, Ag/AgCl was used as a reference electrode and different electrode materials were used as anode and cathode to determine the best electrodes for MO degradation, as shown in Figure 2.1. For the cathode, we compared stainless-steel and graphite electrodes. While for the anode, we compared three types of titanium-based electrodes 1) titanium coated with IrO_2, RuO_2 and TiO_2 (IrO_2-RuO_2-TiO_2 anode), 2) titanium coated with RuO_2 and TiO_2 (RuO_2-TiO_2 anode) and 3) titanium coated with IrO_2 and RuO_2 (IrO_2-RuO_2 anode). The electrode gap between the anode and cathode was maintained at 3.5 cm for all the experiments. The electrochemical cell was connected to a potentiostat (Metrohm, Multi Autolab/M101) to investigate the electrochemical degradation of MO. Subsequently, the best anode and cathode for MO degradation were used in a three-electrode

electrochemical cell similar to that used in the model contaminant degradation experiments. In these experiments, the electrolyte was the mixed industrial wastewater.

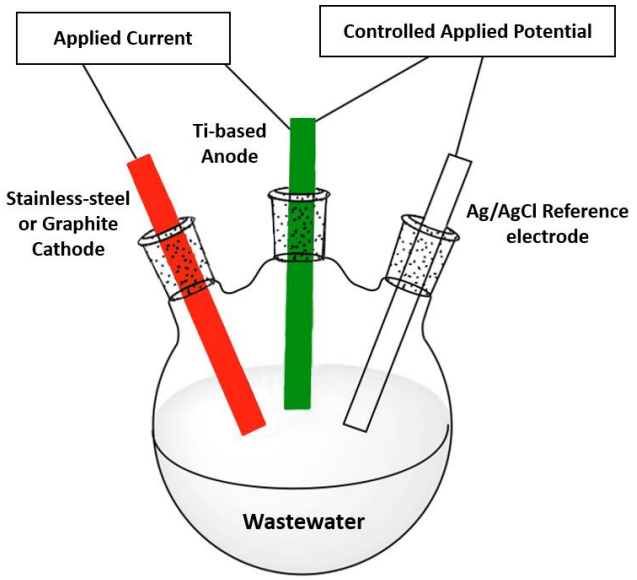

Figure 2.1: Three-electrode electrochemical cell for wastewater degradation

2.3.3 Characterization and analytical procedures

Surface morphology and elemental analysis for the metal oxide coated titanium-based electrodes were performed using Scanning Electron Microscopy (SEM) and Energy Dispersive X-Ray (EDX) spectroscopy, respectively. For the simulated wastewater, MO degradation was measured using a UV-VIS spectrophotometer (Tecan Spark 10 M). While for the industrial wastewater, (1) the organic matter degradation and precipitation were analysed by Total Organic Carbon (TOC) analyzer, (2) the heavy metal content was analysed using Inductively Coupled Plasma-Optical Emission Microscopy (ICP-OES) (Thermo Scientific, iCAP 6000) and Inductively Coupled Plasma-Mass Spectroscopy (ICP-MS) (Thermo Scientific, Xseries 2), (3) the anion concentration was

measured using Ion Chromatography (IC) (Thermo Scientific, Dionex) and (4) the size of suspended particles in solution was estimated by Dynamic Light Scattering (DLS) (Malvern, Zetasizer NanoSampler).

2.4 Results and discussion

2.4.1 Electrochemical degradation of simulated wastewater

Electrochemical degradation experiments were performed for an aqueous solution of methyl orange (MO) as a model organic contaminant to determine the best electrode materials to degrade organic compounds. As aforementioned, the simulated wastewater was 50 ppm MO solution with 0.1 M Na_2SO_4 and 0.01 M NaCl. Electrochemical degradation efficiency was determined by the rate of degradation of the azo bond, indicated by the loss of the orange colour from the MO solution. Three types of titanium-based electrodes were compared for use as anodes (i.e. the working electrode, WE) and validated in comparison to a graphite anode. The three Ti-based electrodes were 1) titanium coated with IrO_2, RuO_2 and TiO_2 (IrO_2-RuO_2-TiO_2 anode), 2) titanium coated with RuO_2 and TiO_2 (RuO_2-TiO_2 anode) and 3) titanium coated with IrO_2 and RuO_2 (IrO_2-RuO_2 anode). SEM images indicated the uniform coating of metal oxides on the Ti-based electrodes, as shown in Figure 2.2. The SEM images also showed the cracked-mud structure which is typical for oxide electrodes [46,47]. The electrochemical degradation of MO was studied using these four anodes, as shown in Figure 2.3. For all four experiments graphite was used as the cathode (counter electrode, CE), a current of 0.5 A was applied to the anode for 30 min, and the WE and CE were kept 3.5 cm from each other. In conventional electrocatalysis a smaller electrode gap is usually preferred to decrease the solution resistance between the electrodes. However, in treating complex wastewater, a slightly larger electrode gap up to 5 cm

has been shown to be beneficial [48,49]. Based on the literature we chose 3.5 cm as an electrode gap in our experiments. In control experiments, graphite WE achieved 15% decolorization efficiency of MO after 5 min and 54% decolorization after 30 min, as shown in Figure 2.3a. In contrast, the three types of titanium-based WEs enhanced the MO decolorization efficiency to 85%, 81%, and 90% after 5 min and to 97 % after 30 min, as shown in Figure 2.3b (IrO_2-RuO_2-TiO_2 Figure 2.3c (RuO_2-TiO_2) and Figure 2.3d (IrO_2-RuO_2), respectively. The electrochemical potential for O_2 evolution on IrO_2 (1.5-1.8 V/SHE) and RuO_2 (1.4-1.7 V/SHE) is lower than for that on graphite (1.8 V/SHE), which benefits the oxidative generation of hydroxyl radicals and chlorates on the Ti-based electrodes [50]. Furthermore, oxidative reactions on the surface of graphite can break the electrode's carbon bonds oxidizing them into CO_2. This electrochemical oxidation of the graphite electrode material competes for the oxidation of organics in solution, diminishing the overall degradation efficiency of organic contaminants [20,50,51].

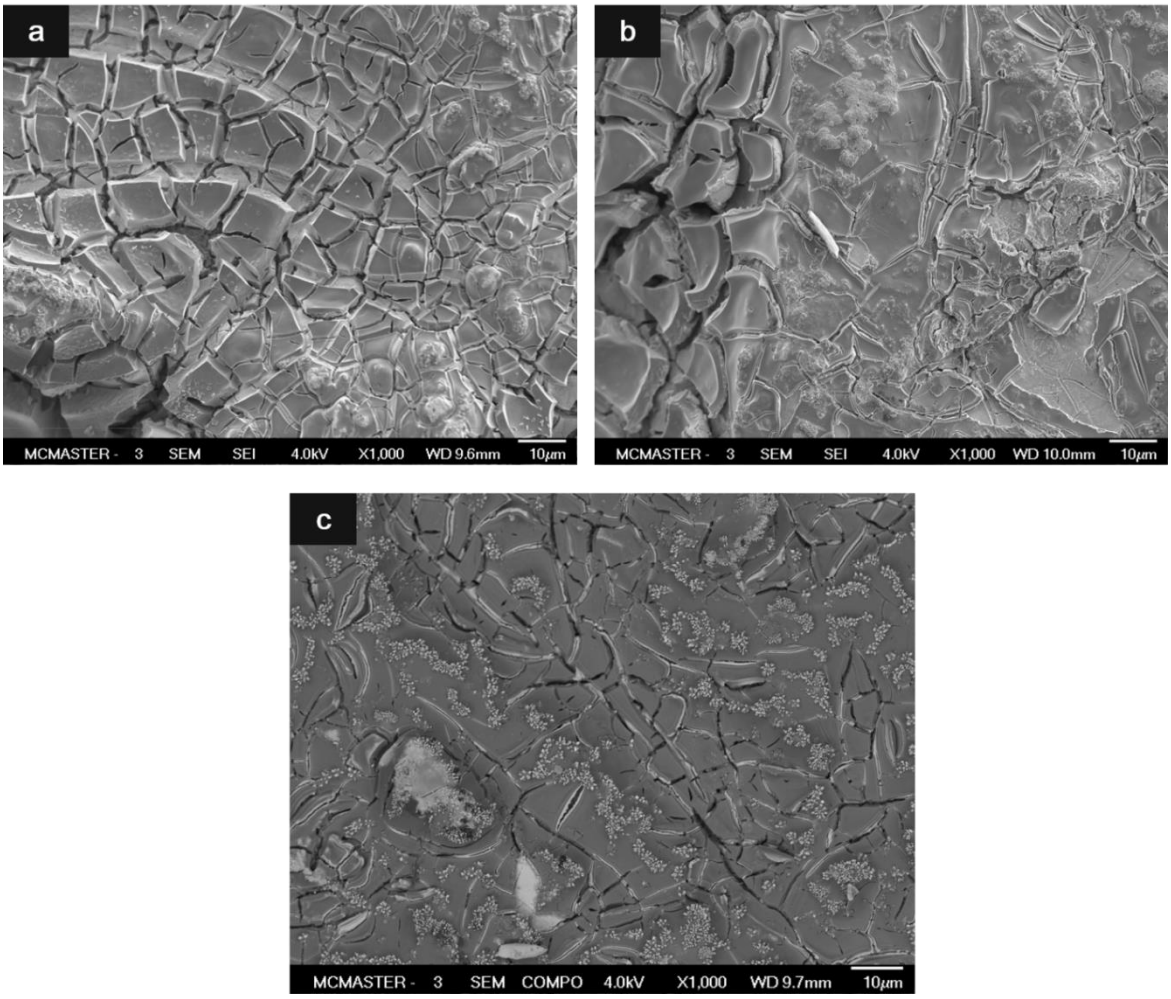

Figure 2.2: SEM images for a) IrO_2-RuO_2-TiO_2 anode , b) RuO_2-TiO_2 anode and c) IrO_2-RuO_2 anode

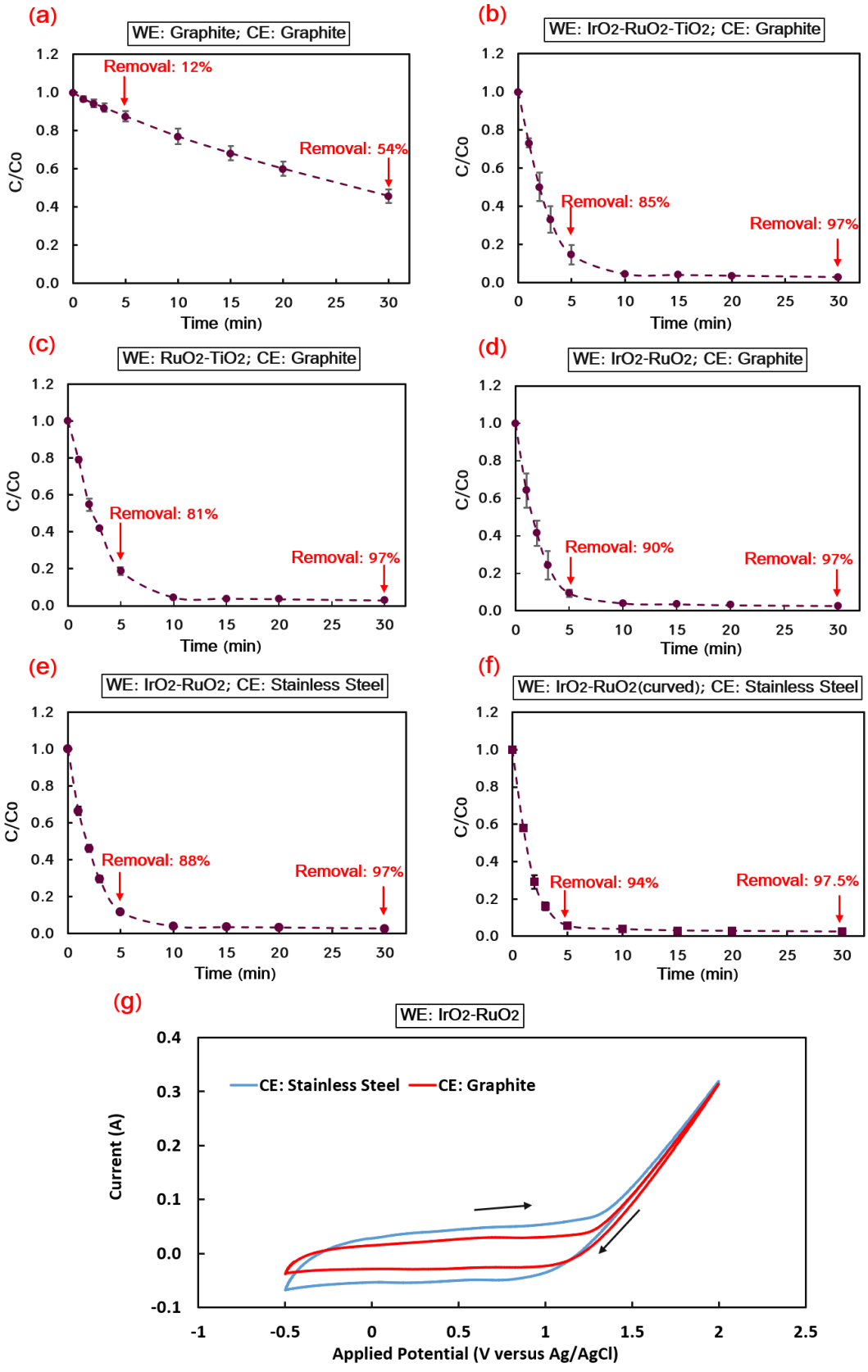
(a)
WE: Graphite; CE: Graphite
Removal: 12%
Removal: 54%
C/C0
Time (min)
(b)
WE: IrO2-RuO2-TiO2; CE: Graphite
Removal: 85%
Removal: 97%
C/C0
Time (min)
(c)
WE: RuO2-TiO2; CE: Graphite
Removal: 81%
Removal: 97%
C/C0
Time (min)
(d)
WE: IrO2-RuO2; CE: Graphite
Removal: 90%
Removal: 97%
C/C0
Time (min)
(e)
WE: IrO2-RuO2; CE: Stainless Steel
Removal: 88%
Removal: 97%
C/C0
Time (min)
(f)
WE: IrO2-RuO2(curved); CE: Stainless Steel
Removal: 94%
Removal: 97.5%
C/C0
Time (min)
(g)
WE: IrO2-RuO2
CE: Stainless Steel
CE: Graphite
Current (A)
Applied Potential (V versus Ag/AgCl)

Figure 2.3: (a, b, c, d) Effect of Anode Materials, (e) Effect of using stainless-steel cathode and (f) Effect of using curved IrO_2-RuO_2 anode on MO degradation at 0.5 A applied current and a 3.5 cm electrode gap. WE refers to the working electrode (Anode in this experiments) and CE refers to the counter electrode (Cathode in this experiments). (g) Cyclic voltammetry curves for stainless-steel and graphite electrodes.

MO degradation can occur by electrochemical oxidation (ECO) at the anode surface. In the case of non-active anodes such as Boron-doped diamond (BDD) or SnO_2, MO degradation occurs through oxidation by hydroxyl radicals ($^{\bullet}OH$) that are generated by water electrolysis. Water splitting occurs at the surface of the anode (A) generating highly reactive $^{\bullet}OH$ (Eq. 2.1) [51]. Hydroxyl radicals are considered the strongest oxidizing agent after fluorine [20] and it efficiently oxidizes aromatic and aliphatic compounds achieving high mineralization efficiency (conversion into CO_2 and inorganic ions) [44,52]. Eq. 2.2 shows the first step of MO oxidation by hydroxyl radicals, where the MO azo-bond breaks to form benzyl carbazate and 4-nitrophenylsulfonate. After the azo bond breaks, many different reactions occur between the hydroxyl radicals and the product compounds until complete mineralization is achieved. These detailed pathways have been previously investigated and discussed [44]. In the case of active anodes (e.g. dimensionally stable anodes (DSA) coated with IrO_2 or RuO_2) that have higher oxidation states due to the presence of transition metals (e.g. Ir or Ru) [53], $^{\bullet}OH$ produced from the electrolysis of water at the metal oxide anode (MO_X) can be further oxidized to aqueous H^+ producing chemically adsorbed superoxide (MO_{X+1}) (Eq. 2.3) [44,54]. MO near the surface of the anode can be oxidized by the superoxide, but at a lower mineralization efficiency, forming carboxylic acids such as oxalic and malic acid [44].

$$H_2O(I) \rightarrow A{\sim}OH^{\bullet} + H^+(aq) + e^- \qquad (2.1)$$

$$C_{14}H_{14}N_3O_3S \xrightarrow{OH\bullet} C_6H_4NO_5S + C_8H_{10}N_2O_2 \qquad (2.2)$$

$$MO_X{\sim}OH^{\bullet} \rightarrow MO_{X+1} + H^+(aq) + e^- \qquad (2.3)$$

When chloride salts are present in solution, active chlorine species (Cl_2, HClO and ClO^-) can be produced by the electrochemical oxidation of chloride at the anode surface as follows [20]:

$$2Cl \rightarrow Cl_2 + 2e^- \qquad (2.4)$$

$$Cl_2 + H_2O \rightarrow HClO + H^+ + Cl^- \qquad (2.5)$$

$$HClO \leftrightharpoons H^+ + ClO^- \qquad (2.6)$$

Active chlorine species are a strong oxidizing agent that can rapidly attack organic molecules and have been demonstrated to have higher rates of reaction than hydroxyl radicals [44]. Interestingly, non-active anodes do not favor the production of active chlorine as the high anodic potential of these electrodes favors the conversion of Cl^- into chlorate (ClO_3^-) and perchlorate (ClO_4^-) which are not strong oxidizing agents at circumneutral pH. In contrast, active anodes, such as those used in this study, have good electrochemical activity for generating active chlorine [20,55].

Degradation of MO can also occur by electrochemical reduction at the cathode, where the generated electrons at the cathode directly reduce MO, breaking its azo bond and producing 4-amin-benzenesulfonic acid and N,N-dimethyl-benzene-1,4-diamine as follows [56]:

$$C_{14}H_{14}N_3O_3S + 4H^+ + 4e^- \rightarrow C_6H_6NO_3S + C_8H_{12}N_2 \qquad (2.7)$$

In our experiments, we believe that the dominant mechanism for MO degradation was anodic ECO rather than cathodic electrochemical reduction. This suggestion is confirmed by the significant increase in MO decolorization when using titanium-based anodes in contrast to using a graphite anode (Figure 2.3). These results align well with a previous study done by Liu et al. which showed a limited electrochemical reduction of MO on carbon paper cathode due to the high electrode resistance. They showed that modifying the carbon cathode with a redox mediator (thionine) was needed to improve the rate of MO reduction [41]. In our experiments, we believe that MO is oxidized by the aid of oxygen and active chlorine because of the presence of NaCl in our solution as well as the use of active anodes which promote the generation of oxygen and active chlorine.

In Figure 2.3 the rate of decolorization of MO using IrO_2-RuO_2 anode was higher than that of IrO_2-RuO_2-TiO_2 anode and RuO_2-TiO_2 anode. 90% of MO was decolorized in the first 5 min when using IrO_2-RuO_2 anode in comparison with 85% and 81% MO removal when using IrO_2-RuO_2-TiO_2 anode and RuO_2-TiO_2 anode, respectively. EDX analysis quantified the elemental compositions of the electrodes and demonstrated that the highest percent of (Ir) existed in the IrO_2-RuO_2 anode (31.0%) followed by IrO_2-RuO_2-TiO_2 anode (22.0%) followed by RuO_2-TiO_2 anode (4.6%), as shown in the supplementary information in Table S2.1. Anodes containing greater amounts of IrO_2 demonstrated greater degradation of MO, suggesting that IrO_2 is critical for enhancing MO degradation. These results match well with previous studies in literature which showed that Ir/Ti anodes achieved better MO degradation than Ru/Ti anodes [44]. One suggestion to explain this trend is that Ir enables greater MO adsorption, leading to direct MO oxidation on the electrode [44]. It is worth mentioning that the molar oxygen percent (calculated from EDX analysis) in each

of the three electrodes is equal to or greater than twice the total molar percentage of the metals (Ti + Ru + Ir), as shown in Table S2.2. This indicates that the pristine electrodes used in these experiments contain a metal oxide layer. IrO_2-RuO_2 anode was determined to be the best anode to be used for the degradation of organic compounds in the mixed industrial wastewater as it showed the highest rate of MO degradation.

In order to determine the cost-effective cathode for organic molecule degradation, a stainless-steel cathode was compared to a graphite electrode for MO degradation experiments. As shown in Figure 2.3e, the electrochemical degradation using stainless-steel (cathode) and IrO_2-RuO_2 (anode) achieved 88 % MO decolorization efficiency within 5 min. The efficiency increased to 97% after 30 min. The MO removal efficiency during the first 5 min (88%) was slightly lower using a stainless-steel cathode as compared to the MO removal efficiency using a graphite cathode (90%), as shown in Figure 2.3d. However, the total MO removal efficiency when using either graphite or stainless-steel cathodes and an IrO_2-RuO_2 anode was the same after 30 min (97%). Cyclic voltammetry (CV) curves illustrate that the stainless-steel electrode showed the same faradic current as the graphite electrode when the same potential was applied, as shown in Figure 2.3g. However, the stainless-steel electrode showed a higher absolute capacitive current than the graphite electrode which suggests that the stainless-steel cathode exhibits higher ion adsorption efficiency than graphite. However, MO decolorization in the case of graphite was slightly greater in the first five min. This result further supports our suggestion that the dominant mechanism for MO degradation is ECO rather than electrochemical reduction, as a change in the efficiency of the cathode had no significant effect on MO degradation. However, stainless-steel was chosen to be used as the cathode for the industrial wastewater experiments, given the near-

identical MO removal efficiencies of the two cathodes, as well as the lower material cost of stainless-steel.

The effect of anode geometry was also investigated. A curved IrO_2-RuO_2 anode and stainless-steel cathode (Figure 2.3f) achieved greater MO removal efficiency than a flat IrO_2-RuO_2 anode and stainless-steel cathode (Figure 2.3e) (94 % vs. 88% MO removal efficiency, respectively) during the first 5 min. The greater available surface area for the curved electrode (1.5 times the area of the flat electrodes) allows greater MO oxidation on the electrode surface.

2.4.2 Electrochemical degradation of mixed industrial wastewater

We investigated the effectiveness of electrochemical treatment using mixed-metal oxide (MMO) anodes on a real mixed industrial wastewater. After identifying the best electrodes to degrade a model organic molecule, we performed electrochemical treatment of mixed industrial wastewater (termed “Sarnia samples”) collected from train tanker cars in Sarnia, Southwestern Ontario.

The wastewater samples were filtered through 30 µm membrane filters to simulate conventional sand filtration to remove any large residual particles. An analysis of the Total organic carbon (TOC) in the filtered samples established an average of 1651 ± 469 ppm, Table S2.3. Gas Chromatography-Mass Spectrometry (GC-MS) (Agilent 5973/6890) analysis was carried out on a filtered sample to survey its organic composition. The mixed industrial wastewater contains a complex mixture of many organic compounds, as shown in Table S2.4. Where, the most abundant compounds are 6-octadecenoic acid, palmitic acid, ethyl 4-ethoxybenzoate, fatty alcohols and alkanes. The probability of proper identification of the organic compounds by GC-MS varied widely across different compounds, as shown in Table S2.4. It was determined that detailed

analysis of the organic composition was not practically feasible. The filtered samples were then analyzed using ICP-OES and ICP-MS to determine the average metal content in the industrial wastewater (Sarnia samples). Among the heavy metals analyzed, the concentrations of Fe, Mn, and Mg were the highest in these samples, while a considerable amount of Al, As, Cr, Cu, Ni and Pb was also detected, and compared to their safe release levels to surface waters according to the Ontario guidelines, as shown in Table 2.1. Table S2.5 shows the detailed metal analysis for the filtered Sarnia samples. IC analysis was also carried out to analyze the anion concentration in the filtered Sarnia samples, where a significant amount of acetate, chloride, sulfate, and formate were found, as shown in Table S2.6.

Table 2.1: Average metal concentrations of 30 µm filtered Sarnia wastewater samples as compared to the Ontario Wastewater Discharge limits from Industrial Facilities

Metals	**Average Concentration measured in Sarnia Samples (ppm)**	**Ontario Wastewater Discharge Limits from Industrial Facilities (ppm) [6–9]**	**Sarnia Wastewater Discharge Limits from Industrial Facilities (ppm) [57]**
Fe	166.68 ± 152.51	50.0	50.0
Mn	18.59 ± 3.26	5.0	5.0
Mg	9.26 ± 2.84	N/A	N/A
As	1.14 ± 0.57	1.0	1.0
Al	0.34 ± 0.15	50.0	50.0
Ni	0.29 ± 0.08	2.0	3.0
Cu	0.054 ± 0.033	2.0	3.0
Cr	0.007 ± 0.004	5.0	3.0
Pb	0.0064 ± 0.0070	2.0	3.0
Cd	0.0023 ± 0.0016	0.02	1.0
Be	0.0012 ± 0.0019	N/A	N/A

Based on methyl orange (MO) degradation experiments, an IrO_2-RuO_2 anode and a stainless-steel cathode were selected for the Sarnia wastewater degradation experiments. IrO_2-RuO_2 showed the highest rate of degradation for MO, while stainless-steel and graphite electrodes did not show a significant difference for MO degradation, so the less expensive stainless-steel was selected. Electrochemical degradation tests were performed on one of the 30 µm filtered Sarnia wastewater samples (pH of 5 and conductivity of 2250 µS/cm) and 0.5 A (20 mA/cm^2) was applied to the anode (resulting in applied potential in between 3-10 V) which was kept 3.5 cm away from the cathode, as shown in Figure 2.4a. After 1-h electrolysis at room temperature, a significant froth layer was formed above the electrolyte surface as shown in Figure 2.4b. Over the course of the following 24 h after the experiment, the treated wastewater sample separated into a three-phase solution. The three-phase solution contained an upper froth layer containing mostly metals, a transparent bulk middle layer, and a bottom layer containing a dense sediment, as shown in Figure 2.4c. The electrochemical treatment of the Sarnia wastewater produced a treated water with significantly lower turbidity than the original wastewater, as observed in Figure 2.4

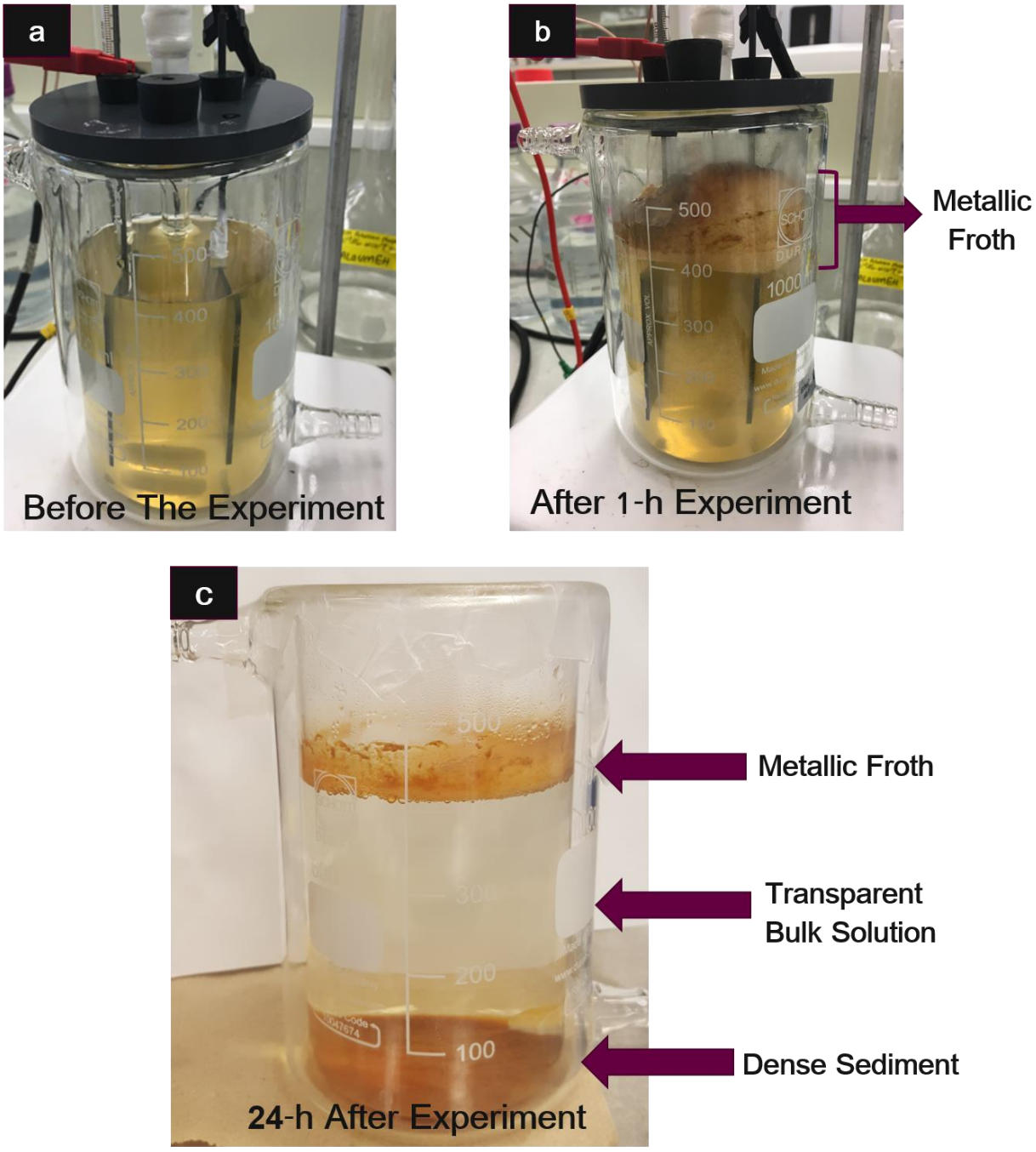

Figure 2.4: Electrochemical treatment of Sarnia wastewater under applied current of 0.5 A, 3.5 cm electrode gap and 1h contact time. The images show the electrochemically treated wastewater (a) before the experiment, (b) immediately after the 1-h experiment and (c) sitting undisturbed for 24-h after the completion of the 1-h experiment.

The treated Sarnia sample was analyzed for their particle size, organic carbon, and heavy metals content to determine the effect of electrochemical treatment time on a real industrial wastewater in comparison to a model solution of MO. The bulk solution, i.e. the yellow middle layer in Figure 2.4b, was analyzed every 10 min for all Sarnia samples treated by electrochemical degradation. Particle size was measured using dynamic light scattering (DLS), to elucidate the fate of the particles within the bulk solution. Figure 2.5 shows that the effective diameters of particles in solution increased over the course of the 1-h experiment, from 1 μm to 9 μm. We assume that the initial 1 μm-sized particles in solution are primarily organic colloids, since metallic colloids of this size would rapidly settle. The 9 μm-sized particles measured from the bulk solution after the 1-h experiment are likely iron hydroxide molecules that may contain flocculated heavy metals or organic compounds. The IrO_2-RuO_2 anodes readily produce hydroxyl radicals ($^{\bullet}OH$) and the cathode produces hydroxyl ions (OH^-) from water electrolysis. OH^- ions reacting with the large amount of dissolved Fe in solution produced iron hydroxide, which is a well-known coagulant. Previous studies have shown a similar order of magnitude for iron hydroxide particle size, where Fedorova et al. have shown iron hydroxide particle size of 10-56 μm for iron concentrations of 25-100 ppm at pH 4-6.2 [58]. Kenari et al. have shown iron hydroxide particle size of 3-8 μm for iron hydroxide concentrations of 5 ppm at pH 6-8 [59]. After 24 h-settling, the solution separated into three distinct phases.

The wastewater solutions were further analyzed 24 h after electrochemical treatment. DLS was used to measure the diameters of particles that remained within the transparent bulk solution, for wastewaters that were exposed to electrochemical treatment for different durations (5 – 60 min). These particles' sizes were compared to those in untreated samples. DLS indicated that the

effective average particle diameter in solution was smaller after 24 h of settling than immediately after treatment, for all solutions electrochemically treated for more than 5 min, as shown in Figure 2.5. The average particle diameter in electrochemically treated solutions was nearly uniformly 4 µm across all electrochemical treatment exposure times, suggesting that the larger colloids settled into the sediment, leaving colloidally stable 4 um particles in solution. Low electrochemical treatment time (5 min) was insufficient to cause coagulation, and therefore no settling of particles occurred.

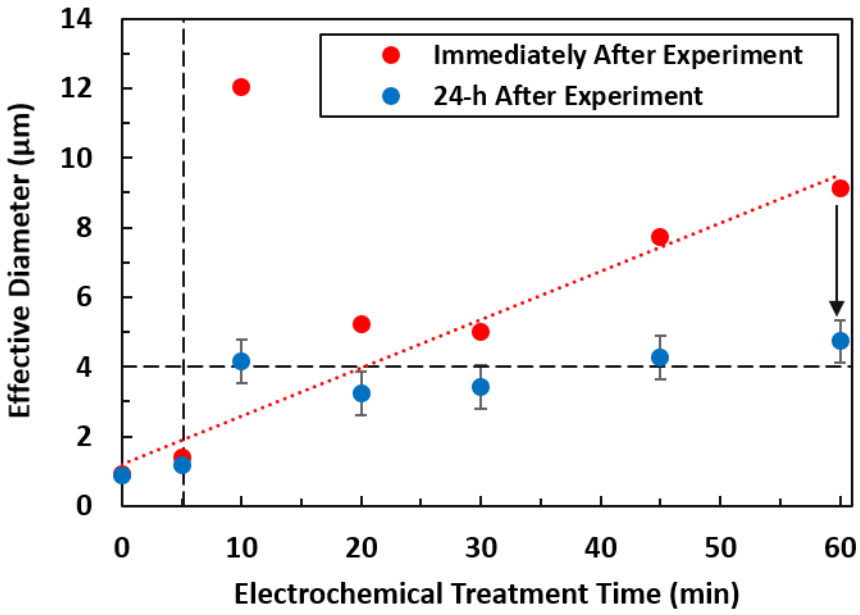

Figure 2.5: Effect of electrochemical treatment time on effective diameter of suspended particles in solution. Data points in red represent the particle sizes measured in the solutions immediately after the electrochemical treatment of a given duration, while data points in blue represent the average particle sizes in those solutions after 24 h of settling.

To determine the efficiency of electrochemical oxidation in-situ coagulation (ECO-IC) for heavy metal removal, samples from the transparent bulk treated solution were collected before and 1-day after the electrochemical treatment experiment and analyzed using ICP-OES and ICP-MS. The

post-treated samples were analyzed from the transparent bulk shown in Figure 2.4c. A significant decrease in heavy metals concentration in the wastewater samples was realized after the ECO-IC treatment, as shown in Figure 2.6. Fe showed the greatest change before and after electrochemical treatment decreasing by an order of magnitude from 190 ppm to 8 ppm as shown in Figure 2.6a. Mn and Mg decreased from 19 ppm to 10 ppm and from 12.5 ppm to 7 ppm, respectively, as shown in Figure 2.6a. The initial Fe and Mn concentrations exceeded the Ontario Wastewater Discharge Limits for Industrial Facilities, which are 50 ppm and 5 ppm (Table 2.1), respectively. After ECO-IC, the final concentration of Fe was below the discharge limits, while the Mn concentration approached the discharge limits. Of particular interest was the change in toxic heavy metal concentration including arsenic, nickel, lead and cadmium. As, Ni, Pb and Cd showed a significant decrease after the ECO-IC process, (As 1070 μg/L to 750 μg/L, Ni 240 μg/L to 150 μg/L, Pb 8 μg/L to 0.4 μg/L, Cd 5.5 μg/L to 0.65 μg/L), as detailed in Figure 2.6b and Figure 2.6c. Of note, the initial As concentration was higher than the Ontario Wastewater Discharge Limits for Industrial Facilities (1000 μg/L) and substantially higher than the Canadian water quality guideline arsenic limits (12.5 μg/L) and the Ontario drinking water quality Maximum Acceptable Concentration (MAC) of arsenic (10 μg/L). After ECO-IC treatment, the Sarnia wastewater was below the Ontario Wastewater Discharge Limits for Industrial Facilities based on its heavy metal concentration [60,61]. Despite being below wastewater discharge limits, the Cd and Pb concentrations in the initial Sarnia wastewater were above the Ontario drinking water MAC (Cd (5 μg/L), Pb (5 μg/L)) before treatment (Cd (5.5 μg/L), Pb (8 μg/L)) and below the MAC after electrochemical treatment (Cd (0.65 μg/L), Pb (0.4 μg/L)) [62,63].

The majority of the heavy metals in the Sarnia wastewater are likely to have been removed through coagulation, while a portion of these heavy metals are likely to have been removed from the wastewater by reduction on the stainless-steel cathode through electrodeposition. The significant decrease in iron concentration in comparison with other metals suggests that most of the iron is removed by coagulation and settling. It is well established that iron reacts with hydroxyl ions produced on the cathode surface from water electrolysis to produce iron hydroxide that can be removed from the solution by precipitation or flotation. Moreover, iron hydroxide is known to be an effective coagulant for removal of other metals. Thus, it is suggested that the dominant mechanism for heavy metal removal in our experiments was coagulation rather than electrodeposition. This suggestion is supported by the significant increase of particles size in the solution during the electrochemical treatment process as shown in Figure 2.5 and by the formation of a prominent metallic froth and a dense sediment layer after the electrochemical treatment, as shown in Figure 2.4b and Figure 2.4c.

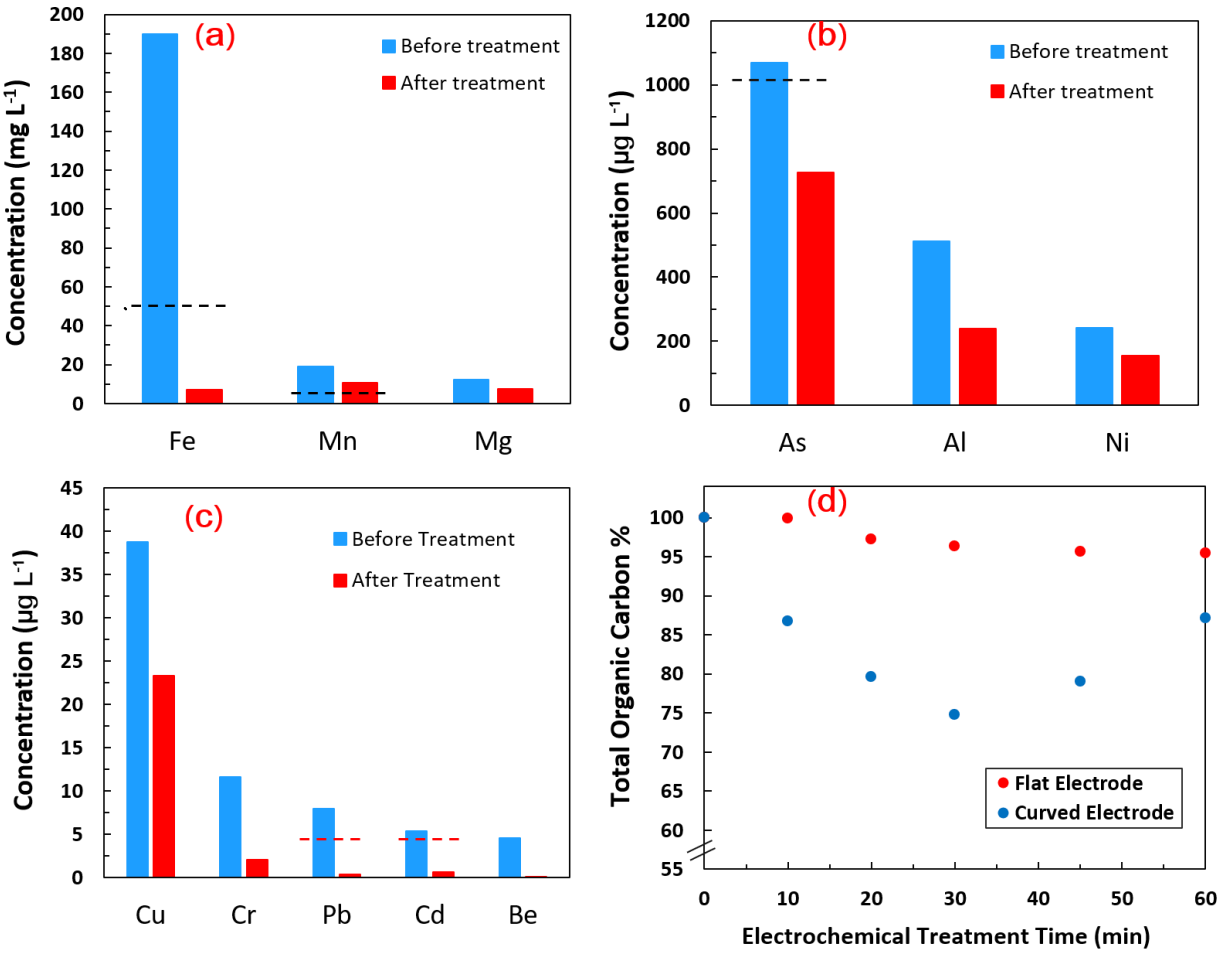

Figure 2.6: (a, b, c) Heavy metal removal and (d) TOC degradation in Sarnia wastewater during 1 h ECO-IC at 0.5 A applied current using IrO_2-RuO_2 anodes, black dashed lines represent Ontario Wastewater Discharge Limits from Industrial Facilities and red dashed lines represent Ontario drinking water MAC.

Total organic carbon (TOC) analysis of the Sarnia wastewater was conducted to measure changes in its organic content before and after electrochemical treatment. As shown in Figure 2.6d, in case of using flat IrO_2-RuO_2 anode, TOC decreased slightly over the 1-h treatment to a maximum of 4.5% reduction in TOC, and the rate of removal decreased exponentially, plateauing after 45 min. It is likely that complete mineralization for a small fraction of the organic molecules lead to the 4.5% reduction in bulk solution TOC, since no sediment was observed over the course of the experiment (Figure 2.4b). We suggest that electrochemically generated active chlorine caused

complete mineralization of some small organic molecules to CO_2. It is suggested that the electrochemical treatment produced active chlorine in the solution because the Sarnia wastewater contains significant amount of chloride (Table S2.6) and the ECO was carried out using active anodes (IrO_2-RuO_2 anode) which favors the production of active chlorine. Furthermore, the presence of dissolved iron in the solution favors the Electro-Fenton reaction which produces hydroxyl radicals ($^{\bullet}OH$). These active chlorine and hydroxyl radicals can lead to the complete mineralization of organic material, as discussed above. While TOC decreased over the course of the 1-h continuous electrochemical degradation, the overall reduction was small, 42.2 ppm decrease representing a 4.5% decrease from the initial TOC. We suggest three reasons for which TOC removal was limited: 1) low the treatment time, 2) limited available electrode surface area for organics oxidation, and 3) a chemical oxidation barrier arising from the limited amount of oxidizing agents (oxygen, hydroxyl radicals and active chlorine). Figure 2.6d shows that the decrease in TOC stabilized after 45 min, which indicates that the electrochemical oxidation of organic compounds in solution was not limited by the process time. GC-MS analysis (Table S2.4) suggested that the mixed organic content of the Sarnia wastewater predominantly contained large organic molecules (e.g. stearic acid, palmitic acid, ethyl 4-ethoxybenzoate). Complete mineralization of large organic molecules through electrochemical oxidation is much more challenging than that of small organic molecules (e.g. simple alkanes). Coupled with the limited amounts of oxidizing agents, this seems to be the most reasonable explanation for the low TOC removal. The solution was well-mixed throughout the experiment, thus small organic molecules were unlikely to be significantly impacted by mass transfer limitations. However, the oxidation pathways for large organic molecules are complicated, and their complete

mineralization requires direct and prolonged contact with the anodes. Electrode surface area may play a role in their extent of mineralization.

To assess the effect of available electrode's surface area on organic compounds degradation, curved anodes were used instead of flat anodes in the ECO-IC treatment process. A curved IrO_2-RuO_2 anode resulted in a 13 % decrease in TOC in a 1-h electrochemical treatment of the Sarnia wastewater sample at 0.5 A applied current and 3.5 cm electrode gap between the center of the curved anode and the stainless-steel counter electrode, Figure 2.6d. The curved electrode achieved nearly 3 times greater TOC removal than the flat IrO_2-RuO_2 anode under the same experimental conditions (Figure 2.6d). The curved electrode has a surface area of 84 cm^2 in comparison with the flat electrode which has a surface area of 56 cm^2, i.e. the surface area of the curved electrode is 1.5 times the area of the flat electrodes. The significant enhancement when using curved electrodes validates our suggestion that the electrochemical degradation of organic compounds was limited by available surface area for oxidation. Interestingly, TOC degradation of the MO model solution (50 ppm) only increased by a factor of 1.07 (from 88% to 94% TOC removal, Figure 2.3e and Figure 2.3f) in comparison with an increase of a factor of 3 (from 4.5% to 13% TOC removal Figure 2.6d) for mixed industrial wastewaters (average initial TOC concentration of 1650 ppm, Table S2.3) when the area of the electrodes was increased by a factor of 1.5. The degradation of a lower concentration model solution (i.e., 50 ppm MO) was not surface area-limited in contrast to the higher contaminated industrial wastewater (i.e., 1650 ppm average initial TOC concentration). The increase in TOC degradation was not linearly correlated with the increase in electrode surface area, where 1.5 times increase in electrode surface area resulted in 3 times greater TOC reduction. These results indicate that other factors other than

the increase in surface area contributed to TOC degradation when using curved electrodes in comparison to flat electrodes. The decrease in electrode gap (between the anode and cathode) due to the increase in the curvature of the anode might have participated in the enhancement of TOC degradation. Previous studies have shown an enhancement in electrochemical oxidation of organic contaminants when decreasing the electrode gap due to the decrease in solution resistance between the electrodes, enhancement in the mass transfer process and the increase in overall oxidation rate [64,65].

The wastewater TOC was also analyzed 24 h after electrochemical treatment with the curved electrodes for different durations (from 5 – 60 min) and compared to the TOC in untreated samples. TOC concentrations do not decrease after 24 h of settling for any of the electrochemically treated solutions treated from 5 – 60 min, as shown in Figure S2.1. This result further supports the suggestion that the decrease in TOC in solution is due to mineralization of organic molecules to inorganic carbon (e.g. CO_2) by ECO rather than removal by the in-situ formed coagulants in solution.

ECO-IC was shown to be effective in substantially reducing the turbidity and heavy metal concentration of real mixed industrial waste waters. The reduction in Fe, Mn, As, and Pb concentrations are a particular benefit. Of note, the three-phase solution can be easily separated in industrial processes by skimming the froth layer and by removing the sediment by gravity settling. Further, the significant increase in average effective diameter of suspended particles in the bulk liquid would enable the further treatment of the wastewater by simple sand or membrane filtration. This proof-of-concept study on real wastewaters suggests that this one-step electrochemical degradation process shows promise as a pre-treatment for complicated and

difficult to treat mixed industrial wastewaters. However, this process is limited in its ability to treat many of the organic molecules present in the wastewaters or to fully remove the high concentration of arsenic present within these samples. The low organics removal efficiency in this mixed industrial wastewater in comparison with the high degradation of MO in the model solutions indicated that degradation of mixed industrial wastewater in practice is more challenging than model solutions prepared in laboratories, and that simple single molecule degradation studies poorly predicts performance in real wastewaters.

2.5 Conclusions

This study investigated the feasibility of combining electrochemical oxidation and in-situ coagulation for treating mixed industrial wastewater containing mixed organic compounds and high concentrations of heavy metals. Electrochemical degradation experiments of methyl orange (MO) solutions identified IrO_2-RuO_2 mixed metal oxide anodes as the best electrodes for organic compound degradation. Stainless-steel and graphite counter electrodes (cathodes) did not show a major difference for MO degradation. Electrochemical degradation was subsequently tested on a real industrial wastewater collected from the steam-cleaning of train tanker cars used to transport industrial solvents. These treatment experiments resulted in a treated solution with a lower organic content, substantially lower heavy metal content, greater effective diameter of the suspended particles, and distinct phases that can be separated for further treatment. It is suggested that the anodic electrochemical oxidation was the dominant mechanism for degrading organic compounds in the solution. However, the electrochemical oxidation was limited by the electrode surface area. Curved electrodes with higher surface area demonstrated an increase in organic compound degradation efficiency. The dominant mechanism for heavy metal removal

from the solution is believed to be coagulation of the heavy metals with the in-situ electrolysis-formed iron hydroxide. Future research will focus on optimizing the removal of Arsenic, quantifying the effect of surface area on the rate of organic compound degradation and combining the electrochemical treatment process with conventional treatment methods (e.g. membranes) to achieve more efficient treatment of industrial wastewater.

2.6 Acknowledgement

This work was funded by the Southern Ontario Water Consortium (SOWC) in partnership with P.W. Custom Fabrications, Canada. We thank Matt Yagar and George Foss for supplying the wastewater samples and for their initial advice on the direction of the project. The authors also acknowledge the Electron Microscopy Facility in the Health Science Centre at McMaster University for the EDX spectroscopy facility and the Canadian Centre for Electron Microscopy (CCEM) for the SEM facility.

2.7 References

[1] L.G. Torres, J. Jaimes, P. Mijaylova, E. Ramírez, B. Jiménez, Coagulation-flocculation pretreatment of high-load chemical-pharmaceutical industry wastewater: Mixing aspects, Water Sci. Technol. 36 (1997) 255–262. doi:10.1016/S0273-1223(97)00395-8.

[2] F.A. Nasr, H.S. Doma, H.S. Abdel-Halim, S.A. El-Shafai, Chemical industry wastewater treatment, Environmentalist. 27 (2007) 275–286. doi:10.1007/s10669-007-9004-0.

[3] A. Asatekin, A.M. Mayes, Oil industry wastewater treatment with fouling resistant membranes containing amphiphilic comb copolymers, Environ. Sci. Technol. 43 (2009) 4487–4492. doi:10.1021/es803677k.

[4] A. Sonune, R. Ghate, Developments in wastewater treatment methods, Desalination. 167 (2004) 55–63.

[5] A.. Patwardhan, Industrial Wastewater Treatment 2nd edition, PHI Learning, 2017.

[6] Canada Institute for Environmental Law and Policy, Spotlight on sustainability: managing sources of municipal wastewater, 2004.

[7] City of Ottawa, Sewer use program-Guide for discharging wastewater from industrial facilities, 2011.

[8] City of Hamilton, By-Law No. 14-090, 2014.

[9] City of Tronoto, Toronto municipal code chapter 681, sewers, 2019.
[10] H. Lin, W. Gao, F. Meng, B.Q. Liao, K.T. Leung, L. Zhao, J. Chen, H. Hong, Membrane bioreactors for industrial wastewater treatment: A critical review, Crit. Rev. Environ. Sci. Technol. 42 (2012) 677–740. doi:10.1080/10643389.2010.526494.
[11] K. Hayat, S. Menhas, J. Bundschuh, H.J. Chaudhary, Microbial biotechnology as an emerging industrial wastewater treatment process for arsenic mitigationA critical review, J. Clean. Prod. 151 (2017) 427–438. doi:10.1016/j.jclepro.2017.03.084.
[12] Woodard & Curran. Inc, Industrial Waste Treatment Handbook, 2005. doi:10.1016/s0304-3894(01)00391-0.
[13] B. Wang, W. Kong, H. Ma, Electrochemical treatment of paper mill wastewater using three-dimensional electrodes with Ti/Co/SnO2-Sb2O5 anode, J. Hazard. Mater. 146 (2007) 295–301. doi:10.1016/j.jhazmat.2006.12.031.
[14] L.C. Chiang, J.E. Chang, T.C. Wen, Indirect oxidation effect in electrochemical oxidation treatment of landfill leachate, Water Res. 29 (1995) 671–678. doi:10.1016/0043-1354(94)00146-X.
[15] R.M. Sterritt, J.N. Lester, Interactions of heavy metals with bacteria, Sci. Total Environ. 14 (1980) 5–17.
[16] C.F. Carolin, P.S. Kumar, A. Saravanan, G.J. Joshiba, M. Naushad, Efficient techniques for the removal of toxic heavy metals from aquatic environment: A review, J. Environ. Chem. Eng. 5 (2017) 2782–2799. doi:10.1016/j.jece.2017.05.029.
[17] F. Fu, Q. Wang, Removal of heavy metal ions from wastewaters: A review, J. Environ. Manage. 92 (2011) 407–418. doi:10.1016/j.jenvman.2010.11.011.
[18] G.K. Kinuthia, V. Ngure, D. Beti, R. Lugalia, A. Wangila, L. Kamau, Levels of heavy metals in wastewater and soil samples from open drainage channels in Nairobi, Kenya: community health implication, Sci. Rep. 10 (2020) 1–13. doi:10.1038/s41598-020-65359-5.
[19] P. Drogui, J.-F. Blais, G. Mercier, Review of Electrochemical Technologies for Environmental Applications, Recent Patents Eng. 1 (2008) 257–272. doi:10.2174/187221207782411629.
[20] Y. Feng, L. Yang, J. Liu, B.E. Logan, Electrochemical technologies for wastewater treatment and resource reclamation, Environ. Sci. Water Res. Technol. 2 (2016) 800–831. doi:10.1039/c5ew00289c.
[21] M.A. Ganzoury, C. Chidiac, J. Kurtz, C.-F. de Lannoy, CNT-sorbents for heavy metals: Electrochemical regeneration and closed-loop recycling, J. Hazard. Mater. 393 (2020). doi:10.1016/j.jhazmat.2020.122432.
[22] N. Zhang, M.A. Halali, C.F. de Lannoy, Detection of fouling on electrically conductive membranes by electrical impedance spectroscopy, Sep. Purif. Technol. 242 (2020) 116823. doi:10.1016/j.seppur.2020.116823.
[23] M. Kobya, E. Demirbas, A. Dedeli, M.T. Sensoy, Treatment of rinse water from zinc phosphate coating by batch and continuous electrocoagulation processes, J. Hazard. Mater. 173 (2010) 326–334. doi:10.1016/j.jhazmat.2009.08.092.
[24] S. Zhao, G. Huang, G. Cheng, Y. Wang, H. Fu, Hardness, COD and turbidity removals from produced water by electrocoagulation pretreatment prior to reverse osmosis membranes, Desalination. 344 (2014) 454–462. doi:10.1016/j.desal.2014.04.014.

[25] H.I. Maarof, W.M.A.W. Daud, M.K.D. Aroua, Recent trends in removal and recovery of heavy metals from wastewater by electrochemical technologies, Rev. Chem. Eng. 33 (2017) 359–386. doi:10.1515/revce-2016-0021.
[26] K. Thella, B. Verma, V.C. Srivastava, K.K. Srivastava, Electrocoagulation study for the removal of arsenic and chromium from aqueous solution, J. Environ. Sci. Heal. - Part A Toxic/Hazardous Subst. Environ. Eng. 43 (2008) 554–562. doi:10.1080/10934520701796630.
[27] I. Kabdaşli, T. Arslan, T. Ölmez-Hanci, I. Arslan-Alaton, O. Tünay, Complexing agent and heavy metal removals from metal plating effluent by electrocoagulation with stainless steel electrodes, J. Hazard. Mater. 165 (2009) 838–845. doi:10.1016/j.jhazmat.2008.10.065.
[28] K.S. Hashim, A. Shaw, R. Al Khaddar, M.O. Pedrola, D. Phipps, Iron removal, energy consumption and operating cost of electrocoagulation of drinking water using a new flow column reactor, J. Environ. Manage. 189 (2017) 98–108. doi:10.1016/j.jenvman.2016.12.035.
[29] P.K. Holt, G.W. Barton, C.A. Mitchell, The future for electrocoagulation as a localised water treatment technology, Chemosphere. 59 (2005) 355–367. doi:10.1016/j.chemosphere.2004.10.023.
[30] J.A.G. Gomes, P. Daida, M. Kesmez, M. Weir, H. Moreno, J.R. Parga, G. Irwin, H. McWhinney, T. Grady, E. Peterson, D.L. Cocke, Arsenic removal by electrocoagulation using combined Al-Fe electrode system and characterization of products, J. Hazard. Mater. 139 (2007) 220–231. doi:10.1016/j.jhazmat.2005.11.108.
[31] A. Shafaei, M. Rezayee, M. Arami, M. Nikazar, Removal of Mn2+ ions from synthetic wastewater by electrocoagulation process, Desalination. 260 (2010) 23–28. doi:10.1016/j.desal.2010.05.006.
[32] C. Barrera-Díaz, B. Frontana-Uribe, B. Bilyeu, Removal of organic pollutants in industrial wastewater with an integrated system of copper electrocoagulation and electrogenerated H2O2, Chemosphere. 105 (2014) 160–164. doi:10.1016/j.chemosphere.2014.01.026.
[33] H. Yang, J. Liang, L. Zhang, Z. Liang, Electrochemical oxidation degradation of methyl orange wastewater by Nb/PbO2 electrode, Int. J. Electrochem. Sci. 11 (2016) 1121–1134.
[34] L. Yu, M. Han, F. He, A review of treating oily wastewater, Arab. J. Chem. 10 (2017) S1913–S1922. doi:10.1016/j.arabjc.2013.07.020.
[35] Y. Kong, Z.L. Wang, Y. Wang, J. Yuan, Z.D. Chen, Degradation of methyl orange in artificial wastewater through electrochemical oxidation using exfoliated graphite electrode, Xinxing Tan Cailiao/New Carbon Mater. 26 (2011) 459–464. doi:10.1016/S1872-5805(11)60092-9.
[36] F. Sopaj, M.A. Rodrigo, N. Oturan, F.I. Podvorica, J. Pinson, M.A. Oturan, Influence of the anode materials on the electrochemical oxidation efficiency. Application to oxidative degradation of the pharmaceutical amoxicillin, Chem. Eng. J. 262 (2015) 286–294. doi:10.1016/j.cej.2014.09.100.
[37] G. Wang, Y. Liu, J. Ye, Z. Lin, X. Yang, Electrochemical oxidation of methyl orange by a Magnéli phase Ti4O7 anode, Chemosphere. 241 (2020) 125084. doi:10.1016/j.chemosphere.2019.125084.

[38] W.G. Dahli, W.S. Pladson, Railcar Cleaning Method And Apparatus, US 6,523,221 B1, 2003.
[39] B. Jansen, C. Nath, Method And Apparatus For Cleaning Railroad Tank Cars, US 9 , 737 , 918 B2, 2017.
[40] N. El Azher, B. Gourich, C. Vial, M.B. Soulami, M. Ziyad, Study of ferrous iron oxidation in Morocco drinking water in an airlift reactor, Chem. Eng. Process. Process Intensif. 47 (2008) 1877–1886. doi:10.1016/j.cep.2007.10.013.
[41] R.H. Liu, G.P. Sheng, M. Sun, G.L. Zang, W.W. Li, Z.H. Tong, F. Dong, M. Hon-Wah Lam, H.Q. Yu, Enhanced reductive degradation of methyl orange in a microbial fuel cell through cathode modification with redox mediators, Appl. Microbiol. Biotechnol. 89 (2011) 201–208. doi:10.1007/s00253-010-2875-x.
[42] Y. Zhao, J. Chu, S.H. Li, Y. Chen, G.P. Sheng, Y.P. Chen, W.W. Li, G. Liu, Y.C. Tian, Y. Xiong, H.Q. Yu, Preparation of Pt-Fe2O3 nano-electrode array on gold nano-wires and its application to the catalytic degradation of methyl orange, Chem. Eng. J. 170 (2011) 440–444. doi:10.1016/j.cej.2010.11.104.
[43] W. Duan, G. Chen, C. Chen, R. Sanghvi, A. Iddya, S. Walker, H. Liu, A. Ronen, D. Jassby, Electrochemical removal of hexavalent chromium using electrically conducting carbon nanotube/polymer composite ultrafiltration membranes, J. Memb. Sci. 531 (2017) 160–171. doi:10.1016/j.memsci.2017.02.050.
[44] E. Isarain-Chávez, M.D. Baró, E. Rossinyol, U. Morales-Ortiz, J. Sort, E. Brillas, E. Pellicer, Comparative electrochemical oxidation of methyl orange azo dye using Ti/Ir-Pb, Ti/Ir-Sn, Ti/Ru-Pb, Ti/Pt-Pd and Ti/RuO2 anodes, Electrochim. Acta. 244 (2017) 199–208. doi:10.1016/j.electacta.2017.05.101.
[45] B.S. Rathi, P.S. Kumar, R. Ponprasath, K. Rohan, N. Jahnavi, An effective separation of toxic arsenic from aquatic environment using electrochemical ion exchange process, J. Hazard. Mater. 412 (2021) 125240. doi:10.1016/j.jhazmat.2021.125240.
[46] B. Adams, M. Tian, A. Chen, Design and electrochemical study of SnO2-based mixed oxide electrodes, Electrochim. Acta. 54 (2009) 1491–1498. doi:10.1016/j.electacta.2008.09.034.
[47] H. Kong, H. Lu, W. Zhang, H. Lin, W. Huang, Performance characterization of Ti substrate lead dioxide electrode with different solid solution interlayers, J. Mater. Sci. 47 (2012) 6709–6715. doi:10.1007/s10853-012-6613-x.
[48] X. He, Z. Chai, F. Li, C. Zhang, D. Li, J. Li, J. Hu, Advanced treatment of biologically pretreated coking wastewater by electrochemical oxidation using Ti/RuO2 – IrO 2 electrodes, J Chem Technol Biotechnol. 88 (2013) 1568–1575. doi:10.1002/jctb.4006.
[49] J. Li, Z. Yang, H. Xu, P. Song, J. Huang, R. Xu, Y. Zhang, Y. Zhou, Electrochemical treatment of mature landfill leachate using Ti/RuO2-IrO2 and Al electrode: Optimization and mechanism Article, RSC Adv. 6 (2016) 47509–47519. doi:10.1039/C6RA05080H.
[50] F.C. Moreira, R.A.R. Boaventura, E. Brillas, V.J.P. Vilar, Electrochemical advanced oxidation processes: A review on their application to synthetic and real wastewaters, Appl. Catal. B Environ. 202 (2017) 217–261. doi:10.1016/j.apcatb.2016.08.037.
[51] M. Rueffer, D. Bejan, N.J. Bunce, Graphite: An active or an inactive anode?, Electrochim. Acta. 56 (2011) 2246–2253. doi:10.1016/j.electacta.2010.11.071.
[52] A.N. Subba Rao, V.T. Venkatarangaiah, Metal oxide-coated anodes in wastewater

treatment, Environ. Sci. Pollut. Res. 21 (2014) 3197–3217. doi:10.1007/s11356-013-2313-6.
[53] M. Panizza, G. Cerisola, Direct and mediated anodic oxidation of organic pollutants, Chem. Rev. 109 (2009) 6541–6569. doi:10.1021/cr9001319.
[54] E. Brillas, C.A. Martínez-Huitle, Decontamination of wastewaters containing synthetic organic dyes by electrochemical methods. An updated review, Appl. Catal. B Environ. 166–167 (2015) 603–643. doi:10.1016/j.apcatb.2014.11.016.
[55] M. Zhou, H. Särkkä, M. Sillanpää, A comparative experimental study on methyl orange degradation by electrochemical oxidation on BDD and MMO electrodes, Sep. Purif. Technol. 78 (2011) 290–297. doi:10.1016/j.seppur.2011.02.013.
[56] Y. Mu, K. Rabaey, R.A. Rozendal, Z. Yuan, J. Keller, Decolorization of azo dyes in bioelectrochemical systems, Environ. Sci. Technol. 43 (2009) 5137–5143. doi:10.1021/es900057f.
[57] City of Sarnia, By-law number of 2021 of the city of Sarnia “Sewer use by-law,” 2021.
[58] A.S. Fedorova, T.A. Nedobukh, M.A. Mashkovtsev, V.S. Semenishchev, The study of processes of iron hydroxide coagulation and sedimentation, AIP Conf. Proc. 1886 (2017). doi:10.1063/1.5002928.
[59] S.L. Dashtban Kenari, B. Barbeau, Size and Zeta Potential of Oxidized Iron and Manganese in Water Treatment: Influence of pH, Ionic Strength, and Hardness, J. Environ. Eng. 142 (2016) 1–9. doi:10.1061/(ASCE)EE.1943-7870.0001101.
[60] Canadian council of ministers of the environment, Canadian water quality guidelines for the protection of aquaticl Life -arsenic, (2001).
[61] Federal-Provincial-Territorial committee on drinking water, Guidelines for Canadian drinking water quality : guideline technical document (arsenic), 2006.
[62] Federal-Provincial-Territorial committee on drinking water, Lead in drinking water, 2017.
[63] Government of Ontario, Safe drinking water act, Ontario Regulation 169/03, 2002.
[64] R. Xie, X. Meng, P. Sun, J. Niu, W. Jiang, Electrochemical oxidation of ofloxacin using a TiO 2 -based SnO2-Sb/polytetrafluoroethylene resin-PbO2 electrode: Reaction kinetics and mass transfer impact, "Applied Catal. B, Environ. 203 (2017) 515–525. doi:10.1016/j.apcatb.2016.10.057.
[65] M. Chen, C. Wang, Y. Wang, X. Meng, Z. Chen, W. Zhang, G. Tan, Kinetic, mechanism and mass transfer impact on electrochemical oxidation of MIT using Ti-enhanced nanotube arrays/ SnO2-Sb anode, Electrochim. Acta. 323 (2019) 134779. doi:10.1016/j.electacta.2019.134779.

Chapter 3

CNT-sorbents for heavy metals: Electrochemical regeneration and closed-loop recycling

Reprinted From MA Ganzoury, C Chidiac, J Kurtz, CF de Lannoy. CNT-sorbents for heavy metals: Electrochemical regeneration and closed-loop recycling. J. Hazard. Mater, 2020, 393. Copyright (2020), with permission from Elsevier.

3.1 Abstract

Heavy metal contamination of aquatic environments is a major concern. Carbon nanotubes (CNTs) are among the most effective adsorbents for heavy metal removal. However, their high cost and their uncertain environmental impact necessitates a closed-loop process through sorbent regeneration and recycling for practical application. Our work demonstrates heavy metal adsorption by carboxylic acid-functionalized single-walled/double-walled carbon nanotubes (f-SW/DWCNTs) and their regeneration using electric fields. We follow a multi-step process: 1) copper in an aqueous solution is adsorbed onto the surface of f-SW/DWCNTs, 2) the copper-saturated f-SW/DWCNTs are filtered onto a microfiltration (MF) membrane, 3) the f-SW/DWCNT coated membrane is used as an anode in an electrochemical cell, 4) an applied electric field desorbs the metals from the CNTs into a concentrated waste, and 5) the CNTs are separated from the membrane, re-dispersed and reused in copper-contaminated water for successive adsorption. With an applied positive electric potential, we achieved ~90% desorption of Cu from f-SW/DWCNTs. We hypothesize that the electric field generated at the anode causes electrostatic repulsion between the anode and the electrostatically adsorbed heavy metal ions. The effect of applied voltages, electrode spacing and electrolyte conductivity on the desorption of Cu from CNTs was also investigated.

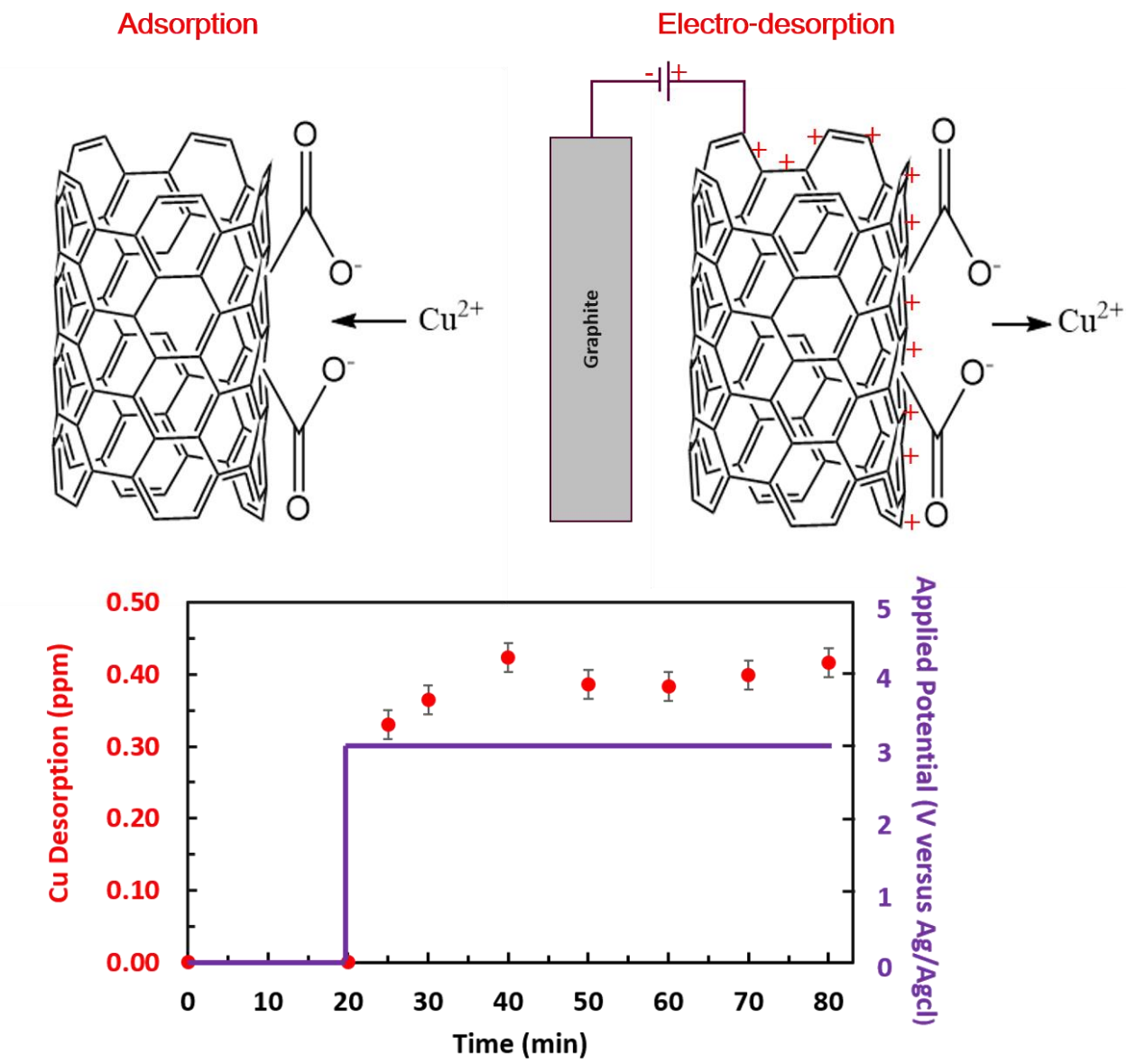

3.2 Introduction

Heavy metals impose severe health hazards to humans, animals and aquatic life [1,2]. Environmental exposure to anthropogenic sources of heavy metals arises from their wide use within metal plating, pesticides, battery technologies and within the pulp and paper industry [3,4]. Heavy metals are discharged from manufactured products into wastewater at all stages of their life cycle from cradle to grave [5]. Discharge occurs at metal extraction, product

manufacturing, use and disposal [6]. Some of these heavy metals are discharged directly into soils, or partition to the solids in wastewater treatment and are applied to soils. In either case, heavy metals accumulated in soils may eventually leach into ground water reservoirs [7]. Heavy metals may also enter drinking water from the piping and solder used in municipal drinking water distribution systems [8]. Natural sources of heavy metals can contaminate water reservoirs through geogenic effects such as natural mineral dissolution [8,9]. Heavy metals of concern include arsenic, zinc, copper, cadmium, chromium, lead and mercury [10,11].The necessity of their removal from sources of water stems from their toxicity, non-biodegradability and their bioaccumulation [12]. Thus, there is a present societal need to find effective techniques for the removal of toxic heavy metals from aqueous systems.

Cu is one of the most abundant heavy metals in wastewater as it is widely used in many industries such as electroplating, etching and metal finishing [13]. Further, Cu is released into drinking water during the corrosion of drinking water piping and fittings [14]. Cu in drinking water can have severe consequences as it is considered a toxic metal at concentrations > 2 ppm [13]. Excessive Cu ingestion can cause acute symptoms such as vomiting and chronic exposure can lead to increased blood pressure, and kidney and liver damage [10,14]. Further, Cu is an ideal model for other heavy metal contaminants. Cu has the same divalent charge as several other common toxic heavy metals including zinc, cadmium, mercury and lead. It's ionic radius is 71 pm which is similar to the ionic radii of nickel (72 pm), chromium (69 pm) and zinc (74 pm) [15,16]. And the in fresh water, Cu predominantly speciates into copper carbonate ($CuCO_3$) and copper hydroxide ($Cu(OH)_2$), which resemble the dominant speciation of other heavy metals in fresh water such as lead carbonate ($PbCO_3$), cadmium carbonate ($CdCO_3$), zinc carbonate ($ZnCO_3$) and

zinc hydroxide ($Zn(OH)_2$) [17,18]. However, Cu is substantially less toxic than other heavy metals such as lead and mercury, enabling safer handling in the laboratory with fewer safety restrictions [1]. All considered, we chose Cu as representative model for heavy metals in this study.

In recent years, researchers have identified adsorption as one of the most promising techniques for the removal of heavy metals from water [14,19]. Adsorption is easily operated in comparison with other technologies such as ion exchange and membrane filtration [1,10]. Adsorption is also considered more cost efficient than flotation which requires high initial cost [1]. The efficiency of various adsorbents for use in the water industry has been extensively studied , i.e. zeolites [20], polymers [21], biomaterials (e.g. biochars, bacteria, algae, fungi and crab shells) [22–24], metal organics framework (MOFs) [2], covalent organics framework (COFs) [25] and carbonaceous materials (e.g. activated carbon, carbon nanomaterials) [26]. The nano-structured materials that have been studied have orders of magnitude greater adsorptive capacity than other adsorbents, owing to their high surface area to volume ratio and high chemical reactivity [27,28]. Carbon nanotubes (CNTs) possess high electrical conductivity, high thermal and chemical stabilities and excellent mechanical properties [29,30] which have enabled them to be used in several environmental applications such as antifouling membranes [31,32], chemical sensors [33], catalyst supports [34,35] and adsorbents for removing contaminants from water [36,37]. Specifically, researchers have focused on the use CNTs as a promising heavy metals adsorbent due to its high porosity, chemical stability and high specific surface area [38]. CNTs can also be chemically functionalized with various chemical moieties, which enhances their adsorption capacity to heavy metals [10,14,39]. However, although CNTs show promise for their treatment

abilities, their use in industry is ultimately hindered by their high cost as well as concerns for their environmental impacts [26,40].

The high cost and some concerns arising from their environmental implications necessitates the development of CNT recycling approaches if they are to be used as adsorbents for heavy metals from water. Acid regeneration of heavy metal-saturated CNTs has been studied as a method to enable their reuse in successive adsorption cycles [10]. For example, Lu et al. showed that exposing Zn-saturated CNTs to nitric acid in a solution with pH 1 achieved a 90% CNT regeneration efficiency [41]. Similarly, Wang et al. studied the desorption of Pb from CNTs using nitric acid in a solution with pH 2, attaining 85% regeneration efficiency [42]. Despite the effectiveness of acid regeneration for CNT reuse, the product stream is a concentrated acid solution containing heavy metals, which will ultimately yield further environmental disposal challenges if employed on a large-scale[43].

Electrochemical techniques have been studied as a sustainable alternative for the regeneration of heavy metal-saturated CNTs. Most of the electrochemical regeneration studies in literature have investigated the adsorption and desorption of heavy metals from CNTs when formed into solid electrodes [15,44–46]. In this setup, adsorption is accomplished by applying a negative potential to the CNT electrode as this allows for electrostatic attraction of heavy metals in solution to the CNTs. The CNT electrode is then regenerated by reversing the applied potential, which in turn causes repulsion of the adsorbed heavy metals from the CNT-electrode surface. This technique has shown promise in metal adsorption and desorption, but several limitations are inherent in the system. For instance, CNTs must be fabricated into electrodes, which requires either stable coatings or growing CNTs on a suitable substrate [44,46]. Metal solutions must be

convected near and/or through the electrode to increase the likelihood of heavy metal adsorption onto the electrode, which requires pumping power and additional engineering design considerations. Moreover, mass transfer limitations within the bulk of the solid electrode limit the efficiency of CNT adsorption. Finally, such a process requires an applied voltage for both adsorption and desorption. In an attempt to mitigate power requirements, Li et al. studied the adsorption of iron on Carbon nanotube-Carbon nanofiber (CNT-CNF) films grown on nickel sheets followed by electrodesorption to regenerate the CNT-CNF adsorbent [47]. This process successfully eliminates power requirements in the adsorption step, however a CNT electrode must still be fabricated and mass transfer limitations during adsorption still exist. Thus, there is still a present need to find an efficient method to employ adsorption and electrodesorption for the removal of heavy metals.

In this study, we combine conventional metal adsorption with an electrode-enabled electrodesorption process in the interest of creating a flexible design that will allow for environmentally benign CNT regeneration. Specifically, well dispersed f-SW/DWCNTs were used to adsorb Cu^{2+} from a $CuSO_4$ solution. After adsorption, the CNTs in solution were filtered onto a microfiltration (MF) membrane. The deposited CNTs formed a temporary electrode, which was charged with a positive potential to desorb the heavy metals concentrating heavy metal in a waste solution, while regenerating the CNTs. The f-SW/DWCNTs were subsequently re-dispersed in a new copper-contaminated solution by mechanically agitating the membrane, thus allowing for successive cycles of adsorption, membrane filtration, electro-regeneration, and f-SW/DWCNTs redispersion. Overall, this process combines adsorption with an environmentally low-impact heavy metal desorption, creating a comparatively greener process for the closed-loop

adsorption of heavy metals by highly efficient CNT adsorbents. In this study, the impact of applied potential, electrolyte conductivity, and electrode spacing on the electro-desorption of Cu from f-SW/DWCNTs was investigated. In addition, the kinetics of desorption and feasibility of f-SW/DWCNTs regeneration was studied.

3.3 Materials and Methods

3.3.1 Materials

f-SW/DWCNTs (functional content 2.73 W %, purity >90 W%, length 5-30 µm and outer diameter 1-4 nm) were purchased from Cheap-Tubes USA. They were either used without further modification or washed for 4 h in 38% (w/w) hydrochloric acid purchased from Anachemia Canada, then rinsed with DI water until a suspension of CNTs had a pH >6. The acid washed f-SW/DWCNTs will be referred to as "HCl treated f-SW/DWCNTs". MF polyethersulfone (PES) membranes (0.2 µm) were purchased from Sterlitech USA. Sodium diethyldithiocarbamate (Na-DDTC) and $CuSO_4.5H_2O$ were purchased from Fisher Scientific USA and Canada, respectively. Ethylenediaminetetraacetic acid (EDTA), tribasic ammonium citrate and NH_4Cl were purchased from Sigma Alderich Canada. Ammonia solution was purchased form EMD Millipore USA.

3.3.2 Adsorption Experiments

5 mg of f-SW/DWCNTs were sonicated in DI water at various times using a probe sonicator (Qsonica Q500) to create a stable CNT suspension. Subsequently, the f-SW/DWCNTs solution was added to $CuSO_4.5H_2O$ solution such that the final Cu^{2+} concentration was 6 ppm, the final volume was 100 mL. The pH was maintained at 6 (original pH of $CuSO_4.5H_2O$ solution) during all the adsorption experiments for two reasons (1) to avoid $Cu(OH)_2$ precipitation at pH >6.5 [48,49] and

(2) to develop non-chemical, and thereby environmentally friendly, methods for removing Cu from aqueous systems. The Cu-CNT solution was then stirred at 300 RPM for various times to allow for the adsorption of Cu onto the f-SW/DWCNT. Once the adsorption experiments were complete, the solution was filtered on a 0.2 µm MF membrane to separate the treated solution from the Cu-CNT complex, as is shown in Figure 3.1 steps 1-2.

3.3.3 Electrodesorption Experiments

As represented in Figure 3.1 step 2, upon adsorption of copper ions (Cu^{2+}) from solution, the Cu-CNT complexes were pressure-deposited onto a MF membrane. After Cu^{2+} adsorption and subsequent removal from solution, the aim was to release Cu^{2+} ions into a concentrated waste solution while regenerating CNTs. Regenerated CNTs could then be reused to continue to remove Cu^{2+} from other contaminated water sources. The Cu-CNT composite on the MF membrane was then used as an anode in an electrochemical cell (Figure 3.1, step 3) in the interest of carrying out electro-desorption and CNT regeneration. The Cu-CNT composite MF membrane anode will be referred to as "f-SW/DWCNTs membrane Electrode" from hereon. Within this electrochemical cell, a graphite plate was used as the cathode, Ag/AgCl was used as the reference electrode and the electrolyte was a 1 M NaCl solution in DI water (300 mL) at neutral pH. The electrochemical cell inner diameter was 6 cm, and the electrolyte solution was stirred at 200 RPM to ensure uniform mixing. The electrochemical cell was connected to a potentiostat (Multi Autolab/M101) for detailed investigation of the electrochemical separation of Cu from f-SW/DWCNTs. Within step 3, we investigated the effect of applied voltage, electrodesorption time, and electrode spacing by varying the distance between the f-SW/DWCNT membrane anode and the graphite

cathode on CNT regeneration. Wherein, Table 3.1 shows the electrodesorption experimental parameters studied.

Table 3.1: Electrodesorption experiments parameters

Experiment	Applied potential (V vs Ag/AgCl)	Electrolyte Conductivity (µS/cm)	Electrode gap (cm)	Time (h)
Experiment 1	Varied from 0-3	570	1.5	1
Experiment 2	3	Varied from 14-570	1.5	1
Experiment 3	3	570	Varied from 1.5-4.5	1
Experiment 4	3	570	1.5	Varied from 0-1

After the electrodesorption, as shown in Figure 3.1 step 4, we then evaluated the ability of electro-desorbed f-SW/DWCNTs to re-adsorb Cu^{2+} from a new solution of $CuSO_4$. This was achieved by mechanically agitating the membrane to remove CNTs (another alternative method for CNT removal from polymeric membranes using ultra-sonication is illustrated in SI). The membrane surface was mechanically agitated by scarping with a spatula to remove CNTs, which were then re-dispersed in solution via sonication for consecutive adsorption-electrodesorption cycles. Steps 1–4 were repeated in successive cycles to investigate the reusability of CNTs for adsorption and concentration of heavy metals.

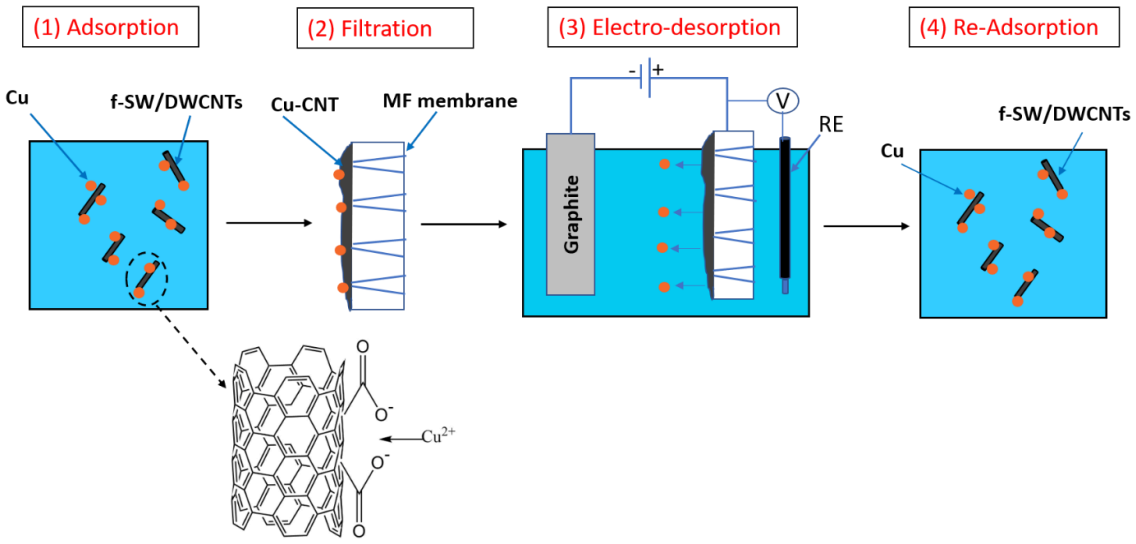

Figure 3.1: Schematic approach for Cu adsorption-electrodesorption process on f-SW/DWCNTs.

3.3.4 Cu Analysis

Initial Cu concentration before the adsorption experiment, final Cu concentration after the adsorption and filtration steps (steps 1-2 in Figure 3.1) and Cu concentration after the electro-desorption step (step 3 in Figure 3.1) were measured for each experiment to determine the percent of Cu adsorbed and electro-desorbed from the CNTs. These concentrations were measured using spectrophotometric methods, as they are less costly than inductively coupled plasma (ICP) and atomic absorption spectroscopy (AAS) analyses [50]. In this method, Na-DDTC reacts with Cu^{2+} ions to give Cu-DDTC which yields a yellow-brown color that can be detected by a UV-VIS spectrophotometer [51–53]. Previous research has demonstrated that aqueous-based spectrophotometric analysis can accurately measure Cu^{2+} concentrations up to 7 ppm [50,52], thus we investigated Cu^{2+} adsorption up to a maximum concentration of 6 ppm. We used a UV-VIS spectrophotometer (Tecan Spark 10M) to quantify the concentration of Cu^{2+} in aqueous solution up to 6 ppm. Although Cu^{2+}aqueous solutions were prepared using DI water, EDTA and

tribasic ammonium citrate were used as a masking agent to prevent any possibility for side reactions in this process [50,53]. Moreover, in the interest of controlling solution pH, ammonia solution was added to raise the pH to 8.3 and NH_4Cl was used as a buffering agent [50]. Figure S3.1a illustrates the obtained Cu^{2+} UV-VIS spectra in EDTA and tribasic ammonium citrate aqueous solution with 0.0625 ppm detection limit. While, Figure S3.1b shows calibration curve relating the Cu^{2+} concentration to the absorbance at 460 nm wavelength. Anova regression analysis for the obtained calibration curves are shown also in the SI.

3.4 Results and Discussion

3.4.1 Adsorption Experiments

Carboxylic acid-functionalized single wall/double wall CNTs (f-SW/DWCNTs) were used to adsorb Cu^{2+} ions from aqueous solutions. Functionalized CNTs were chosen for this study as several reports have shown that carboxylic-acid functionalized CNTs enhance adsorption [49,54,55]. At neutral pH the carboxylic acid-functional groups lower the isoelectric point of the f-SW/DWCNTs, such that the f-SW/DWCNTs will have more negative charges on their surface [56]. The presence of negatively charged carboxylic acid functional groups decreases the attraction of f-SW/DWCNTs for each other, enabling their greater dispersibility in aqueous solutions [57,58], while also enhancing greater electrostatic attraction of positive metal ions to the f-SW/DWCNT surfaces [59]. Mass of adsorbed Cu^{2+} per mass of f-SW/DWCNTs (mg Cu^{2+}/ gm f-SW/DWCNTs) was calculated using the following equation:

$$\text{Mass of adsorbed Cu} = \frac{(C_i - C_f)\,V}{m} \qquad (3.1)$$

where C_i is the initial copper concentration in ppm, C_f is the copper concentration after the adsorption experiment in ppm, V is the solution volume in liter and m is the mass of CNTs in gm. Probe sonication was used to disperse f-SW/DWCNTs in the Cu^{2+} contaminated aqueous solutions. Probe sonication was used to enhance the dispersion of CNTs and increase the available surface area for Cu^{2+} adsorption. Initially we investigated the effects of sonication time on Cu^{2+} adsorption onto f-SW/DWCNTs. Batches of CNTs were sonicated for 15, 30, 40 and 60 min and then added to aqueous solutions of 6 ppm Cu^{2+}. The Cu-CNT solution was then stirred at 300 RPM for 3 h. As seen in Figure 3.2a, it was found that f-SW/DWCNTs which were sonicated for 30 min achieved significantly greater adsorption of Cu^{2+} than f-SW/DWCNTs which were sonicated for both greater and lesser amounts of time. Of note, f-SW/DWCNTs sonicated for an excess of 30 min demonstrated lower Cu^{2+} adsorption. It is hypothesized that this trend is due to a trade-off between the dispersion and damage of CNTs upon increasing sonication time. Specifically, increasing sonication time has been found to induce buckling and wall fracture of CNTs [60–64], which may lead to lower heavy metal adsorption on f-SW/DWCNTs. Following the impact of sonication time, we investigated the rate of adsorption of Cu^{2+} onto f-SW/DWCNTs. f-SW/DWCNTs were exposed to $CuSO_4$ solutions for 10 min, and 1, 3 and 5 h, and the amount of Cu^{2+} that was removed from solution was measured by UV-Vis. It was found that maximum Cu^{2+} adsorption to f-SW/DWCNTs was achieved after 1 h, and further exposure of Cu^{2+} to f-SW/DWCNTs did not increase the adsorption capacity (Figure 3.2b). This result is in agreement with previous reports from the literature which suggest that saturation time of Cu^{2+} on f-SW/DWCNTs occurred between 1 and 2 h [14,49]. Considering these results, all subsequent adsorption experiments were carried out with a sonication time of 30 min and adsorption time

of 3 h to ensure maximum Cu^{2+} adsorption onto f-SW/DWCNTs, which was determined to be 24.4 $\pm$ 4 mg/g (the initial mass of Cu^{2+} in the solution was 0.6 mg and the mass of Cu adsorbed on 5mg f-SW/DWCNTs was approximately 0.123 mg (i.e. 20 % Cu^{2+} removal efficiency)). These adsorption results are in agreement with that found by Li et al. and Wang et al. which reported adsorption capacities of 24.5 and 29.6 mg/g for Cu^{2+} adsorption on oxidized multiwalled CNTs, respectively [30,65]. Cu^{2+} adsorption experiments were also carried out using HCl treated f-SW/DWCNTs with a sonication time of 30 min and adsorption time of 3 h showing nearly the same Cu^{2+} adsorption as untreated f-SW/DWCNTs at the same conditions, see Figure 3.2c.

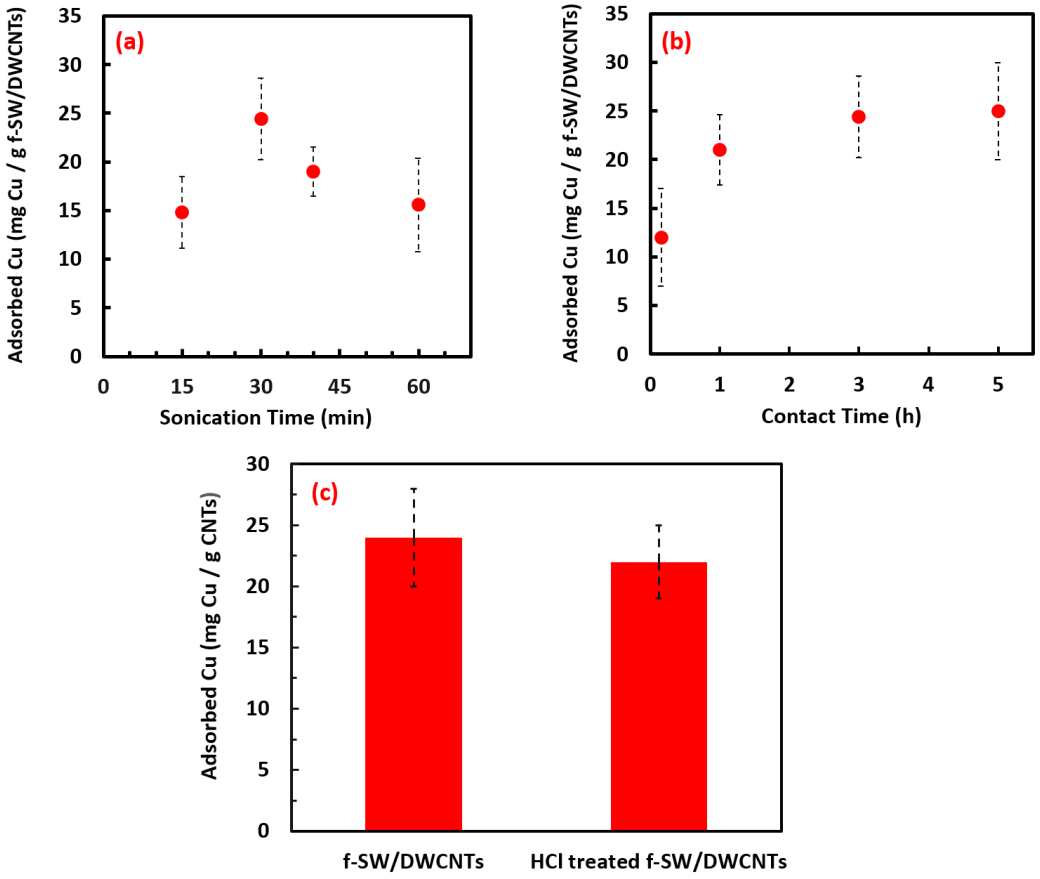

Figure 3.2: (a) The effect of f-SW/DWCNTs sonication time on the adsorbance of Cu^{2+} onto f-SW/DWCNTs at 3 h contact time (b) The effect of contact time on the adsorbance of Cu^{2+} onto

f-SW/DWCNTs at 30 min sonication time (c) The effect of using f-SW/DWCNTs and HCl treated f-SW/DWCNTs (both sonicated for 30 min) on the adsorbance of Cu^{2+} at 3 h contact time, the bars represent the calculated propagated error of standard deviations from repeated experiments.

Scanning electron microscopy (SEM) and energy dispersive X-Ray spectroscopy (EDX) analyses was performed on Cu saturated f-SW/DWCNTs (obtained from Cu adsorption experiments) and bare f-SW/DWCNTs deposited on MF PES membranes. The Cu saturated f-SW/DWCNTs membrane is shown in Figure 3.3a. The cross-section SEM image of this membrane is shown in Figure 3.3b, where the thickness of f-SW/DWCNTs on the PES is ranging between 10 to 25 µm. Top view SEM images combined with EDX Cu mapping images for Cu saturated f-SW/DWCNTs and bare f-SW/DWCNTs are shown in Figure 3.3c and Figure 3.3d, respectively. These images indicate a significant amount of Cu on the Cu saturated f-SW/DWCNTs in comparison with bare f-SW/DWCNTs. The EDX elemental analysis showed 1.1 Cu wt% in the Cu saturated f-SW/DWCNTs in comparison with 0.2 Cu wt% in the bare f-SW/DWCNTs. On the other hand, EDX elemental analysis showed no Cu in HCl treated f-SW/DWCNTs. However, the Cu adsorption capacity on HCl treated f-SW/DWCNTs was nearly the same as on untreated f-SW/DWCNTs as aforementioned, which indicates that the Cu impurities in the f-SW/DWCNTs did not affect the Cu^{2+} adsorption onto the f-SW/DWCNTs. See Table S3.1 for the EDX elemental analysis.

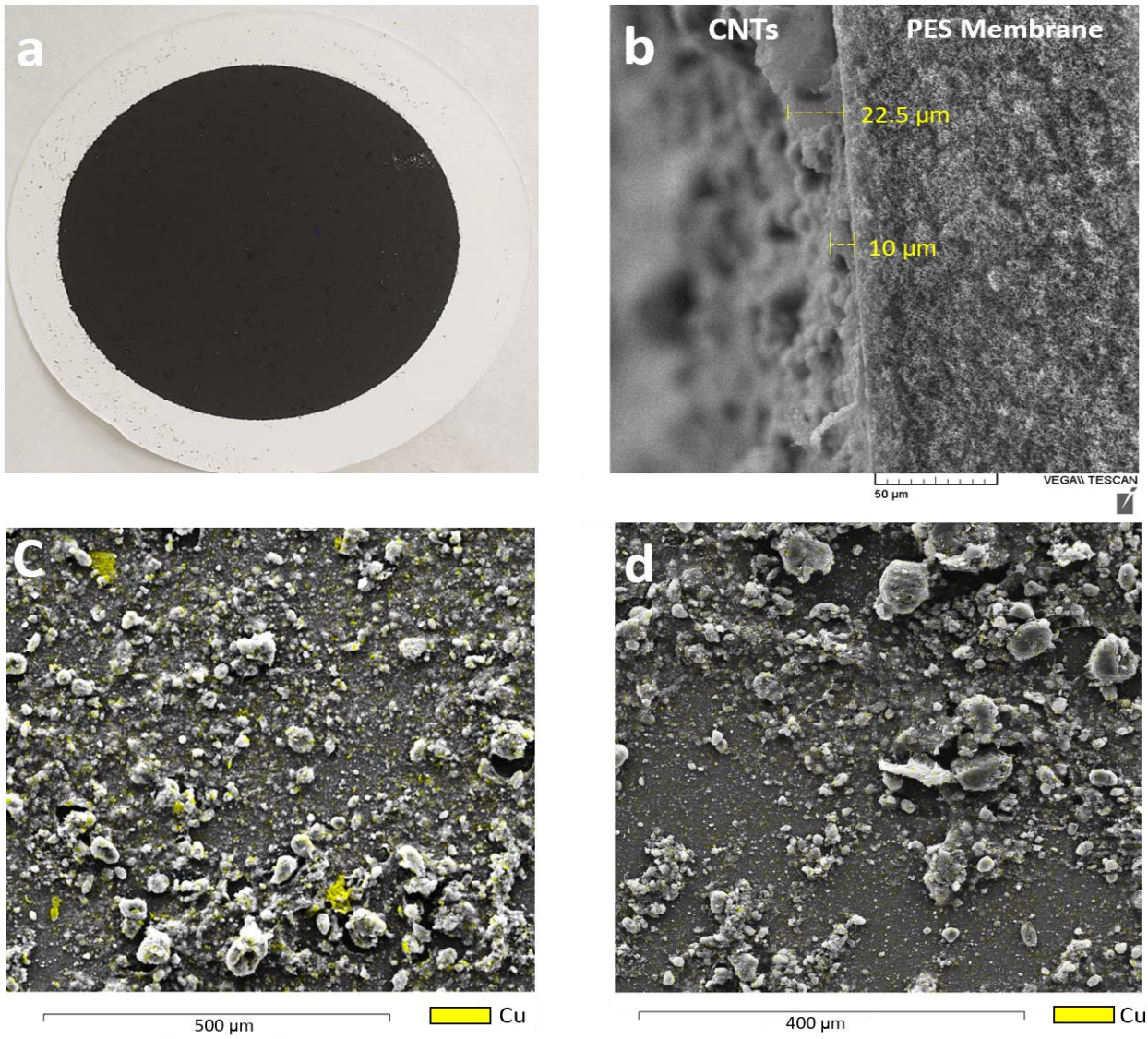

Figure 3.3: Cu saturated f-SW/DWCNTs deposited on a MF PES membrane after adsorption experiments (a) macroscopic top view, (b) cross-section SEM image, and (c) top view SEM image combined with EDX Cu mapping images; bare f-SW/DWCNTs deposited on MF PES membrane (d) top view SEM image combined with EDX Cu mapping images demonstrating the absence of copper in control experiments.

3.4.2 Electrodesorption Experiments

Following adsorption of Cu^{2+} onto f-SW/DWCNTs for the removal of Cu^{2+} from water, we investigated electric field-enabled regeneration of Cu-saturated f-SW/DWCNTs. To this end,

Cu-saturated f-SW/DWCNTs were filtered from the water through dead-end microfiltration (MF). The permeate was an aqueous solution with a lower Cu^{2+} concentration, while the MF membrane was coated in Cu-saturated f-SW/DWCNTs, which created a porous electrically conductive membrane, termed a f-SW/DWCNTs membrane electrode. This f-SW/DWCNTs membrane electrode was then used as a temporary electrode for the regeneration of CNTs and the removal and concentration of Cu^{2+} ions into a concentrated waste stream. An external electric potential was applied to the f-SW/DWCNTs membrane electrode to remove Cu from the f-SW/DWCNTs. Figure 3.4a illustrates the effect of applying positive potential to f-SW/DWCNTs membrane electrode for Cu desorption (Experiment 1 in Table 3.1). As seen in Figure 3.4a, the percentage of Cu desorbed from the electrode increased with increasing applied potential when varied from 1V to 3V versus Ag/AgCl electrode. It is hypothesized that this enhanced desorption with increasing positive applied potential is a result of the increased number of free positive charges on the anode surface. More free positive charges allow for a greater electrostatic repulsive force between the f-SW/DWCNTs and the adsorbed Cu^{2+} ions leading to greater desorption.

Next, we studied the impact of electrolyte concentration on the desorption of Cu from the f-SW/DWCNTs membrane electrodes (Experiment 2 in Table 3.1). As shown in Figure 3.4b, increasing the electrolyte conductivity from 14 to 100 µS/cm showed a significant enhancement in Cu desorption from CNTs, while increasing the electrolyte conductivity further from 100 to 570 µS/cm showed no statistical impact on Cu desorption. An increase in the electrolyte conductivity increases the number of available ions in solution. With an applied positive potential to the f-SW/DWCNTs membrane electrode, Cu^{2+} cations are repelled from this anode, while anions in solution will be attracted to CNT adsorption sites, replacing Cu^{2+} cations facilitating their

desorption. At higher conductivity (> 100 µS/cm), the increased number of ions available in solution do not show any significant increase in Cu desorption. This is likely due to the saturation of the anode electric double layer. The effect of electrode gap distance was subsequently studied (Experiment 3 in Table 3.1). As seen in Figure 3.4c, electrode gap distance has no statistical impact on Cu desorption from CNTs. In theory, decreasing electrode spacing decreases solution resistance and thus induces higher currents. These higher currents are believed to create a more positive charge on the anode surface and in turn lead to higher electrostatic repulsions. We hypothesize that Cu desorption was not noticeably enhanced with decreasing electrode spacing because the system's high desorption capacity (approximately 90%) was achieved at an electrode spacing of 4.5 cm. A study of greater electrode spacing was not practical in our lab-scale set-up. Importantly, the 90% regeneration of CNTs achieved in this study surpasses that observed for other carbonaceous materials employed in Cu eletrodesorption experiments [43]. For instance, Pan et al showed that carboxyl-functionalized graphene aerogels demonstrated only a regeneration efficiency of 35% at 3V and required 0.62 mM HCl electrolyte in order to attain an efficiency of 90% [43]. They proposed that H^+ ions in HCl substituted for the Cu^{2+} ions that had adsorbed to the functionalized graphene through chemical interaction with the carboxylic groups ($-COO^-$). However, in our experiments we achieved 90% regeneration efficiency without the use of any acid. This suggests that the chemical interaction between the Cu^{2+} ions and carboxylic functional groups on CNTs is not the dominant adsorption mechanism in our case.

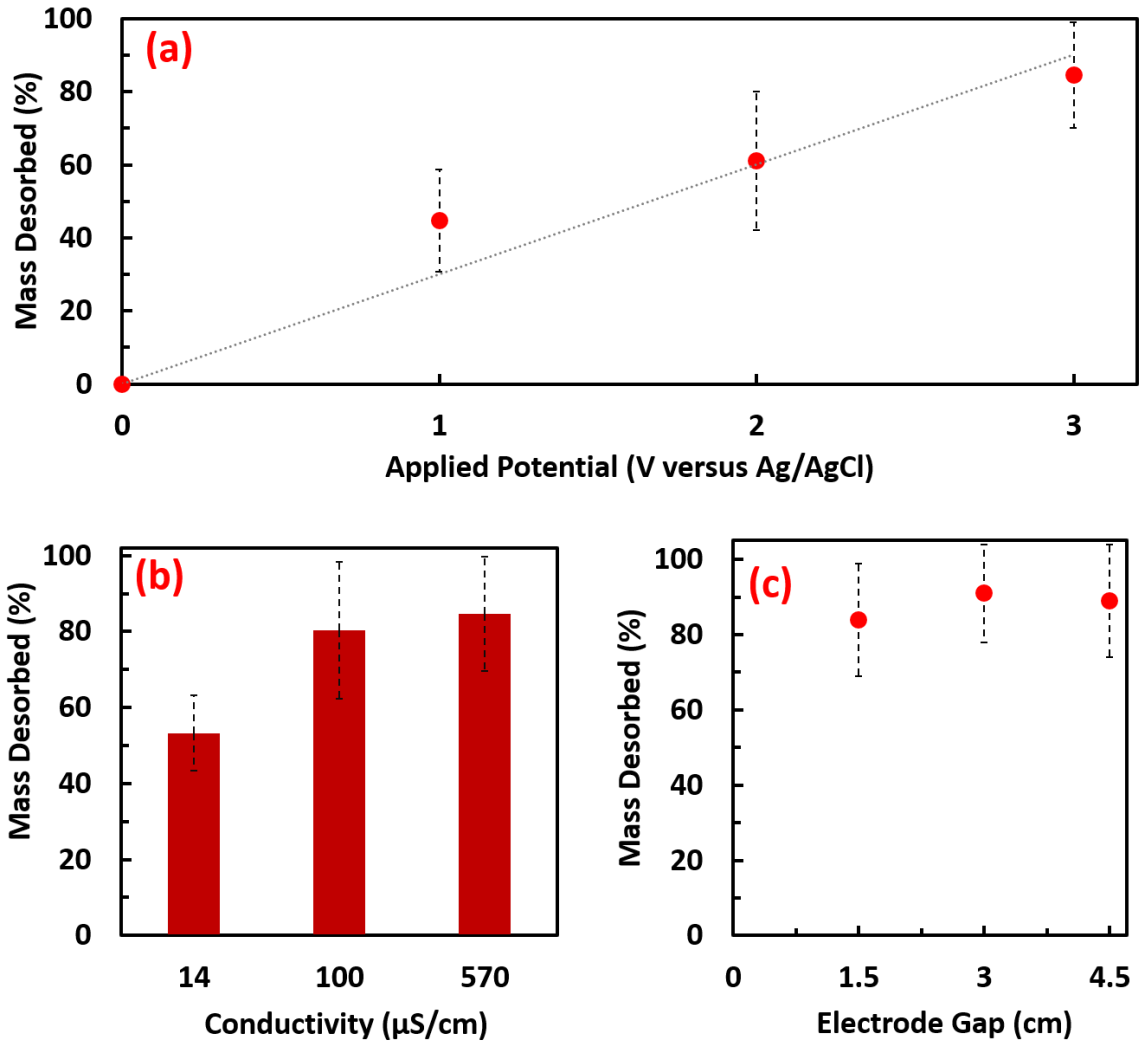

Figure 3.4: (a) The effect of applied potential on the mass percent of Cu desorbed from f-SW/DWCNTs membrane electrodes (at 1-h contact time , electrolyte conductivity 570 µS/cm and Electrode gap of 1.5 cm) ; the line represents the regression model fit with R^2 of 0.948. (b) The effect of conductivity on the mass percent of Cu desorbed (at 1-h contact time, Electrode gap of 1.5 cm and applied potential of 3V) (c) The effect of electrode gap on the mass percent of Cu desorbed (at 1-h contact time , electrolyte conductivity 570 µS/cm and applied potential of 3V), where the error bars represent the calculated propagated error of standard deviations from repeated experiments.

The rate of Cu desorption from CNTs is critical to identifying the rate limiting steps in the adsorption desorption cycle, as well as to establish how effective electric field desorption is in comparison to other desorption techniques. Figure 3.5 shows the effect of contact time on Cu

desorption (Experiment 4 in Table 3.1). Initially, the f-SW/DWCNTs membrane electrode was left in the electrolyte solution for 20 min without applying potential. After 20 min, a 3V applied potential versus Ag/AgCl electrode was applied for 1 h. Over the entire length of the experiment, before and after applied potential, the cumulative concentration of Cu^{2+} in the solution was measured at different time intervals. As demonstrated in Figure 3.5, there was no Cu desorption from the f-SW/DWCNTs membrane electrode in the initial 20 min while there was no applied potential. Cu desorption was only measurable after a potential was applied demonstrating that Cu desorption is driven entirely by the applied potential. As such, we suggest that the competition for f-SW/DWCNT adsorption sites by electrolyte ions does not lead to any significant desorption of Cu ions in the absence of an applied positive potential. While electorlyte ions do not desorb Cu ions without an applied potential, electrolyte ions may facilitate the desorption process in the presence of an applied poential (Figure 3.4b). Over 90% of the adsorbed Cu was desorbed from the f-SW/DWCNTs membrane electrode over the course of 1 h at an applied potential of 3 V. 80% of the adsorbed Cu was desorbed from the f-SW/DWCNTs within the first 5 min after the application of the 3 V step-function. In the subsequent 20 min, 10% of the initial amount of adsorbed Cu was desorbed. In the last 35 min, no more copper was desorbed. These results suggest that there may be two steps to Cu desorption: The first occurs in the first 5 min and requires minimal energy (~ 20 J) while the second occurs in the following 20 min and requires a greater amount of energy (~ 58 J). Previous studies have hypothesized three primary mechanisms for metals adsorption onto CNTs; 1) physisorption of metals to the outer surface of CNTs, 2) electrostatic attraction of metals to the negatively charged functional groups on the surface of CNTs and 3) chemical bonding of the metal ions to the functional groups on the surface of CNTs

[29,66]. Previous studies have shown that while bare CNTs can physisorb Cu from solution, a more than 200 % increase in adsorption is possible using functionalized CNTs, in particular carboxyl functionalized CNTs [49]. It has been hypothesized that this increase in adsorption is due to both electrostatic and chemical interactions between Cu^{2+} in solution and the functional groups on CNTs [10,49]. In our experiments, the applied positive potential desorbed the majority of the Cu within the first five min indicating weak adsorption of Cu to f-SW/DWCNT by electrostatic attraction as opposed to chemical bonding. To assess the effect of mass transfer on Cu desorption kinetics, we calculated an estimate of the time needed for Cu to diffuse through the f-SW/DWCNTs membrane electrode (approximated thickness 25 µm, as shown in Figure 3.3b) into the solution. Without any additional driving forces (e.g. electric fields, convection) that would enhance diffusional flux, Cu ions would diffuse through the membrane on the order of seconds (calculation details are provided in the SI). This estimation indicates that Cu desorption from the CNTs rather than Cu diffusion through the membrane is the rate determining step for the remaining 10% of desorbed Cu in our experiments.

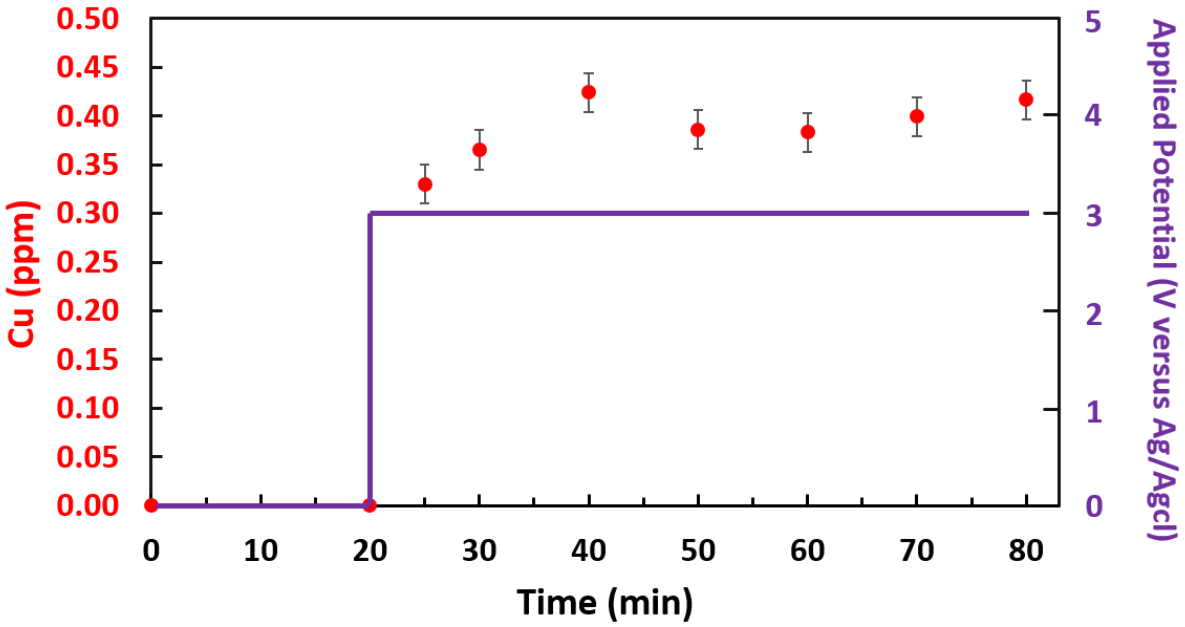

Figure 3.5: The cumulative desorption rate of Cu (potential = 3V, K = 570 µS/cm and Electrode gap = 1.5 cm). Error bars represent the calculated propagated error of standard deviations from repeated experiments.

Cyclic voltammetry (CV) was performed on f-SW/DWCNTs membrane electrodes at 100 and 10 mV/s scan rates as shown in Figure 3.6a and Figure 3.6b, respectively. No peaks were observed between 0-4 V for both scan rates. As aforementioned, the electrodesorption kinetics experiments (Figure 3.5) indicated that the majority of Cu (about 80%) was desorbed from the CNTs by electrostatic repulsion, while a small percent (less than 10%) was desorbed by chemical bond breaking (i.e., electrochemical oxidation). Nevertheless, the absence of CV peaks indicated the absence of Cu redox reactions onto the CNTs membrane anode. It is believed that the low percent of Cu desorption via electrochemical oxidation produced insignificant electric currents that was not detected as peaks on the CV curves. At higher applied potentials (> 0.62 V versus Ag/AgCl), water splitting can theoretically occur if no overpotential is required. It is possible that

oxygen evolution from water splitting may contribute to the desorption of Cu ions. To investigate whether water splitting, rather than electrostatic repulsion may be the major cause of Cu desorption, Linear sweep voltammetry (LSV) was conducted on the f-SW/DWCNTs membrane electrodes. In Figure 3.6e, LSV of f-SW/DWCNTs membrane electrode shows that more than 1V is required for the oxygen evolution reaction (OER). However significant Cu desorption was seen at an applied voltage of 1V, at which potential minimal water splitting would have occurred. Furthermore, the current density at an applied potential of 3 V is approximately 3 mA/cm^2, which is substantially lower than the conventional benchmark for significant OER of 10 mA/cm^2 [67–69]. In addition, insignificant gas production was observed at the f-SW/DWCNTs membrane anode at 3 V, as shown in the video attached in the supplementary information. These results are in agreement with previous studies that showed that CNTs need to be doped with catalysts such as Ni , Co and perovskites in order to favor the kinetics of oxygen production [70]. As such, we concluded that the mechanism for Cu desorption was electrostatic desorption from f-SW/DWCNTs rather than from any physical shearing or chemical effect as a result of oxygen production arising from water electrolysis.

Interestingly, the CV curves overlap at voltages greater than 2.6 V (Figure 3.6a) at high scan rates (100 mV). Overlapping current responses are likely a result of slow Cu diffusion from the f-SW/DWCNTs membrane electrode. Higher currents on the reverse scan may be due to Cu ions that have not had sufficient time to leave the bulk f-SW/DWCNTs. This result is supported by previous studies which have explained that at higher reverse scan rates, slow kinetics of species formation in front of the electrode surface leads to higher reverse currents [71–73]. Conversely, at lower scan rates (Figure 3.6b), there is sufficient time for complete Cu desorption and diffusion

from the f-SW/DWCNT bulk to occur, which ultimately results in a lower current on the reverse scan, evidenced by the non-intersecting CV scans. Controls of CV curves on bare f-SW/DWCNTs membrane electrodes with no Cu adsorbed (Figure 3.6c and Figure 3.6d) confirms this hypothesis, as the forward scan has a significantly higher current than the reverse scan for both high and low scan rates.

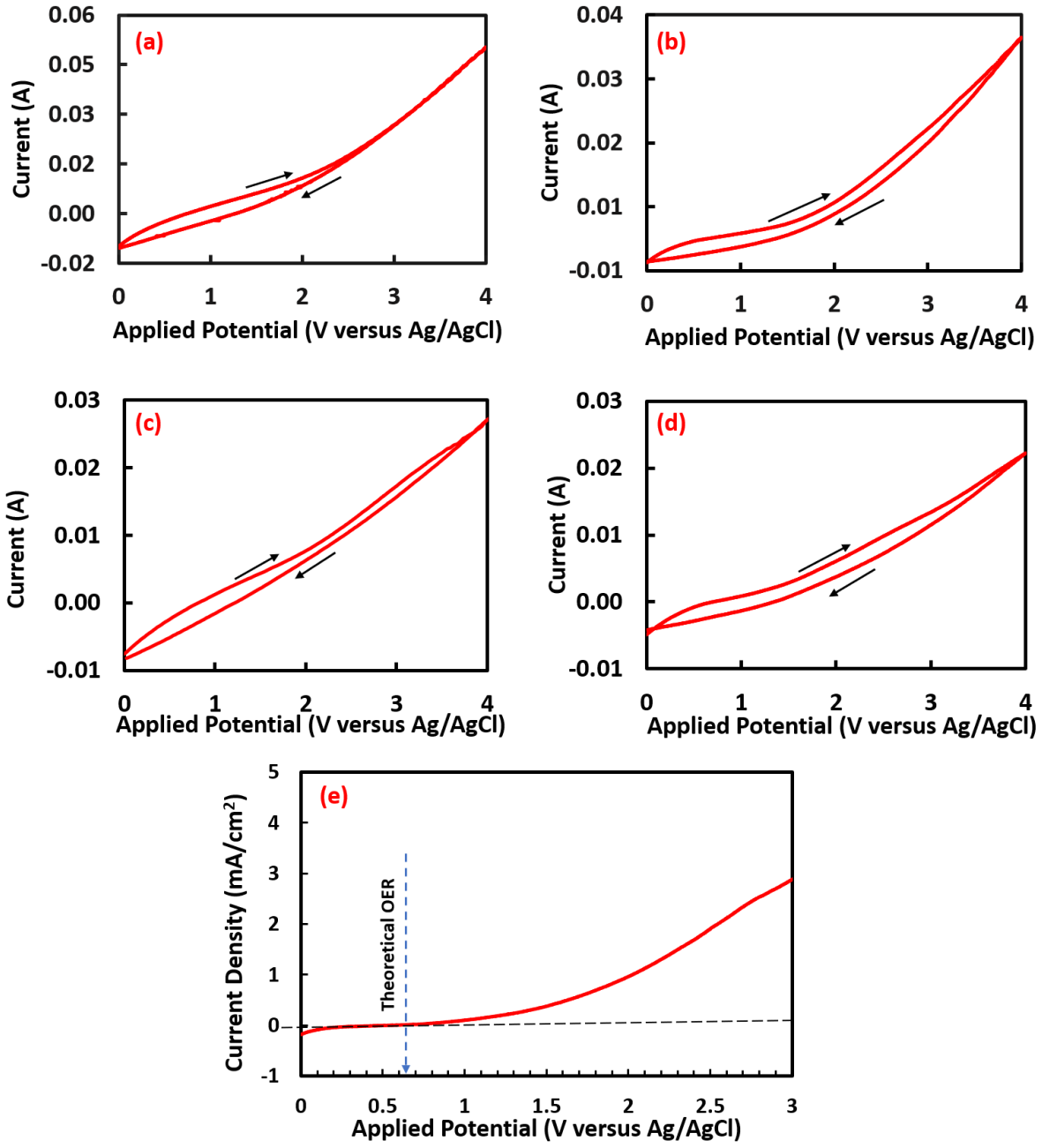

Figure 3.6: Cyclic voltammetry for f-SW/DWCNTs membrane electrode saturated with Cu at (a) 100 mV/s (b) 10 mV/s scan rate; and for bare f-SW/DWCNTs electrode at (c) 100 mV/s (d) 10 mV/s scan rates. (e) linear sweep voltammetry for f-SW/DWCNTs membrane electrode at 10 mV/s scan rate indicating the theoretical potential for the oxygen evolution reaction (OER) at 0.62 V, which lies at lower applied potential than the observed change in current density.

Finally, the reusability of the CNTs was investigated by utilizing them through consecutive cycles. Figure 3.7a demonstrates the regeneration ability of the CNTs in 4 consecutive adsorption-electrodesorption cycles. As seen by Figure 3.7a, the mass of adsorbed and desorbed Cu was approximately equivalent within the first 4 cycles. Figure 3.7b, shows the Cu-CNT complexes filtered on MF membranes subsequent to the adsorption step, the MF membranes after the CNTs were removed from them subsequent to electrodesorption, and the suspension of CNTs that were removed from the MF membranes to be used in the subsequent Cu adsorption cycle.

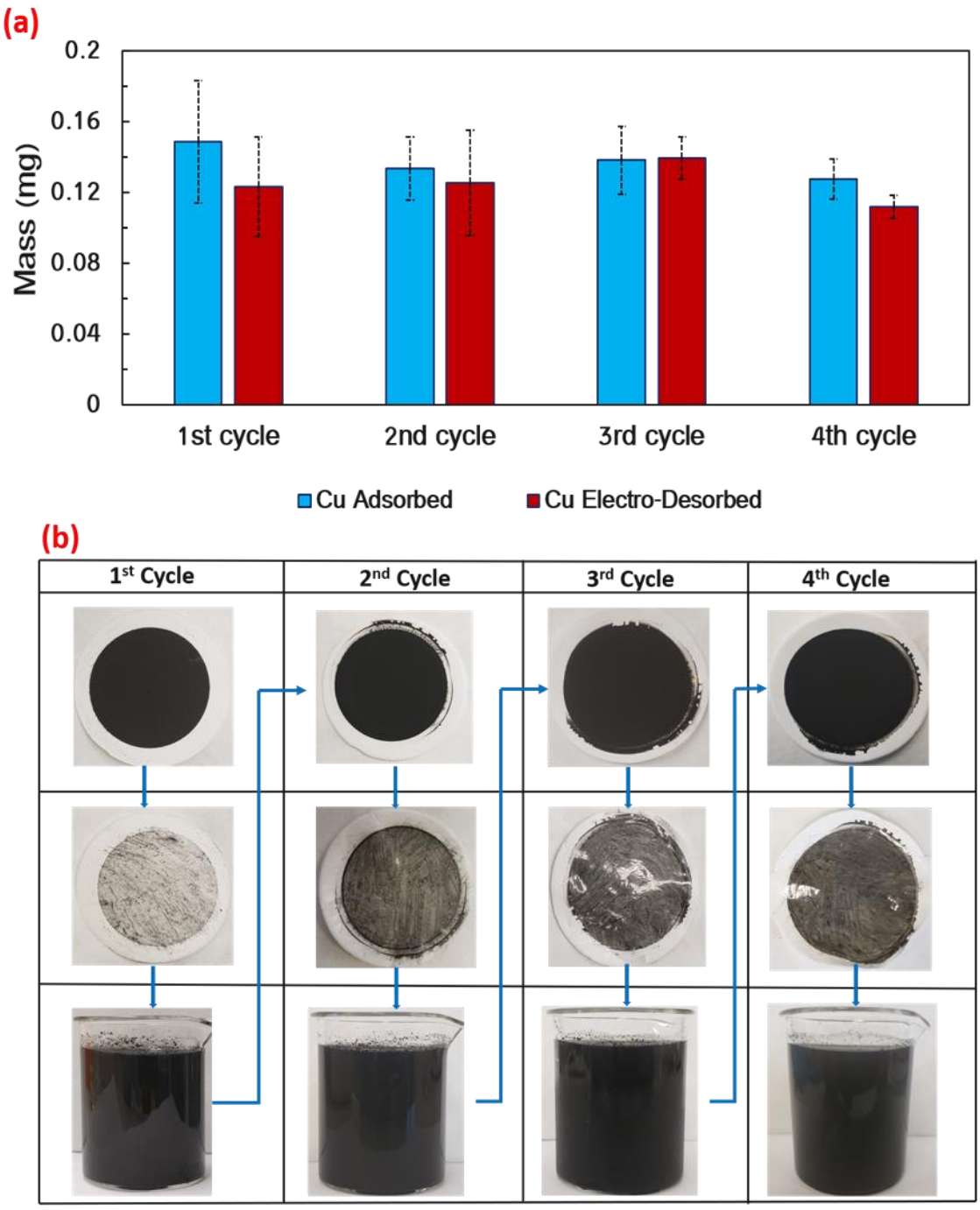

Figure 3.7: (a) Mass of Cu adsorbed/desorbed in five adsorption electro-desorption cycles using the same batch of CNTs, the bars represent the calculated propagated error of standard deviations from repeated experiments (b) The first row shows the Cu-CNT complexes filtered on MF membranes after Cu adsorption, the second row shows the MF membranes after the CNTs were removed from them subsequent to electrodesorption, and the third row shows the removed CNTs sonicated in DI water to be used in the next Cu adsorption cycle.

Based on the results obtained from this work, we propose an adsorption-electrodesorption process to be utilized in large batch scale applications (see Figure 3.8). In the first stage, CNTs will be mixed with heavy metal-contaminated solutions to allow for the adsorption process. This CSTR, will be partitioned at one end with a conductive electrode and at the other with a porous surface. In the second step, a pressure will be applied to filter the water and retain the CNTs-Metal complex on the porous medium. In the third step, the conductive cathode and anode (the CNT-Metal complexes deposited on the porous membrane) will establish an electrochemical cell for the electro-mediated regeneration of the CNTs. In the fourth step, pressure will be applied to the porous medium to remove the CNTs in order to reuse them for subsequent heavy metal adsorption. In the fifth step, a new heavy metal-contaminated solution will be added to the regenerated CNTs and the closed loop process continues. To achieve an effective closed loop process, two areas of research focus are essential: effective removal of CNTs from porous membranes, and longer-term testing of recyclability. The affinity of variously functionalized CNTs to different hydrophobic porous membrane materials is the focus of future studies, while longer term testing of the reusability of CNTs is encouraged for validation of the proposed process. Finally, it is important to note that the proposed adsorption-electrodesorption process, shown in Figure 3.8, will require two more steps than conventional adsorption-acid desorption processes. These two steps are the filtration of metal-CNTs complex onto the porous medium (step 2 in Figure 3.8) and the CNT removal from the porous medium (step 4 in Figure 3.8). Despite the additional steps, the adsorption-electrodesorption process (step 3 in Figure 3.8) will ensure a continuous closed-loop process that avoids the handling and usage of large volumes of acids. Moreover, our adsorption-electrodesorption process eliminates the concentrated acid stream,

which would required several additional steps for its proper treatment and disposal. This externality is not often addressed in conventional processes.

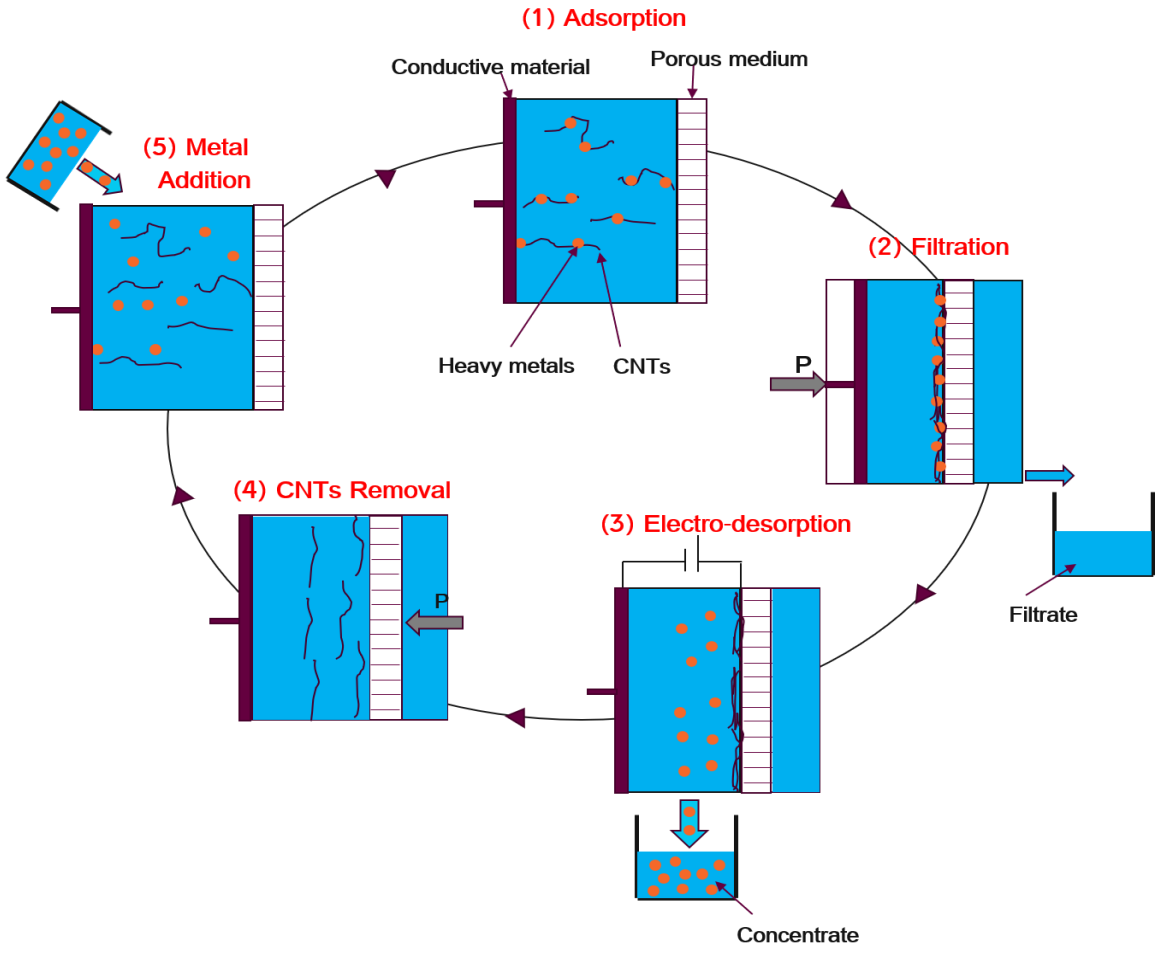

Figure 3.8: Proposed industrial close-loop adsorption-electrodesorption process.

3.5 Conclusion

This study investigated the feasibility of combining Cu adsorption onto CNTs with electrochemical methods for their regeneration. Overall, it was found that the adsorption of Cu onto CNTs can be maximized utilizing a sonication time of 30 min and an adsorption time of 3 h. Cu-saturated f-SW/DWCNT were successfully formed into temporary membrane electrodes and the application of an electric field achieved over 90% Cu ion removal from f-SW/DWCNTs into a waste recovery

stream. Electric field mediated desorption successfully regenerated the CNTs for subsequent Cu ion adsorption experiments. Cu removal from the CNT composite was found to increase with increasing applied potential and solution conductivity, while electrode distance was found to have no statistical impact. It was hypothesized that the driving force for this regeneration process stems from electrostatic repulsion between the f-SW/DWCNT membrane anode and the positively charged adsorbed Cu ions. This hypothesis was supported by fast desorption kinetics and by insignificant oxygen production limiting the possibility of shear effects. Finally, this study demonstrated the feasibility of CNT regeneration within 4 consecutive cycles. This paper outlines important trends between electrodesorption and operational parameters while demonstrating the feasibility of CNT regeneration in conventional adsorption processes. Future research will focus on developing more effective approaches in separating CNTs from membranes to avoid CNT mass loss during successive cycles, building a continuous process for the adsorptive water treatment followed by concentrated heavy metal recovery in a waste stream, and the application to other heavy metals.

3.6 References

[1] F. Fu, Q. Wang, Removal of heavy metal ions from wastewaters: A review, J. Environ. Manage. 92 (2011) 407–418. doi:10.1016/j.jenvman.2010.11.011.

[2] S.W. Lv, J.M. Liu, C.Y. Li, N. Zhao, Z.H. Wang, S. Wang, A novel and universal metal-organic frameworks sensing platform for selective detection and efficient removal of heavy metal ions, Chem. Eng. J. 375 (2019) 122111. doi:10.1016/j.cej.2019.122111.

[3] R. Rostamian, M. Najafi, A.A. Rafati, Synthesis and characterization of thiol-functionalized silica nano hollow sphere as a novel adsorbent for removal of poisonous heavy metal ions from water: Kinetics, isotherms and error analysis, Chem. Eng. J. 171 (2011) 1004–1011. doi:10.1016/j.cej.2011.04.051.

[4] M.A. Barakat, New trends in removing heavy metals from industrial wastewater, Arab. J. Chem. 4 (2011) 361–377. doi:10.1016/j.arabjc.2010.07.019.

[5] N. Verma, G. Kaur, Trends on Biosensing Systems for Heavy Metal Detection, Elsevier Ltd, 2016. doi:10.1016/bs.coac.2016.04.001.

[6] S.A. Nabi, M. Shahadat, R. Bushra, A.H. Shalla, Heavy-metals separation from industrial effluent, natural water as well as from synthetic mixture using synthesized novel composite adsorbent, Chem. Eng. J. 175 (2011) 8–16. doi:10.1016/j.cej.2011.01.022.
[7] P.B. Tchounwou, C.G. Yedjou, A.K. Patlolla, D.J. Sutton, Heavy Metals Toxicity and the Environment, Mol. Clin. Environ. Toxicol. 101 (2012) 133–164. doi:10.1007/978-3-7643-8340-4.
[8] S. Chowdhury, M.A.J. Mazumder, O. Al-Attas, T. Husain, Heavy metals in drinking water: Occurrences, implications, and future needs in developing countries, Sci. Total Environ. 569–570 (2016) 476–488. doi:10.1016/j.scitotenv.2016.06.166.
[9] J.R. Parga, D.L. Cocke, J.L. Valenzuela, J.A. Gomes, M. Kesmez, G. Irwin, H. Moreno, M. Weir, Arsenic removal via electrocoagulation from heavy metal contaminated groundwater in la Comarca Lagunera México, J. Hazard. Mater. 124 (2005) 247–254. doi:10.1016/j.jhazmat.2005.05.017.
[10] Ihsanullah, A. Abbas, A.M. Al-Amer, T. Laoui, M.J. Al-Marri, M.S. Nasser, M. Khraisheh, M.A. Atieh, Heavy metal removal from aqueous solution by advanced carbon nanotubes: Critical review of adsorption applications, Sep. Purif. Technol. 157 (2016) 141–161. doi:10.1016/j.seppur.2015.11.039.
[11] C.A. Basha, M. Somasundaram, T. Kannadasan, C.W. Lee, Heavy metals removal from copper smelting effluent using electrochemical filter press cells, Chem. Eng. J. 171 (2011) 563–571. doi:10.1016/j.cej.2011.04.031.
[12] X. Li, Y. Li, Z. Ye, Preparation of macroporous bead adsorbents based on poly(vinyl alcohol)/chitosan and their adsorption properties for heavy metals from aqueous solution, Chem. Eng. J. 178 (2011) 60–68. doi:10.1016/j.cej.2011.10.012.
[13] S.A. Al-Saydeh, M.H. El-Naas, S.J. Zaidi, Copper removal from industrial wastewater: A comprehensive review, J. Ind. Eng. Chem. 56 (2017) 35–44. doi:10.1016/j.jiec.2017.07.026.
[14] V.K. Gupta, S. Agarwal, A.K. Bharti, H. Sadegh, Adsorption mechanism of functionalized multi-walled carbon nanotubes for advanced Cu (II) removal, J. Mol. Liq. 230 (2017) 667–673. doi:10.1016/j.molliq.2017.01.083.
[15] C. Nie, Y. Zhan, L. Pan, H. Li, Z. Sun, Electrosorption of different cations and anions with membrane capacitive deionization based on carbon nanotube/nanofiber electrodes and ion-exchange membranes, Desalin. Water Treat. (2011) 266–271. doi:10.5004/dwt.2011.2092.
[16] V. Chantawong, N.W. Harvey, V.N. Bashkin, Comparison of Heavy Metal Adsorptions By Thai Kaolin, Adsorpt. J. Int. Adsorpt. Soc. (2003) 111–125.
[17] T.M. Florence, G.E. Batley, Chemical Speciation In Natural Waters, C R C Crit. Rev. Anal. Chem. 9 (1980) 219–296. doi:10.1080/10408348008542721.
[18] World Health Organization, Copper in Drinking-water, 2004.
[19] A. Tripathi, M. Rawat Ranjan, Heavy Metal Removal from Wastewater Using Low Cost Adsorbents, J. Bioremediation Biodegrad. 06 (2015). doi:10.4172/2155-6199.1000315.
[20] E. Erdem, N. Karapinar, R. Donat, The removal of heavy metal cations by natural zeolites, J. Colloid Interface Sci. 280 (2004) 309–314. doi:10.1016/j.jcis.2004.08.028.
[21] K. Dutta, S. De, Aromatic conjugated polymers for removal of heavy metal ions from wastewater: A short review, Environ. Sci. Water Res. Technol. 3 (2017) 793–805.

doi:10.1039/c7ew00154a.
[22] M. Minamisawa, H. Minamisawa, S. Yoshida, N. Takai, Adsorption Behavior of Heavy Metals on Biomaterials, J. Agric. Food Chem. 52 (2007) 5606–5611. doi:10.1021/jf0496402.
[23] P.X. Pinto, S.R. Al-Abed, D.J. Reisman, Biosorption of heavy metals from mining influenced water onto chitin products, Chem. Eng. J. 166 (2011) 1002–1009. doi:10.1016/j.cej.2010.11.091.
[24] K. Yin, Q. Wang, M. Lv, L. Chen, Microorganism remediation strategies towards heavy metals, Chem. Eng. J. 360 (2019) 1553–1563. doi:10.1016/j.cej.2018.10.226.
[25] N. Huang, L. Zhai, H. Xu, D. Jiang, Stable Covalent Organic Frameworks for Exceptional Mercury Removal from Aqueous Solutions, J. Am. Chem. Soc. 139 (2017) 2428–2434. doi:10.1021/jacs.6b12328.
[26] C. Lu, C. Liu, G.P. Rao, Comparisons of sorbent cost for the removal of Ni2+ from aqueous solution by carbon nanotubes and granular activated carbon, J. Hazard. Mater. 151 (2008) 239–246. doi:10.1016/j.jhazmat.2007.05.078.
[27] A.E. Burakov, E. V. Galunin, I. V. Burakova, A.E. Kucherova, S. Agarwal, A.G. Tkachev, V.K. Gupta, Adsorption of heavy metals on conventional and nanostructured materials for wastewater treatment purposes: A review, Ecotoxicol. Environ. Saf. 148 (2018) 702–712. doi:10.1016/j.ecoenv.2017.11.034.
[28] C. Santhosh, V. Velmurugan, G. Jacob, S.K. Jeong, A.N. Grace, A. Bhatnagar, Role of nanomaterials in water treatment applications: A review, Chem. Eng. J. 306 (2016) 1116–1137. doi:10.1016/j.cej.2016.08.053.
[29] X. Ren, C. Chen, M. Nagatsu, X. Wang, Carbon nanotubes as adsorbents in environmental pollution management: A review, Chem. Eng. J. 170 (2011) 395–410. doi:10.1016/j.cej.2010.08.045.
[30] Y.-H. Li, Z. Luan, Z. Di, Y. Zhu, C. Xu, D. Wu, B. Wei, J. Ding, Competitive adsorption of Pb , Cu and Cd ions from aqueous solutions by multiwalled carbon nanotubes, Carbon N. Y. 41 (2003) 2787–2792. doi:10.1016/s0008-6223(03)00392-0.
[31] G.S. Ajmani, D. Goodwin, K. Marsh, D.H. Fairbrother, K.J. Schwab, J.G. Jacangelo, H. Huang, Modification of low pressure membranes with carbon nanotube layers for fouling control, Water Res. 46 (2012) 5645–5654. doi:10.1016/j.watres.2012.07.059.
[32] W. Yu, Y. Liu, L. Shen, Y. Xu, R. Li, T. Sun, H. Lin, Magnetic field assisted preparation of PES-Ni@MWCNTs membrane with enhanced permeability and antifouling performance, Chemosphere. 243 (2020) 125446. doi:10.1016/j.chemosphere.2019.125446.
[33] A.Z. Philip G. Collins, Keith Bradley, Masa Ishigami, Extreme oxygen sensitivity of electronic properties of carbon nanotubes, Science (80-.). 287 (2000) 1801–1804. doi:10.1126/science.287.5459.1801.
[34] G. Che, B.B. Lakshmi, E.R. Fisher, C.R. Martin, Carbon nanotubule membranes for electrochemical energy storage and production, Nature. 393 (1998) 346–349. doi:10.1038/30694.
[35] P. J.M, N. Coustel, B. Coq, V. Bretons, P.S. Kumbhar, R. Dutartre, P. Geneste, P. Bernier, P.M. Ajayan, Application of Carbon Nanotubes as Supports in Heterogeneous Catalysis, J. Am. Chem. SOC. 116 (1994) 7935–7936. doi:10.1121/1.384235.
[36] J.L. Gong, B. Wang, G.M. Zeng, C.P. Yang, C.G. Niu, Q.Y. Niu, W.J. Zhou, Y. Liang, Removal

of cationic dyes from aqueous solution using magnetic multi-wall carbon nanotube nanocomposite as adsorbent, J. Hazard. Mater. 164 (2009) 1517–1522. doi:10.1016/j.jhazmat.2008.09.072.
[37] C. Lu, Y.L. Chung, K.F. Chang, Adsorption of trihalomethanes from water with carbon nanotubes, Water Res. 39 (2005) 1183–1189. doi:10.1016/j.watres.2004.12.033.
[38] Y. Ge, Z. Li, D. Xiao, P. Xiong, N. Ye, Sulfonated multi-walled carbon nanotubes for the removal of copper (II) from aqueous solutions, J. Ind. Eng. Chem. 20 (2014) 1765–1771. doi:10.1016/j.jiec.2013.08.030.
[39] V.K. Gupta, O. Moradi, I. Tyagi, S. Agarwal, H. Sadegh, R. Shahryari-Ghoshekandi, A.S.H. Makhlouf, M. Goodarzi, A. Garshasbi, Study on the removal of heavy metal ions from industry waste by carbon nanotubes: Effect of the surface modification: A review, Crit. Rev. Environ. Sci. Technol. 46 (2016) 93–118. doi:10.1080/10643389.2015.1061874.
[40] P. Laux, C. Riebeling, A.M. Booth, J.D. Brain, J. Brunner, C. Cerrillo, O. Creutzenberg, I. Estrela-Lopis, T. Gebel, G. Johanson, H. Jungnickel, H. Kock, J. Tentschert, A. Tlili, A. Schäffer, A.J.A.M. Sips, R.A. Yokel, A. Luch, Challenges in characterizing the environmental fate and effects of carbon nanotubes and inorganic nanomaterials in aquatic systems, Environ. Sci. Nano. 5 (2018) 48–63. doi:10.1039/c7en00594f.
[41] C. Lu, H. Chiu, C. Liu, Removal of zinc(II) from aqueous solution by purified carbon nanotubes: Kinetics and equilibrium studies, Ind. Eng. Chem. Res. 45 (2006) 2850–2855. doi:10.1021/ie051206h.
[42] H.J. Wang, A.L. Zhou, F. Peng, H. Yu, L.F. Chen, Adsorption characteristic of acidified carbon nanotubes for heavy metal Pb(II) in aqueous solution, Mater. Sci. Eng. A. 466 (2007) 201–206. doi:10.1016/j.msea.2007.02.097.
[43] M. Pan, C. Shan, X. Zhang, Y. Zhang, C. Zhu, G. Gao, B. Pan, Environmentally Friendly in Situ Regeneration of Graphene Aerogel as a Model Conductive Adsorbent, Environ. Sci. Technol. 52 (2018) 739–746. doi:10.1021/acs.est.7b02795.
[44] H. Wang, C. Na, Binder-free carbon nanotube electrode for electrochemical removal of chromium, ACS Appl. Mater. Interfaces. 6 (2014) 20309–20316. doi:10.1021/am505838r.
[45] Y.X. Liu, D.X. Yuan, J.M. Yan, Q.L. Li, T. Ouyang, Electrochemical removal of chromium from aqueous solutions using electrodes of stainless steel nets coated with single wall carbon nanotubes, J. Hazard. Mater. 186 (2011) 473–480. doi:10.1016/j.jhazmat.2010.11.025.
[46] Y.X. Liu, J.M. Yan, D.X. Yuan, Q.L. Li, X.Y. Wu, The study of lead removal from aqueous solution using an electrochemical method with a stainless steel net electrode coated with single wall carbon nanotubes, Chem. Eng. J. 218 (2013) 81–88. doi:10.1016/j.cej.2012.12.020.
[47] H. Li, L. Pan, Y. Zhang, Z. Sun, Ferric ion adsorption and electrodesorption by carbon nanotubes and nanofibres films, Water Sci. Technol. 59 (2009) 1657–1663. doi:10.2166/wst.2009.162.
[48] C.H. Wu, Studies of the equilibrium and thermodynamics of the adsorption of Cu2+ onto as-produced and modified carbon nanotubes, J. Colloid Interface Sci. 311 (2007) 338–346. doi:10.1016/j.jcis.2007.02.077.
[49] O. Moradi, The removal of ions by functionalized carbon nanotube: Equilibrium, isotherms and thermodynamic studies, Chem. Biochem. Eng. Q. 25 (2011) 229–240.

[50] J. van Staden, A. Botha, Spectrophotometric determination of Cu(II) with sequential injection analysis, Talanta. 49 (1999) 1099–1108. doi:10.1016/S0039-9140(99)00062-4.
[51] M.N. Uddin, M. Abdus Salam, M.A. Hossain, Spectrophotometric measurement of Cu(DDTC)2 for the simultaneous determination of zinc and copper, Chemosphere. 90 (2013) 366–373. doi:10.1016/j.chemosphere.2012.07.029.
[52] D. Xiao, H. Li, H. He, R. Lin, P. Zuo, Adsorption performance of carboxylated multi-wall carbon nanotube–Fe3O4 magnetic hybrids for Cu(II) in water, New Carbon Mater. 29 (2014) 15–25.
[53] P. Wang, S.. Shi, D. Zhou, Sequential Determination of Nickel and Copper in Waste Waters by Reversed Flow Injection Spectrophotometr, Microchem. J. 52 (1995) 146–154.
[54] A.B. Dichiara, M.R. Webber, W.R. Gorman, R.E. Rogers, Removal of Copper Ions from Aqueous Solutions via Adsorption on Carbon Nanocomposites, ACS Appl. Mater. Interfaces. 7 (2015) 15674–15680. doi:10.1021/acsami.5b04974.
[55] G.P. Rao, C. Lu, F. Su, Sorption of divalent metal ions from aqueous solution by carbon nanotubes: A review, Sep. Purif. Technol. 58 (2007) 224–231. doi:10.1016/j.seppur.2006.12.006.
[56] S. Mallakpour, E. Khadem, Carbon Nanotubes for Heavy Metals Removal, Elsevier Inc., 2019. doi:10.1016/b978-0-12-814132-8.00009-5.
[57] O. V. Kharissova, B.I. Kharisov, E.G. De Casas Ortiz, Dispersion of carbon nanotubes in water and non-aqueous solvents, RSC Adv. 3 (2013) 24812–24852. doi:10.1039/c3ra43852j.
[58] M.A. Halali, C.F. De Lannoy, The Effect of Cross-Linkers on the Permeability of Electrically Conductive Membranes, Ind. Eng. Chem. Res. 58 (2019) 3832–3844. doi:10.1021/acs.iecr.8b05691.
[59] X. Yang, Y. Wan, Y. Zheng, F. He, Z. Yu, J. Huang, H. Wang, Y.S. Ok, Y. Jiang, B. Gao, Surface functional groups of carbon-based adsorbents and their roles in the removal of heavy metals from aqueous solutions: A critical review, Chem. Eng. J. (2019) 608–621. doi:10.1016/j.cej.2019.02.119.
[60] A. Montazeri, N. Montazeri, K. Pourshamsian, A. Tcharkhtchi, The effect of sonication time and dispersing medium on the mechanical properties of multiwalled carbon nanotube (MWCNT)/epoxy composite, Int. J. Polym. Anal. Charact. 16 (2011) 465–476. doi:10.1080/1023666X.2011.600517.
[61] K.L. Lu, R.M. Lago, Y.K. Chen, M.L.H. Green, P.J.F. Harris, S.C. Tsang, Mechanical damage of carbon nanotubes by ultrasound, Carbon N. Y. 34 (1996) 814–816. doi:10.1016/0008-6223(96)89470-X.
[62] K.B. Shelimov, R.O. Esenaliev, A.G. Rinzler, C.B. Huffman, R.E. Smalley, Purification of single-wall carbon nanotubes by ultrasonically assisted filtration, Chem. Phys. Lett. 282 (1998) 429–434. doi:10.1016/S0009-2614(97)01265-7.
[63] J.S. Taurozzi, V.A. Hackley, M.R. Wiesner, Ultrasonic dispersion of nanoparticles for environmental, health and safety assessment issues and recommendations, Nanotoxicology. 5 (2011) 711–729. doi:10.3109/17435390.2010.528846.
[64] F. Hennrich, R. Krupke, K. Arnold, J.A.R. Stütz, S. Lebedkin, T. Koch, T. Schimmel, M.M. Kappes, The mechanism of cavitation-induced scission of single-walled carbon nanotubes, J. Phys. Chem. B. 111 (2007) 1932–1937. doi:10.1021/jp065262n.

[65] J. Wang, Z. Li, S. Li, W. Qi, P. Liu, F. Liu, Y. Ye, L. Wu, L. Wang, W. Wu, Adsorption of Cu(II) on Oxidized Multi-Walled Carbon Nanotubes in the Presence of Hydroxylated and Carboxylated Fullerenes, PLoS One. 8 (2013). doi:10.1371/journal.pone.0072475.
[66] H. Wang, A. Zhou, F. Peng, H. Yu, J. Yang, Mechanism study on adsorption of acidified multiwalled carbon nanotubes to Pb(II), J. Colloid Interface Sci. 316 (2007) 277–283. doi:10.1016/j.jcis.2007.07.075.
[67] L. Lu, W. Vakki, J.A. Aguiar, C. Xiao, K. Hurst, M. Fairchild, X. Chen, F. Yang, J. Gu, Z.J. Ren, Unbiased solar H2 production with current density up to 23 mA cm-2 by Swiss-cheese black Si coupled with wastewater bioanode, Energy Environ. Sci. 12 (2019) 1088–1099. doi:10.1039/c8ee03673j.
[68] A.G. Scheuermann, C.E.D. Chidsey, P.C. McIntyre, Understanding photovoltage in insulator-protectedwater oxidation half-cells, J. Electrochem. Soc. 163 (2016) H192–H200. doi:10.1149/2.0601603jes.
[69] T. Kou, S. Wang, J.L. Hauser, M. Chen, S.R.J. Oliver, Y. Ye, J. Guo, Y. Li, Ni Foam-Supported Fe-Doped β-Ni(OH) 2 Nanosheets Show Ultralow Overpotential for Oxygen Evolution Reaction, ACS Energy Lett. 4 (2019) 622–628. doi:10.1021/acsenergylett.9b00047.
[70] Y. Cheng, S.P. Jiang, Advances in electrocatalysts for oxygen evolution reaction of water electrolysis-from metal oxides to carbon nanotubes, Prog. Nat. Sci. Mater. Int. 25 (2015) 545–553. doi:10.1016/j.pnsc.2015.11.008.
[71] S.S.R. Cloud-owen, Impact of cyclic voltammetry on mixed culture single chamber microbial fuel cell performance and anodic bacterial viability, The Pennsylvania State University, 2009.
[72] J. Heinze, A. Rasche, M. Pagels, B. Geschke, On the origin of the so-called nucleation loop during electropolymerization of conducting polymers, J. Phys. Chem. B. 111 (2007) 989–997. doi:10.1021/jp066413p.
[73] M. Zhou, V. Rang, J. Heinze, Electropolymerization of pyrrole and electrochemical study of polypyrrole 4. Electrochemical oxidation of non-conjugated pyrrole oligomers, Acta Chem. Scand. 53 (1999) 1059–1062. doi:10.3891/acta.chem.scand.53-1059.

Chapter 4

Gold Adsorption from Acidic Solutions using Functionalised CNT-Sorbents and their Electrochemical Regeneration in Neutral Solutions

.

Pending submission to Chemical Engineering Journal

4.1 Abstract

Acidic wastewater generated from e-waste leaching is rich in precious metals including gold, silver, palladium, and platinum. Adsorption is preferred technique for precious metal separation over other conventional methods (e.g., chemical precipitation and solvent extraction) due to its low chemical consumption and ease of operation. Carbon nanotubes (CNTs) have shown promise for gold adsorption due to their high specific surface area, high stability under acidic conditions and ability to be functionalised by different chemical moieties to enhance selective adsorption. In this study, we clearly demonstrated the effect of various functional groups on the sidewalls of multiwall carbon nanotubes (MWCNTs) on gold adsorption, and we introduced a chemical-free electrochemical technique for Au elution from MWCNTs. Pristine MWCNTs (P-MWCNTs), carboxylic functionalised MWCNTs (COOH-MWCNTs), and amide functionalised MWCNTs (NH_2-MWCNTs) of the same approximate lengths and diameters were compared for their affinity for Au adsorption from acidic (pH~1) $AuCl_4^-$ solutions mimicking acidic e-waste leachate. Au adsorption affinity onto MWCNTs followed the order of P-MWCNT > NH_2-MWCNT > COOH-MWCNTs. XPS supported the hypothesis that chemisorption was the dominant mechanism for Au adsorption by the functionalised MWCNTs, while a combination of physisorption and chemisorption governed adsorption of Au on P-MWCNTs. Au elution from Au-saturated MWCNTs was subsequently achieved using chemical-free electrochemical desorption in a neutral solution. Au-loaded MWCNTs were deposited on a PES membrane. The Au-MWCNTs membrane was used as an anode in an electrochemical cell to investigate Au electro-desorption using anodic oxidation. The Au electro-desorption was shown to have a direct relationship with both the applied current (ranging between 1 to 13 mA) and the mass of the Au absorbed on the MWCNTs

(ranging between 7.5 to 91.5 mg Au/g MWCNTs). This study demonstrated the effect of CNT chemical moieties on Au extraction from acidic wastewater. In addition, it demonstrated an environmentally friendly approach for the subsequent Au elution from the CNTs sorbents. This study will improve the utilization of functionalised CNT sorbents for gold separation and preconcentration from e-waste leachate with a minimal chemical consumption.

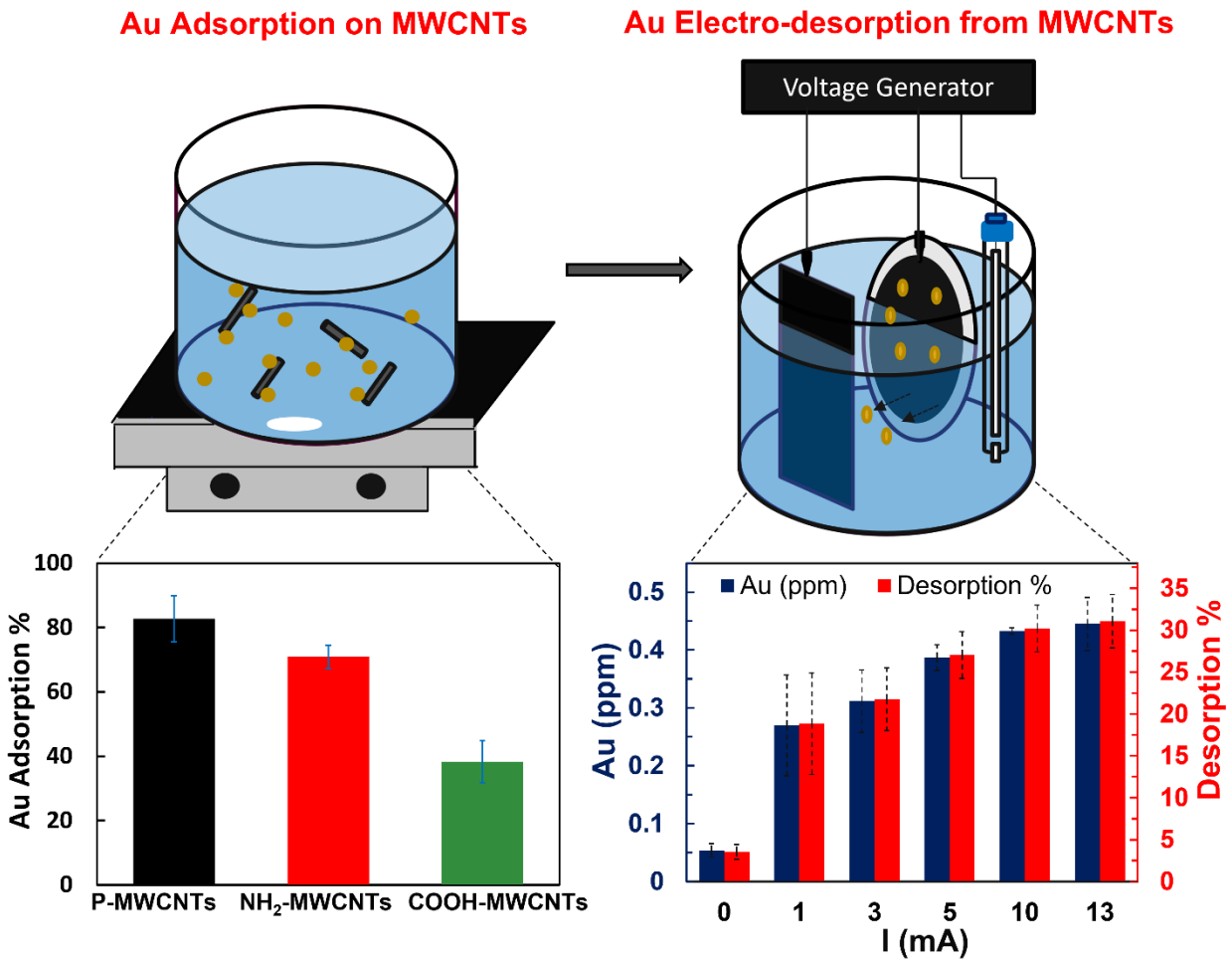

4.2 Introduction

The global e-waste generation rate averages around 50 million tons per year [1]. E-waste contains large amounts of base metals (e.g., iron, nickel, copper, zinc) as well as considerable amounts of precious metals (e.g., gold, silver, palladium) [2,3]. For example in 2016, 44.7 million tons of e-

waste were generated, of which only 20% was effectively recycled producing 71.2 tons gold, 3276 tons silver and 14 tons palladium [4]. Extracting precious metals (especially gold) is one of the major goals for e-waste recycling [5]. Aqua regia (a mixture of 3 parts concentrated hydrochloric acid and 1 part concentrated nitric acid) or hydrochloric acid containing chlorine gas (Cl_2/HCl) are usually used to leach gold from e-waste. Nevertheless, the other metals in the e-waste are also dissolved in the acidic solution resulting in a poor gold selectivity [5–8]. Thus, a subsequent process is required to extract the gold from the e-waste acidic lixiviant solution. Conventional recycling processes such as chemical precipitation and solvent extractio57n consume large amounts of reagents and have low metal selectivity [6,9]. Adsorption is a preferred technique for gold recycling due to the low chemical consumption, low space requirements, and ease of operation [8–10]. Due to its large surface area and high selectivity, activated carbon (AC) has been widely used in the last three decades as an adsorbent for selective gold removal from e-waste leachate [6,7,10–13]. However, the usage of AC is recently limited by its high price resulting from the depletion of coal reserves and the high energy required for its production [14,15]. Ion exchange resins have also shown promise for gold extraction due to their high loading capacity. However, resins are not commercially competitive with AC due to their lower selectivity and the swelling and entanglement problems that occur to the resins' polymer chains [5,16]. Biosorbents (e.g., chitosan beads, biopolymer composites, banana peels) have been demonstrated at the lab scale as gold adsorbents due to their low cost, high selectivity, and abundance [8,9,17,18]. Nevertheless, biosorbents scaling up is limited by their localized distribution and the variation in their production rate due to seasonal changes [19–21]. Recently, carbon nanotubes (CNTs) have been used as sorbents in gold separation and preconcentration due to their high specific surface

area, scalability, high mechanical and chemical stability, and enhanced specificity towards Au adsorption via functionalization by chemical moieties [6,12,22–27]. Pristine multiwall carbon nanotubes (P-MWCNTs) have shown promise for Au adsorption from acidic $AuCl_4^-$ solutions in the absence and presence of Cu ions [6]. Carboxylic functionalised MWCNTs (COOH-MWCNTs) have demonstrated a high selectivity for Au adsorption in acid solutions containing Zn, Cd, Mn and Pb [23]. Polysilsesquioxane functionalised CNTs (assumed to be MWCNTs) have shown higher selectivity for Au adsorption than other metals (i.e., Pt, Hg, Ag, Ni, Cu and Pb) in acidic wastewater [24]. High Au adsorption from acidic Au solutions was also demonstrated in the case of using triphosphonic acid modified MWCNTs sorbents [22]. To this end, pristine and functionalised CNTs were shown to be promising for gold extraction from acidic media. However, a systematic study to compare the effect of different functionalised CNTs on gold adsorption efficiency under the same experimental conditions has not been performed.

One of the major limitations for all sorbents is the process by which the adsorbed Au is removed to both recover Au and regenerate the sorbents. Strong acids or mixed reagents are used to recover Au from sorbents, which adds cost through chemical consumption, increases handling hazards, and contributes additional environmental challenges during disposal [25,28]. Au elution from adsorbents is efficiently achieved using thiourea including from biosorbents [8,9,17], activated carbons [10,29] and CNTs [12,22,25,30]. During this process, one Au atom is chelated between two sulfur atoms of two thiourea molecules [5]. While using thiourea for gold elution is highly effective, the process requires acidic conditions (pH 1.4-1.8). Hydrochloric acid or nitric acid are usually used to set the required pH, which adds cost through chemical consumption, increases handling hazards, and contributes additional environmental challenges during disposal

[5,8,25]. Unlike most biosorbents, CNTs and activated carbon are electrically conductive materials which enables their electrical regeneration. In contrast to activated carbon, CNTs can be easily made into temporary electrodes by depositing them onto porous substrates. Previously, we have demonstrated a chemical-free electrochemical regeneration approach for recovering Cu from electrically conductive CNTs. CNTs were used for Cu adsorption from an aqueous solution, then they were deposited on a microfiltration (MF) membrane to form a temporary electrode to electrochemically remove Cu and regenerate the CNTs [31]. Similar electrochemical technique is investigated for gold elution for the first time to achieve chemical-free regeneration.

In this study, we used CNTs as sorbents for Au adsorption from simulated acidic e-waste leachate and simultaneously recovered Au while regenerating these sorbents using our recently introduced chemical-free electrochemical technique. Our study aimed to fill two gaps presented in the literature: First, we systematically studied the effect of the most common CNT functional groups on gold adsorption under identical experimental conditions. P-MWCNTs, COOH-MWCNTs, and amide MWCNTs (NH_2-MWCNTs) of the same approximate length and diameter were compared for their affinity for Au adsorption from acidic (pH~1) $AuCl_4^-$ solutions simulating acidic e-waste leachate. Second, we explored gold elution from CNT sorbents using a novel electrochemical technique and identified the impact of Au concentration and applied current on Au recovery.

4.3 Materials and Methods

4.3.1 Materials

P-MWCNTs, COOH-MWCNTs and NH_2-MWCNTs (OD 17.5 nm, ID 9 nm, Length 5-20 μm, Purity >95%, consists of 9 concentric single wall CNTs) were purchased from NanoLab USA. According to the manufacturer, P-MWCNTs were produced by chemical vapor deposition (CVD), COOH-MWCNTs were produced by oxidizing the P-MWCNTs in H_2SO_4/HNO_3 reflux, and NH_2-NH-O-MWCNTs (which are notated as NH_2-MWCNTs for simplicity) were produced by the amidation of the COOH-MWCNTs using ethylene diamine. The MWCNTs fabrication process is shown in Figure S4.1. Hydrogen tetrachloroaurate (III) ($AuCl_4 \cdot H_3O$), salicylaldehyde reagent (2-hydroxy-1-naphaldhyde), sodium chloride (NaCl) and 1M hydrochloric acid (HCl) were purchased from Sigma Alderich Canada. Ortho-phenylenediamine and ethanol (C_2H_5OH) were purchased from Fisher Scientific Canada. MF polyethersulfone (PES) membranes (0.2 μm) were purchased from Sterlitech USA. Graphite electrodes (surface area of 56 cm^2) were purchased from McMaster-Carr Canada. All stock and buffer solutions were prepared in 0.05 μS/cm DI water from a Millipore system.

4.3.2 CNTs Characterization

The three types of MWCNTs used in this study (P-MWCNTs, COOH-MWCNTs and NH_2-MWCNTs) were characterized prior to the Au adsorption experiments to determine their chemical and physical properties. MWCNTs chemical compositions were determined using XPS analysis performed by PHI Quantera II Scanning XPS Microprobe. The XPS peaks were fitted using instrument built-in Multi Pack and CASA XPS software to determine the elemental atomic percentages. Surface charges of the MWCNTs in acidic media were determined by measuring the

Zeta potentials of the MWCNTs in 0.2 M HCl (pH~1) solution using a zeta potential analyzer (ZetaPlus, Brookhaven Instruments). Elemental analysis of the MWCNTs was done using Energy dispersive X-Ray (EDX) spectroscopy. MWCNTs' specific surface area (SSA) was measured using nitrogen adsorption-desorption isotherms performed by a physisorption instrument (Quantahrome iQ). The MWCNTs samples were degassed for 24 h at 105 ^{O}C prior to the SSA measurements. The SSA was measured using the Brunauer-Emmet-Teller (BET) equation:

$$\frac{1}{\left(\frac{P_O}{P}-1\right)W} = \frac{B-1}{B\,W_m}\left(\frac{P}{P_O}\right) + \frac{1}{B\,W_m} \qquad (4.1)$$

where W represents the weight of gas adsorbed at a given relative pressure (P/P_O) , B is a second parameter related to the adsorption heat, and W_m represents the weight of gas required to form a monolayer on the adsorbant surface which is used to calculate the SSA based on multipoint BET method.

4.3.3 Au Adsorption Experiments

5 mg of P-MWCNTs, COOH-MWCNTs and NH_2-MWCNTs were sonicated in DI water using a probe sonicator (Qsonica Q500) to form stable MWCNTs suspensions. Based on our previous study for Cu adsorption on CNTs, 30 min sonication time was selected as it represented an ideal trade-off between sufficient CNT dispersion and low oxidative damage of CNT sidewalls, which increased with increasing sonication time [31]. Immediately after the MWCNTs sonication, $HAuCl_4 \cdot 3H_2O$ in HCl solution was added to the MWCNTs solutions such that the final Au(III) concentration was 10 ppm, HCl concentration was 0.2 M, the total solution volume was 50 mL and the solution had pH~1. The Au-MWCNTs solutions were stirred at 400 RPM for 4 h to allow for Au adsorption on the MWCNTs (step 1 in Figure 4.1). Afterwards, the solution was filtered on 0.2 µm PES MF

membrane to separate the Au-MWCNTs complex from the treated solution (step 2 in Figure 4.1). The Au concentration of the treated solutions was measured to compare the affinities of different types of MWCNTs for Au adsorption in acidic media. Au Adsorption % was determined using the following equation:

$$\text{Au Adsorption } \% = \frac{C_i - C_f}{C_i} x100 \qquad (4.2)$$

where C_i and C_f are the initial and final Au concentrations, respectively. To determine the chemical states of the Au on the MWCNTs sorbents, the same procedures were repeated for the three types of MWCNTs (P-MWCNTs, COOH-MWCNTs and NH_2-MWCNTs). However, this time they were applied for adsorbing Au from 75 ppm Au(III) solution to produce highly Au saturated MWCNTs. These MWCNTs were then characterized using XPS. Au adsorption isotherm experiments were then conducted using different concentrations of Au solutions (1 ppm - 87.5 ppm) with a constant mass of NH_2-MWCNT sorbents (5 mg) for 24 h. The equilibrium adsorption capacity (q_e) was calculated using the following equation:

$$q_e = \frac{(C_i - C_e)\, V}{m} \qquad (4.3)$$

where C_e is the Au equilibrium concentration after 24 h, V is the volume of the Au solution (50 mL), and m is the mass of NH_2-MWCNT sorbents (5mg). Afterwards, the kinetics of Au adsorption was studied by taking samples (during 10 ppm Au(III) adsorption experiments onto 5 mg NH_2-MWCNTs) at different times (1, 2, 8, 18, 30, 60, 120, and 180 minutes) and measuring the Au Adsorption %. All the experiments in this section were repeated in at least duplicate.

4.3.4 Au Electro-desorption Experiments

A temporary membrane electrode was formed to desorb Au from the MWCNTs following the same methodology we detailed in our previous study for desorbing Cu from CNTs [31]. Briefly, Au-MWCNTs complex was pressure-deposited on 0.2 µm PES MF membrane (step 2 in Figure 4.1), which was then utilized as an anode in a three-electrode electrochemical cell to study the feasibility of Au desorption under electric field (step 3 in Figure 4.1). Graphite was used as a cathode in the electrochemical cell, Ag/AgCl was used as a reference electrode and 5 mM NaCl solution (Conductivity 0.5 mS/cm, V= 175 mL, pH= 5) was used as an electrolyte solution. The electrochemical cell inner diameter was 6 cm, and the electrolyte solution was stirred at 200 RPM to ensure uniform mixing. The electrode gap between the anode and cathode was maintained at 2 cm in all experiments. The electrochemical cell was connected to a potentiostat (Metrohm, Multi Autolab/M101) to investigate the electrochemical desorption of Au from MWCNTs. Au desorption was studied under varying applied currents (1 mA - 13 mA), and different masses of Au adsorbed on the MWCNTs (7.5 mg Au/ g MWCNTs - 91.5 mg Au/ g MWCNTs). All the experiments in this section were repeated in at least duplicate.

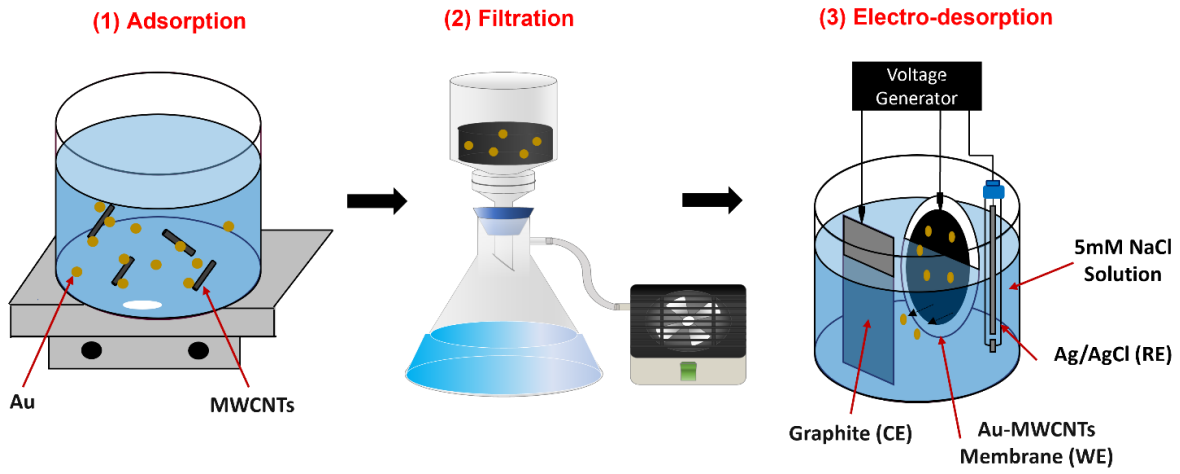

Figure 4. 1: Schematic approach for Au adsorption-electro-desorption process on MWCNTs.

4.3.5 Au Analysis

Au concentration was measured before and after the adsorption experiments using spectrophotometric methods which is less expensive than using other methods such as atomic absorption microscopy (AAS) or inductively coupled plasma-optical emission spectrometry (ICP-OES). A Schiff reagent (bis(salicylaldehyde) ortho-phenylenediamine (BSOPD)) was prepared in the laboratory by reacting a salicylaldehyde, 2-hydroxy-1-naphaldhyde with ortho-phenylenediamine, as described elsewhere [32,33]. BSOPD reacts with gold in acidic media to form a yellowish-brown complex which can be detected using UV-VIS spectrophotometer at (488 nm) wavelength. In our study, UV-VIS spectrophotometer (Tecan Spark 10 M) was used to quantify Au(III) concentration up to 30 ppm in a 0.2 M HCl solution. Figure S4.2a shows the Au(III) UV-VIS spectra with a detection limit 0.12 ppm, and Figure S4.2b illustrates the calibration curve relating the Au(III) concentration to the UV-VIS absorbance at (488 nm) wavelength. Anova regression analysis for the Au calibration curve is also shown in the SI. To confirm the validity of the UV-VIS spectrophotometry method for detecting gold, the Au adsorption capacity (q_e) on 5 mg NH_2-MWCNTs (for adsorption experiments using a 10 ppm Au(III) concentration allowed to achieve adsorption equilibrium over 24 h) was quantified using UV-VIS spectrophotometry and ICP-OES. Figure S4.3 shows values for q_e within 5% of each other using the two techniques.

Au concentration in the electrolyte solution after the electro-desorption experiments was detected using ICP-OES to avoid any possible interaction between the UV-VIS reagent (BOSBD) with (1) the NaCl present in the electrolyte solution or with (2) any electrochemical side product that may have been produced, which could overestimate the Au concentration in solution.

4.4 Results and discussions

4.4.1 CNTs Characterization

Prior to their usage in Au adsorption experiments, MWCNTs were characterized to determine their physical and chemical properties (i.e., chemical composition, electric charge, and specific surface area) that would impact Au adsorption. To determine the chemical composition of the MWCNTs used in this study, XPS analysis was performed on P-MWCNTs, COOH-MWCNTs and NH_2-MWCNTs. As shown in Figure 4.2a, C1s peaks were shown in the three types of MWCNTs, and a N1s peak was shown in case of NH_2-MWCNTs. Figure 4.2 a also shows a small intensity O1s peak in the P-MWCNTs and higher intensity O1s peaks in the COOH-MWCNTs and NH_2-MWCNTs. COOH-MWCNTs were produced by oxidizing P-MWCNTs, which means that they have a higher percentage of oxygen. NH_2-MWCNTs were produced through the amidation (i.e., reaction with ethylene diamine) of COOH-MWCNTs. During amidation, the COOH's hydroxyl group is replaced by an amide group, while COOH's carbonyl group does not participate in this process, as shown in Figure S4.1, which explains the presence of oxygen in the NH_2-MWCNTs. Further, perfect conversion of hydroxyl groups into NH_2 groups during the amidation process does not occur, leaving extra oxygen atoms on the NH_2-MWCNTs. Figure 4.2a also shows the oxygen Auger (O_{KLL}) peaks representing the energy emitted due to the Auger Effect, resulting from electrons falling from higher energy states to fill the electrons vacancies released by the X-ray scattering [34,35]. Due to their higher oxygen percent, the functionalised MWCNTs showed higher intensity O_{KLL} peaks compared to the P-MWCNTs. The XPS peaks were fitted to determine the elemental atomic percentages, as shown in Table S4.1. These percentages were used to calculate the atomic percentage of functional group presence in the functionalized MWCNTs. This showed that the

COOH groups occupy 6% of the COOH-MWCNTs' composition and that the NH_2 groups occupy 4.5% of the NH_2-MWCNTs' composition. The detailed calculations are shown in the SI.

To determine the electric charge of the MWCNTs under relevant acidic conditions to mimic electronic waste leachate, the zeta potentials of P-MWCNTs, COOH-MWCNTs and NH_2-MWCNTs were measured in 0.2 M HCl solution (pH ~1). Figure 4.2b shows that NH_2-MWCNTs have a higher positive zeta potential (13 mV) as compared to P-MWCNTs which were measured to only have a slight positive zeta potential (3 mV). COOH-MWCNTs have a negative zeta potential (-5 mV). NH_2 groups (having pK_a~10.5-10.7) and NH groups (having pK_a~10-10.2) protonated in acidic conditions, resulted in an overall positive charge on the NH_2-MWCNTs [36,37]. COOH groups (having pKa ~ 5) should have a neutral charge in acidic conditions, however a negative charge was observed on the COOH-MWCNTs due to the partial ionization of the COOH groups into COO^- [38,39]. P-MWCNTs showed a slight positive zeta potential, which may be caused by the adsorbed H^+ protons on the CNTs in the acidic media [39].

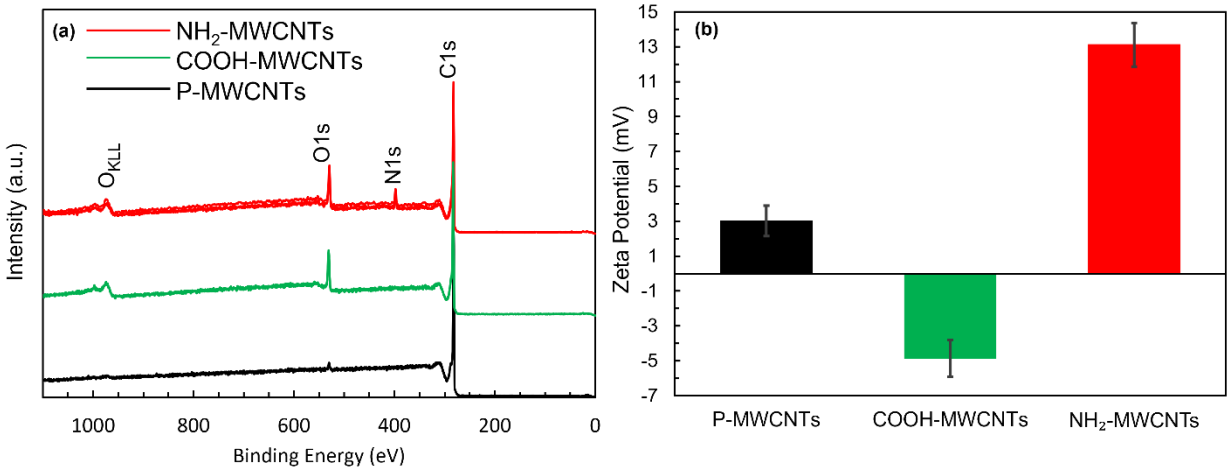

Figure 4. 2: (a) XPS survey spectrum for P-MWCNTs, COOH-MWCNTs and NH_2-MWCNTs (collected at three different locations for each sample). (b) zeta potentials of P-MWCNTs,

COOH-MWCNTs and NH_2-MWCNTs measured in 0.2 M HCl solution (pH~1). Error bars represent the calculated propagated error of standard deviations from repeated experiments.

A semi-quantitative elemental analysis was performed for the MWCNTs using EDS to identify impurities that might affect Au adsorption, especially for the elements present outside the range studied in the XPS analysis. As shown in Figure S4.4, iron and sulfur concentrations were negligible in the three types of MWCNTs (P-MWCNTs, COOH-MWCNTs and NH_2-MWCNTs). On the other hand, impurities from magnesium (which appears at binding energy 1300-1320 eV on XPS; outside the studied range in our XPS analysis) were significant in all three types of MWCNTs. However, we hypothesize that Mg impurities will not affect Au adsorption onto MWCNTs. According to the Hard and Soft (Lewis) Acids and Bases (HSAB) theory, hard acids should interact with hard bases and soft acids should interact with soft bases [40,41]. Mg is considered a hard acid and Au is regarded as a soft acid thus interaction is likely to be unfavorable.

BET analysis was performed to determine the specific surface are (SSA) of the MWCNTs used in this study. Figure 4.3 shows the N_2 adsorption isotherms for P-MWCNTs, COOH-MWCNTs and NH_2-MWCNTs. The adsorption isotherms of the three types of MWCNTs showed mesoporous structures, indicating existence of abundant mesopores ranging between 2–50 nm [42,43]. SSAs of the MWCNTs were calculated from the isotherms using the BET multipoint method, showing 203.02 m^2/g for P-MWCNTs, 194.23 m^2/g for COOH-MWCNTs, and 91.14 m^2/g for NH_2-MWCNTs. The decrease in CNTs SSA upon functionalization has been illustrated in previous studies. Xu et al. showed that the SSA of COOH functionalised CNTs was drastically decreased upon further functionalization with polysilsesquioxane [24]. Chakraborty et al. have also demonstrated a significant decrease in SWCNTs SSA after functionalization with different alkyl halides [44]. In our

study, the NH_2-MWCNTs have only 4.5% NH_2 functional groups (as shown from the XPS analysis) which should not significantly decrease the SSA. However, MWCNTs used in this study were composed of 9 rolled graphitic sheets with an average 17.5 nm OD and 9.0 nm ID (as detailed by the manufacturer). Therefore, the thickness of each graphitic sheet was calculated to be 0.53 nm. The ratio of the surface area of the outer graphitic sheet (π.OD.L) to the total surface area of the MWCNTs sheets (π.$(\sum_{n=0}^{n=8} ID + 0.53 * 2 * n)$.L) was calculated to be 14.7%, which was assumed to be the same ratio for the carbon atoms in the outer sheet to the total carbon atoms in the MWCNTs. Taking into consideration that the functional groups are only formed on the outer graphitic surface, ~30% (4.5/14.7%) of the carbon atoms in the outer layer should be functionalised with NH_2 groups. Most of the accessible adsorption sites for adsorbates in solution should be on the outer layer of the MWCNTs, indicating that the 55% reduction in the NH_2-MWCNTs SSA measured by N_2 adsorption is reasonable, especially when considering the bending and stretching vibrations occurring to the functional groups which will increase the total inaccessible surface area of the MWCNTs to N_2 adsorption.

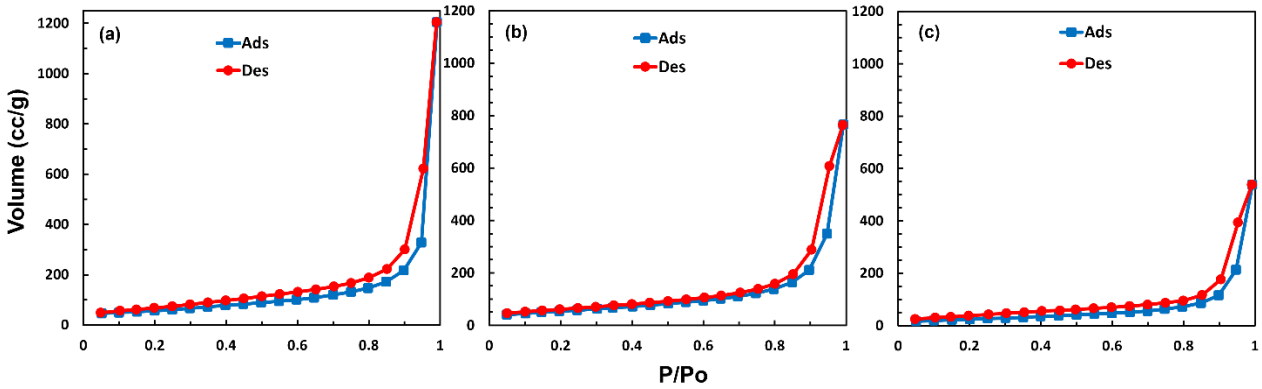

Figure 4. 3: Nitrogen adsorption–desorption isotherms for (a) P-MWCNTs, (b)COOH-MWCNTs and (c) NH_2-MWCNTs

4.4.2 Adsorption Experiments

The adsorption affinities of P-MWCNTs, COOH-MWCNTs and NH2-MWCNTs for Au from 10 ppm Au(III) acidic solutions (pH~1) were compared. As shown in Figure 4.4a, P-MWCNTs have shown the highest Au adsorption ($83 \pm 7\%$), followed by NH_2-MWCNTs which have shown ($71 \pm 3.5\%$) Au adsorption, while COOH-MWCNTs demonstrated the lowest Au adsorption ($38 \pm 6.5\%$). At acidic conditions (pH~1), Au(III) is speciated to $AuCl_4^-$ [45]. Since COOH-MWCNTs are negatively charged at pH~1 (as shown in Figure 4.2 b); they repelled $AuCl_4^-$ ions, decreasing their overall adsorption ability. NH_2-MWCNTs which are positively charged at pH~1, should have a high electrostatic attraction for $AuCl_4^-$ ions. As a result, NH_2-MWCNTs have a higher Au adsorption affinity compared to COOH-MWCNTs. Although P-MWCNTs have a lower positive charge compared to NH_2-MWCNTs (as shown in Figure 4.2 b), they were shown to have a higher Au adsorption in comparison with NH_2-MWCNTs. We hypothesize that the higher SSA in the case of P-MWCNTs (203.02 m^2/g) in comparison to NH_2-MWCNTs (91.14 m^2/g) allowed for more adsorption sites, increasing the overall Au adsorption. These results indicated a trade-off between the effect of electric charge and SSA on Au adsorption onto MWCNTs.

To determine Au adsorption mechanisms onto the three types of MWCNTs used in this study, high-resolution Au(4f) XPS analysis was performed on Au-loaded MWCNTs (Figure 4.4b). The XPS analysis was done on three different locations on each sample, where each curve shown in Figure 4.4b represents one analyzed location. In the case of Au-loaded COOH-MWCNTs, two peaks were shown at binding energies of 83.96 eV and 87.63 eV corresponding to Au(0) peaks [6,46], indicating the complete reduction of Au(III) to Au(0) onto the COOH-MWCNTs. In the case of Au-loaded NH_2-MWCNTs, two significant peaks for Au(0) were also shown at binding energies of

83.96 eV and 87.63 eV, together with very small peaks of Au(X) at a binding energy of 89.87 eV, where Au(X) could be either Au(I) or Au(III) [24,46,47]. These results also indicate that most of Au(III) that adsorbed on NH_2-MWCNTs was reduced to Au(0). Thus, the XPS analysis indicated that chemisorption was the dominant mechanism for Au(III) adsorption on the functionalised MWCNTs. Indeed, amide and hydroxyl groups have high affinities for Au reduction as follows [8,17]:

$$AuCl_4^- + 3R\text{-}NH_3^+ \rightarrow Au^o + 3\ R\text{-}NH_2 + 3H^+ + 4Cl^- \qquad (4.4)$$

$$AuCl_4^- + 3R\text{-}OH \rightarrow Au^o + 3\ R{=}O + 3H^+ + 4Cl^- \qquad (4.5)$$

In the case of P-MWCNTs, two significant Au(0) peaks were also shown at binding energies of 83.96 eV and 87.63 eV, together with two other major peaks for Au(X) at binding energies of 86.16 eV and 89.87 eV [24,46,47]. This indicates that both chemisorption of Au(III) reduced to Au(0) or Au(I) and physisorption of Au(III) likely occurred onto P-MWCNTs . Delocalized π electrons on P-MWCNTs can reduce Au(III) to Au(I) (Eq. 4.6) or Au(0) (Eq. 4.7), but their reducing strength is not as great as that of the functional groups on functionalised MWCNTs, evident by the presence of Au(X) peaks.

$$AuCl_4^- + 2e^- \rightarrow AuCl_2^- + 2Cl^- \qquad (4.6)$$

$$AuCl_4^- + 3e^- \rightarrow Au^o + 4Cl^- \qquad (4.7)$$

The percentages of Au(0) and Au (X) from the total Au adsorbed on P-MWCNTs were determined by calculating their peak areas .Based on the calculated peak areas, the average amount Au(X) adsorbed on P-MWCNTs was (58.35%) in comparison with (41.65%) for Au(0). An example for the

peak fitting analysis for one of the three P-MWCNTs XPS curves is shown in Figure 4.4c, and the analysis for the other two curves are shown in Figure S4.5 and Figure S4.6.

Survey XPS spectrum analysis for the Au-loaded MWCNTs were also performed, as shown in Figure S4.7. The XPS peaks were fitted to determine the atomic percent of the elements, as shown in Table S4.2. The highest Au atomic percent (0.53%) was shown on P-MWCNTs, followed by (0.46%) Au atomic percent on NH_2-MWCNTs, and (0.15%) Au atomic percent on COOH-MWCNTs. These results further confirm that P-MWCNTs have the highest Au adsorption affinity, followed by NH_2-MWCNTs, while COOH-MWCNTs have the lowest Au adsorption capacity. Table S4.2 also shows the absence of chloride on COOH-MWCNTs, validating the complete reduction of $\mathrm{AuCl_4^-}$ into Au(0). While significant chloride (1.44%) was shown on P-MWCNTs, confirming the incomplete reduction of $\mathrm{AuCl_4^-}$ into Au(0) onto the P-MWCNTs. In the case of NH_2-MWCNTs, a lower chloride percent (0.34%) was shown, proving that the majority of $\mathrm{AuCl_4^-}$ was reduced to Au(0) onto the NH_2-MWCNTs.

Au(I) or Au (III) XPS peaks have close binding energies [24,46,47], thus it is difficult to differentiate between them. To determine the valency of Au(X) ions on the P-MWCNTs, the chloride atomic percent on the P-MWCNTs (1.44%) (Table S4.2) was divided by the Au(X) atomic percent (which is the product of the Au(X) percentage calculated from the peak fitting (58.35%) and the total Au atomic percent adsorbed on the P-MWCNTs (0.53%) (Table S4.2)). The Cl/Au(X) atomic ratio was >4 (calculated to be ~4.6), indicating that the Au(X) corresponds to Au(III) ($\mathrm{AuCl_4^-}$) peaks which has an atomic Cl:Au ratio of 4:1. These results suggest the absence of partial reduction of Au(III) ($\mathrm{AuCl_4^-}$) into Au(I) ($\mathrm{AuCl_2^-}$) onto the P-MWCNTs. The Au species on P-MWCNTs were

therefore either adsorbed as Au(III) through physisorption (~58.35%), or completely reduced to Au(0) through chemisorption (~41.65%).

After the adsorption experiment, the Au-loaded MWCNTs were filtered on PES membranes to be used as temporary electrodes for gold electro-desorption (step 2 in Figure 4.1). However, it was shown that the P-MWCNTs (having the highest Au adsorption) did not form a uniform surface on the PES membrane in comparison with the NH_2-MWCNTs, and COOH-MWCNTs, as shown in Figure 4.4d, Figure 4.4e, and Figure 4.4f. The presence of charged functional groups decreases the attraction of MWCNTs for each other, enabling their greater dispersibility in aqueous solutions. Therefore, they formed more uniform surfaces upon filtering on the PES membranes in comparison with P-MWCNTs. The non-uniformity of P-MWCNTs hindered electron transfer when used as electrodes. NH_2-MWCNTs were thus deemed to be the optimal adsorbents for Au adsorption-electro-desorption since they have considerable Au adsorption while also producing a uniform and electrically conductive temporary electrode on the membrane substrate. As such, NH_2-MWCNTs were used in all subsequent experiments throughout.

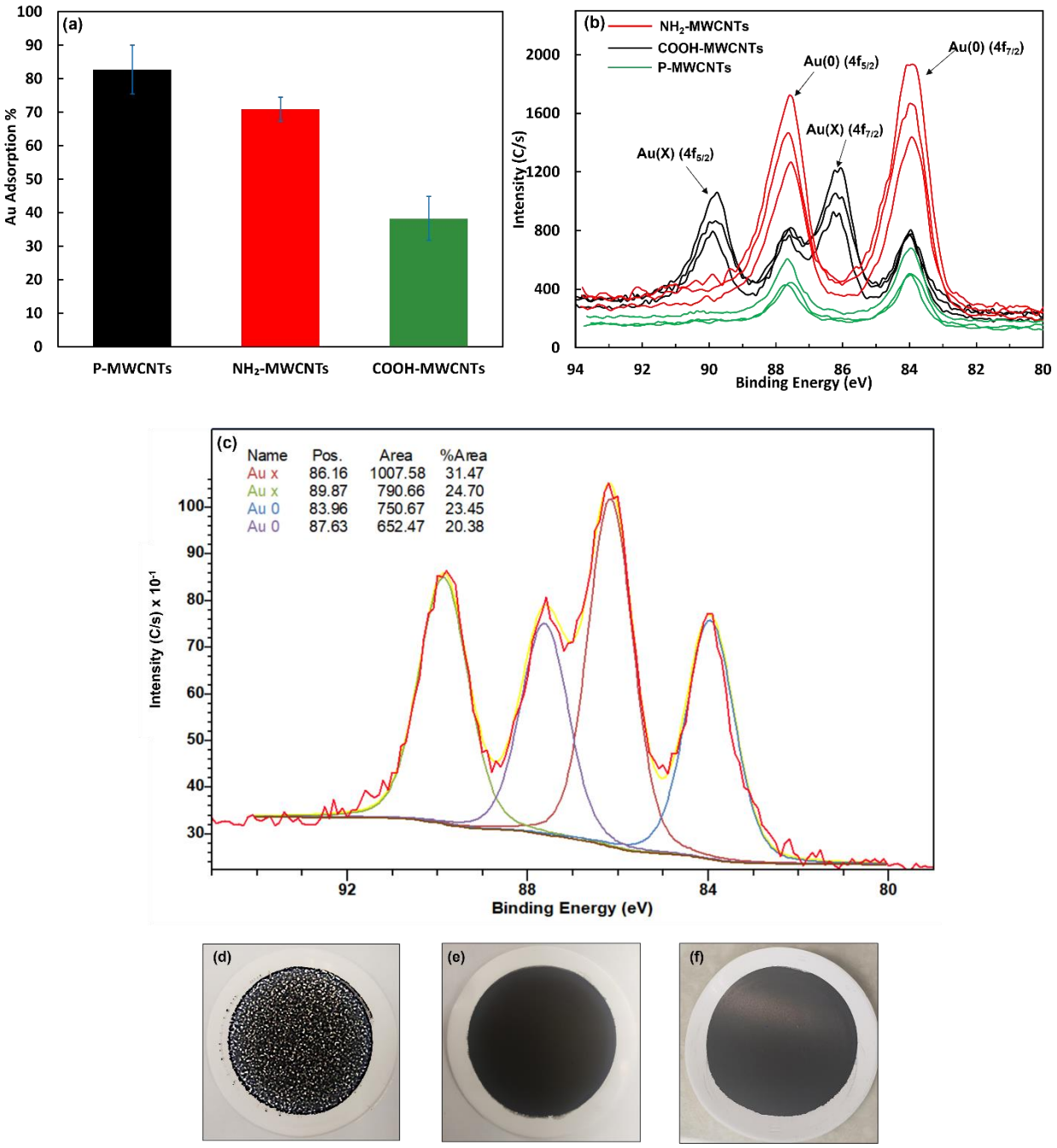

Figure 4. 4: (a) Au adsorption onto MWCNTs from 10 ppm Au(III) acidic solutions (pH~1). (b) Au 4f high resolution XPS spectrum for MWCNTs (collected at three different locations for each sample). (c) Peak fitting analysis for the middle XPS curve of the P-MWCNTs using CASA XPS software, red curve represents the original XPS curve, and the yellow curve represents the fitting curve. Digital images for 5 mg (d) P-MWCNTs , (e) NH_2-MWCNTs , and (f) COOH-MWCNTs deposited on PES membranes.

Adsorption isotherms were performed using a fixed mass of NH_2-MWCNTs (5 mg) while varying the Au(III) initial concentration between (1-87.5 ppm). The adsorption isotherm showed a direct relation between the Au adsorption capacity (q_e) and the Au equilibrium concentration (C_e), as shown in Figure 4.5a. The isotherm data was modelled using the linearized forms of the Langmuir equation (Eq. 4.8) and the Freundlich equation (Eq. 4.9).

$$\frac{C_e}{q_e} = \frac{C_e}{q_{max}} + \frac{1}{K_L \ q_{max}} \qquad (4.8)$$

$$\log q_e = \frac{1}{\mathrm{n}} \log C_e + \log K_F \qquad (4.9)$$

where q_{max} (mg Au/ g MWCNTs) represents the maximum Au adsorption capacity on the NH_2-MWCNTs, K_L is Langmuir constant, K_F is Freundlich constant and n represents the adsorption intensity. Figure 4.5c and Figure 4.5d show the adsorption isotherm data fitted with Langmuir and Freundlich models, respectively. Since the R^2 value for Langmuir model (0.9506) was closer to unity than the R^2 value for Freundlich model (0.9126), the Langmuir model was considered more appropriate to describe the Au adsorption behavior onto NH_2-MWCNTs. This result predicted a monolayer Au adsorption on NH_2-MWCNTs in agreement with other studies in the literature which indicated a monolayer of Au adsorbed on MWCNTs [6,22–24]. The maximum Au Adsorption Capacity (q_{mFax}) was calculated from the slope of the Langmuir equation to be (138.9 mg Au/ g NH_2-MWCNTs). Anova regression analysis for the Langmuir model is also shown in the SI. The Kinetics of Au adsorption on NH_2-MWCNTs were studied by measuring Au Adsorption % in different time intervals during 10 ppm Au(III) adsorption experiments, as shown in Figure 4.5b.

71.5% Au Adsorption was achieved in the first 1 minute and quickly plateaued at 77% Au adsorption after 1h. These results indicated very fast kinetics for Au adsorption on NH_2-MWCNTs.

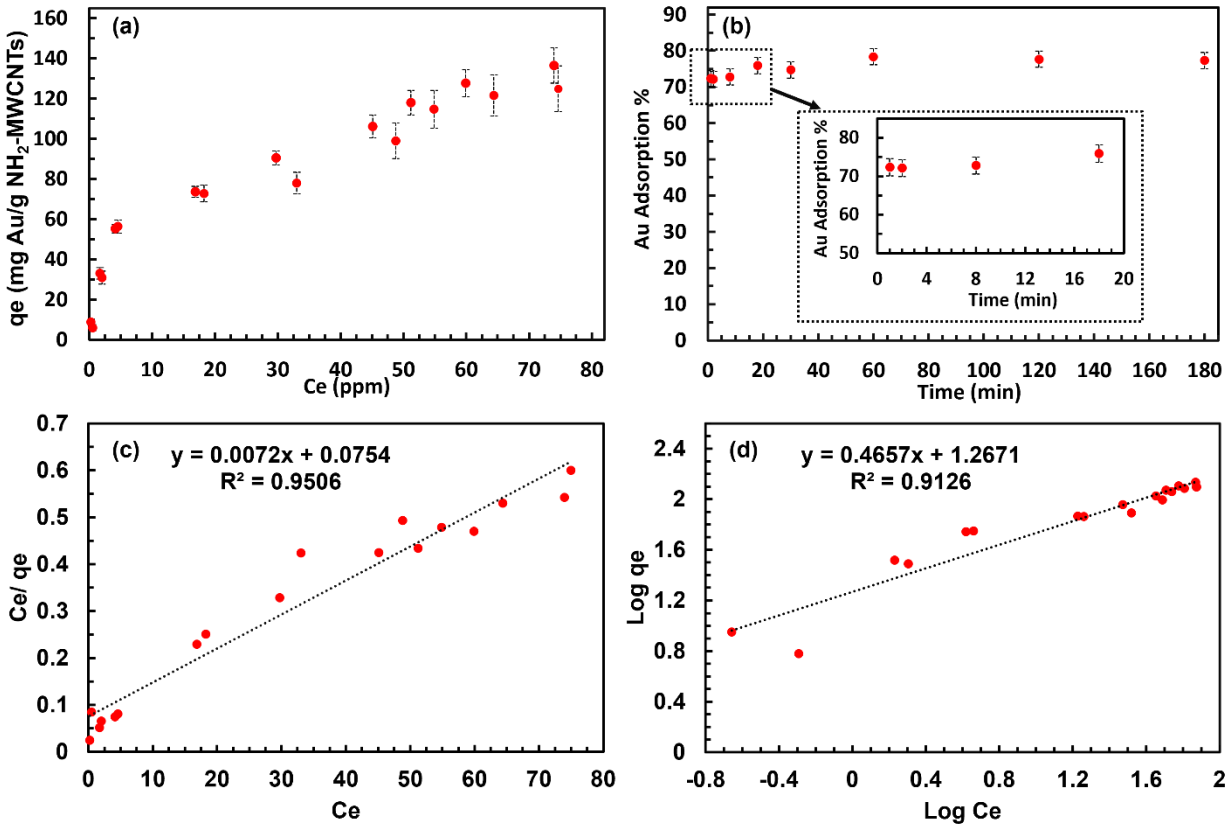

Figure 4. 5: (a) Au adsorption isotherm constructed using a fixed mass of NH_2-MWCNTs (5mg) while varying the Au(III) initial concentration between (1-87.5 ppm). (b) Au adsorption kinetics on 5 mg NH_2-MWCNTs in a 10 ppm Au(III) solution. Isotherm data fitted using (c) Langmuir equation and (d) Freundlich equation. Error bars represent the calculated propagated error of standard deviations from repeated experiments.

4.4.3 Electro-desorption Experiments

Previous studies have shown the efficient Au elution from CNTs using thiourea [12,22,25,30], nevertheless the occurrence of thiourea elution requires strongly acidic conditions which are expensive to operate and are not environmentally sustainable [5,8,25]. Therefore, we sought to develop a Au elution technique using a chemical-free process in neutral solutions. We

investigated Au elution from MWCNTs through electro-desorption in neutral NaCl electrolyte solution. Au is known to be inert for electrical oxidation at neutral conditions; therefore gold is often used as an inert electrode in many anodic applications [48–50]. However, in the presence of chloride in the electrolyte solution, anodic corrosion of Au electrodes occurs [51,52]. Chloride acts as a ligand that can react with Au ions that are produced by anodic oxidation and can thus enable Au to be dissolved in solution. This behavior resembles Au dissolution using aqua regia, where HNO_3 oxidizes the Au into Au(III) ions, and HCl provides the chloride ligands to react with Au(III) ions to form aqueous species ($AuCl_4^-$) [5], as follows:

$$Au + HNO_3 + 4HCl \rightarrow AuCl_4^- + NO + H_3O^+ + H_2O \qquad (4.10)$$

In this study, we utilize the concept of Au anodic corrosion in the presence of chloride ligands for Au elution from MWCNTs. Following the adsorption process (step 1 in Figure 4.1), Au-loaded NH_2-MWCNTs (50 ± 6 mg Au/ g NH_2-MWCNTs) were deposited on a PES membrane (step 2 in Figure 4.1). The Au-NH_2-MWCNTs membrane was used as anode in an electrochemical cell (step 3 in Figure 4.1) to investigate Au desorption using anodic oxidation. A 5mM NaCl aqueous solution with an initial conductivity (0.5 mS/cm), an initial pH (5) and a total volume (175 mL) was used as an electrolyte solution for these experiments. Preliminary calculations have shown that the molar ratio of Cl^- ions (in the electrolyte solution) to the Au (adsorbed on the NH_2-MWCNTs) approaches Cl:Au = 645:1, which indicates the availability of adequate chloride ligands to react with Au on the NH_2-MWCNTs. Figure 4.6a illustrates the effect of applied current on Au desorption from NH_2-MWCNTs. After 1 h of zero applied current, low concentration of Au was desorbed in the electrolyte solution (0.05 ppm) which is equivalent to (3.5%) Au desorption from the original mass of Au adsorbed. This low Au desorption percent is believed to be the loosely attached (i.e.,

physiosorbed) Au to the NH_2-MWCNTs. Applying 1 mA for 1 h resulted in Au ions desorption in the electrolyte solution with Au concentration (0.27 ppm) which is equivalent to (19%) Au desorption from the original mass of Au adsorbed. Applying 1 mA resulted in 1.5 V vs. Ag/AgCl at the Au-NH_2-MWCNTs membrane anode (as shown in Table S4.3) which exceeded the Au/$AuCl_4^-$ oxidation potential (0.8 V vs. Ag/AgCl). It is hypothesized that the Au that was originally adsorbed by reduction on the NH_2-MWCNTs (as indicated by the XPS analysis) was desorbed by anodic oxidation by inducing electric potential greater than Au/ $AuCl_4^-$ oxidation potential in the presence of chloride ligands. This result demonstrated the feasibility of Au electrochemical elution from CNTs. The Au-NH_2-MWCNTs membrane electrode used for this study was loaded with an average of 50 mg Au/g NH_2-MWCNTs (0.25 mg Au/ 5 mg NH_2-MWCNTs). Using the molecular weight of Au and Avogadro's number, the number of Au atoms on the electrodes was calculated to be 7.64×10^{17}. Knowing that each Au atom requires 3 electrons for oxidation, the complete Au oxidation will require 2.29×10^{18} electrons. Applying 1 mA will provide 6.242×10^{15} electrons per second, indicating that enough electrons are provided for complete Au oxidation. Nevertheless, electrons are also consumed by ohmic losses in the wires and connections attached to the electrodes [53], the charge transfer resistance at the solid/liquid interface [54], and through water electrolysis reactions (where the oxygen evolution reaction (OER) theoretically occurs at 0.62 V vs. Ag/AgCl in comparison with 0.8 V vs. Ag/AgCl for Au/$AuCl_4^-$) [55]. Figure 4.6a also shows that Au desorption increased by increasing the applied current from 1 mA to 13 mA. Increasing the applied current increased the desorbed Au concentration from 0.27 ppm (19% Au desorption) to a maximum of 0.45 ppm (31% Au desorption). This relationship between Au desorption and applied current indicates that a

greater current, induced by a higher electric potential, increases the energy available for redox reactions. This study provides a proof-of-concept for implementation in large-scale applications with larger power generators, where higher applied currents can be used to increase Au desorption.

The pH of the electrolyte solution was altered variously by different magnitude of applied currents. At applied currents below 10 mA, the pH of the electrolyte solution was not significantly changed from the initial electrolyte pH (pH~5), as shown in Table S4.3. However, at 10 mA and 13 mA applied currents, the pH of the electrolyte solution increased above neutral pH (pH~8). At a pH below 6, Au speciates to $AuCl_4^-$ in solutions containing chloride ions. Whereas at a pH ranging between 6 and 8.5 Au speciates to $AuCl_3(OH)^-$ [45]. To study the effect of the different Au speciation forms in the electrolyte solution on Au electro-desorption, the pH of the electrolyte solution was controlled between 5-6 (by titrating the solution with non-interfering 0.2 M HCl solution) during the electrochemical desorption experiments at 10 mA and 13 mA applied currents. The Au desorption in the pH controlled experiments did not show a significant change from the uncontrolled experiments (see Figure S4.8), suggesting that Au electro-desorption is not affected by the different forms of Au speciation in electrolyte solutions that exist in pH between 5-8.

Figure 4.6b shows the correlation between the initial mass of Au adsorbed on the NH_2-MWCNTs and the Au desorbed under 10 mA applied current for 1h. Increasing the Au mass from 7.5 ± 1.5 mg Au/g NH_2-MWCNTs to 50.0 ± 6.0 mg Au/g NH_2-MWCNTs, increased the Au desorbed concentration in the electrolyte from 0.14 ppm to 0.43 ppm. While increasing the Au mass from

50.0 ± 6.0 mg Au/g NH_2-MWCNTs to 91.5 ± 9.5 mg Au/g NH_2-MWCNTs, increased the Au concentration in the electrolyte from 0.43 ppm to 0.87 ppm. These results indicated a direct relationship between the mass of Au adsorbed on the MWCNTs and the Au desorbed. Increasing the mass of gold on the MWCNTs is hypothesized to increase the probability of the interaction between the flowing electrons and the Au atoms, favoring more Au oxidation in the solution. While the desorbed Au concentration increased with greater adsorbed Au on the NH_2-MWCNTs, the total desorption percent decreased with increasing initial adsorbed Au. Au desorption percent was the highest in the case of 7.5 ± 1.5 mg Au/g NH_2-MWCNTs (65%) and decayed to (31%) in the case of 50.0 ± 6.0 mg Au/g NH_2-MWCNTs and to (33%) in the case of 91.5 ± 9.5 mg Au/g NH_2-MWCNTs, as shown in Figure 4.6b.

The pH of initial electrolyte solution (pH_i~5) was altered by the mass of Au adsorbed onto the NH_2-MWCNTs. For the cases of 7.5 ± 1.5 mg Au/g NH_2-MWCNTs and 50.0 ± 6.0 mg Au/g NH_2-MWCNTs, the final solution pH was 8. For the case of 91.5 ± 9.5 mg Au/g NH_2-MWCNTs, the final solution pH was 6.9 (as shown in Table S4.4). The smaller increase in the electrolyte pH with increasing Au mass can be related to the increased gold redox reactions. These gold redox reactions may have competed with water electrolysis reactions, buffering the electrolyte by consuming hydroxide ions as they were produced.

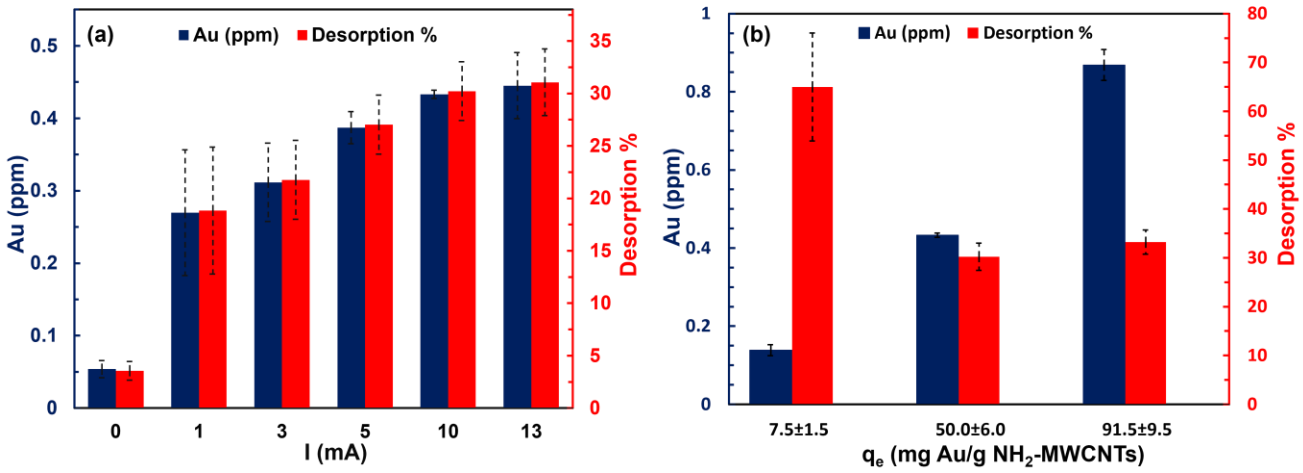

Figure 4. 6: (a) Effect of applied current on Au electro-desorption from NH_2-MWCNTs loaded with 50±6 mg Au/ g NH_2-MWCNTs, (b) Effect of Au mass adsorbed on Au electro-desorption from NH_2-MWCNTs at 10 mA applied current, for 1h electrochemical experiments. Error bars represent the calculated propagated error of standard deviations from repeated experiments.

Cyclic voltammetry (CV) curves were obtained for Au-NH_2-MWCNTs membrane electrodes loaded with different masses of Au (50±6 mg Au/ g MWCNTs, and 91.5±9.5 mg Au/ g MWCNTs) between 0-3 V at 10 mV/s scan rate, as shown in Figure S4.9a and Figure S4.9b. The electrolyte used for these experiments was NaCl solution having a higher conductivity (5 mS/cm) than that used for the previous electro-desorption experiments (0.5 mS/cm) to increase the ionic strength to limit analyte transport by migration [56]. No stirring was applied during the experiments to limit analyte transport by convection [56]. The CV curves showed broad concavities between 0.5-0.8V (see Figure S4.9a and Figure S4.9b), however these concavities can not be confirmed as clear Au oxidation peaks. In our previous study for chlorine reduction on CNTs membranes electrodes, we realized that there was an absence of reduction peaks on the CV curves at 100 and 500 ppm chlorine concentrations in the electrolyte solution even though chlorine reduction was confirmed by FTIR analysis [57]. To understand this behavior, we performed CV control experiments in 60

ppm Au solution using a bare NH_2-MWCNTs membrane electrode and a titanium dioxide electrode (see Figure S4.9c and Figure S4.9d). No clear peaks were shown in the case of the bare NH_2-MWCNTs membrane electrode (Figure S4.9c) although Au was visibly reduced to its elemental state (a yellow metallic sheen) and deposited on the bare NH_2-MWCNTs membrane electrode after the CV experiments (Figure S4.9e and Figure S4.9f). In contrast, use of the titanium dioxide electrode presented clear Au oxidation and reduction peaks at 1 V and 0.93 V respectively (Figure S4.9d). This behavior may be the result of the lower induced current at the CNT membranes in comparison with other more conductive electrodes. The temporary electrode formed from CNTs likely was insufficiently conductive and only presented small redox peaks that were poorly visible in CV curves. To this end, we hypothesize that Au was desorbed from the Au-NH_2-MWCNTs electrodes in this study via electrochemical oxidation. This hypothesis was based on the XPS results (Figure 4.4b) that showed that the vast majority of Au was originally adsorbed by chemical reduction on the NH_2-MWCNTs. Nevertheless, the low current intensity induced at the Au-NH_2-MWCNTs membranes electrodes did not clarify the Au oxidation peaks on the CV curves.

This section demonstrated the feasibility of gold electro-desorption from MWCNTs via anodic oxidation in a low concentration NaCl electrolyte solution. These results open new avenues for gold elution from sorbents using environmentally friendly electrochemical techniques instead of the conventionally used gold elution methods which have high acidic consumption.

4.5 Conclusion

In this study, we investigated novel MWCNTs sorbents for Au adsorption from acidic media and their electrochemical regeneration in neutral solutions. This process enables downstream

resource recovery of precious metals, turning an environmental pollutant into a valuable resource with minimal chemical consumption. In the first part of the study, we presented a clear demonstration for the effect of functional groups attached to the CNTs on gold adsorption under the same experimental conditions. P-MWCNTs, COOH-MWCNTs, and NH_2-MWCNTs having the same ranges of length and diameter were compared for their affinity for Au adsorption from $AuCl_4^-$ acidic solutions. The results indicated a trade-off between the effect of electric charge and SSA on Au adsorption onto MWCNTs. Negatively charged MWCNTs have a negative effect on Au adsorption from acidic solutions regardless of their SSA. In contrast, for positively charged MWCNTs, the SSA area has a more dominant effect on Au adsorption than the magnitude of the strength of the surface charge groups. In the second part of the study, we demonstrated for the first time the feasibility of electrochemical gold elution from graphitic sorbents in neutral solutions with low Cl^- concentrations by applying sufficiently high currents (>1 mA) to the sorbent. The Au electro-desorption showed a direct relationship with the applied current and the mass of Au adsorbed on the MWCNTs sorbents. The mechanism for Au electrodesorption from MWCNTs is believed to be Au electrochemical oxidation reactions. This study demonstrated the effect of CNTs' functional groups on Au extraction from acidic solutions, which can enhance the efficiency of CNTs sorbents for Au separation from acidic wastewater (e.g., e-waste leachate). Additionally, it introduced an electrochemical approach for the subsequent Au desorption from the CNTs sorbents, which opens new avenues for environmentally friendly Au elution from graphitic sorbents.

4.6 Acknowledgements

The authors thank the support of the Natural Sciences and Engineering Research Council of Canada (NSERC, Discovery Grant).

4.7 References

[1] A. Yoshida, A. Terazono, F.C. Ballesteros, D.Q. Nguyen, S. Sukandar, M. Kojima, S. Sakata, E-waste recycling processes in Indonesia, the Philippines, and Vietnam: A case study of cathode ray tube TVs and monitors, Resour. Conserv. Recycl. 106 (2016) 48–58. doi:10.1016/j.resconrec.2015.10.020.

[2] Y. Barrueto, P. Hernández, Y.P. Jiménez, J. Morales, Properties and application of ionic liquids in leaching base/precious metals from e-waste. A review., Hydrometallurgy. 212 (2022) 105895. doi:10.1016/j.hydromet.2022.105895.

[3] A. Islam, T. Ahmed, M.R. Awual, A. Rahman, M. Sultana, A.A. Aziz, M.U. Monir, S.H. Teo, M. Hasan, Advances in sustainable approaches to recover metals from e-waste-A review, J. Clean. Prod. 244 (2020) 118815. doi:10.1016/j.jclepro.2019.118815.

[4] Y. Ding, S. Zhang, B. Liu, H. Zheng, C. chi Chang, C. Ekberg, Recovery of precious metals from electronic waste and spent catalysts: A review, Resour. Conserv. Recycl. 141 (2019) 284–298. doi:10.1016/j.resconrec.2018.10.041.

[5] H. Salimi, Extraction and Recovery of Gold from both Primary and Secondary Sources by Employing A Simultaneous Leaching and Solvent Extraction Technique and Gold Leaching In Acidified Organic Solvents, University of Saskatchewan, 2017.

[6] S.K. Pang, K.C. Yung, Prerequisites for achieving gold adsorption by multiwalled carbon nanotubes in gold recovery, Chem. Eng. Sci. 107 (2014) 58–65. doi:10.1016/j.ces.2013.11.026.

[7] F. Wang, J. Zhao, M. Zhu, J. Yu, Y.S. Hu, H. Liu, Selective adsorption-deposition of gold nanoparticles onto monodispersed hydrothermal carbon spherules: A reduction-deposition coupled mechanism, J. Mater. Chem. A. 3 (2015) 1666–1674. doi:10.1039/c4ta05597g.

[8] J.K. Bediako, J.W. Choi, M.H. Song, Y. Zhao, S. Lin, A.K. Sarkar, C.W. Cho, Y.S. Yun, Recovery of gold via adsorption-incineration techniques using banana peel and its derivatives: Selectivity and mechanisms, Waste Manag. 113 (2020) 225–235. doi:10.1016/j.wasman.2020.05.053.

[9] S.I. Park, I.S. Kwak, S.W. Won, Y.S. Yun, Glutaraldehyde-crosslinked chitosan beads for sorptive separation of Au(III) and Pd(II): Opening a way to design reduction-coupled selectivity-tunable sorbents for separation of precious metals, J. Hazard. Mater. 248–249 (2013) 211–218. doi:10.1016/j.jhazmat.2013.01.013.

[10] L. Zhang, Z. Li, X. Du, X. Chang, Activated carbon functionalized with 1-amino-2-naphthol-4-sulfonate as a selective solid-phase sorbent for the extraction of gold(III), Microchim. Acta. 174 (2011) 391–398. doi:10.1007/s00604-011-0643-y.

[11] Z. Supiyeva, K. Avchukir, V. Pavlenko, M. Yeleuov, A. Taurbekov, G. Smagulova, Z. Mansurov, The investigation of electroreduction of AuCl-4 in the case of gold

electrosorption using activated carbon, Mater. Today Proc. 25 (2019) 33–38. doi:10.1016/j.matpr.2019.11.013.
[12] M.R. Nabid, R. Sedghi, R. Hajimirza, H.A. Oskooie, M.M. Heravi, A nanocomposite made from conducting organic polymers and multi-walled carbon nanotubes for the adsorption and separation of gold(III) ions, Microchim. Acta. 175 (2011) 315–322. doi:10.1007/s00604-011-0680-6.
[13] B. Altansukh, K. Haga, N. Ariunbolor, S. Kawamura, A. Shibayama, Leaching and adsorption of gold from waste printed circuit boards using iodine-iodide solution and activated carbon, Eng. J. 20 (2016) 29–40. doi:10.4186/ej.2016.20.4.29.
[14] F. Fu, Q. Wang, Removal of heavy metal ions from wastewaters: A review, J. Environ. Manage. 92 (2011) 407–418. doi:10.1016/j.jenvman.2010.11.011.
[15] C.F. Carolin, P.S. Kumar, A. Saravanan, G.J. Joshiba, M. Naushad, Efficient techniques for the removal of toxic heavy metals from aquatic environment: A review, J. Environ. Chem. Eng. 5 (2017) 2782–2799. doi:10.1016/j.jece.2017.05.029.
[16] B. Li, Y. Zhang, D. Ma, Z. Xing, T. Ma, Z. Shi, X. Ji, S. Ma, Creation of a new type of ion exchange material for rapid, high-capacity, reversible and selective ion exchange without swelling and entrainment, Chem. Sci. 7 (2016) 2138–2144. doi:10.1039/c5sc04507j.
[17] W. Wei, D.H.K. Reddy, J.K. Bediako, Y.S. Yun, Aliquat-336-impregnated alginate capsule as a green sorbent for selective recovery of gold from metal mixtures, Chem. Eng. J. 289 (2016) 413–422. doi:10.1016/j.cej.2015.12.104.
[18] S. Richards, J. Dawson, M. Stutter, The potential use of natural vs commercial biosorbent material to remediate stream waters by removing heavy metal contaminants, J. Environ. Manage. 231 (2019) 275–281. doi:10.1016/j.jenvman.2018.10.019.
[19] J.B. Dunn, M. Biddy, S. Jones, H. Cai, P.T. Benavides, J. Markham, L. Tao, E. Tan, C. Kinchin, R. Davis, A. Dutta, M. Bearden, C. Clayton, S. Phillips, K. Rappé, P. Lamers, Environmental, Economic, and Scalability Considerations and Trends of Selected Fuel Economy-Enhancing Biomass-Derived Blendstocks, ACS Sustain. Chem. Eng. 6 (2018) 561–569. doi:10.1021/acssuschemeng.7b02871.
[20] R. Evans, P.A. English, S.C. Anderson, S. Gauthier, C.L.K. Robinson, Factors affecting the seasonal distribution and biomass of E. pacifica and T. spinifera along the Pacific coast of Canada: A spatiotemporal modelling approach, PLoS One. 16 (2021) 1–21. doi:10.1371/journal.pone.0249818.
[21] T.A. Aragaw, F.M. Bogale, Biomass-Based Adsorbents for Removal of Dyes From Wastewater: A Review, Front. Environ. Sci. 9 (2021). doi:10.3389/fenvs.2021.764958.
[22] Z. Jia, P. Yin, Z. Yang, X. Liu, Y. Xu, W. Sun, H. Cai, Q. Xu, Triphosphonic acid modified multi-walled carbon nanotubes for gold ions adsorption, Phosphorus, Sulfur Silicon Relat. Elem. 196 (2020) 106–118. doi:10.1080/10426507.2020.1818748.
[23] H.A. Shaheen, H.M. Marwani, E.M. Soliman, Selective adsorption of gold ions from complex system using oxidized multi-walled carbon nanotubes, J. Mol. Liq. 212 (2015) 480–486. doi:10.1016/j.molliq.2015.09.040.
[24] T. Xu, R. Qu, Y. Zhang, C. Sun, Y. Wang, X. Kong, X. Geng, C. Ji, Preparation of bifunctional polysilsesquioxane/carbon nanotube magnetic composites and their adsorption properties for Au (III), Chem. Eng. J. 410 (2021). doi:10.1016/j.cej.2020.128225.
[25] H. Ebrahimzadeh, E. Moazzen, M.M. Amini, O. Sadeghi, Novel ion imprinted polymer

coated multiwalled carbon nanotubes as a high selective sorbent for determination of gold ions in environmental samples, Chem. Eng. J. 215–216 (2013) 315–321. doi:10.1016/j.cej.2012.11.031.
[26] C. Gao, H. He, L. Zhou, X. Zheng, Y. Zhang, Scalable functional group engineering of carbon nanotubes by improved one-step nitrene chemistry, Chem. Mater. 21 (2009) 360–370. doi:10.1021/cm802704c.
[27] A.O. Rashed, A. Merenda, T. Kondo, M. Lima, J. Razal, L. Kong, C. Huynh, L.F. Dumée, Carbon nanotube membranes – Strategies and challenges towards scalable manufacturing and practical separation applications, Sep. Purif. Technol. 257 (2021) 117929. doi:10.1016/j.seppur.2020.117929.
[28] F.H. Moghaddam, M.A. Taher, M. Behzadi, M. Naghizadeh, Modified carbon nanotubes as a sorbent for solid-phase extraction of gold, and its determination by graphite furnace atomic absorption spectrometry, Microchim. Acta. 182 (2015) 2123–2129. doi:10.1007/s00604-015-1550-4.
[29] Z. Tu, S. Lu, X. Chang, Z. Li, Z. Hu, L. Zhang, H. Tian, Selective solid-phase extraction and separation of trace gold, palladium and platinum using activated carbon modified with ethyl-3-(2-aminoethylamino)-2-chlorobut-2-enoate, Microchim. Acta. 173 (2011) 231–239. doi:10.1007/s00604-011-0552-0.
[30] F.J. Alguacil, Adsorption of Gold(I) and Gold(III) using multiwalled carbon nanotubes, Appl. Sci. 8 (2018). doi:10.3390/app8112264.
[31] M.A. Ganzoury, C. Chidiac, J. Kurtz, C.-F. de Lannoy, CNT-sorbents for heavy metals: Electrochemical regeneration and closed-loop recycling, J. Hazard. Mater. 393 (2020). doi:10.1016/j.jhazmat.2020.122432.
[32] M.M. Abd-Elzaher, Synthesis and spectroscopic characterization of some tetradentate Schiff bases and their nickel, copper and zinc complexes, Synth. React. Inorg. Met. Chem. 30 (2000) 1805–1816. doi:10.1080/00945710009351870.
[33] R. Soomro, M.J. Ahmed, N. Memon, H. Khan, A Simple and Selective Spectrophotometric Method for the Determination of Trace Gold in Real, Environmental, Biological, Geological and Soil Samples Using Bis(Salicylaldehyde) Orthophenylenediamine, Anal. Chem. Methods Appl. (2011) 231–254. doi:10.4137/aci.s977.
[34] A. McAllister, D. Bayerl, E. Kioupakis, Radiative and Auger recombination processes in indium nitride, Appl. Phys. Lett. 112 (2018) 251108. doi:10.1063/1.5038106.
[35] A. Yokoya, T. Ito, Photon-induced Auger effect in biological systems : a review, Int. J. Radiat. Biol. 93 (2017) 743–756. doi:10.1080/09553002.2017.1312670.
[36] V.K. Rajan, K. Muraleedharan, The pKa values of amine based solvents for CO2 capture and its temperature dependence — An analysis by density functional theory, Int. J. Greenh. Gas Control. 58 (2017) 62–70. doi:10.1016/j.ijggc.2017.01.009.
[37] M.D. Cantu, S. Hillebrand, E. Carrilho, Determination of the dissociation constants (pKa) of secondary and tertiary amines in organic media by capillary electrophoresis and their role in the electrophoretic mobility order inversion, J. Chromatogr. A. 1068 (2005) 99–105. doi:10.1016/j.chroma.2004.12.009.
[38] T. Sun, H. Fan, Q. Zhuo, X. Liu, Z. Wu, Covalent incorporation of aminated carbon nanotubes into epoxy resin network, High Perform. Polym. 26 (2014) 892–899. doi:10.1177/0954008314533810.

[39] C. Lu, H. Chiu, Adsorption of zinc(II) from water with purified carbon nanotubes, Chem. Eng. Sci. 61 (2006) 1138–1145. doi:10.1016/j.ces.2005.08.007.
[40] R.M. Lopachin, T. Gavin, A. Decaprio, D.S. Barber, Application of the Hard and Soft , Acids and Bases (HSAB) Theory to Toxicant À Target Interactions, Chem. Res. Toxicol. 25 (2012) 239–251.
[41] M.M. Jones, W.K. Vaughn, HSAB Theory and Acute Metal Ion Toxicity and Detoxification Processes, J. Inorg. Nucl. Chem. 40 (1978) 2081–2088.
[42] P. Schneider, Adsorption isotherms of microporous-mesoporous solids revisited, Appl. Catal. A, Gen. 129 (1995) 157–165. doi:10.1016/0926-860X(95)00110-7.
[43] L. Qi, X. Tang, Z. Wang, X. Peng, Pore characterization of different types of coal from coal and gas outburst disaster sites using low temperature nitrogen adsorption approach, Int. J. Min. Sci. Technol. 27 (2017) 371–377. doi:10.1016/j.ijmst.2017.01.005.
[44] S. Chakraborty, J. Chattopadhyay, H. Peng, Z. Chen, A. Mukherjee, R.S. Arvidson, R.H. Hauge, W.E. Billups, Surface area measurement of functionalized single-walled carbon nanotubes, J. Phys. Chem. B. 110 (2006) 24812–24815. doi:10.1021/jp065044u.
[45] J.A. Peck, C.D. Tait, B.I. Swanson, G.E.B. Jr, Speciation of aqueous gold (II1) chlorides from ultraviolet / visible absorption and Raman / resonance Raman spectroscopies, 55 (1991).
[46] J. Sylvestre, S. Poulin, A. V Kabashin, E. Sacher, M. Meunier, J.H.T. Luong, Surface Chemistry of Gold Nanoparticles Produced by Laser Ablation in Aqueous Media, Phys. Chem. B. 108 (2004) 16864–16869. doi:10.1021/jp047134.
[47] X. Yang, Q. Pan, Y. Ao, J. Du, Z. Dong, M. Zhai, L. Zhao, Facile preparation of L-cysteine – modified cellulose microspheres as a low-cost adsorbent for selective and efficient adsorption of Au (III) from the aqueous solution, Environ. Sci. Pollut. Res. 27 (2020) 38334–38343.
[48] S. Cherevko, A.A. Topalov, I. Katsounaros, K.J.J. Mayrhofer, Electrochemical Dissolution ofGold in Acidic Medium, Electrochem. Commun. (2012). doi:10.1016/j.elecom.2012.11.040.
[49] S. Cherevko, A.A. Topalov, A.R. Zeradjanin, I. Katsounaros, K.J.J. Mayrhofer, Gold dissolution : towards understanding of noble metal corrosion, RSC Adv. 3 (2013) 16516–16527. doi:10.1039/c3ra42684j.
[50] N. Zhang, H. Lee, Y. Wu, M.A. Ganzoury, C. De Lannoy, Integrating biofouling sensing with fouling mitigation in a two-electrode electrically conductive membrane filtration system, Sep. Purif. Technol. 288 (2022) 120679. doi:10.1016/j.seppur.2022.120679.
[51] R.P. Frankenthal, D.J. Siconolfi, The Anodic Corrosion of Gold in Concentrated Chloride Solutions, J. Electrochem. Soc. 129 (1982) 1192.
[52] D.S. Rico, E.R. Duran, Electrochemical Study on Electrodissolution of Gold in Acidic Medium Using Chlorides as Ligands, J. OfThe Electrochem. Soc. 164 (2017) 994–1002. doi:10.1149/2.0351714jes.
[53] P. Clauwaert, P. Aelterman, T.H. Pham, L. De Schamphelaire, M. Carballa, K. Rabaey, W. Verstraete, Minimizing losses in bio-electrochemical systems : the road to applications, Appl Microbiol Biotechnol. 79 (2008) 901–913. doi:10.1007/s00253-008-1522-2.
[54] B.L. Corso, I. Perez, T. Sheps, P.C. Sims, O.T. Gu, P.G. Collins, Electrochemical Charge-Transfer Resistance in Carbon Nanotube Composites, Nano Lett. 14 (2014) 1329–1336.

[55] N.-T. Suen, S.-F. Hung, Q. Quan, N. Zhang, Y.-J. Xu, H.M. Chen, There, Electrocatalysis for the oxygen evolution reaction: recent development and future perspectives, Chem. Soc. Rev. 46 (2017) 337. doi:10.1039/c6cs00328a.
[56] K.J. Rountree, B.D. Mccarthy, E.S. Rountree, T.T. Eisenhart, J.L. Dempsey, A Practical Beginner' s Guide to Cyclic Voltammetry, J. Chem. Educ. 95 (2018) 197–206. doi:10.1021/acs.jchemed.7b00361.
[57] H.J. Lee, N. Zhang, M.A. Ganzoury, Y. Wu, C.F. De Lannoy, Simultaneous Dechlorination and Advanced Oxidation Using Electrically Conductive Carbon Nanotube Membranes, ACS Appl. Mater. Interfaces. 13 (2021) 34084–34092. doi:10.1021/acsami.1c06137.

Chapter 5

Electrolyte Ion Migration through Electrochemical Membranes: Potential Source of Error in Batch Electrochemical Cells

Submitted to The Canadian Journal of Chemical Engineering

5.1 Abstract

Electrochemical membranes (ECMs) and porous electrodes have gained much attention in a broad range of applications including water and wastewater treatment, energy production and storage, and carbon dioxide capture. Lab scale batch experiments (electrochemical stirred cells) are the baseline for developing ECMs and porous electrodes. We observed electrochemical dissolution of metal fasteners (alligator clips), used to hold porous conductive and non-conductive membranes in batch electrochemical cells, despite being kept outside the electrolyte solution. The electrolyte ions migrated through the porous membranes by the action of capillary forces forming a closed electrochemical circuit with the alligator clips. This unexpected leaching can lead to misleading results for electrochemical experiments on porous electrodes and ECMs. In this study, we compared (1) porous membranes versus non-porous electrodes, (2) hydrophilic versus hydrophobic membranes, and (3) conductive versus non-conductive membranes in their ability to cause capillary wetting-induced corrosion of metal alligator clips. We proposed a simple solution for the problem: separating the metal alligator clips from the porous membrane electrode with a non-porous conductive graphite foil, which keeps the electrochemical circuit open. We have validated this solution and propose it as a standard method for experiments using porous electrodes and electrically conductive membranes.

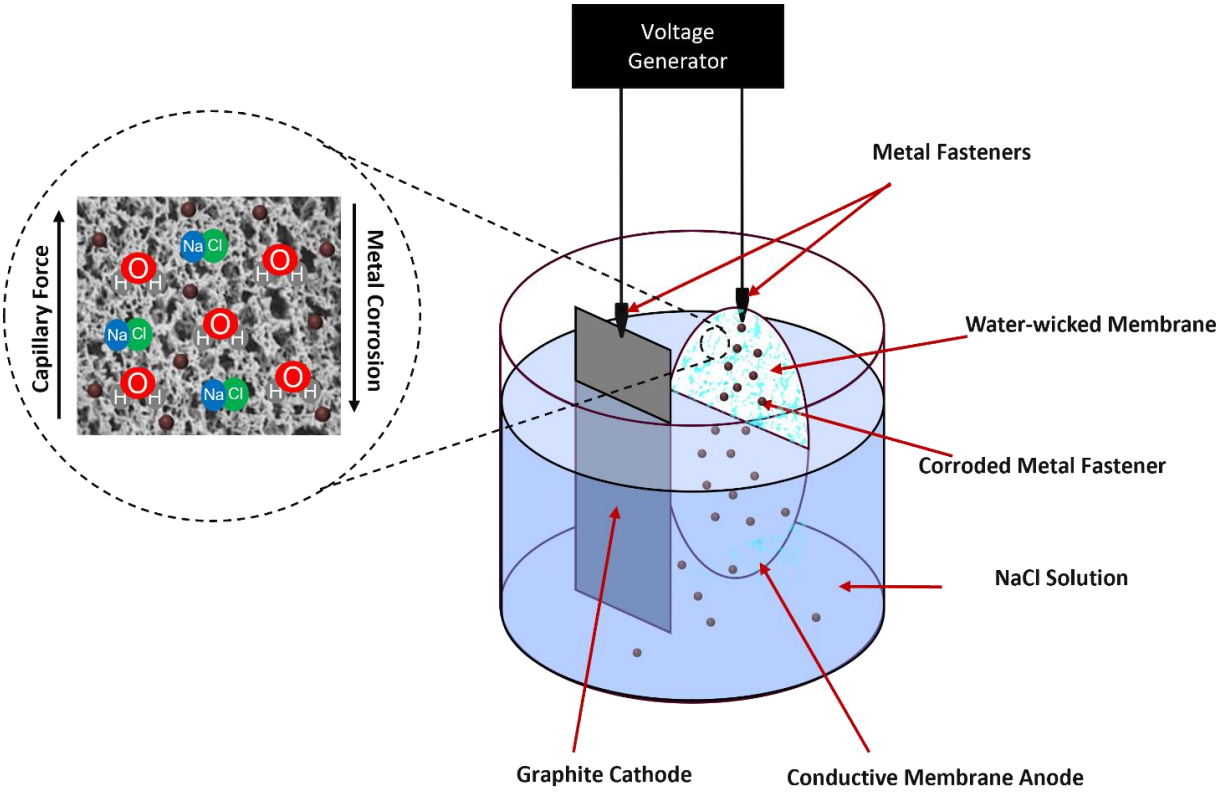

5.2 Introduction

Much research efforts have been directed towards applications and material improvements of electrochemical membranes (ECMs) and porous electrodes for water treatment [1–10]. ECMs have gained increasing attention and importance for their ability to both separate solutes in solutions and perform electrochemical reactions. As such, ECMs have demonstrated an ability to prevent surface fouling, degrade contaminants, remove chlorine, and detect foulants, among other abilities provided by a porous electrochemical surface [11–16]. Similarly, porous electrodes have gained importance for their ability to increase electrode surface area and increase mass transfer of reactants by flowing solutes through the electrodes [17–19]. Batch experiments on a lab scale are usually the baseline for developing ECMs and porous electrodes. Wherein the ECM

or Porous electrode is used as a working electrode in a batch electrochemical cell (BECC) containing the water/wastewater required to be treated, as illustrated in Figure 5.1. ECMs have been evaluated in BECCs for a variety of applications including hexavalent chromium removal from drinking water [20], de-chlorination of treated drinking water [21], detection of chlorine in solution [22], detection of foulants on membrane surfaces [23], and to evaluate the stability of conductive coatings on ECMs [24,25]. ECMs have been used as either anodes or cathodes, inducing oxidation or reduction reactions at their surface. These membranes have been formed from polymeric substrates coated or crosslinked with a variety of materials including carbon nanotubes (CNTs) [20,21], graphitic materials [26,27], conductive polymer [25,28] and metal thin films [22,29].

As the electrochemical systems and the electrolyte solutions become more complex, it is imperative to identify confounding chemical and electrochemical parameters that could lead to misleading results when using ECMs and porous electrodes in batch experiments. In BECCs, ECMs and porous electrodes are conventionally connected to a power generator by conductive wires rods that are attached to the ECM and porous electrode with metal fasteners, usually metal alligator clips, as shown in Figure 5.1. The most commonly used alligator clips are composed of stainless-steel or copper which are low cost and have high electrical conductivity. It is always recommended to keep the metal alligator clips outside of the electrolyte solution to prevent their corrosion and their involvement in the electrochemical reactions.

In this study, we demonstrate that metal alligator clips fastened to ECMs become involved in the electrochemical reactions in BECCs even when kept outside the electrolyte solution. We hypothesize that electrolyte ions can migrate through porous ECMs and porous electrode by

capillary forces and thereby can interact with the metal alligator clips, resulting in their participation in electrochemical reactions. The redox reactions of the alligator clips in electrochemical reactions can lead to deceptive results, in particular when using ECMs to treat water in BECCs. For instance, the anodic oxidation of metal alligator clips can lead to metal dissolution in the wastewater that is being treated, which can confound measurements of treatment efficiency. Furthermore, metal alligator clip dissolution can confuse ECM electrochemical characterization (e.g., by CV curves) during pollutant degradation. The reaction of alligator clips and other non-inert connectors within porous electrode and porous ECM systems will be of particular concern when these porous electrodes are used as anodes, and they will be of increasing concern during longer term experiments needed to validate such systems for industrial application and/or in high ionic strength electrolyte solutions such as seawater and brine, mining effluents, and some industrial wastewaters.

5.3 Materials and Methods

In our experiments, we used a three-electrode batch electrochemical cell (resembling electrochemical cells used in literature for batch ECMs experiments), as shown in Figure 5.1. A graphite counter electrode (CE), Ag/AgCl reference electrode (RE), and concentrated NaCl electrolyte solution (conductivity (50 mS/cm), pH (6.2)) were used for all electrochemical experiments carried out in this study. A highly conductive electrolyte solution (i.e., concentrated NaCl solution) was chosen for this study as an extreme condition to accelerate and intensify the interaction of the electrolyte ions with the alligator clips to clearly illustrate the interference of alligator clips in the electrochemical reactions. Various materials were used as working electrodes (WE) to assess the effect of wettability, conductivity and porosity on electrolyte ion

migration through electrodes to the alligator clips causing their dissolution and interference in the electrochemical reactions. A working electrode ECM (i.e., polyether sulfone (PES) membranes coated with amide functionalized multiwall carbon nanotubes (NH_2-MWCNTs)), was compared to working electrodes composed of non-conductive but porous membranes (hydrophilic polyether sulfone (PES) and hydrophobic polyvinylidene fluoride (PVDF)), and nonporous but conductive graphite electrodes. The electrode gap between the WE and CE (graphite) was maintained at 20 mm in all experiments. Stainless-steel alligator clips (kept outside the electrolyte solution) were used to hold the WE and CE and the distance between the bottom of the alligator clips (holding the WE) and surface of the water was maintained at 6 mm. New unused alligator clips were used for each experiment. 6mA anodic current in a chrono potentiometric mode was applied for 1 h using a potentiostat (Metrohm, Multi Autolab/M101) connected to the electrochemical cell, unless stated otherwise. The electrochemical cell inner diameter was 6 cm, and the electrolyte solution was stirred at 200 RPM to ensure uniform mixing.

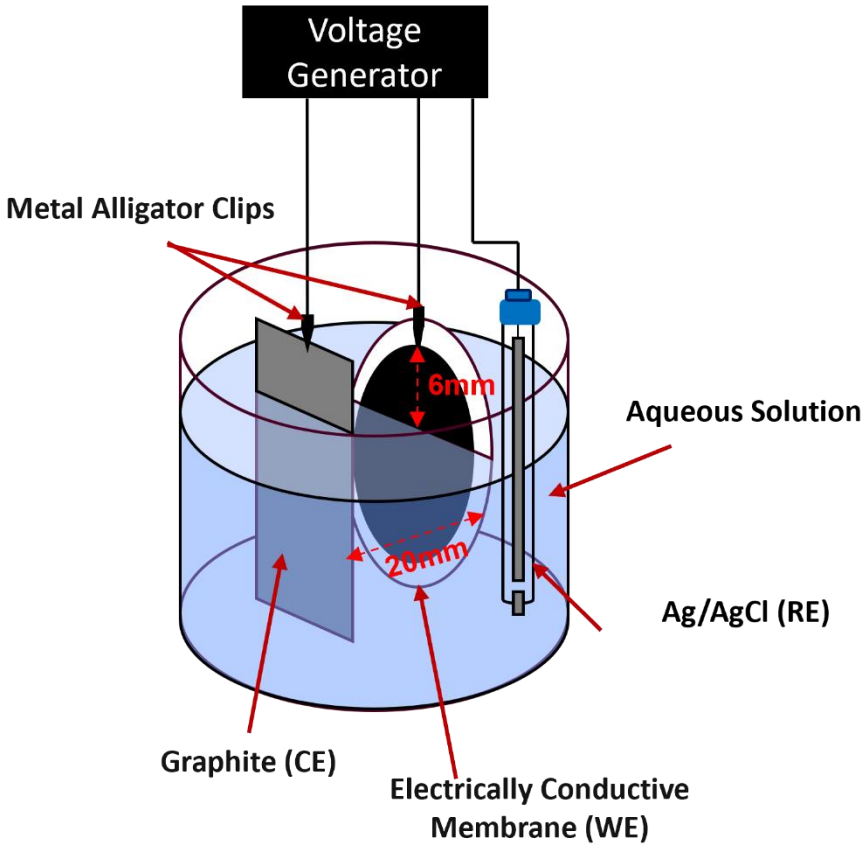

Figure 5.1: Batch electrochemical cell using electrically conductive membrane as working electrode for treating water/wastewater

5.4 Results and Discussion

Initially, a bare PES membrane was used as an anode in a BECC, as shown in Figure 5.2a. Interestingly, the bare non-conductive membrane produced a closed electrochemical circuit when a 6mA current was applied, with an average potential of 5.2V vs. Ag/AgCl induced at the anode. pH of the electrolyte solution increased from 6.2 to 11.8 by the end of the 1-h electrochemical reaction, as shown in Table S5.1. Water electrolysis occurred at the cathode producing hydrogen gas (Eq. 5.1), and a chlorination reaction occurred at the anode producing chlorine gas (Eq. 5.2). The chlorination reaction (Eq. 5.2) is more favorable at the anode than the

oxygen evolution reaction (OER) (Eq. 5.3) in a concentrated NaCl electrolyte solution [30–33]. As a result, hydroxide ions generated from the hydrogen evolution reaction (Eq. 5.1) are not consumed in the OER, raising the electrolyte solution pH. The bare, dry PES membrane is a non-conductive polymeric material and would act as a resistor to the flow of electrons, preventing a closed electrochemical circuit. Nevertheless, the stainless-steel alligator clip (kept outside the electrolyte solution) was observed to be participating in the electrochemical reaction. Therefore, electrolyte ions must have migrated through the porous polymeric membrane by action of capillary forces, to form a closed electrochemical circuit with the stainless-steel alligator clip. Anodic electro-dissolution of the stainless-steel alligator clip occurred, producing orange precipitates, which became large enough to visually observe in the electrolyte solution two h after the end of the electrochemical experiment, as shown in the third column of Figure 5.2a. Iron, the main constituent of stainless-steel, dissolved by anodic oxidation (Eq. 5.4) and reacted with the abundant hydroxide ions in the electrolyte solution, producing iron hydroxide (orange precipitate) [34,35]. This was confirmed by a control experiment in which a stainless-steel alligator clip was immersed directly in the electrolyte solution and used as an anode in the same electrochemical cell (Figure 5.2c). Dissolution of iron in such an electrochemical cell is well established and the orange precipitate generated in this electrolyte solution was identical to that produced using a bare PES membrane anode held by a stainless-steel alligator clip maintained outside the electrolyte solution (Figure 5.2a) [36]. As the only source of iron in either of these cells is the alligator clip, it is evident that iron was dissolving from the alligator clip and migrating through the membrane, despite being held outside the electrolyte solution.

$$2H_2O\ (l) + 2e^- \rightarrow H_2\ (g) + 2OH^-\ (aq) \qquad (5.1)$$

$$2Cl^- (aq) \rightarrow Cl_2 (g) + 2e^- \quad (5.2)$$

$$4OH^- (aq) \rightarrow 2H_2O (l) + O_2 (g) + 4e^- \quad (5.3)$$

$$Fe(s) \rightarrow Fe^{2+} (aq) + 2e^- \quad (5.4)$$

In contrast, Figure 5.2b shows a non-porous graphite electrode used as an anode in the same BECC. No precipitate was generated in the electrolyte solution after applying 6mA for 1-h, which confirms that non-porous electrodes do not enable electrolyte ion migration to the alligator clips, thereby preventing their electro-dissolution. The average potential at the graphite anode was (1.34 V vs. Ag/AgCl) and the pH of the electrolyte solution increased from 6.20 to 8.22 by the end of the 1-h electrochemical reaction. The increase in pH resulted from hydroxide generation as aforementioned. However, the increase in pH was less than that when using the bare PES membrane as an anode, which suggests that at the graphite anode the OER (Eq. 5.3) occurs together with the chlorine evolution reaction (Eq. 5.2), likely because graphite has higher electrical conductivity than the PES membrane.

To further analyze the electrochemically generated precipitates, each electrolyte solution was filtered through 0.2 μm MF PES membranes 2 h after the completion of each electrochemical experiment. Precipitates were retained on the MF membranes and weighed after drying. The orange precipitates in Figure 5.2a, c as compared to the lack thereof on membranes in Figure 5.2b, confirms that non-porous electrodes prevent alligator clip corrosion, while a sufficiently water wicking porous membrane will allow electrolyte ion migration and thereby cause the alligator clip to corrode. Directly immersing the stainless-steel alligator clip electrode in the electrolyte solution (Figure 5.2c) produced a dark red precipitate of iron oxides. 10.4 mg of precipitate was formed when the stainless-steel alligator clip was immersed directly in the

electrolyte solution while 3.8 mg of precipitate formed when the bare PES membrane electrode was suspended in the electrolyte solution by a stainless-steel alligator clip. As expected, when directly immersed in the electrolyte solution the stainless-steel alligator clip would undergo greater corrosion by electro-dissolution. Figure 5.2d shows the use of a copper alligator clip as an anode in an electrochemical cell under 20mA applied current. As expected, the copper alligator clip also corroded by electro-oxidation producing a bluish-green CuO precipitate in the electrolyte solution, indicated that copper alligator clips would similarly corrode when used to suspend porous ECMs in BECCs. Copper corrosion was achieved by applying 20 mA to the copper alligator clip to reach an average potential at the WE of > 0.14 V vs. Ag/AgCl (the potential required for copper oxidation). This potential was not reached when applying 6 mA to the copper alligator clip, since a patina formed over the clip and acted as a passivation layer reducing the copper's conductivity. In contrast, in the case of the stainless-steel alligator, iron was oxidized into rust (iron oxides) which did not not form a protective layer on the alligator clip, and the rust flaked off in the solution allowing iron oxidation at a lower current than that required for the patina-coated copper alligator clip [37].

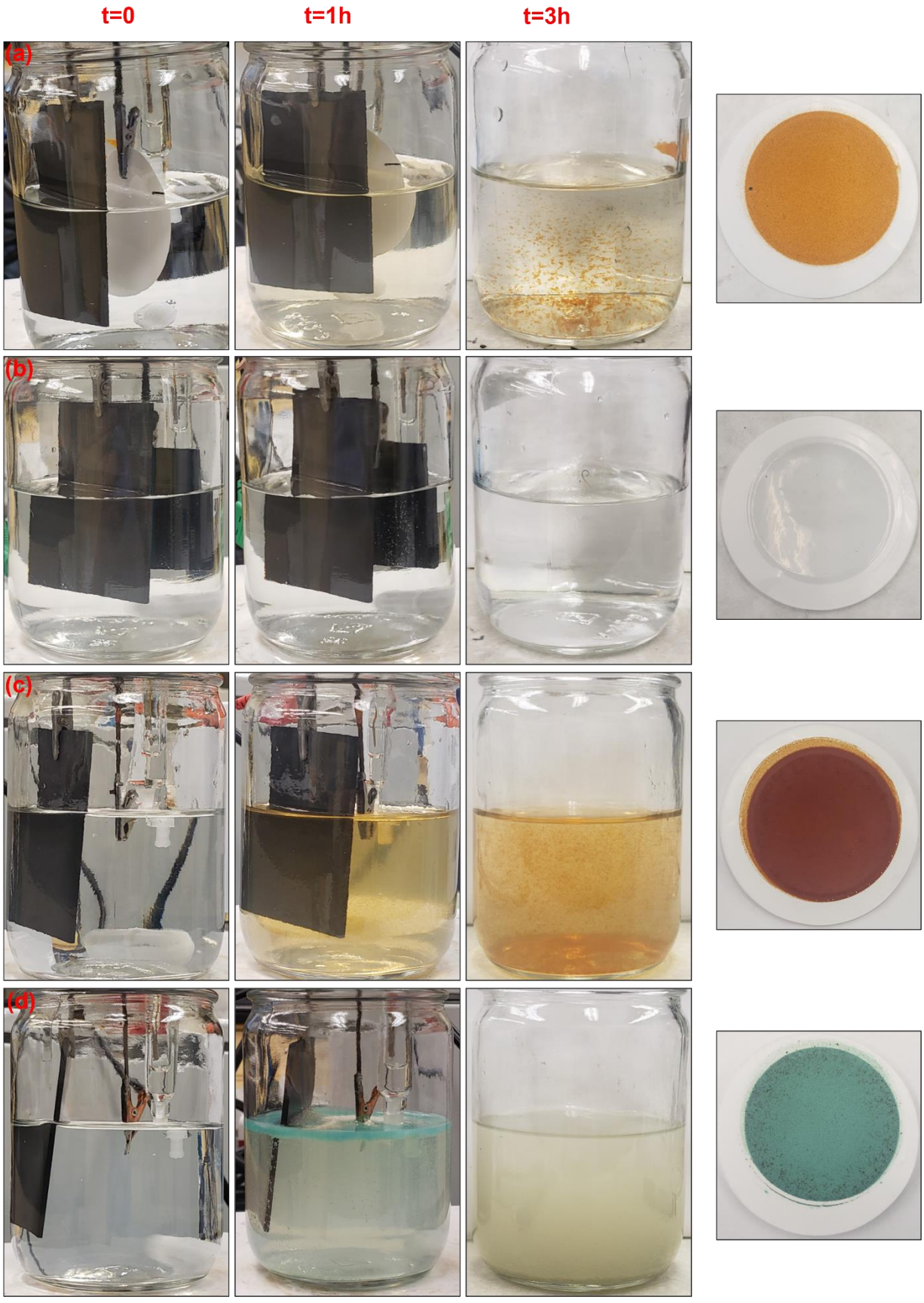
t=0
t=1h
t=3h
(a)
(b)
(c)
(d)

Figure 5.2: (a) PES membrane, (b) Graphite, (c) Stainless-steel alligator clip and (d) Copper alligator clip each used as anodes in a batch electrochemical cell (BECC). The first column shows the BECC before the electrochemical experiment, the second column shows the BECC after a 1-h electrochemical experiment, the third column shows the BECC 2-h after the end of the electrochemical experiment, and the fourth column shows the precipitate from each BECC filtered onto a 0.2 µm MF membrane

We then studied the effect of membrane conductivity and wettability on electrolyte ion migration through membranes by comparing the corrosion of stainless-steel alligator clips that suspended a bare PES membrane (Figure 5.3a), NH_2-MWCNTs coated on a PES membrane (Figure 5.3b), and a bare PVDF membrane (Figure 5.3c) used as anodes in BECC. PES membranes are known to be hydrophilic, however when they are coated with hydrophobic CNTs the hydrophilicity of the membranes decreases while its conductivity substantially increases. PVDF membranes are known to be more hydrophobic membranes than either PES or CNT-coated PES membrane. In order to confirm the difference in membranes' wettability, we performed dynamic contact angle experiments on a bare PES membrane, NH_2-MWCNTs coated on a PES membrane, and a bare PVDF membrane. The contact angle for the initial attachment of a water droplet on a PVDF membrane was 54.7^o compared to 28.1^o in the case of a PES membrane and 25.2^o in the case of NH_2-MWCNTs coated on a PES membrane (Figure S5.1). While the required time to reach complete wetting (i.e., zero contact angle) was 7s for a PVDF membrane, 6s for NH_2-MWCNTs coated on a PES membrane, and 3s for a PES membrane (Figure S5.1 and Figure S5.2). These results confirm that PVDF membranes are more hydrophobic than PES and CNT-coated PES membranes. The results also indicated that CNT-coated PES membranes have a higher hydrophobicity than PES membranes despite their similar surface contact angles for the initial attachment of water droplets. The required time to reach complete wetting in the case of CNT-

coated PES membrane was twice as long as that for a bare PES membrane. In all three cases, significant orange precipitates were generated in the electrolyte solution (third column of Figure 5.3) indicating that decreasing the wettability (i.e., increasing the hydrophobicity) of the membrane was not sufficient to prevent the electrolyte ion migration through the membrane. However, it was clear that the there were greater amounts of orange precipitates formed in the case of the PES membrane than when using the more hydrophobic membranes (third column of Figure 5.3). The last column in Figure 5.3 shows the precipitate on MF PES membranes (0.2 μm) collected by filtering the electrolyte solution 2 h after each electrochemical experiment. An orange precipitate was collected and weighed after drying in each case. Iron oxide precipitates weighed 3.8 mg using PES as an anode, 2.7 mg using NH_2-MWCNTs coated PES membrane anodes and 1.8 mg PVDF membrane anodes (1.8 mg). These results confirm that the increase in hydrophilicity enhances the electrolyte ion migration inside the membrane allowing for a higher corrosion rate of the alligator clips. Electrolyte solution pH increased over the course of the 1-h long electrochemical experiments from 6.2 to 11.8 when using the PES membrane as an anode, from 6.2 to 11.6 when using the NH_2-MWCNTs coated PES membrane as an anode, and from 6.2 to 11.9 when using the PVDF membrane as an anode, as shown in Table S5.1. The increase in electrolyte solution pH in all cases confirms the closed electrochemical circuit, which results in water electrolysis and chlorine evolution, increasing the electrolyte solution pH by hydroxide generation, as previously explained. The average potentials at the WE were 5.2V vs Ag/AgCl for the PES membrane anode, 3.2V vs Ag/AgCl for the NH_2-MWCNTs coated PES membrane anode, and 8.4V vs Ag/AgCl for the PVDF membrane anode. Tellingly, the hydrophobic PVDF membrane electrode required a higher average applied potential to achieve the same current (6 mA) as

compared to the hydrophilic PES membrane. This is likely because of the lower ion current density of electrolyte ions migrating through the hydrophobic membrane as compare to that through the more hydrophilic membrane. In the case of the NH_2-MWCNTs coated PES membrane electrode, the average potential was lower still than either of the insulating bare PES and PVDF membranes due to the higher conductivity of CNTs which lowers the required electric potential to achieve the same 6mA current.

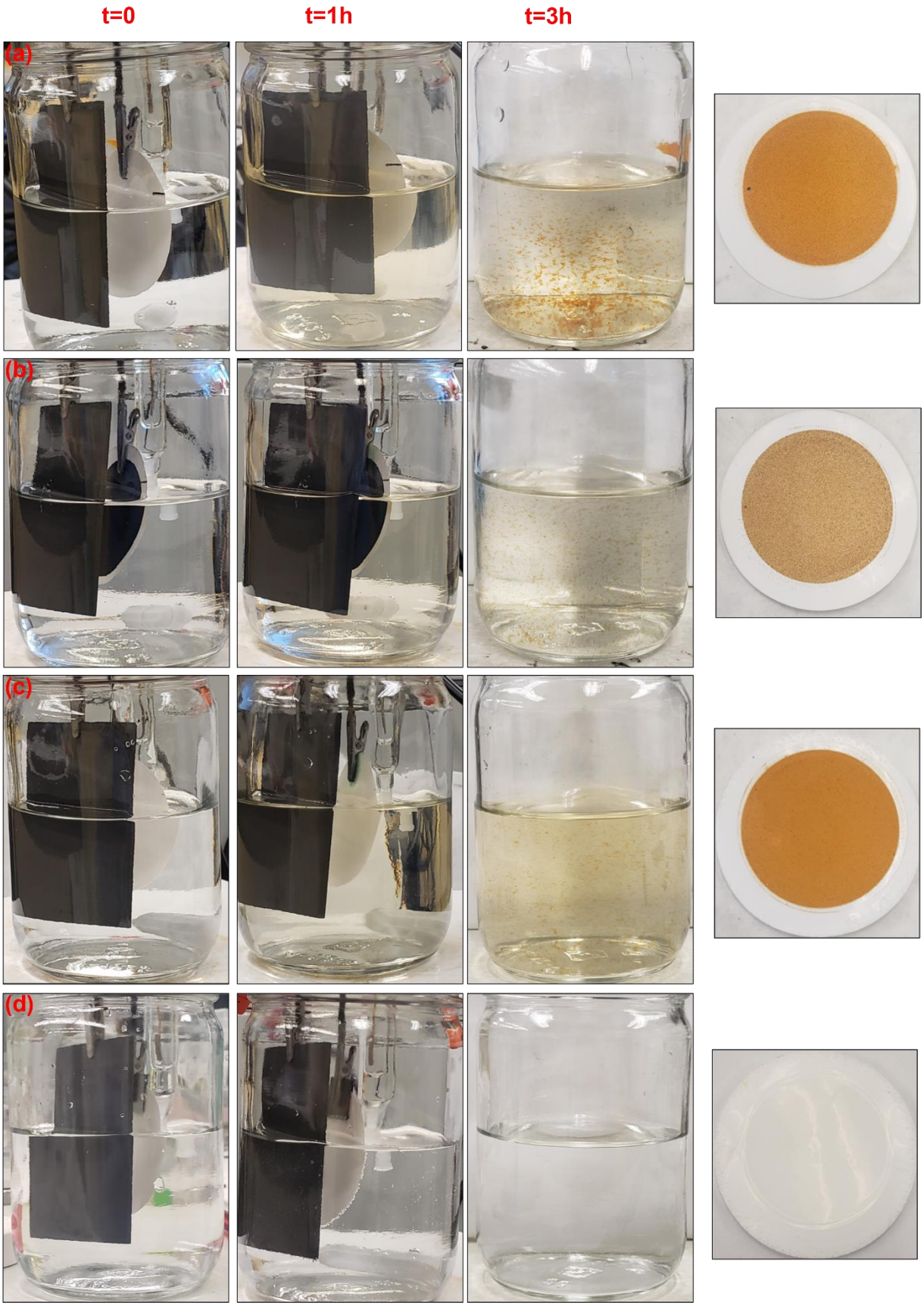
t=0
t=1h
t=3h
(a)
(b)
(c)
(d)

Figure 5.3: a) PES membrane, (b) NH_2-MWCNTs coated PES membrane, (c) PVDF membrane and (d) PES membrane (separated from the stainless-steel alligator clip by a thin graphite sheet) each used as anodes in BECC. The first column shows the BECC before the electrochemical experiment, the second column shows the BECC after a 1-h electrochemical experiment, the third column shows the BECC 2-h after the end of the electrochemical experiment, and the fourth column shows the precipitate from each BECC filtered onto a 0.2 µm MF membranes.

In order to mitigate alligator clip corrosion, an inert conductive material resistive to electro-dissolution (e.g., Pt, Au) could be used to fabricate the alligator clips. However, noble metals are costly in comparison with stainless-steel and copper. Alternatively, the porous membranes can be separated from the metal alligator clips in the electrochemical cells using an inert conductive current collector (e.g., graphite). Figure 5.3d shows a bare PES membrane used as an anode in a BECC while being separated from the stainless-steel alligator clip by a thin graphite sheet. As expected, applying 6mA for 1-h did not generate orange precipitates in the electrolyte solution 2 h after the electrochemical experiment, and no precipitate was shown after filtering the electrolyte solution through MF membranes.

5.5 Conclusion

In conclusion, it was shown that metal alligator clips holding porous ECMs in BECC participate in electrochemical reactions, even when these alligator clips are kept outside the electrolyte. Electro-induced corrosion of alligator clips occurs with both hydrophilic and hydrophobic porous membranes, producing iron oxide precipitates in the electrolyte solution, although hydrophobic membranes were shown to produce fewer precipitates. We hypothesize that the electrolyte solution wets the electrode enabling ions to migrate through the porous membrane by capillary forces. Thus, considerations should be taken when using porous ECMs suspended by metal alligator clips for water treatment experiments in BECCs to avoid alligator clips' electro-

dissolution which can lead to misleading results. Similar considerations are also necessary when testing the stability of these ECMs for long-term experiments in either BECCs or electrochemical cross-flow systems to validate their industrial applicability. Finally, these study findings should also be applied to all porous electrodes tested in BECCs for their many applications including hydrogen production [38,39], organic molecule electrochemical reactions (e.g. glycerol oxidation [40], ketone oxidation [41] and pyridine oxidation [42]), fuel cells [43,44], and water and wastewater treatment (e.g. organic contaminant degradation [45,46] and water desalination [47]), where the capillary migration of electrolyte solutions and alligator clips' corrosion are expected to occur in the same manner.

5.6 Acknowledgements

The authors thank the support of the Natural Sciences and Engineering Research Council of Canada (NSERC, Discovery Grant).

5.7 References

[1] E. Sechi, A. Vacca, M. Mascia, S. Palmas, Nickel-based nanoporous electrodes for water treatment, Chem. Eng. Trans. 47 (2016) 97–102. doi:10.3303/CET1647017.

[2] P.M. Biesheuvel, H.V.M. Hamelers, M.E. Suss, Theory of Water Desalination by Porous Electrodes with Immobile Chemical Charge, Colloids Interface Sci. Commun. 9 (2015) 1–5. doi:10.1016/j.colcom.2015.12.001.

[3] F. He, P.M. Biesheuvel, M.Z. Bazant, T.A. Hatton, Theory of water treatment by capacitive deionization with redox active porous electrodes, Water Res. 132 (2018) 282–291. doi:10.1016/j.watres.2017.12.073.

[4] W. Tang, D. He, C. Zhang, P. Kovalsky, T.D. Waite, Comparison of Faradaic reactions in capacitive deionization (CDI) and membrane capacitive deionization (MCDI) water treatment processes, Water Res. 120 (2017) 229–237. doi:10.1016/j.watres.2017.05.009.

[5] B.P. Chaplin, Critical review of electrochemical advanced oxidation processes for water treatment applications, Environ. Sci. Process. Impacts. 16 (2014) 1182–1203. doi:10.1039/c3em00679d.

[6] S. Nayak, B.P. Chaplin, Fabrication and characterization of porous, conductive, monolithic Ti4O7 electrodes, Electrochim. Acta. 263 (2018) 299–310.

doi:10.1016/j.electacta.2018.01.034.
[7] M.J. Larocque, A. Gelb, D.R. Latulippe, C.-F. de Lannoy, Meta-analysis of electrically conductive membranes: A comparative review of their materials, applications, and performance, Sep. Purif. Technol. 287 (2022) 120482. doi:10.1016/j.seppur.2022.120482.
[8] M.A. Halali, C.F. De Lannoy, The Effect of Cross-Linkers on the Permeability of Electrically Conductive Membranes, Ind. Eng. Chem. Res. 58 (2019) 3832–3844. doi:10.1021/acs.iecr.8b05691.
[9] C.F. De Lannoy, D. Jassby, K. Gloe, A.D. Gordon, M.R. Wiesner, Aquatic biofouling prevention by electrically charged nanocomposite polymer thin film membranes, Environ. Sci. Technol. 47 (2013) 2760–2768.
[10] C.F. de Lannoy, E. Soyer, M.R. Wiesner, Optimizing carbon nanotube-reinforced polysulfone ultrafiltration membranes through carboxylic acid functionalization, J. Memb. Sci. 447 (2013) 395–402. doi:10.1016/j.memsci.2013.07.023.
[11] C.F. de Lannoy, D. Jassby, D.D. Davis, M.R. Wiesner, A highly electrically conductive polymer-multiwalled carbon nanotube nanocomposite membrane, J. Memb. Sci. 415–416 (2012) 718–724. doi:10.1016/j.memsci.2012.05.061.
[12] T. Mantel, E. Jacki, M. Ernst, Electrosorptive removal of organic water constituents by positively charged electrically conductive UF membranes, Water Res. 201 (2021) 117318. doi:10.1016/j.watres.2021.117318.
[13] A. Karkooti, M. Rastgar, N. Nazemifard, M. Sadrzadeh, Graphene-based electro-conductive anti-fouling membranes for the treatment of oil sands produced water, Sci. Total Environ. 704 (2020) 135365. doi:10.1016/j.scitotenv.2019.135365.
[14] S.F. Anis, B.S. Lalia, A. Lesimple, R. Hashaikeh, N. Hilal, Electrically conductive membranes for contemporaneous dye rejection and degradation, Chem. Eng. J. 428 (2022) 131184. doi:10.1016/j.cej.2021.131184.
[15] N.H. Barbhuiya, U. Misra, S.P. Singh, Synthesis, fabrication, and mechanism of action of electrically conductive membranes: A review, Environ. Sci. Water Res. Technol. 7 (2021) 671–705. doi:10.1039/d0ew01070g.
[16] L. Xu, L. Liu, K. Wang, S. Zhao, Q. Liu, Y. Zhang, J. Wang, Development of a novel electrocoagulation membrane reactor with electrically conductive membranes as cathode to mitigate membrane fouling, J. Memb. Sci. 618 (2021) 118713. doi:10.1016/j.memsci.2020.118713.
[17] J. Friedl, U. Stimming, Determining Electron Transfer Kinetics at Porous Electrodes, Electrochim. Acta. 227 (2017) 235–245. doi:10.1016/j.electacta.2017.01.010.
[18] P.M. Biesheuvel, Y. Fu, M.Z. Bazant, Diffuse charge and Faradaic reactions in porous electrodes, Phys. Reviw E. 061507 (2011). doi:10.1103/PhysRevE.83.061507.
[19] R. Zhao, P.M. Biesheuvel, H. Miedema, H. Bruning, A. Van Der Wal, Charge Efficiency: A Functional Tool to Probe the Double-Layer Structure Inside of Porous Electrodes and Application in the Modeling of Capacitive Deionization, J. Phys. Chem. Lett. 1 (2010) 205–210. doi:10.1021/jz900154h.
[20] W. Duan, G. Chen, C. Chen, R. Sanghvi, A. Iddya, S. Walker, H. Liu, A. Ronen, D. Jassby, Electrochemical removal of hexavalent chromium using electrically conducting carbon nanotube/polymer composite ultrafiltration membranes, J. Memb. Sci. 531 (2017) 160–171. doi:10.1016/j.memsci.2017.02.050.

[21] H.J. Lee, N. Zhang, M.A. Ganzoury, Y. Wu, C.F. De Lannoy, Simultaneous Dechlorination and Advanced Oxidation Using Electrically Conductive Carbon Nanotube Membranes, ACS Appl. Mater. Interfaces. 13 (2021) 34084–34092. doi:10.1021/acsami.1c06137.
[22] Y.T. Chiang, S.C. Chou, B.Y. Sun, P.W. Wu, A conductive silver membrane for electrochemical detection of free chlorine in aqueous solution, Sensors Actuators B Chem. 348 (2021) 130724. doi:10.1016/j.snb.2021.130724.
[23] N. Zhang, M.A. Halali, C.F. de Lannoy, Detection of fouling on electrically conductive membranes by electrical impedance spectroscopy, Sep. Purif. Technol. 242 (2020) 116823. doi:10.1016/j.seppur.2020.116823.
[24] M.A. Halali, M. Larocque, C.F. de Lannoy, Investigating the stability of electrically conductive membranes, J. Memb. Sci. 627 (2021) 119181. doi:10.1016/j.memsci.2021.119181.
[25] W. Duan, A. Ronen, S. Walker, D. Jassby, Polyaniline-Coated Carbon Nanotube Ultrafiltration Membranes: Enhanced Anodic Stability for in Situ Cleaning and Electro-Oxidation Processes, ACS Appl. Mater. Interfaces. 8 (2016) 22574–22584. doi:10.1021/acsami.6b07196.
[26] Y. Liu, J.H.D. Lee, Q. Xia, Y. Ma, Y. Yu, L.Y.L. Yung, J. Xie, C.N. Ong, C.D. Vecitisd, Z. Zhou, Graphene-based Electrochemical Filter for Water Purification, Mater. Chem. A. 2 (2014) 16554–16562. doi:10.1039/C4TA04006F.
[27] F. Gao, X. Du, X. Hao, X. Ma, L. Chang, N. Han, A novel electrical double-layer ion transport carbon-based membrane with 3D porous structure : High permselectivity for dilute zinc ion separation, Chem. Eng. J. 380 (2020) 122413. doi:10.1016/j.cej.2019.122413.
[28] K. Wang, L. Xu, K. Li, L. Liu, Y. Zhang, J. Wang, Development of polyaniline conductive membrane for electrically enhanced membrane fouling mitigation, J. Memb. Sci. 570–571 (2019) 371–379. doi:10.1016/j.memsci.2018.10.050.
[29] N. Zhang, H. Lee, Y. Wu, M.A. Ganzoury, C. De Lannoy, Integrating biofouling sensing with fouling mitigation in a two-electrode electrically conductive membrane filtration system, Sep. Purif. Technol. 288 (2022) 120679. doi:10.1016/j.seppur.2022.120679.
[30] Y. Kuang, M.J. Kenney, Y. Meng, W. Hung, Y. Liu, J. Erick, Solar-driven , highly sustained splitting of seawater into hydrogen and oxygen fuels, PNAS. 116 (2019). doi:10.1073/pnas.1900556116.
[31] S. Hsu, J. Miao, L. Zhang, J. Gao, H. Wang, H. Tao, S. Hung, A. Vasileff, S.Z. Qiao, B. Liu, An Earth-Abundant Catalyst-Based Seawater Photoelectrolysis System with 17 . 9 % Solar-to-Hydrogen Efficiency, Adv. Mater. 1707261 (2018) 1–8. doi:10.1002/adma.201707261.
[32] L. Yu, Q. Zhu, S. Song, B. Mcelhenny, D. Wang, C. Wu, Z. Qin, J. Bao, Y. Yu, S. Chen, Z. Ren, high-performance alkaline seawater electrolysis, Nat. Commun. 10 (2019) 1–10. doi:10.1038/s41467-019-13092-7.
[33] F. Dionigi, T. Reier, Z. Pawolek, M. Gliech, P. Strasser, Design Criteria , Operating Conditions , and Nickel – Iron Hydroxide Catalyst Materials for Selective Seawater Electrolysis, ChemSusChem. 9 (2016) 962–972. doi:10.1002/cssc.201501581.
[34] D.M. Drazi, C.S. Hao, The Anodic Dissolution Process on Active Iron in Alkaline Solutions, Electrochim. Acta. 27 (1982) 1409–1415.
[35] C.M. Van Genuchten, T. Behrends, P. Kraal, S.L.S. Stipp, K. Dideriksen, Controls on the

formation of Fe (II , III) (hydr) oxides by Fe (0) electrolysis, Electrochim. Acta. 286 (2018) 324–338. doi:10.1016/j.electacta.2018.08.031.
[36] M.A. Ahangarnokolaei, H. Ganjidoust, B. Ayati, Optimization of parameters of electrocoagulation/flotation process for removal of Acid Red 14 with mesh stainless steel electrodes, J. Water Reuse Desalin. 8 (2018) 278–292. doi:10.2166/wrd.2017.091.
[37] OpenStax College, Chemistry 2e, OSC Rice University, 2012.
[38] A.A. Abdelhafiz, M.A. Ganzoury, A.W. Amer, A.A. Faiad, A.M. Khalifa, S.Y. Alqaradawi, M.A. El-Sayed, F.M. Alamgir, N.K. Allam, Defect engineering in 1D Ti-W oxide nanotube arrays and their correlated photoelectrochemical performance, Phys. Chem. Chem. Phys. 20 (2018). doi:10.1039/c8cp01413b.
[39] H.H. Farrag, S. Youssef, N.K. Allam, A.M. Mohammad, Emerging nanoporous anodized stainless steel for hydrogen production from solar water splitting, J. Clean. Prod. 274 (2020) 122826. doi:10.1016/j.jclepro.2020.122826.
[40] N. Arjona, S. Rivas, L. Álvarez-Contreras, M. Guerra-Balcázar, J. Ledesma-García, E. Kjeang, L.G. Arriagae, Glycerol electro-oxidation in alkaline media using Pt and Pd catalysts electrodeposited on three dimensional porous carbon electrodes, New J. Chem. 41 (2017) 1854–1863. doi:10.1039/C6NJ03739A.
[41] W. Zhao, J. Xing, D. Chen, D. Jin, J. Shen, Electrochemical degradation of Musk ketone in aqueous solutions using a novel porous Ti /SnO2 -Sb2O3 / PbO2 electrodes, J. Electroanal. Chem. 775 (2016) 179–188. doi:10.1016/j.jelechem.2016.05.050.
[42] D. Li, J. Tang, X. Zhou, J. Li, X. Sun, J. Shen, L. Wang, W. Han, Electrochemical degradation of pyridine by Ti / SnO2-Sb tubular porous electrode, Chemosphere. 149 (2016) 49–56. doi:10.1016/j.chemosphere.2016.01.078.
[43] J.S. Yi, T. Van Nguyen, Multicomponent Transport in Porous Electrodes of Proton Exchange Membrane Fuel Cells Using the Interdigitated Gas Distributors, J. Electrochem. Soc. 146 (1999) 38–45.
[44] N. Hedayat, Y. Du, H. Ilkhani, Review on fabrication techniques for porous electrodes of solid oxide fuel cells by sacrificial template methods, Renew. Sustain. Energy Rev. 77 (2017) 1221–1239. doi:10.1016/j.rser.2017.03.095.
[45] R. Mei, Q. Wei, C. Zhu, W. Ye, B. Zhou, L. Ma, Z. Yu, 3D macroporous boron-doped diamond electrode with interconnected liquid fl ow channels : A high-e ffi ciency electrochemical degradation of RB-19 dye wastewater under low current, Appl. Catal. B Environ. 245 (2019) 420–427. doi:10.1016/j.apcatb.2018.12.074.
[46] J. Fan, G. Zhao, H. Zhao, S. Chai, T. Cao, Fabrication and application of mesoporous Sb-doped SnO 2 electrode with high specific surface in electrochemical degradation of ketoprofen, Electrochim. Acta. 94 (2013) 21–29. doi:10.1016/j.electacta.2013.01.129.
[47] M.M. Taha, S.E. Anwar, M. Ramadan, H.M. Al-bulqini, M.S. Abdallah, N.K. Allam, Controlled fabrication of mesoporous electrodes with unprecedented stability for water capacitive deionization under harsh conditions in large size cells, Desalination. 511 (2021) 115099. doi:10.1016/j.desal.2021.115099.

Chapter 6

Limitations on using Metal Feed Spacer Electrodes in Electro-assisted RO Filtration

6.1. Abstract

This study investigates electro-assisted RO filtration of calcium sulfate solutions by applying an electric potential to metal conductive feed spacers separating RO membranes. Calcium sulfate is a secondary pollutant produced during metal-rich mining wastewater treatment. Calcium hydroxide is conventionally used to precipitate metals from mining effluents. While effective, it reacts with sulfates in the feed water, producing a high amount of calcium sulfates in the treated solution. Calcium sulfate is then deposited as gypsum scale during RO filtration of the treated solution, causing severe membrane fouling leading to low permeate flux and possible damage on the RO membranes. Using antiscalants for gypsum mitigation during RO filtration can be costly and leads to a high chemical consumption which produces a secondary environmental disposal challenge. Using electrochemical technologies for gypsum mitigation can reduce the environmental impacts caused by antiscalants. Some studies have shown that the application of electrical potentials to electrically conductive membranes could be effective in reducing mineral scaling. However, fabricating electrically conductive RO membranes that maintain rejection is non-trivial and requires significant changes to RO membrane manufacturing. A simpler approach may be to replace conventional polymeric membrane spacers with electrically conductive metal spacers and to apply an electrical potential to these spacers to prevent mineral scaling formation on the RO membranes. In this study, we investigate gypsum mitigation by applying electric potentials on low-cost stainless steel metal meshes used as feed spacers for an RO membrane during the cross-flow filtration of calcium sulfate solutions. This study analyzes the overall impact of anodic or cathodic electric potentials on gypsum scale mitigation. Cathodic potentials (greater than the water electrolysis potential) generate hydrogen bubbles that can physically remove

formed gypsum on the membrane surface. However, cathodic potentials can electrostatically attract calcium cations to deposit on the membrane surface. Anodic potentials are expected to repel calcium cations inducing a nucleation free zone near the RO membrane and generate oxygen bubbles as well which reduce the gypsum scaling on the membrane. Nevertheless, anodic potential is also known of causing anodic corrosion of the metal spacers, which can generate additional foulants in the feed solution. This study quantitatively evaluating whether the benefits achieved in applying electric potentials to the metal feed spacers outweighs the limitations of such an approach.

6.2. Introduction

RO filtration is currently the leading water treatment technology used in seawater desalination, potable reuse applications, and treatment of mining effluent as membranes are modular, mobile, and energy efficient enabling on-site treatment even in remote locations [1,2]. However, membrane fouling is a primary challenge when using RO filtration in water treatment. Contaminants accumulation on the membrane surfaces lead to decreased permeate flux, lower selectivity, and sometimes physical damage to the membrane surfaces [1,3]. Mineral scaling is one of the most common membrane fouling problems especially when treating brackish and sea water, and mining effluents [4]. Mining effluents are rich in metals as well as sulfates dissolved from the mined rocks [5,6]. In the presence of water and oxygen, sulfates are converted into sulfuric acid producing the acid that leads to acid mine drainage (AMD) – the acidic water that flows from metal mines. Calcium hydroxide is conventionally used to precipitate the metals in AMD and to neutralise the acidic solution [7,8]. However, a secondary pollutant (calcium sulfate) is produced in the treated solution by the reaction of calcium with sulfuric acid. This solution is

usually filtered in RO systems to produce a water stream that is of adequate quality to be released into the environment [9–11]. During the filtration process, calcium sulfate forms an intransigent gypsum ($CaSO_4.2H_2O$) scale on the membranes [12,13]. Gypsum has a sharp crystal structure that can puncture the polyamide thin films that are the RO membrane active surfaces as the gypsum precipitates and grows [14]. Damage to RO membrane active layers irreversibly eliminates membrane selectivity for salts. Moreover, gypsum scale is a dense mineral structure that severely hinders water flux across the membrane, both limiting productivity and reducing the selectivity of RO membranes. The formation of gypsum can be so dense and uniform in some cases as to nearly eliminate water flux across the membrane [15].

Several studies have shown that the addition of antiscalants containing phosphonates, carboxylic acids and acrylic acids to the feed to the RO membranes can mitigate minerals scaling [16–18]. Nevertheless, the high chemical antiscalants consumption can cause secondary environmental waste challenges [19,20]. Using electrochemical technologies for mineral scale mitigation can reduce the costs and environmental impacts of using antiscalants. Recent research has shown that the application of electrical potentials to electrically conductive membranes (including RO membranes) is effective in reducing mineral scaling [4,21–23]. Applying a positive potential to the an electrically conductive membrane, which would thus operate as an anode, was hypothesized to prevent calcium ions from accumulating near the membrane [4]. Further, applied positive potential was thought to reduce the density of gypsum scale [4]. Negative applied potentials sufficiently large to achieve water electrolysis prevented the silicate minerals from attaching to the membrane operating as a cathode [24]. Water electrolysis produces hydrogen gas at the cathode membrane which dissolved the silicate minerals attached to the

membrane [24]. Nevertheless, modifying RO membranes with electrically conductive surface layers that maintain the high rejection required for monovalent salt separation is challenging and research is still ongoing. Significant hurdles exist in modifying and manufacturing, thus these membranes may not be commercially developed for several years [25].

In spiral wound membrane modules, polymeric feed spacers are used to separate membrane sheets and to promote feed solution mixing near the membrane surface [26]. A simpler approach to fabricating electrically conductive RO membranes for electro-assisted filtration is to replace the polymeric feed spacers with flexible meshes made of electrically conductive metals(e.g., copper, stainless steel, titanium) and to apply electric potential directly to these conductive spacers [27,28]. A titanium feed spacer has been previously used to detach microorganisms from an RO membrane using either positive or negative applied potentials [27]. Positive potential was thought to detach microorganisms by generating translational motions, while negative potential was hypothesized to induce electrostatic repulsion with the negatively charged microorganisms [27]. Applying a negative potential to a titanium feed spacer during humic acid filtration assisted in cleaning the membrane via hydrogen bubble generation [28]. To date, the use of metal feed spacers for mineral scaling mitigation during electro-assisted membrane filtration has not been investigated.

In this study, we investigated gypsum mitigation on a RO membrane by applying electric potentials on a low-cost metal feed spacer (i.e., stainless steel) on the surface of a RO membrane. Gypsum was used as the model scalant as this is the most challenging scale to remove from RO membranes. Negative potentials applied at the spacer surface at magnitudes greater than the hydrogen evolution potential (-0.42 V vs. SHE at neutral pH) generate hydrogen bubbles that can

physically remove formed gypsum and dissolve gypsum scale that formed on the membrane surface. However, negative applied potentials will electrostatically attract calcium divalent cations to deposit on the membrane surface. Applying positive potential at the spacer surface was expected to repel calcium cations inducing a nucleation free zone near the RO membrane, which could reduce the rate of gypsum scaling on the membrane. Applying positive potential above oxygen evolution potential (0.82 V vs. SHE at neutral pH) will also generate oxygen bubbles which can induce steric mixing effect, which decrease gypsum scaling on the membrane. However, a positive applied potential is also known to cause anodic dissolution of the metal spacers (iron the main constituent of stainless steel theoretically dissolves at 0.44 V vs. SHE at neutral pH), which can generate additional foulants in feed solution. Herein, we investigated the overall effect of applying positive/negative electric potentials on gypsum scale mitigation. Further, we evaluated whether the advantages gained by applying electric potentials on the metal feed spacers outweighed the limitations associated with anodic dissolution and enhanced calcium deposition. We have also presented a techno-economic analysis for using various conductive feed spacers .

6.3. Experimental

6.3.1 Materials

Commercial BW30 Polyamide RO membranes were purchased from Dow FilmTec USA. 304 stainless steel mesh (aperture size 1.45 mm, open area (i.e., porosity) 73%, thickness 20 mil (0.5 mm), length (84 mm), and width (50 mm)), was purchased from McMaster-Carr Canada to be used as a feed spacer. A titanium mesh (aperture size 0.2 mm, open area 20%, thickness 20 mil (0.5 mm), length (84 mm), and width (50 mm)) was obtained from Delta Scientific Laboratory

Canada to be compared with the stainless steel feed spacer. Calcium hydroxide and sulfuric acid were obtained from Sigma Aldrich Canada. All stock and buffer solutions were prepared in 0.05 µS/cm DI water from a Millipore system.

6.3.2 Model for Estimating Gypsum Nucleation Free Zone near the RO Membrane

Prior to $CaSO_4$ electro-assisted filtration experiments, the Modified Poisson Boltzmann equation was solved numerically in MATLAB to estimate the gypsum nucleation free zone induced near the membrane at positive applied potentials. When a charged surface is placed in an ionic solution, the solution ions rearrange to screen the surface charges, counterions are attracted to the surface and co-ions are repelled from the surface [29]. Ionic species redistribution around the charged surfaces creates an ionic cloud, known as the electric double layer, which has an electrostatic potential [29]. The Modified Poisson-Boltzmann (MPB) equation describes the electrical potential distribution as function of distance from a planar charged surface as follows [30]:

$$\varepsilon_e \frac{d^2\varphi}{dx^2} = \frac{-eN_A \sum_{i=1}^{m} z_i c_i^{\infty} \exp\left(-\frac{z_i e\,\varphi}{k\,T}\right)}{1 + \sum_{i=1}^{m} \frac{c_i^{\infty}}{c_i^{max}} \left[\exp\left(-\frac{z_i e\,\varphi}{k\,T}\right) - 1\right]} \qquad (6.1)$$

where ε_e is the solution electric permittivity, φ is the electric potential, x is the distance from the charged surface, N_A is Avogadro's number, e is the electron charge, z_i is the valence of ionic species, k is the Boltzmann constant, T is the solution temperature, c_i^{∞} is the bulk concentration of ionic species and c_i^{max} is the maximum ion concentration that can accumulate on the charged surface and is calculated from:

$$c_i^{max} = \frac{P}{\frac{4}{3}\pi R_i^3 N_A} \qquad (6.2)$$

where P is defined as the packing factor, which is equal to 1 in case of perfect packing, 0.64 in case of random close packing and 0.52 for simple cubic packing [30]. In our study P is assumed to be 0.64 (i.e., random close packing of ions on the charged membranes). R_i is the ionic radius of ions in the solution. In this study, membrane fouling will be investigated in $CaSO_4$ solutions, the ionic radii for Ca^{2+} and $SO4^{2-}$ were taken as 0.1 nm [31] and 0.258 nm [32], respectively.

In order to be solved numerically, the MPB equation should be written in a dimensionless form. The dimensionless form of the MPB equation for planar coordinates was deduced to be:

$$\frac{d^2\emptyset}{d\,Y^2}\,Y^2 + \frac{d\,\emptyset}{d\,Y}\,Y^2 = \frac{\frac{-1}{2\,\mathrm{I}}\sum_{i=1}^{m} z_i c_i^{\infty} \exp\,(-z_i \emptyset\,)}{1 + \sum_{i=1}^{m} \frac{c_i^{\infty}}{c_i^{max}}\left[\exp(-z_i\emptyset) - 1\right]} \qquad (6.3)$$

Where $\emptyset$ is the dimensionless potential, Y is the dimensionless distance from the membrane, I is the ionic strength of the solution and K is kappa which is the inverse of Debye length:

$$\emptyset = \frac{\mathrm{e}\,\varphi}{\mathrm{k\,T}} \quad (6.4) \quad \text{and} \quad \mathrm{Y} = \exp(-\mathrm{Kx}) \quad (6.5)$$

$$\mathrm{I} = \frac{1}{2}\sum_{\mathrm{i=1}}^{\mathrm{m}} \mathrm{z_i^2 c_i^{\infty}} \quad (6.6) \quad \text{and} \quad \mathrm{K} = \sqrt{\frac{\mathrm{e^2\,N_A}}{\varepsilon_{\mathrm{e}}\,\mathrm{k\,T}}\,2\mathrm{I}} \quad (6.7)$$

After solving the MPB equation to get the electrical potential distribution, the concentrations of co-ions and counter ions as function of the distance from a charged surface can be calculated from [30]:

$$c_i = \frac{c_i^{\infty} \exp\left(-\frac{z_i e\,\varphi}{k\,T}\right)}{1 + \sum_{i=1}^{m} \frac{c_i^{\infty}}{c_i^{max}}\left[\exp\left(-\frac{z_i e\,\varphi}{k\,T}\right) - 1\right]} \qquad (6.8)$$

For this study, the conductive spacers attached to the RO membrane was considered as a planar charged surface (the spacers have length to thickness ratio (168) and width to thickness ratio (100)). The MPB equation (Eq. 6.3) was solved numerically using boundary value problem fourth

order method (BVP4C) in MATLAB to get the electrical potential distribution as a function of the distance from the charged spacer in $CaSO_4$ solution. The boundary conditions for this problem are $\varphi_{x=0} = \varphi_{applied}$ and $\varphi_{x=\infty} = 0$. These boundary conditions in the dimensionless form are corresponding to:

$$\emptyset_{Y=1} = \frac{\mathrm{e}\,\varphi_{applied}}{\mathrm{k\,T}} \quad (6.9) \quad \text{and} \quad \emptyset_{Y=0} = 0 \quad (6.10)$$

The concentration of Ca^{2+} ions near the spacer surface was calculated from Eq. 6.8 at different applied anodic potentials at the spacer surface ($\varphi_{applied}$ = 1,3,6 V). The gypsum nucleation free zone was estimated to be the distance free from calcium ions near the spacer surface. Appendix A shows the MATLAB code used for solving the MPB equation for a flat plate (i.e., the conductive spacer) charged with 1 V in 2.5 mM (340 ppm) $CaSO_4$ solution.

6.3.3 Electro-Assisted RO Filtration Experiments

2.5 mM (340 ppm) $CaSO_4$ solution (initial conductivity ~ 500 µS/cm, pH_i ~ 7.5) was prepared by adding $Ca(OH)_2$ to H_2SO_4 solution. The $CaSO_4$ solution was filtered in a cross-flow filtration system while applying electric potentials to a stainless steel mesh spacer attached to a RO membrane to investigate gypsum scale mitigation under an applied electric field. The custom-built lab-scale cross-flow filtration system (shown in Figure 6.1) consists of a membrane cross-flow cell, a control valve (Badger meter Inc., USA), a high pressure pump (Wanner Engineering Inc., USA), and a feed water tank equipped with a chiller (VWR Co., USA) to maintain a constant temperature (25±2 °C). The membrane cross-flow cell held a stainless steel spacer attached to rectangular flat sheet membrane (effective area of 42 cm^2), the cell is equipped with a graphite electrode which was used as a counter electrode to the spacer working electrode in the electrochemical filtration experiments. A schematic for the cross-flow cell is shown in Figure S6.1. The two electrodes were

connected to stainless steel rods which is connect to an external power supply to apply an electric potential. An open-source software package was applied using a Visual Basic control program on an Arduino Nano microcontroller to coordinate input/output operations between computers, sensors, and actuators. This system was used to control the feed pressure and cross-flow velocity as well as to automate data acquisition. The solution in the feed tank was continuously filtered by the RO membrane at a constant pressure of 250 psi. The retentate and permeate were recirculated into the feed tank. RO Membrane samples were compacted for 18 h with deionized water before being used in the $CaSO_4$ solution filtration experiments. Salt rejection (*i.e.*, Salt rejection (%) = 100 × (1 – C_p/C_f)) was determined by measuring the permeate conductivity (C_p) and the feed conductivity (C_f) using a conductivity meter (Thermo Scientific, USA). Normalised flux (*i.e.*, Normalised flux (%) = 100 × (J_V/J_{vi})) was determined by comparing the measured permeate flux of $CaSO_4$ exposed membranes (J_c) to their permeate flux before $CaSO_4$ exposure (J_{vi}).

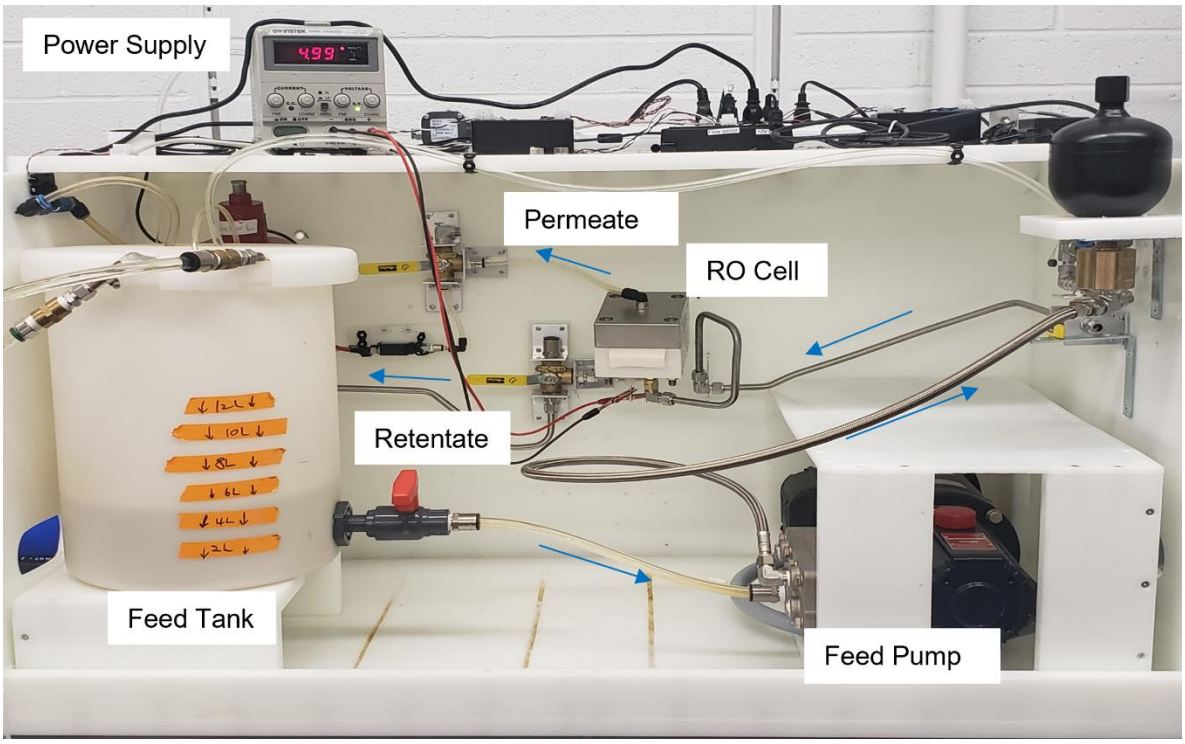

Figure 6. 1: Custom-built lab-scale cross-flow filtration system.

6.4 Results and Discussions

6.4.1 Estimating Gypsum Nucleation Free Zone near the RO Membrane

Before the $CaSO_4$ electro-assisted filtration experiments, gypsum nucleation free zone near the conductive spacers was estimated for positive applied potentials using the modified Poisson-Boltzman model. Applying positive potentials on the conductive spacer on the surface of the RO membrane was expected to repel Ca^{2+} cations from the spacer creating a gypsum nucleation free zone. The nucleation free zone was supposed to reduce the scale formation on the membrane surface enhancing the permeate flux. At negative potentials, sulfate anions are also supposed to repel from the membrane surface creating a nucleation free zone. However, the calcium cations will be attracted and deposited on the negatively charged spacer reducing the permeate flux.

Therefore, the nucleation free zone at negative applied potentials is not expected to enhance the scale mitigation and was not computed in this study.

Figure 6.2 shows the Ca^{2+} cations concentration as function of the distance from the charged surface (i.e., conductive spacer) at positive applied potentials on the spacer surface. The nucleation free zone (i.e., the Ca^{2+} ions free zone) was estimated to be 0.95 nm in case of 1V applied potential and increased to 1.49 nm and 2.00 nm upon increasing the applied potentials to 3V and 6V respectively, assuming theoretical conditions with no thermal losses. Increasing the applied potential increased the electrostatic repulsion force between the positively charged spacer and the metal cations increasing the crystal's nucleation free zone near the charged spacer, which can lead to better fouling control and higher permeate flux.

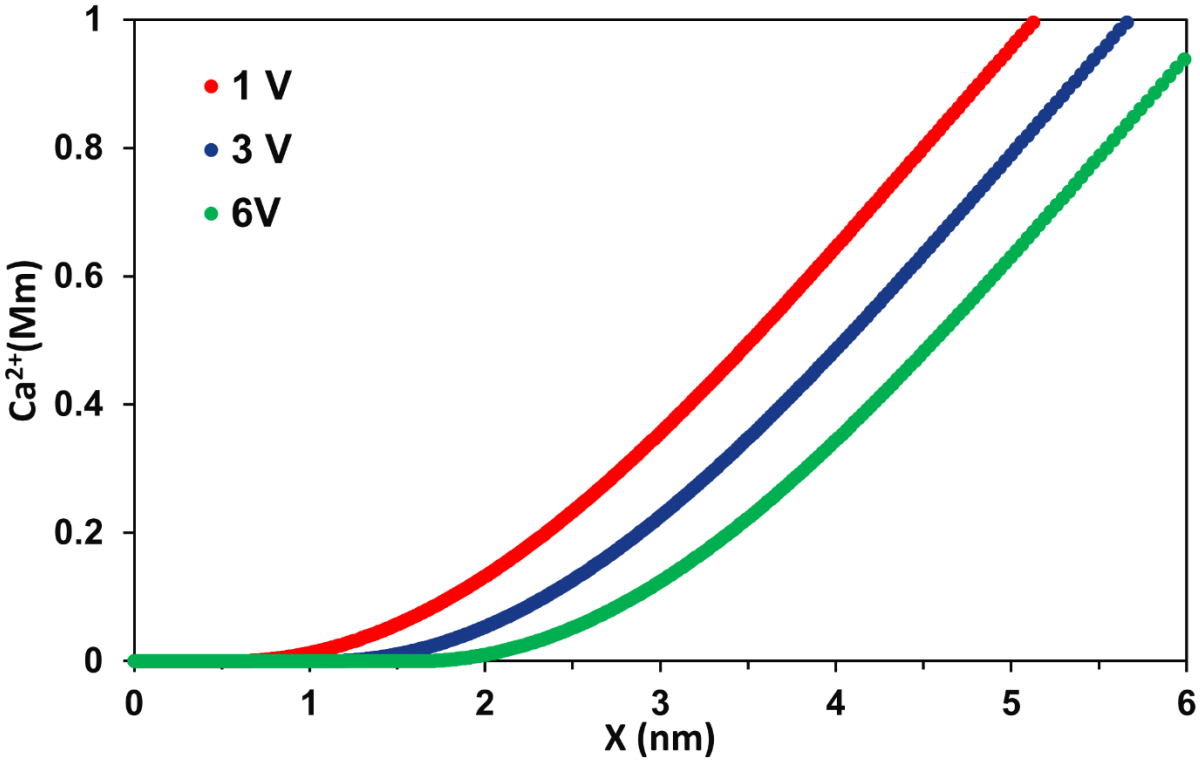

Figure 6. 2: Ca^{2+} cations concentration as function of the distance from the charged spacer at positive applied potentials

6.4.2 Electro-Assisted RO Filtration experiments

Electric potentials were applied between the stainless-steel spacer and the graphite counter electrode while filtering 340 ppm $CaSO_4$ solution in a cross-flow filtration cell. Applying -3V electric potential to the spacer/graphite pair while using the spacer as cathode did not affect the permeate flux in comparison with the control experiment at 0V, as shown in Figure 6.3. This result indicates that the generated hydrogen bubbles at the spacer cathode did not produce sufficient mixing or shear forces to overcome the calcium deposition on the membrane. Figure 6.3 also shows that increasing the applied potential to -7V caused a significant decline in the flux in comparison with the control experiment at 0V, suggesting that enhanced electrostatic attraction of the divalent calcium cations to the spacer cathode increased membrane scaling. Increasing the applied potential to -7V was expected to significantly increase hydrogen gas production which was predicted to limit scale formation on the membrane surface. Nevertheless, the enhanced electrostatic attraction of calcium cations to the spacers seemed to enhance the formation of gypsum scale. An image for the RO membrane is shown in Figure 6.3 when this membrane was used to filter the $CaSO_4$ electrolyte solution with a spacer cathode charge to -7V applied potential. The image illustrates a white precipitate on the membrane surface related to calcium deposition. The salt rejection in case of using cathodic spacers exceeded 96% at -3V and -7V applied potentials, indicating that the electric field did not affect the ions rejection. While the pH of the permeate increased from 7.5 (in case of control) to 8.3 and 9.5 in case of applying -3V and -7V respectively. Using the spacer as cathode produced hydrogen gas and hydroxide ions (OH^-) near the membrane increasing the permeate pH, but had no effect on reducing gypsum formation and increased gypsum scaling with the application of -7V potential.

Applying 3V to the spacer/graphite pair while using the spacer as an anode did not show a significant enhancement in the permeate flux in comparison with the control experiments at 0V, as shown in Figure 6.3. In order to estimate the potential at the spacer surface corresponding to the applied potential between the spacer/graphite pair in the cross-flow cell, a three-electrode batch electrochemical cell (having a stainless steel spacer working electrode, graphite counter electrode and Ag/AgCl reference electrode) connected to a potentiostat and a voltameter was utilized. Applying 3V to the spacer/graphite pair approximately induces 2.3V vs. Ag/AgCl (2.5V vs. SHE) at the spacer surface. Using PBM model, a nucleation freezone of 1.37 nm will be produced when applying 2.5 V to the spacer surface. However, this nucleation free zone did not enhance gypsum mitigation on the RO membrane as shown by the unchanged permeate flux in Figure 6.3. Under anodic potentials, the spacer undergoes anodic corrosion and thus oxidative dissolution of iron in the electrolyte, producing iron-based foulants which were hypothesized to have a negative effect on the permeate flux and negated any enhancement resulting from the either induced nucleation free zone or steric repulsion from O_2 gas generation. A 7V potential between the spacer/graphite pair (6V vs. SHE at the spacer surface) was then applied to demonstrate that the production of iron foulants from the spacer anodic corrosion in the electrolyte would counter-act any benefit obtained from the nucleation free zone (2.00 nm at 6V) induced near the membrane surface or from the steric effect from O_2 gas generation . As expected, the permeate flux significantly decreased when applying 7V in comparison with 3V and 0V control experiments, as shown in Figure 6.3. A digital image for the RO membrane used for $CaSO_4$ solution filtration in the 7V applied potential experiment is shown in Figure 6.3. The image shows an orange-red precipitate on the membrane surface indicating the anodic dissolution of iron (the main

constituent of the stainless steel spacer) which produced extra foulants in the solution decreasing the overall flux. Control experiment in a batch electrochemical cell using stainless steel spacer anode and graphite cathode showed the formation of significant red precipitates after 1h of applying 7V in $CaSO_4$ electrolyte confirming the anodic dissolution of the stainless steel spacer, see Figure S6.2. Similar to the case of using cathodic spacers, the salt rejection for the control and the electro filtration experiments at 3V and 7V exceeded 96%. On the other hand, the pH of the permeate was affected by the electro-filtration. Applying 3V and 7V on the spacer decreased the permeate pH from to 7.5 to 6 and 4.5 respectively. Using the spacer as an anode promoted water electrolysis and H^+ protons production near the membrane which decreased the permeate pH, but had no impact on reducing gypsum scale. The initial permeate flows for the performed experiments in this section were nearly constant (4.94 ± 0.06 mL/min), which ensured an accurate comparison between the different experiments. Figure S6.4 shows that the permeate flow during applied potential experiments has the same trend as the normalized flux (Figure 6.3) when compared to the control experiments at 0V.

To validate these results, a titanium spacer that was previously used for electro assisted filtration of solutions rich in organic and biofoulants [27,28], was used in place of the stainless steel spacer during $CaSO_4$ solution electrofiltration. The titanium spacer electrofiltration experiments demonstrated the same flux decline behaviour as the stainless steel spacer experiments when using the titanium spacer as either an anode or a cathode under 7V applied potential, as shown in Figure S6.3a. Figure S6.3b presents control experiments with the titanium spacer anode and a graphite cathode in a batch electrochemical cell, demonstrating anodic dissolution of titanium into titanium dioxide (white precipitate) under 7V applied potential for 1h in $CaSO_4$ electrolyte.

The conclusions from these set of experiments are twofold: First, the use of conductive spacers as cathodes for gypsum mitigation during electro-assisted filtration will not be effective as the reduction in permeate flux caused by the deposited calcium cations on the membrane will overcome any potential cleaning effect realized by hydrogen bubble generation via water electrolysis. This result can also be extended to electrochemical membranes (ECMs) as the competition between the calcium deposition and hydrogen bubbles cleaning effect will occur in the same manner. Second, the use of conductive metal spacers for gypsum mitigation during electro-assisted filtration will not be effective due to metal anodic dissolution. However, the use of anodically inert electrically conductive spacers, such as graphite or CNTs coated spacers may benefit from the nucleation free zone induced near the membrane via the anodic potential and enhance the overall permeate flux. Anodically inert spacers are expected to be more expensive than the stainless steel spacers used in this study. Therefore, an economic analysis was performed to compare the cost of different types of conductive spacers, as follows.

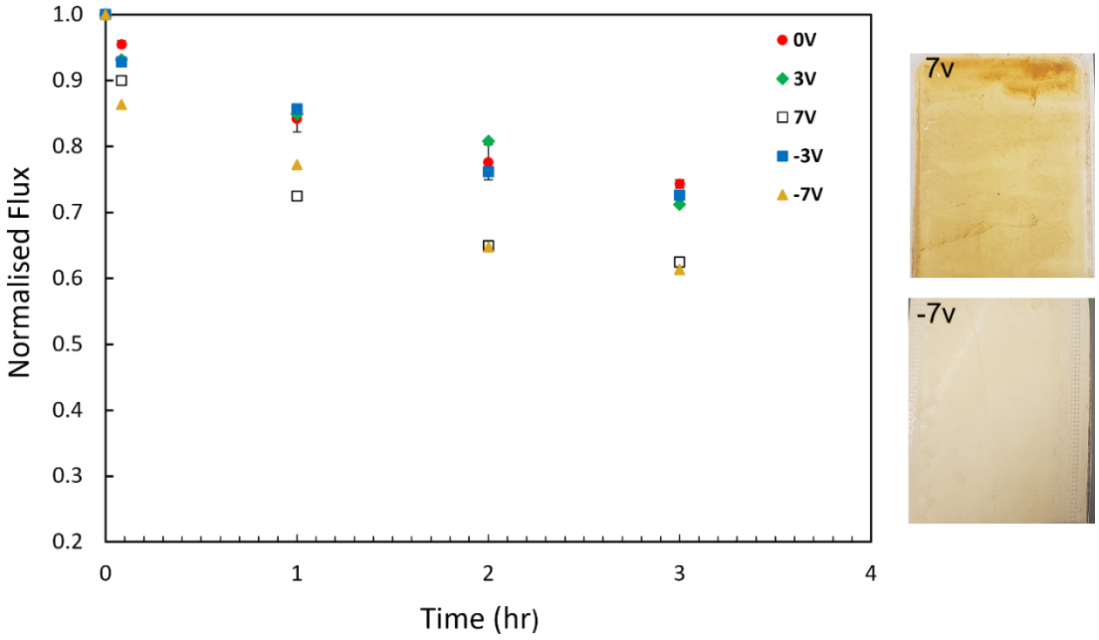

Figure 6. 3: (Left side) Normalised permeate flux as function of filtration time under different

applied potentials in a cross-flow filtration cell, initial permeate flux = 58.5 L/m^2/h, applying 3V and 7V to the stainless steel spacer/graphite pair while using the spacer as anode was notated as "3V" and "7V", while applying 3V and 7V while using spacer cathode was notated as "-3V" and "-7V". (Right side) Digital images for the RO membranes after the electro-assisted filtration experiments.

6.4.3 Economic Analysis for Different Spacer Materials

To draw a comparison between conductive spacers fabricated form different materials, a techno economic analysis was preformed to compare the cost of stainless-steel spacers with that of polymetric spacers coated with CNTs and 3D printed graphene spacers. The stainless steel spacer that was used for this study (purchased from McMaster-Carr Co. Canada) costs \$58.29/m^2 , the cost of which included material costs as well as the operational and capital costs to produce it.

Polypropylene spacers are widely used as feed spacers for RO membranes, however they are not electrically conductive. Coating polypropylene (PP) spacers with a conductive material that is inert to electric anodic dissolution (e.g., CNTs) can enable their use in electro-filtration applications. Commercial PP spacers (having 76% open area (i.e. porosity), diamond shaped hole size 2.79 mm (i.e. aperature), thickness 31 mil, and 9x9 strands per inch) are sold by Industrial Netting Co. USA for 3 \$/m^2. Rao et al. have shown that the mass of CNTs required for coating a PP membrane was 4.17 g CNTs/m^2 [33], and previous demonstration from our group have shown that 1.73 g CNTs/m^2 are required for coating PES membranes. Thus, the required mass of CNTs for coating PP spacers were assumed to be in the range between 1.73-4.17 g CNTs/m^2 . The thermal cost for spray coating the PP membrane with CNTs was \$2/m^2 [33]. We assumed that spray coating would be among the most efficient methods to coat a polypropylene spacer thus the same thermal cost was assumed for the spray coating of PP spacers. The approximate cost of functionalized CNTs (CNTs functionalization is necessary for effective dispersion of CNTs in the

spraying solution to allow uniform coating on the spacer surface) is $17 /g from Cheap Tubes Co. USA. Taking into consideration the void fraction of the spacer and that both sides of the spacer need to be coated, the total surface area of the spacer to be coated per m^2 polypropylene spacer sheet was estimated to be 0.9165 m^2. Adding the thermal cost for spraying ($2/$m^2$), the propylene spacer cost ($3/$m^2$), and the CNTs cost (mass of CNTs per unit area (1.73-4.17 g CNTs/m^2) x price of CNTs per mass ($17 /g CNTs) for a total CNT cost ($29.41-70.89/$m^2$)). All of these are scaled by the required area to be coated per unit area (0.9165). Thus, the total materials and energy cost for coating a PP spacer with CNTs is $31.54-69.55/$m^2$. The capital cost of thermal spray coaters according to a market survey varies between $20,000-$80,0000 depending on the size and brand. This capital cost would be amortized over the lifetime of the coater and the total surface area coated in that time.

An alternative approach to making conductive spacers is to use 3D printing. Using 3D printing for the production of graphite conductive spacers has been previously reported [34]. Graphene blended polymer spacers (square-shaped hole size 4.95 mm (i.e. aperture), thickness 50 mil) was produced by fusion 3D printing of polylactic acid filaments blended with 8% graphene. The materials cost was $570/$m^2$ and electric cost was $0.963 /$m^2$ [34]. The capital cost for the Industrial fusion 3D Printers cost varies between $20,000-$100,000 according to the Fusion3 Co USA.

Table 6.1 shows a summary for the techno-economic analysis comparing the stainless-steel spacer, PP spacer coated with CNTs, and 3D printed graphite spacer. The CNT-coated PP spacer fabrication does not require high materials and energy cost in comparison with the stainless-steel spacer, nevertheless the capital cost is higher but this will be amortized over the total surface

area of membranes produced in the lifetime of the device. In comparison, the 3D printed graphite spacer showed a significantly higher materials cost compared with both the stainless steel and the CNT-coated PP spacers, and required a higher capital cost than the spray-coating technique. Taking into consideration that the stainless-steel spacer electrochemically dissolves when used as an anode in electro assisted filtration, CNT-coated polymeric spacers might be a reasonable choice for anodic spacers due to it relatively low materials and energy cost.

Table 6. 1: Techno-economic analysis for different types of conductive spacers

Cost	Stainless steel spacer	PP coated with CNTs spacer	3D printed graphite spacer
Materials	$58.29/m^2	$29.54-67.55/m^2	$570/m^2
Energy		$2/m^2	$0.963 /m^2
Capital		$20,000-$80,0000	$20,000-$100,000

6.5 Conclusion

In this study, we investigated gypsum scale mitigation during filtration of calcium sulfate solution while applying electric potentials on a low-cost stainless steel feed spacer attached to a RO membrane. We examined the effect of using the feed spacers as either a cathode or an anode on gypsum scale mitigation. It was determined that using conductive feed spacers as cathodes for gypsum mitigation during electro-assisted filtration is not effective as the cleaning effect of hydrogen bubble generation via water electrolysis was insufficient to prevent the reduction in permeate flux caused by deposited calcium cations on the membrane . Further, it was determined that using anodic metal spacers for gypsum mitigation during electro-assisted filtration is not effective either, as the metal spacers anodically dissolve. However, the use of anodes that are anodically stable and resistant to anodic-dissolution may be used to produce a

nucleation free zone near the membrane surface via anodic potential which may maintain overall permeate flux. A high-level techno economic analysis suggests that using CNT-coated PP spacers would be an economically feasible technological approach to making conductive spacers to limit mineral scaling. Future experiments will focus on validating the expected positive effects of using anodic CNT-coated polymeric spacers on scale mitigation in electro-assisted filtration processes.

6.6 Acknowledgment

This work was funded by the Natural Sciences and Engineering Research Council of Canada (NSERC) in partnership with Hatch Ltd., Canada.

6.7 References

[1] M. Qasim, M. Badrelzaman, N.N. Darwish, N.A. Darwish, N. Hilal, Reverse osmosis desalination: A state-of-the-art review, Desalination. 459 (2019) 59–104. doi:10.1016/j.desal.2019.02.008.

[2] K.P. Lee, T.C. Arnot, D. Mattia, A review of reverse osmosis membrane materials for desalination — Development to date and future potential, J. Memb. Sci. 370 (2011) 1–22. doi:10.1016/j.memsci.2010.12.036.

[3] M. Qasim, N.N. Darwish, S. Mhiyo, N.A. Darwish, N. Hilal, The use of ultrasound to mitigate membrane fouling in desalination and water treatment, Desalination. 443 (2018) 143–164. doi:10.1016/j.desal.2018.04.007.

[4] W. Duan, A. Dudchenko, E. Mende, C. Flyer, X. Zhu, D. Jassby, Electrochemical mineral scale prevention and removal on electrically conducting carbon nanotube-polyamide reverse osmosis membranes, Environ. Sci. Process. Impacts. 16 (2014) 1300–1308. doi:10.1039/c3em00635b.

[5] D.C. Buzzi, L.S. Viegas, M.A.S. Rodrigues, A.M. Bernardes, J.A.S. Tenório, Water recovery from acid mine drainage by electrodialysis, Miner. Eng. 40 (2013) 82–89. doi:10.1016/j.mineng.2012.08.005.

[6] A.O. Aguiar, L.H. Andrade, B.C. Ricci, W.L. Pires, G.A. Miranda, M.C.S. Amaral, Gold acid mine drainage treatment by membrane separation processes: An evaluation of the main operational conditions, Sep. Purif. Technol. 170 (2016) 360–369. doi:10.1016/j.seppur.2016.07.003.

[7] D. Feng, C. Aldrich, H. Tan, Treatment of acid mine water by use of heavy metal precipitation and ion exchange, Miner. Eng. 13 (2000) 623–642. doi:10.1016/S0892-6875(00)00045-5.

[8] S. Heviánková, I. Bestová, M. Kyncl, The application of wood ash as a reagent in acid mine

drainage treatment, Miner. Eng. 56 (2014) 109–111. doi:10.1016/j.mineng.2013.10.032.
[9] H. Kyllönen, A. Grönroos, E. Järvelä, J. Heikkinen, C. Tang, Experimental Aspects of Scaling Control in Membrane Filtration of Mine Water, Mine Water Environ. 36 (2017) 193–198. doi:10.1007/s10230-016-0415-3.
[10] City of Ottawa, Sewer use program-Guide for discharging wastewater from industrial facilities, 2011.
[11] City of Tronoto, Toronto municipal code chapter 681, sewers, 2019.
[12] A. Matin, F. Rahman, H.Z. Shafi, S.M. Zubair, Scaling of reverse osmosis membranes used in water desalination: Phenomena, impact, and control; future directions, Desalination. 455 (2019) 135–157. doi:10.1016/j.desal.2018.12.009.
[13] Y.A. Le Gouelleec, M. Elimelech, Control of calcium sulfate (gypsum) scale in nanofiltration of saline agricultural drainage water, Environ. Eng. Sci. 19 (2002) 387–397. doi:10.1089/109287502320963382.
[14] M. Uchymiak, E. Lyster, J. Glater, Y. Cohen, Kinetics of gypsum crystal growth on a reverse osmosis membrane, J. Memb. Sci. 314 (2008) 163–172. doi:10.1016/j.memsci.2008.01.041.
[15] A. Rahardianto, W. Shih, R. Lee, Y. Cohen, Diagnostic characterization of gypsum scale formation and control in RO membrane desalination of brackish water, J. Memb. Sci. 279 (2006) 655–668. doi:10.1016/j.memsci.2005.12.059.
[16] M.M. Kim, J. Au, A. Rahardianto, J. Glater, Y. Cohen, F.W. Gerringer, C.J. Gabelich, Impact of conventional water treatment coagulants on mineral scaling in RO desalting of brackish water, Ind. Eng. Chem. Res. 48 (2009) 3126–3135. doi:10.1021/ie800937c.
[17] K. Chauhan, R. Kumar, M. Kumar, P. Sharma, G.S. Chauhan, Modified pectin-based polymers as green antiscalants for calcium sulfate scale inhibition, Desalination. 305 (2012) 31–37. doi:10.1016/j.desal.2012.07.042.
[18] H. Lee, M. Amin, T. Baker, S. Sarathy, A comparative study of RO membrane scale inhibitors in wastewater reclamation : Antiscalants versus pH adjustment, Sep. Purif. Technol. 240 (2020) 116549. doi:10.1016/j.seppur.2020.116549.
[19] I. Marian, N. Adroer, E. Cortada, D. Vidal, J. Aumatell, Environmentally friendly antiscalant effective in inhibition of scale formation and dispersing organic and colloidal matter in seawater desalination plants, Desalin. Water Treat. 55 (2015) 3485–3497. doi:10.1080/19443994.2014.947776.
[20] T.M. Missimer, R.G. Maliva, Environmental issues in seawater reverse osmosis desalination: Intakes and outfalls, Desalination. 434 (2018) 198–215. doi:10.1016/j.desal.2017.07.012.
[21] L. Tang, A. Iddya, X. Zhu, A. V. Dudchenko, W. Duan, C. Turchi, J. Vanneste, T.Y. Cath, D. Jassby, Enhanced Flux and Electrochemical Cleaning of Silicate Scaling on Carbon Nanotube-Coated Membrane Distillation Membranes Treating Geothermal Brines, ACS Appl. Mater. Interfaces. 9 (2017) 38594–38605. doi:10.1021/acsami.7b12615.
[22] R. Hashaikeh, B.S. Lalia, V. Kochkodan, N. Hilal, A novel in situ membrane cleaning method using periodic electrolysis, J. Memb. Sci. 471 (2014) 149–154. doi:10.1016/j.memsci.2014.08.017.
[23] P. Gayen, J. Spataro, S. Avasarala, A.M. Ali, J.M. Cerrato, B.P. Chaplin, Electrocatalytic Reduction of Nitrate Using Magnéli Phase TiO2 Reactive Electrochemical Membranes

Doped with Pd-Based Catalysts, Environ. Sci. Technol. 52 (2018) 9370–9379. doi:10.1021/acs.est.8b03038.
[24] L. Tang, A. Iddya, X. Zhu, A. V. Dudchenko, W. Duan, C. Turchi, J. Vanneste, T.Y. Cath, D. Jassby, Enhanced Flux and Electrochemical Cleaning of Silicate Scaling on Carbon Nanotube-Coated Membrane Distillation Membranes Treating Geothermal Brines, ACS Appl. Mater. Interfaces. 9 (2017) 38594–38605. doi:10.1021/acsami.7b12615.
[25] Y. Zhao, M. Sun, L.R. Winter, S. Lin, Z. Wang, J.C. Crittenden, J. Ma, Emerging Challenges and Opportunities for Electrified Membranes to Enhance Water Treatment, Environ. Sci. Technol. 56 (2022) 3832–3835. doi:10.1021/acs.est.1c08725.
[26] B. Gu, C.S. Adjiman, X.Y. Xu, The effect of feed spacer geometry on membrane performance and concentration polarisation based on 3D CFD simulations, J. Memb. Sci. 527 (2017) 78–91. doi:10.1016/j.memsci.2016.12.058.
[27] Y. Baek, H. Yoon, S. Shim, J. Choi, J. Yoon, Electroconductive Feed Spacer as a Tool for Biofouling Control in a Membrane System for Water Treatment, Environ. Sci. Technol. Lett. 1 (2014) 179–184. doi:10.1021/ez400206d.
[28] H.S. Abid, D.J. Johnson, B. Clifford, D.T. Gethin, P. Bertoncello, R. Hashaikeh, N. Hilal, Periodic electrolysis technique for in situ fouling control and removal with low-pressure membrane filtration, Desalination. 433 (2018) 10–24. doi:10.1016/j.desal.2018.01.019.
[29] H. Saboorian-Jooybari, Z. Chen, Analytical solutions of the Poisson-Boltzmann equation within an interstitial electrical double layer in various geometries, Chem. Phys. 522 (2019) 147–162. doi:10.1016/j.chemphys.2019.01.026.
[30] J.J. López-García, J. Horno, C. Grosse, Poisson-Boltzmann description of the electrical double layer including ion size effects, Langmuir. 27 (2011) 13970–13974. doi:10.1021/la2025445.
[31] B. Tansel, J. Sager, T. Rector, J. Garland, R.F. Strayer, L. Levine, M. Roberts, M. Hummerick, J. Bauer, Significance of hydrated radius and hydration shells on ionic permeability during nanofiltration in dead end and cross flow modes, Sep. Purif. Technol. 51 (2006) 40–47. doi:10.1016/j.seppur.2005.12.020.
[32] http://www.wiredchemist.com/chemistry/data/thermochemical-radii-anions (accessed on 02-04-2020.).
[33] U. Rao, A. Iddya, B. Jung, C.M. Khor, Z. Hendren, C. Turchi, T. Cath, E.M.V. Hoek, G.Z. Ramon, D. Jassby, Mineral Scale Prevention on Electrically Conducting Membrane Distillation Membranes Using Induced Electrophoretic Mixing, Environ. Sci. Technol. 54 (2020) 3678–3690. doi:10.1021/acs.est.9b07806.
[34] N. Yanar, E. Yang, H. Park, M. Son, H. Choi, Efficacy of Electrically-Polarized 3D Printed Graphene-blended Spacers on the Flux Enhancement and Scaling Resistance of Water Filtration Membranes, ACS Sustain. Chem. Eng. 9 (2021) 6623–6631. doi:10.1021/acssuschemeng.0c09362.

Chapter 7

Contributions and Future Perspectives

7.1 Contributions

Efficient industrial wastewater treatment is required nowadays for industrial wastewaters to meet both environmental and social needs within economic feasibility. Removing toxic contaminants (e.g., toxic metals and organic pollutants) is necessary for the safe disposal of industrial wastewater, while extracting useful resources (e.g., precious metals) can make treatment economically beneficial. This thesis investigated the replacement conventional removal and treatment methods for metal and associated contaminants from industrial wastewaters with novel electrochemical approaches to lower the environmental impact, decrease the chemical consumption, decrease the overall capital costs by reducing the number of unit operations, while extracting precious metals as an economic benefit.

Chapter 2 demonstrated for the first time the feasibility of combining electrochemical oxidation and in-situ coagulation for treating mixed industrial wastewater containing high concentrations of toxic metals together with organic pollutants. Electrochemical oxidation experiments of methyl orange model solution identified IrO_2-RuO_2 mixed metal oxide anodes as the optimum electrodes for organic compound degradation. These anodes together with stainless-steel cathodes were used to degrade a highly contaminated mixed industrial wastewater using an electrochemical oxidation-in-situ coagulation (ECO-IC) process. ECO-IC resulted in a treated solution with a substantially lower heavy metal content, lower organic content, greater effective diameter of the suspended particles, and distinct phases that can be separated for further treatment. The dominant mechanism for heavy metal removal from the solution is the coagulation of the toxic metals with the in-situ electrolysis-formed iron hydroxide. While anodic

electrochemical oxidation was the dominant mechanism for degrading organic compounds in the solution. The findings of this study demonstrate the feasible use of ECO-IC process towards the efficient treatment of real mixed industrial wastewater rich with toxic metals and organic contaminants. Such a process could decrease the chemical consumption and the stagewise unit operations required for treating these highly contaminated wastewaters, which will have economic and environmental benefits. However, the ECO-IC process is limited to industrial wastewaters rich in metals that can form metal hydroxide coagulants (i.e., iron or aluminium).

Chapter 3 reported the invention of a closed loop continuous process for adsorption and electrodesorption of toxic metals from aqueous solutions using CNT sorbents. The closed-loop continuous regenerative process enables the feasible use of highly effective, but expensive CNT sorbents for metal removal from waste solutions. The desorption process is based on electrochemical regeneration of CNTs from metals, which avoids the need for acids or other solvents to regenerate the CNTs. Copper (a model toxic metal) desorption from functionalized carbon nanotubes via electric fields was demonstrated. 90% of the copper adsorbed onto the CNT surfaces was desorbed by applying 3V anodic potential for 1h. The mechanism of desorption was hypothesized to be electrostatic repulsion between the CNT anode and the Cu cations rather than Cu electrochemical oxidation and/or the shearing from bubbles generated by water electrolysis at the CNT surface. This study demonstrated the use of CNTs for effective removal of copper (a model toxic metal) and their environmentally benign electrodesorption into a concentrate stream.

Based on the results from chapter 3, chapter 4 investigated gold (a model of precious metals) extraction from industrial wastewaters using CNTs and their subsequent elution from the CNTs

via a chemical-free electrochemical technique. Such a process could enable downstream resource recovery of precious metals, turning an environmental pollutant into a valuable resource with minimal chemical consumption. In the first part of the study, the effect of functional groups attached to MWCNTs on gold extraction from acidic solutions simulating e-waste leachate was investigated. The study demonstrated a trade-off between the effect of functional group electric charge and specific surface area (SSA) on Au adsorption onto MWCNTs. Negatively charged MWCNTs have a negative impact on Au adsorption from acidic solutions regardless of their SSA. On the other hand, for positively charged MWCNTs, the SSA area has a more dominant effect on Au adsorption than the magnitude of the strength of the surface charge groups. In the second part of the study, Au electrochemical elution from sorbents was demonstrated for the first time. Au electrodesorption from MWCNTs sorbents showed a direct relationship with the applied current and the mass of Au adsorbed on the MWCNTs. The mechanism for Au electrodesorption from MWCNTs is believed to be Au electrochemical oxidation reactions. This chapter provided a better understanding of the effect of CNTs' functional groups on Au extraction from acidic wastewater and demonstrated a chemical free approach for the subsequent Au elution from the CNTs sorbents in neutral solution.

Chapter 5 demonstrated the electrochemical dissolution of metal fasteners (metal alligator clips) holding porous conductive and non-conductive membranes in batch electrochemical cells, even when these alligator clips are kept outside the electrolyte. It was identified that the electrolyte ions migrated through the porous membranes by the action of capillary forces forming a closed electrochemical circuit with the alligator clips. This phenomenon has not been previously reported in either the porous electrode or electrochemical membrane (ECM) literature, yet has

significant implications for batch electrochemical cell experiments, and may confound experimental results. A simple solution was proposed to this problem: separating the metal fasteners from the porous membrane electrode with a non-porous conductive graphite foil, which will maintain an open electrochemical circuit. This solution was validated and proposed as a standard method for experiments using porous electrodes and electrically conductive membranes. The findings of this study will decrease the source of errors when testing ECMs and porous electrodes in batch experiments. This will have significant implication for the many emerging applications of porous electrodes and ECMs in water treatment including metal removal, organic pollutant degradation and desalination.

Chapter 6 demonstrated the electro-assisted filtration of calcium sulfate solutions using RO membranes. Calcium sulfate is a secondary pollutant produced during metal removal from acid mine drainage. Calcium sulfates deposited as gypsum scale during RO filtration of mining waste solution, reducing the permeate flux and possibly damaging the RO membranes. In this research, conventional gypsum mitigation using antiscalants was replaced by an electrochemical method to minimize the chemical consumption and reduce the associated environmental disposal challenges. Electrically conductive metal feed spacers were charged with electrical potential to prevent gypsum scale formation on the RO membranes during the filtration of calcium sulfate solutions. It was identified that applying cathodic potentials on the metal spacers to prevent scaling by hydrogen bubble scouring will not be effective as the crystallization of gypsum on the membrane is resistant to the cleaning effect of hydrogen bubble generation via water electrolysis. Applying anodic potential on the metal spacers during electro-assisted filtration caused anodic dissolution of the metal spacers. The foulants produced from the spacer

dissolution decreased the permeate flux and prevented any scale mitigation resulting from a gypsum nucleation free zone induced near the membranes via the anodic potential. The results of this research suggest that using inert feed spacers to electro-dissolution (e.g., CNTs or graphite coated polymeric spacers) may benefit from the nucleation free zone induced near the membrane during applying anodic potential and to enhance the overall permeate flux.

7.2 Future Perspectives

This thesis recommends that future researchers should investigate the following aspects.

1. ECO-IC process was introduced for the simultaneous removal of metals and associated organic pollutants from highly contaminated mixed industrial wastewater. A significant decrease in the metal concentrations was shown, however the organic pollutant degradation was limited by electrode available surface area for oxidation. Future research should focus on quantifying the effect of electrode surface area and porosity on the rate of organic compound degradation. Additionally, it is recommended to combine the ECO-IC process with conventional treatment methods (e.g., membranes) to achieve more efficient treatment of industrial wastewater.

2. A closed loop cycle for metals adsorption and electrochemical desorption from waste solutions using CNTs sorbents was introduced. This approach was used for metal (i.e., copper or gold) removal from single metal solutions in batch systems. Future research should investigate using this process for the selective adsorption of metals from mixed metal solutions. Future studies should also focus on building a continuous process for the adsorptive water treatment followed by concentrated metal recovery in a waste stream, and should continue developing industrial efficient techniques for CNT removal from polymeric membranes.

3. A limitation on gypsum scale mitigation via charging metallic feed spacers in electro-assisted filtration process was shown in this study. The results suggested that anodically inert feed spacers are a more appropriate alternative to metal feed spacers in the study of mineral scale mitigation during RO filtration. Economic analysis has shown that polypropylene (PP) spacers coated with CNTs will be a cost-effective option as inert feed spacers. Future studies should experimentally investigate the effect of charging CNT-coated PP spacers on scale mitigation during RO filtration.

Appendix A

Supporting Information

Chapter 2 Supporting Information

Table S2. 1: EDX Analysis for the titanium-based electrodes

Elements Wt%	IrO_2-RuO_2-TiO_2 anode	RuO_2-TiO_2 anode	IrO_2-RuO_2 anode
O	29.0	37.8	33.4
Ti	30.9	21.8	18.4
Ir	22.0	4.6	31.0
Ru	13.6	35.2	13.5
C	2.4	--	--
Sn	1.1	--	2.2
P	--	0.7	--
Co	0.6	--	1.5
Si	0.3	0.2	--

Table S2. 2: Elements Mole percent in titanium-based electrodes calculated from the EDX Analysis

Elements mole%	IrO_2-RuO_2-TiO_2 anode	RuO_2-TiO_2 anode	IrO_2-RuO_2 anode
O	61.71	73.71	74.20
Ti	21.98	14.19	13.71
Ir	3.90	0.75	5.74
Ru	4.58	10.83	4.75
C	6.80	--	--
Sn	0.32	--	0.66
P	--	0.26	--
Co	0.35	--	0.92
Si	0.36	0.25	--

Table S2. 3 : TOC analysis for filtered Sarnia samples

Sample #	TOC (ppm)
Sample 1	2250
Sample 2	2036
Sample 3	1980
Sample 4	1970
Sample 5	1402
Sample 6	1401
Sample 7	1249
Sample 8	920
Average	**1651**
Standard deviation	**469**

Table S2. 4: Organic content characterization for 30 µm filtered Sarnia wastewater samples

Compound	Formula	Relative Fraction %	Probability %
6-octadecenoic acid	$C_{18}H_{34}O_2$	23.794	10.6
Palmitic acid	$C_{16}H_{32}O_2$	14.873	72.9
Alkanes	C_nH_{2n+2}	12.995	8.16
Ethyl 4-ethoxybenzoate	$C_{11}H_{14}O_3$	12.269	94.8
Fatty alcohols	$C_{12}H_{26}O$	9.192	7.23
Behenyl alcohol	$C_{22}H_{46}O$	7.227	5.85
1,2-octadecanediol	$C_{18}H_{38}O_2$	6.330	4.16
Stearic acid	$C_{18}H_{36}O_2$	4.424	35.9
Lauric acid	$C_{12}H_{14}O_2$	2.487	27.9
Hexaethylene glycol	$C_{12}H_{26}O_7$	2.124	0.26
Stearyl alcohol	$C_{18}H_{38}O$	1.809	19.6
Hexadecyl trichloroacetate	$C_{18}H_{33}Cl_3O_2$	1.666	---

Table S2. 5: Metal analysis for filtered Sarnia samples

Sample #	Fe (ppm)	Mn (ppm)	Mg (ppm)	As (ppm)	Al (ppm)	Ni (ppm)
Sample 1	101.70	8.38	15.26	0.81	0.15	0.35
Sample 2	418.30	12.31	20.38	0.85	0.26	0.35
Sample 3	99.85	6.37	22.77	2.14	0.32	0.35
Sample 4	23.53	7.02	15.35	0.83	0.47	0.18
Sample 5	190.00	12.22	19.19	1.07	0.51	0.24
Average	166.68	9.26	18.59	1.14	0.34	0.29
Standard deviation	152.51	2.84	3.26	0.57	0.15	0.080

Sample #	Cu (ppm)	Cr (ppm)	Pb (ppm)	Cd (ppm)	Be (ppm)
Sample 1	0.092	0.0023	0.0027	0.0016	0.00008
Sample 2	0.026	0.010	0.0022	0.0016	0.00008
Sample 3	0.026	0.0042	0.0011	0.0030	0.00008
Sample 4	0.088	0.0063	0.018	0.0034	0.0011
Sample 5	0.038	0.012	0.0079	0.0054	0.0046
Average	0.054	0.0069	0.0064	0.0030	0.0012
Standard deviation	0.033	0.0039	0.0070	0.0016	0.0020

Table S2. 6: Anions analysis for filtered Sarnia samples

Sample #	Acetate (ppm)	Chloride (ppm)	Formate (ppm)	Sulfate (ppm)	Lactate (ppm)
Sample 1	262.36	489.14	77.65	72.48	1.97
Sample 2	1190.54	641.04	12.80	67.79	1.08
Sample 3	369.67	298.56	58.40	29.23	2.06
Sample 4	225.01	438.06	137.38	51.99	9.18
Sample 5	1156.25	337.69	12.61	11.04	1.00
Average	640.77	440.90	59.77	46.51	3.06
Standard deviation	489.26	135.37	51.90	26.05	3.46

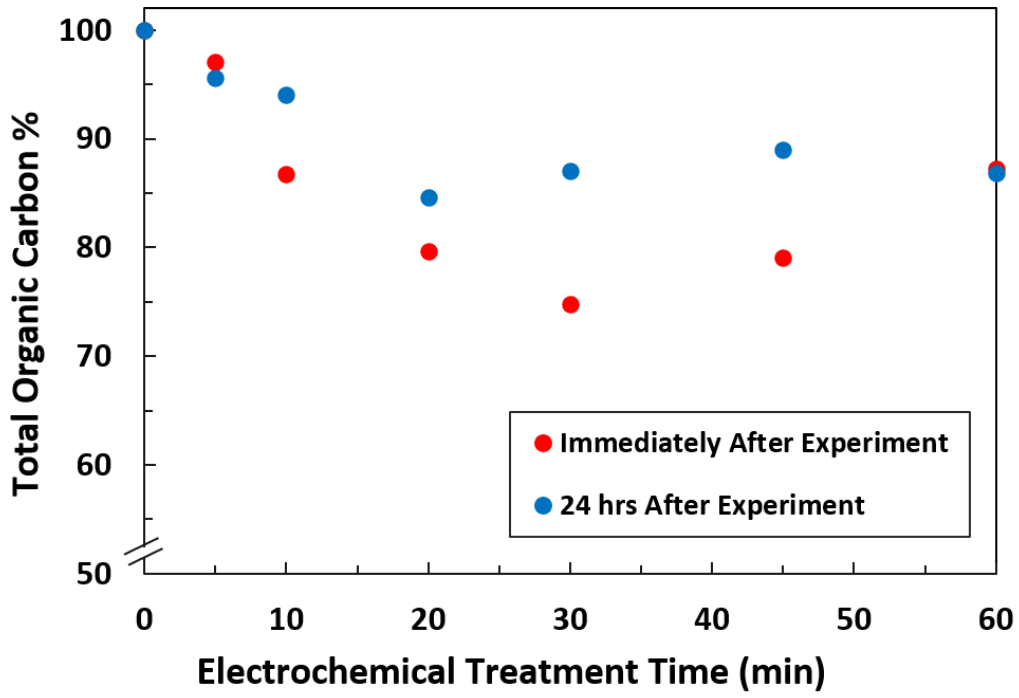

Figure S2. 1: TOC degradation in Sarnia wastewater during 1h ECO-IC at 0.5 A applied current using a curved IrO_2-RuO_2 anode

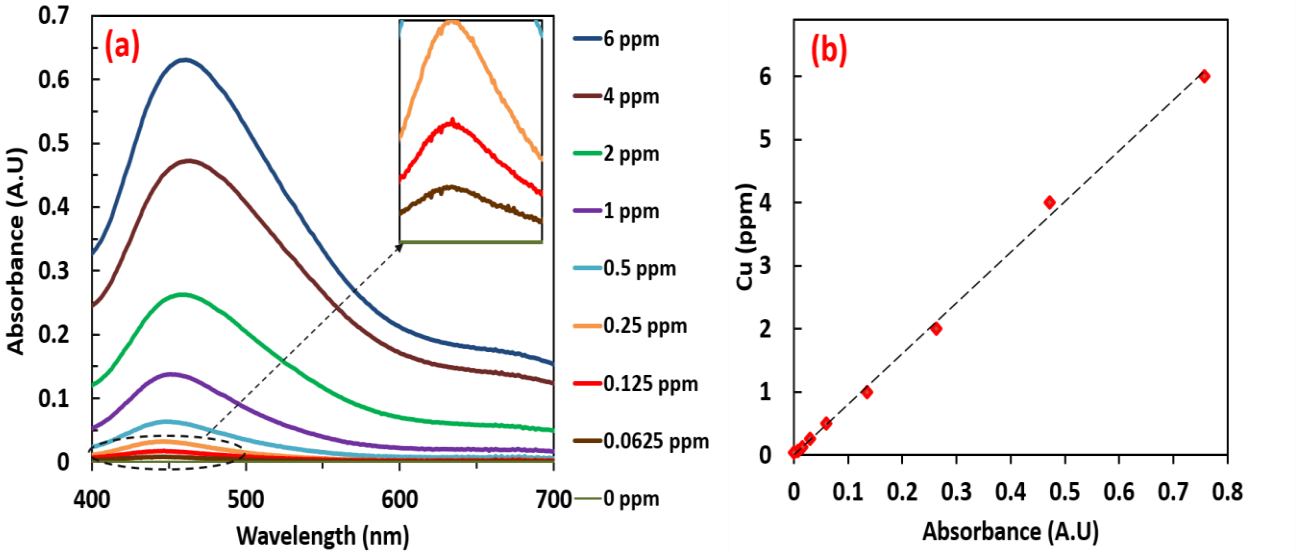

Figure S3. 1: (a) UV-Vis spectra of Cu-DDTC complex in EDTA and tribasic ammonium citrate aqueous solution, (b) A representative calibration curve relating the Cu^{2+} concentration to the absorbance at 460 nm wavelength; the line represents the regression model fit with R^2 of 0.998 and standard error of 0.094 ppm.

Table S3. 1: EDX analysis for f-SW/DWCNTs, HCl treated f-SW/DWCNTs and Cu saturated f-SW/DWCNTs

Elements (wt%)	f-SW/DWCNTs	HCl treated f-SW/DWCNTs	Cu saturated f-SW/DWCNTs
C	84.3	84.5	82.9
O	7.3	7.7	7.7
Al	0.1	0.2	0.1
S	4.8	4.8	5.3
Ti	1.4	1.3	1.3
Cr	1.2	0.9	1.1
Fe	0.4	0.4	0.3
Co	0.3	-	0.2
Cu	**0.2**	**-**	**1.1**
Cl	-	0.1	-
Ca	-	0.1	-

Cu Diffusion Time across the CNTs Membrane

Diffusion time of Cu across the CNTs film on the membrane to the solution (assuming steady state conditions and no additional driving force from applied electric fields) was calculated using the following equation :

$$t = \frac{\Delta X^2}{D} \qquad (S\ 3.1)$$

where ΔX is the thickness of CNTs film, assumed to be 25 µm depending on the SEM analysis. D is the diffusivity of $CuSO_4$ in water, assumed to be equal 5.6x 10^{-6} cm^2/s based on experimental data [1]. Using these values for ΔX and D, the diffusion time of Cu across the CNTs film was calculated using Eq. S3.1 to be 1.1 s. To confirm this estimate, the diffusivity of $CuCl_2$ was also calculated to be 1.78x10^{-5} cm^2/s using Nernst-Haskell equation :

$$D_{AB} = 8.928X10^{-10}T\ \frac{(\frac{1}{n_+} + \frac{1}{n_-})}{(\frac{1}{\lambda_+} + \frac{1}{\lambda_-})} \qquad (S\ 3.2)$$

Where n_+ and n_- are the valencies of Cu and Cl ,respectively. λ_+ (108 W.g-equiv/cm^5) and λ_- (76.3 W.g-equiv/cm^5) are the limiting ionic conductances of Cu and Cl ,respectively [2]. The diffusion time was then recaclulated by Eq. S3.1 using the the diffusivity of $CuCl_2$ to be 0.35 s, which is the same order of magnitude for that calculated using diffusivity of $CuSO_4$.

Detaching CNTs from the Polymeric Membranes vis Ultra-sonication

In the proposed closed-loop adsorption-electrodesorption cycle, mechanical separation was utilized to detach CNTs from PES membranes electrodes so that the CNTs can be recycled in subsequent adsorption cycles. In order to find more industrial effective alternatives for CNTs detachment from polymeric membranes, ultra-sonication was investigated. 5 mg of f-SW/DWCNTs was deposited on PES and PVDF membranes as shown in Figure S3.2a and Figure S3.2b. The CNTs membranes was then ultra-sonicated in 40 KHz bath-sonicator to investigate the possibility of CNTs detachment. After 5 min sonication, the CNTs-PES membrane was destroyed (as shown in Figure S3.2c) indicating that ultra-sonication is not good option for separating CNTs from PES membranes. On the other hand, the CNTs was efficiently detached from the PVDF membrane after 5 min sonication. Figure S3.2d shows the cleaned PVDF membranes after the sonication process. This result indicates the feasibility of CNTs detachment via ultrasonication from

PVDF membranes electrodes, which provides other alternatives for the mechanical detaching process. It worth mentioning that properties of the PVDF membrane (i.e., membrane mass, water permeability, and particles retention efficiency) were nearly the same after the sonication process, which allows it use in subsequent filtration cycles.

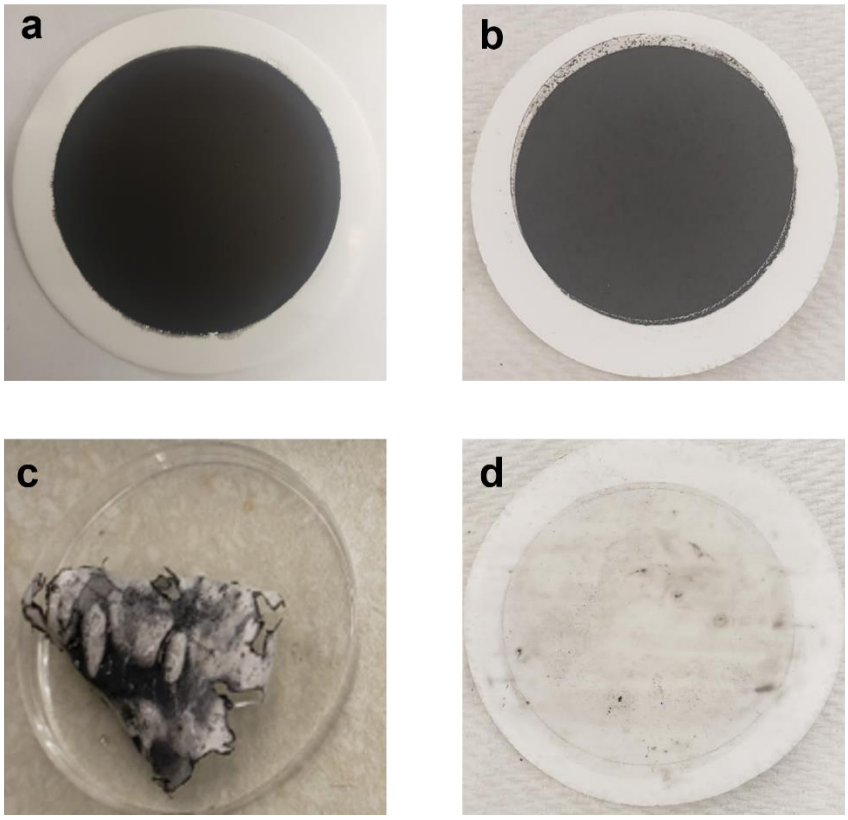

Figure S3. 2: 5 mg of f-SW/DWCNTs deposited on (a) PES and (b) PVDF membranes before the ultra - sonication process. (c) PES and (d) PVDF membranes after 5 min ultrasonication process.

Videos Taken from our Experiments Showing the Bubbles Generation at the Electrodes

Insignificant bubbles at CNTs anode at 3V:

https://www.youtube.com/shorts/XyTDTT1E51I

Significant bubbles at cathode at 3V:

https://www.youtube.com/shorts/Ldumnww4pF4

Regression Analysis for Figure S3.1b

Regression Statistics

Multiple R	0.99937861
R Square	0.99875761
Adjusted R Square	0.87375761
Standard Error	0.09435899
Observations	9

Anova

	Df	*SS*	*MS*	*F*	*Significance F*
Regression	1	57.2608	57.2608	6431.183	1.23E-11
Residual	8	0.071229	0.008904		
Total	9	57.33203			

	Coefficients	*Standard Error*	*t Stat*	*P-value*	*Lower 95%*	*Upper 95%*
Intercept	0	#N/A	#N/A	#N/A	#N/A	#N/A
X Variable 1	8.03387654	0.10018	80.19465	6.52E-13	7.802862	8.264891

Residual Output

Observation	*Predicted Y*	*Residuals*
1	6.07923438	-0.07923
2	3.78877618	0.211224
3	2.11371292	-0.11371
4	1.08296656	-0.08297
5	0.48203259	0.017967
6	0.23619597	0.013804
7	0.12773864	-0.00274
8	0.06186085	0.000639
9	0	0

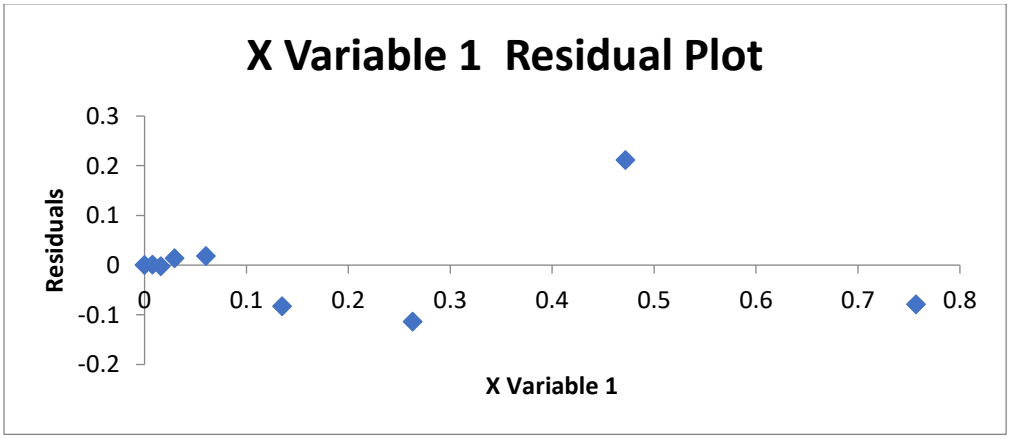

Regression Analysis for Figure 3.4a

Regression Statistics

Multiple R	0.974008
R Square	0.948691
Adjusted R Square	0.782024
Standard Error	15.09246
Observations	7

Anova

	Df	SS	MS	F	Significance F
Regression	1	25269.8	25269.8	110.9383	0.000133
Residual	6	1366.695	227.7824		
Total	7	26636.49			

	Coefficients	Standard Error	t Stat	P-value	Lower 95%	Upper 95%
Intercept	0	#N/A	#N/A	#N/A	#N/A	#N/A
X Variable 1	30.04152	2.852207	10.53272	4.3E-05	23.06242	37.02062

Residual Output

Observation	*Predicted Y*	*Residuals*
1	90.12455	-7.26536
2	90.12455	-3.66957
3	60.08303	-15.966
4	60.08303	17.79879
5	30.04152	2.23699
6	30.04152	26.90221
7	0	0

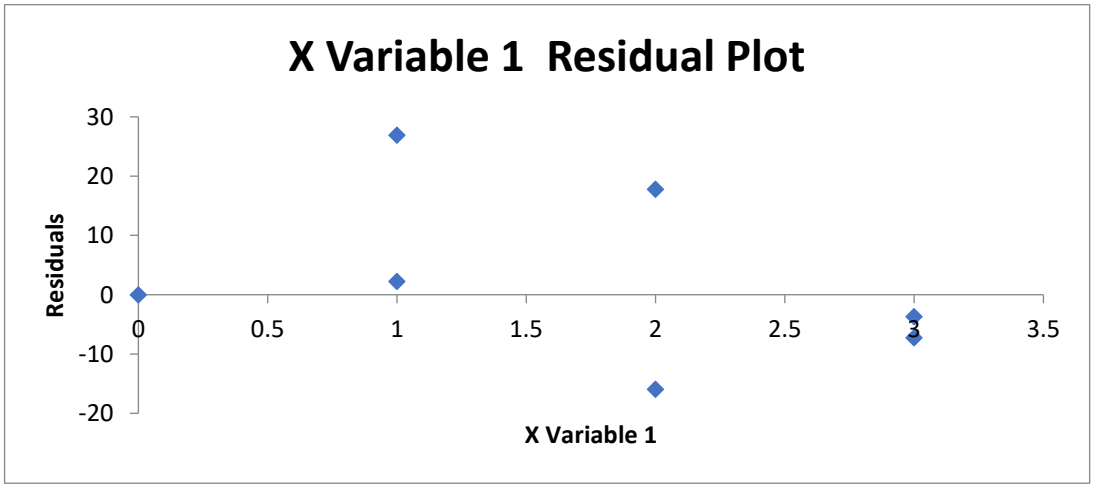

References

[1] A. Emanuel, D.R. Olander, Diffusion Coefficients of Copper Sulfate in Water and Water in n-Butyl Alcohol, J. Chem. Eng. Data. 8 (1963) 31–32. doi:10.1021/je60016a008.

[2] C. J. Geankoplis, Transport Processes and Separation Process Principles (includes unit operations), Prentice Hall Professional Technical Reference, 2003.

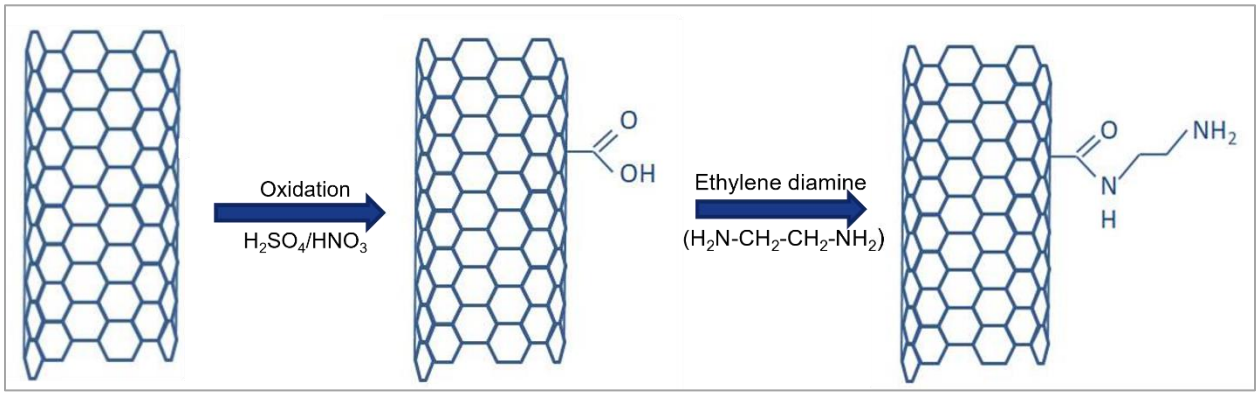

Figure S4. 1: The MWCNTs fabrication process

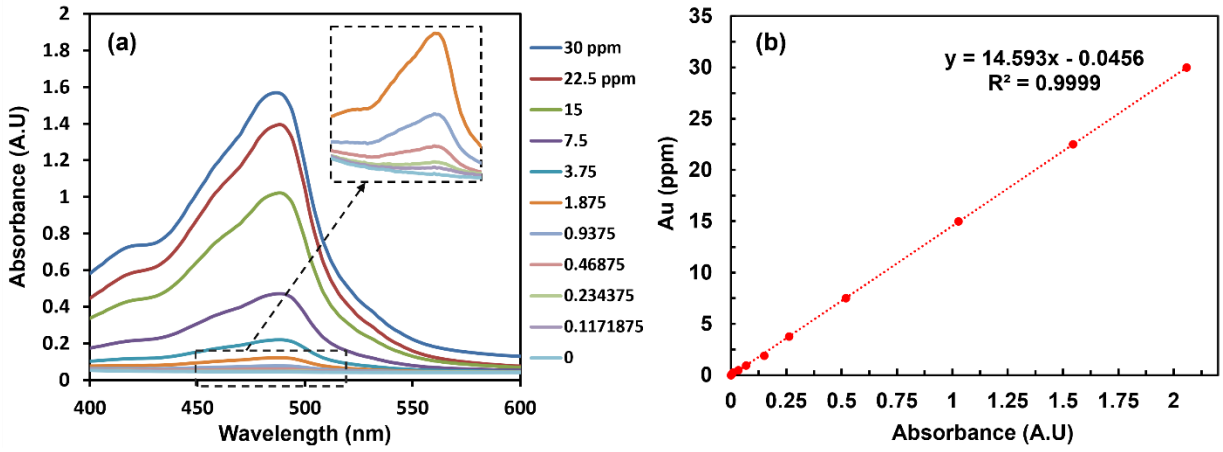

Figure S4. 2: (a) UV-Vis spectra of Au-BSOPD complex in 0.2 M HCl solution, (b) A representative calibration curve relating the Au(III) concentration to the absorbance at 488 nm wavelength; the line represents the regression model fit with R^2 of 0.9999 and standard error of 0.11 ppm.

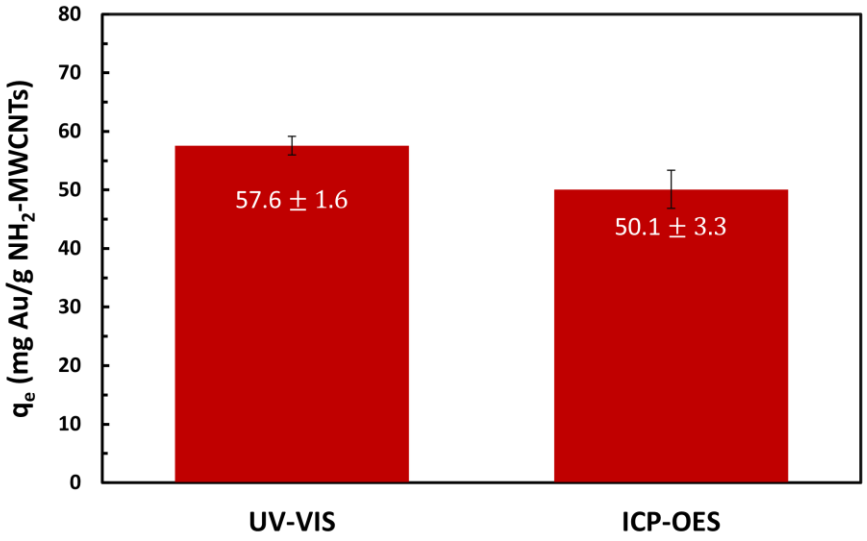

Figure S4. 3: Au adsorption capacity on 5 mg NH_2-MWCNTs (for adsorption experiments started with 10 ppm Au (III) and run for 24 h) quantified using UV-VIS spectrophotometry and ICP-OES

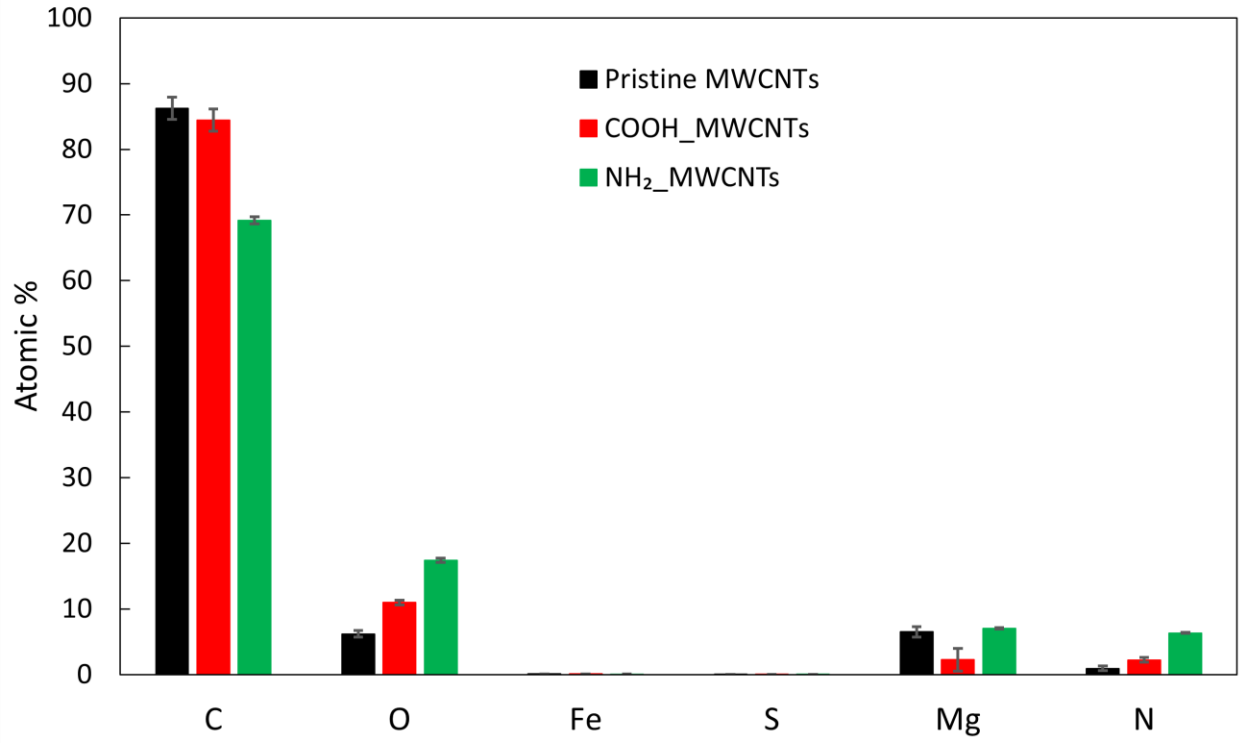

Figure S4. 4: EDS analysis performed on P-MWCNTs, COOH-MWCNTs and NH_2-MWCNTs

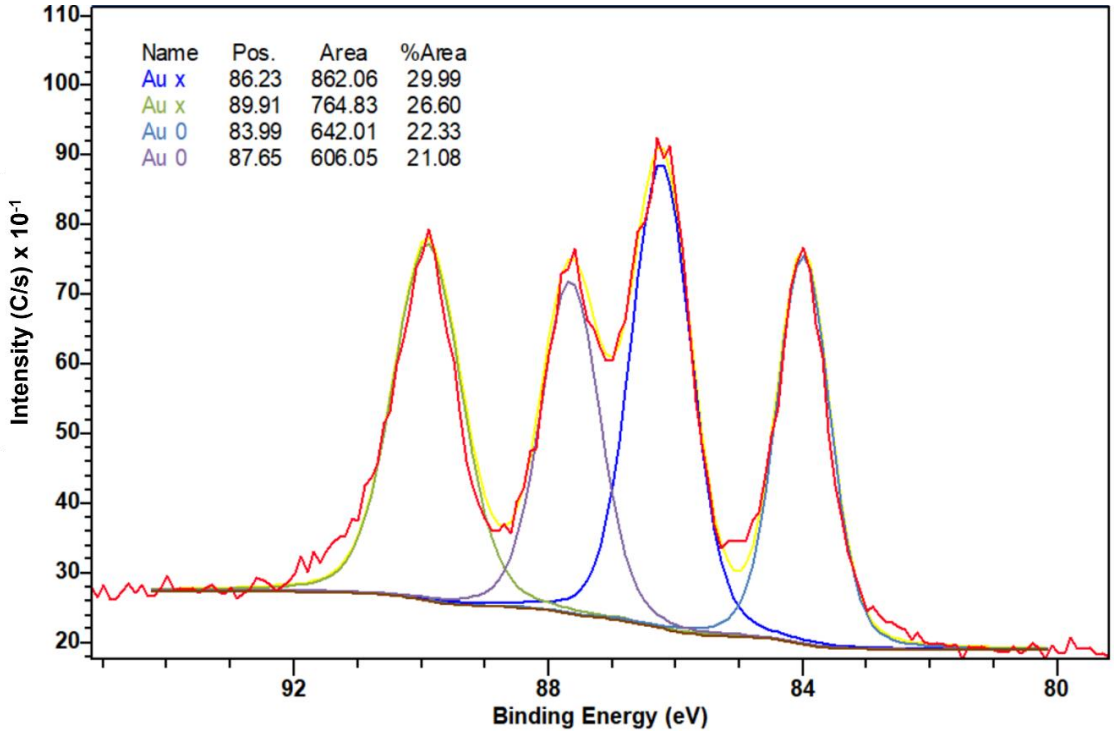

Figure S4. 5: Peak fitting analysis for the lowest intensity XPS curve of the P-MWCNTs (shown in Figure 4.4b) using CASA XPS software

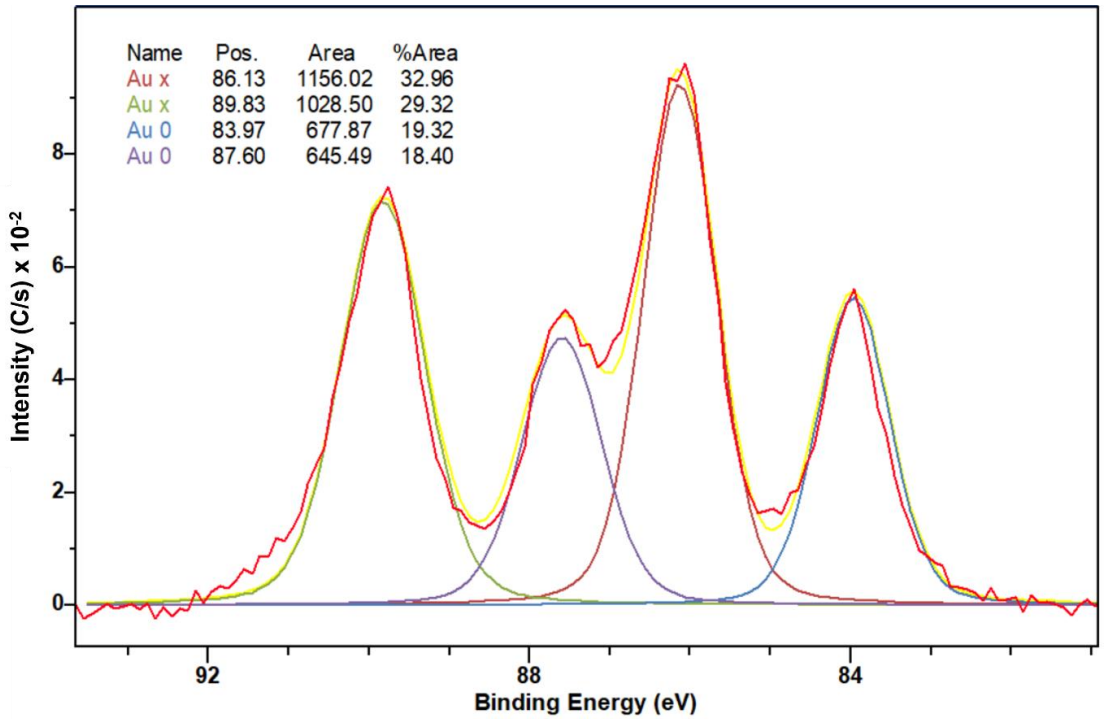

Figure S4. 6: Peak fitting analysis for the highest intensity XPS curve of the P-MWCNTs (shown in Figure 4.4b) using CASA XPS software

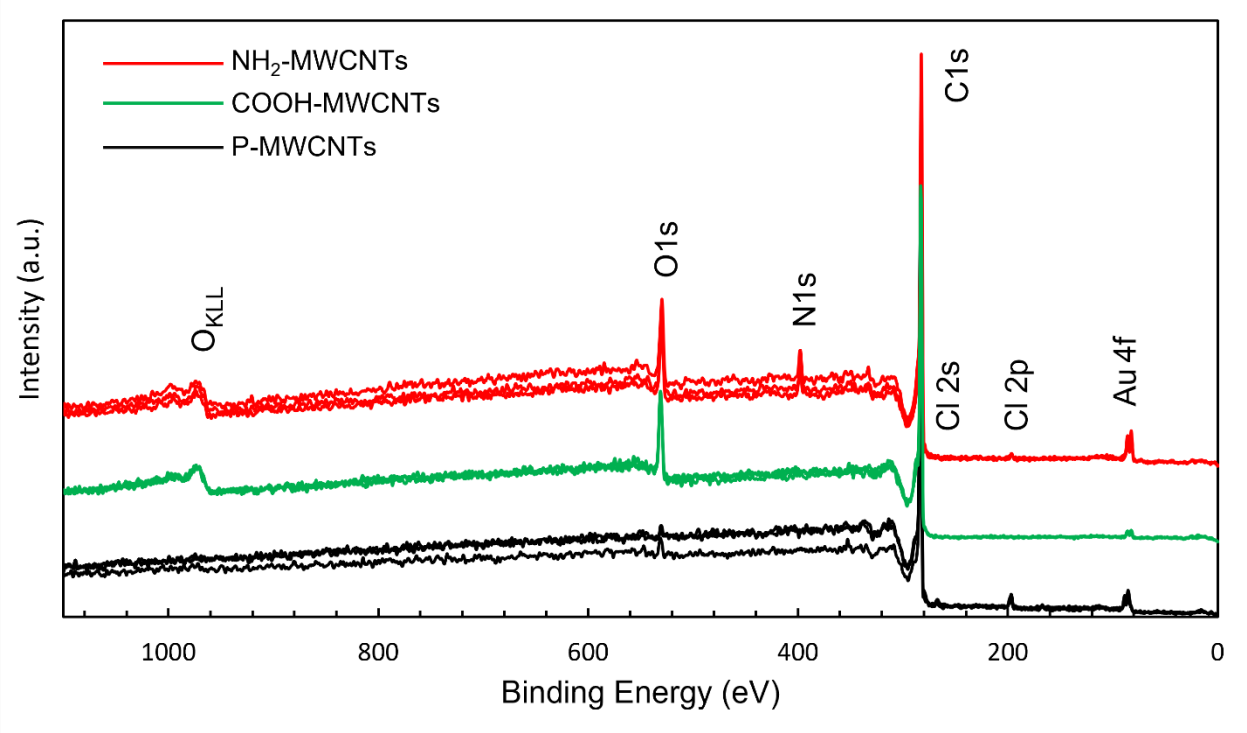

Figure S4. 7: XPS survey spectrum for Au loaded P-MWCNTs, COOH-MWCNTs and NH_2-MWCNTs (collected at three different locations for each sample)

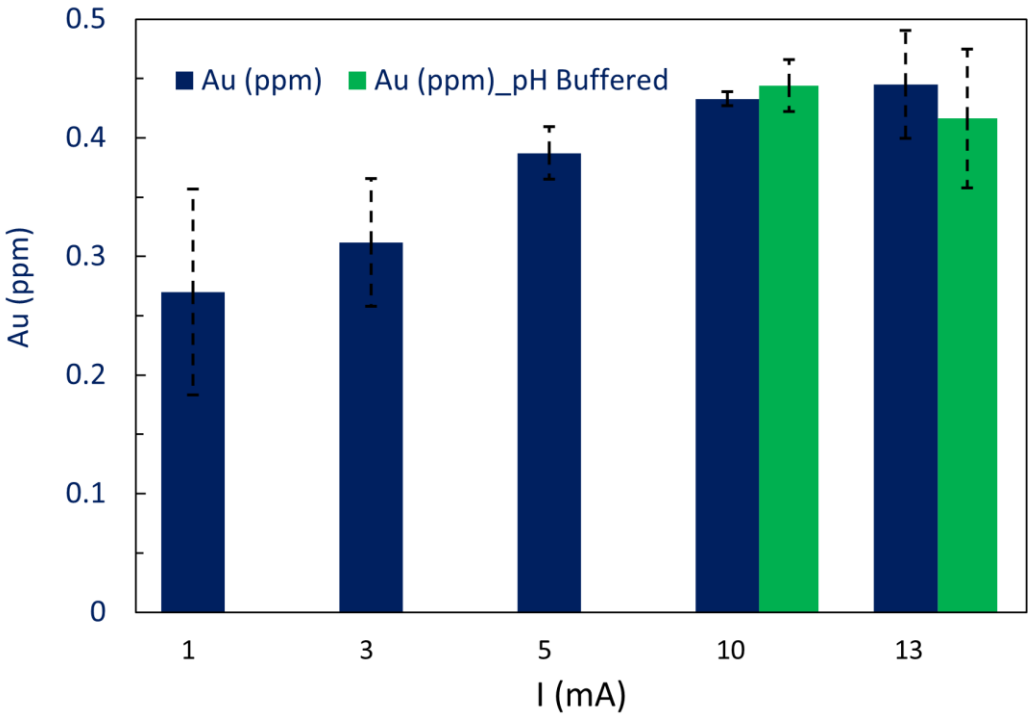

Figure S4. 8: Effect of applied current on Au electrodesorption from NH_2-MWCNTs loaded with 50±6 mg Au/ g MWCNTs for 1h electrochemical experiments, uncontrolled pH experiments (blue bars) and pH buffered experiments (green bars)

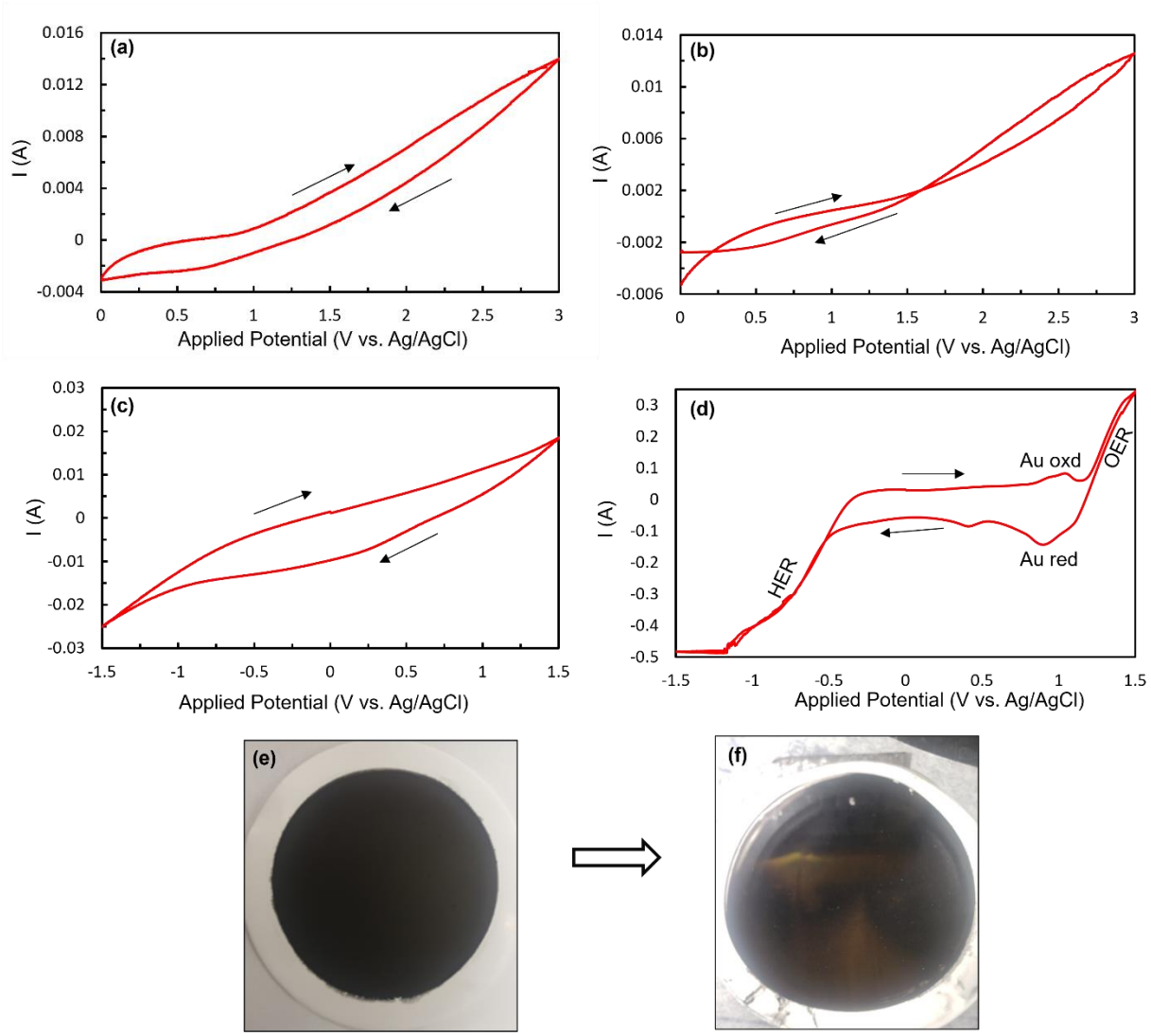

Figure S4. 9: Cyclic voltammetry for Au-NH_2-MWCNTs membrane electrode loaded with (a) 50$\pm$6 mg, (b) 91.5$\pm$9.5 mg Au/ g NH_2-MWCNTs in NaCl solution having conductivity (5 mS/cm); and for (c) bare NH_2-MWCNTs membrane electrode, (d) titanium dioxide electrode in 60 ppm Au (III) electrolyte solution at 10 mV/s scan rate. Digital images for the bare NH_2-MWCNTs membrane electrode (e) before and (f) after being used in the cyclic voltammetry experiments in 60 ppm Au(III) electrolyte solution.

Table S4. 1: Elements average atomic %, calculated from fitting the XPS peaks in Figure 4.2a

Elements (atomic %)	P-MWCNTs	COOH-MWCNTs	NH_2-MWCNTs
C	98.36	87.92	82.09
O	1.64	12.08	11.13
N	NA	NA	6.77

Functional groups atomic percentage preliminary calculations

P-MWCNTs:

- O/C atomic ratio = 1.64/98.36 = 0.0167

COOH-MWCNTs:

- O/C atomic ratio = 12.08/87.92 = 0.1374
- O/C atomic ratio (without background oxygen) = 0.1374 - 0.0167 = 0.1207
- COOH groups /C atomic ratio = 0.1207/2 = 0.06035 → 6 % COOH groups

NH_2-MWCNTs:

- N/C atomic ratio = 6.77/82.09 = 0.0825
- Equivalent C atom is added with each N atom during the amidation process with ethylene diamine (H_2N-CH_2-CH_2-NH_2)
- Actual N/C molar ratio = 0.0825/(1-0.0825) = 0.0899
- NH_2-NH-O groups/C atomic ratio= 0.0899/2 = 0.0449 → 4.5 mol % NH-NH_2 groups

Table S4. 2: Elements average atomic % for Au-loaded MWCNTs , calculated from fitting the XPS peaks in Figure S4.7

Elements (atomic %)	P-MWCNTs	COOH-MWCNTs	NH_2-MWCNTs
C	96.08	88.31	83.46
O	1.95	11.53	10.82
N	NA	NA	4.86
Au	0.53	0.15	0.46
Cl	1.44	NA	0.36

Table S4. 3: The effect of applied current for 1h at Au-NH_2-MWCNTs membrane anodes loaded with 50±6 mg Au/ g NH_2-MWCNTs, on the anode electric potentials and on the electrolyte solutions final pH

Applied Current (mA)	Average Anodic Potential vs. Ag/AgCl (V)	pH_f
1	1.5	4.75
3	3.95	5.0
5	>10	5.5
10	>10	8.0
13	>10	8.1

Table S4. 4: The effect of Au mass adsorbed on NH_2-MWCNTs, on the anode electric potentials and on the electrolyte solutions final pH at 10 mA applied current for 1h

Au Mass (mg Au/ g NH_2-MWCNTs)	Average Anodic Potential vs. Ag/AgCl (V)	pH_f
7.5 ± 1.5	>10	8.1
50.0 ± 6.0	>10	8.0
91.5 ± 9.5	>10	6.9

Regression Analysis for Figure S4.2b (UV-VIS Calibration Curve)

Regression Statistics

Multiple R	0.999948
R Square	0.999896
Adjusted R Square	0.999885
Standard Error	0.112126
Observations	11

Anova

	Df	*SS*	*MS*	*F*	*Significance F*
Regression	1	1089.139	1089.139	86630.4	3.07E-19
Residual	9	0.11315	0.012572		
Total	10	1089.252			

	Coefficients	*Standard Error*	*t Stat*	*P-value*	*Lower 95%*	*Upper 95%*
Intercept	-0.0456	0.042406	-1.07542	0.310171	-0.14153472	0.050325426
X Variable 1	14.59259	0.049579	294.3304	3.07E-19	14.4804367	14.70474742

Residual Output

Observation	*Predicted Y*	*Residuals*
1	29.99179	0.008213
2	22.49703	0.002968
3	14.95558	0.04442
4	7.535247	-0.03525
5	3.782032	-0.03203
6	2.149121	-0.27412
7	0.964203	-0.0267
8	0.443247	0.025503
9	0.090106	0.144269
10	0.020062	0.097125
11	-0.0456	0.045605

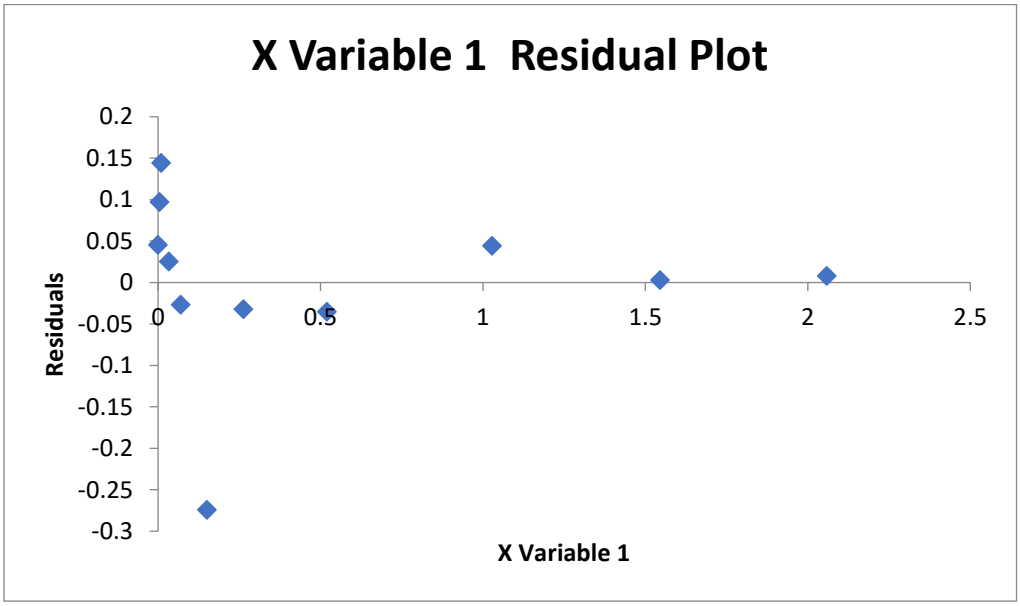

Regression Analysis for Figure 4.5c (Langmuir Model)

Regression Statistics

Multiple R	0.974989
R Square	0.950603
Adjusted R Square	0.947516
Standard Error	0.046217
Observations	18

Anova

	Df	*SS*	*MS*	*F*	*Significance F*
Regression	1	0.657686	0.657686	307.9054	7.12E-12
Residual	16	0.034176	0.002136		
Total	17	0.691862			

	Coefficients	*Standard Error*	*t Stat*	*P-value*	*Lower 95%*	*Upper 95%*
Intercept	0.075434	0.017262	4.369963	0.000476	0.03884	0.112028
X Variable 1	0.007237	0.000412	17.54723	7.12E-12	0.006363	0.008112

Residual Output

Observation	*Predicted Y*	*Residuals*
1	0.090053	-0.02457
2	0.108541	-0.02735
3	0.20744	0.043037
4	0.314544	0.109248
5	0.428592	0.06417
6	0.47268	0.005968
7	0.5416	-0.0116
8	0.087738	-0.03622
9	0.105517	-0.03043
10	0.197493	0.031454
11	0.290582	0.038152
12	0.40195	0.022987
13	0.446019	-0.01199
14	0.509198	-0.03951
15	0.610924	-0.06876
16	0.618228	-0.01823
17	0.079132	0.005964
18	0.077028	-0.05232

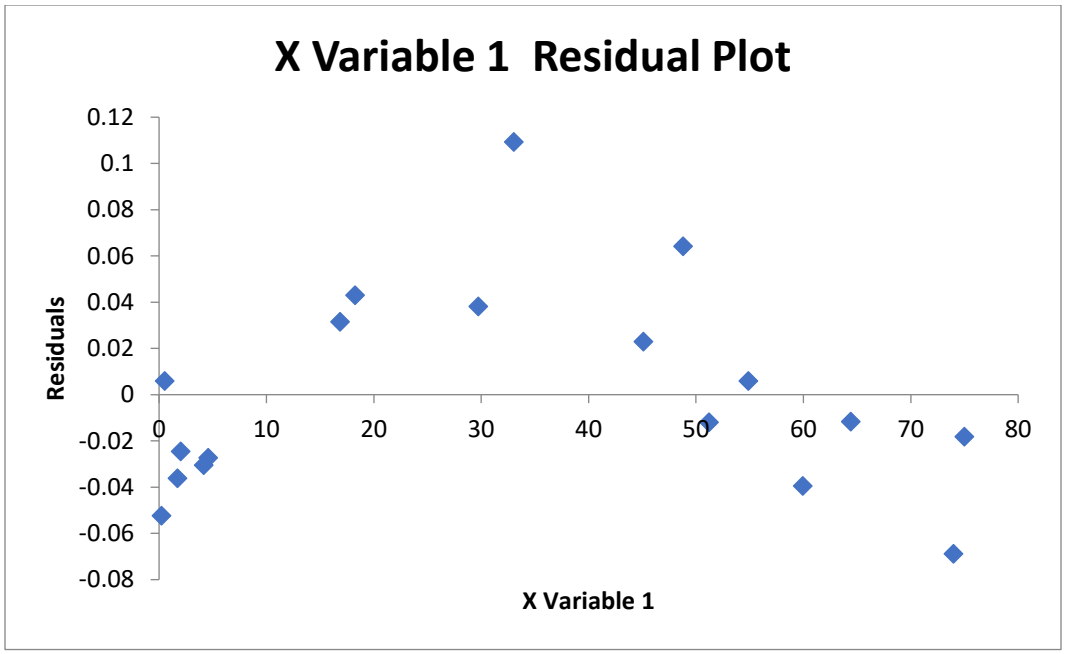
X Variable 1 Residual Plot
Residuals
X Variable 1
0.12
0.1
0.08
0.06
0.04
0.02
0
-0.02
-0.04
-0.06
-0.08
0
10
20
30
40
50
60
70
80

Chapter 5 Supporting Information

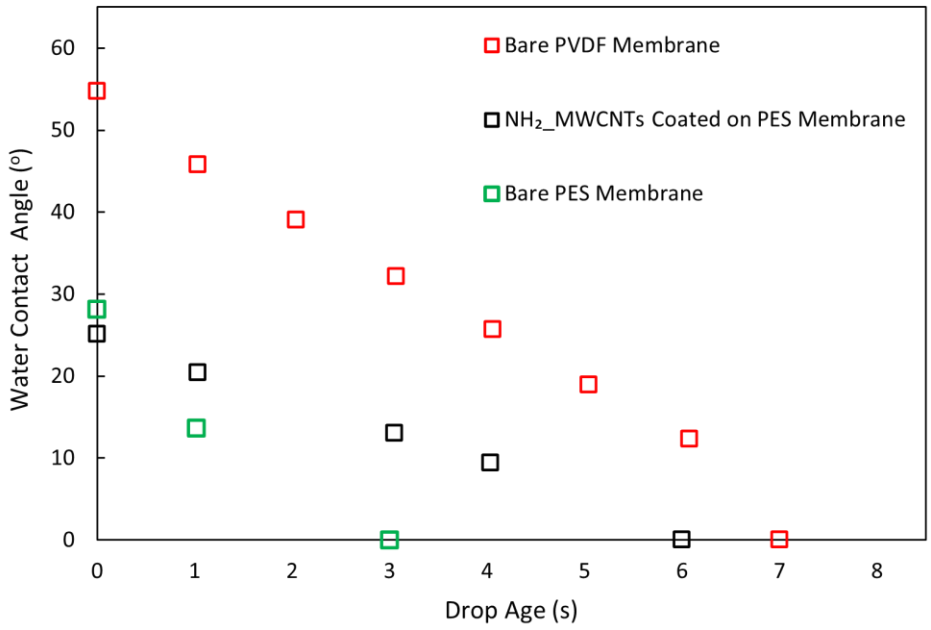

Figure S5. 1: Change of water contact angle with time on different membrane substrates

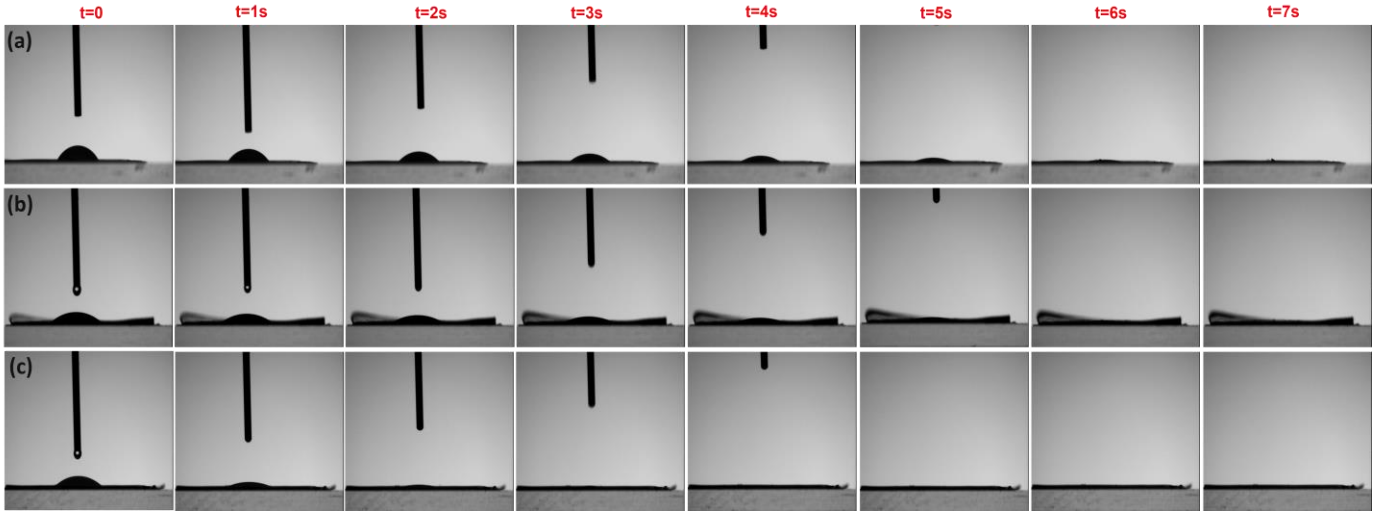

Figure S5. 2: Change of water drop size with time on (a) a PVDF membrane, (b) NH_2-MWCNTs coated on a PES membrane and (c) a PES membrane

Table S5. 1: Change in Electrolyte Solution pH with Different Anodes used in BECC after a 1-h electrochemical experiment

Anode	pH_i	pH_f
PES Membrane	6.2	11.8
PVDF Membrane	6.2	11.9
NH_2-MWCNTs coated PES membrane	6.2	11.6
Graphite	6.2	8.22
PES Membrane (separated from the stainless-steel alligator clip by a thin graphite sheet)	6.2	10.6
Stain-less steel Alligator Clip	6.2	6.4
Copper Alligator Clip	6.2	10.5

In the stain-less steel alligator clip control experiment, the electrolyte solution pH was not significantly changed after 1h electrochemical experiment. The mass of the generated metal precipitate in this experiment was higher than other experiments and the precipitate generation kinetics was also faster. Thus, the generated OH^- ions were immediately consumed to produce metal hydroxides leading to a minimal change in the electrolyte pH. In the NH_2-MWCNTs coated PES membrane experiment, the electrolyte solution pH increased to 11.6 after 1-h electrochemical experiment and then decreased to 7.2 after 40 h from the experiment indicating slow consumption of the produced OH^- ions by the generated precipitate.

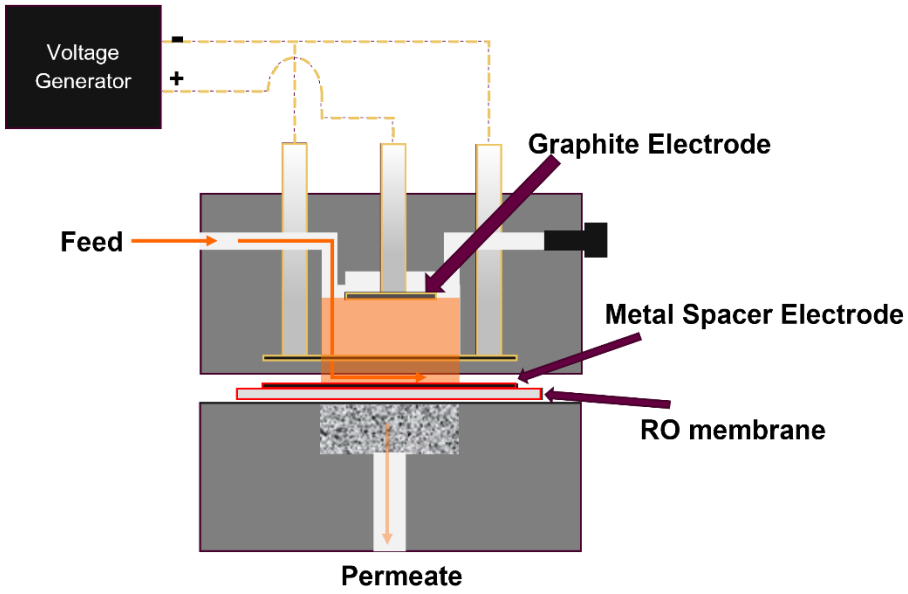

Figure S6. 1: Schematic for the electrochemical cross-flow cell.

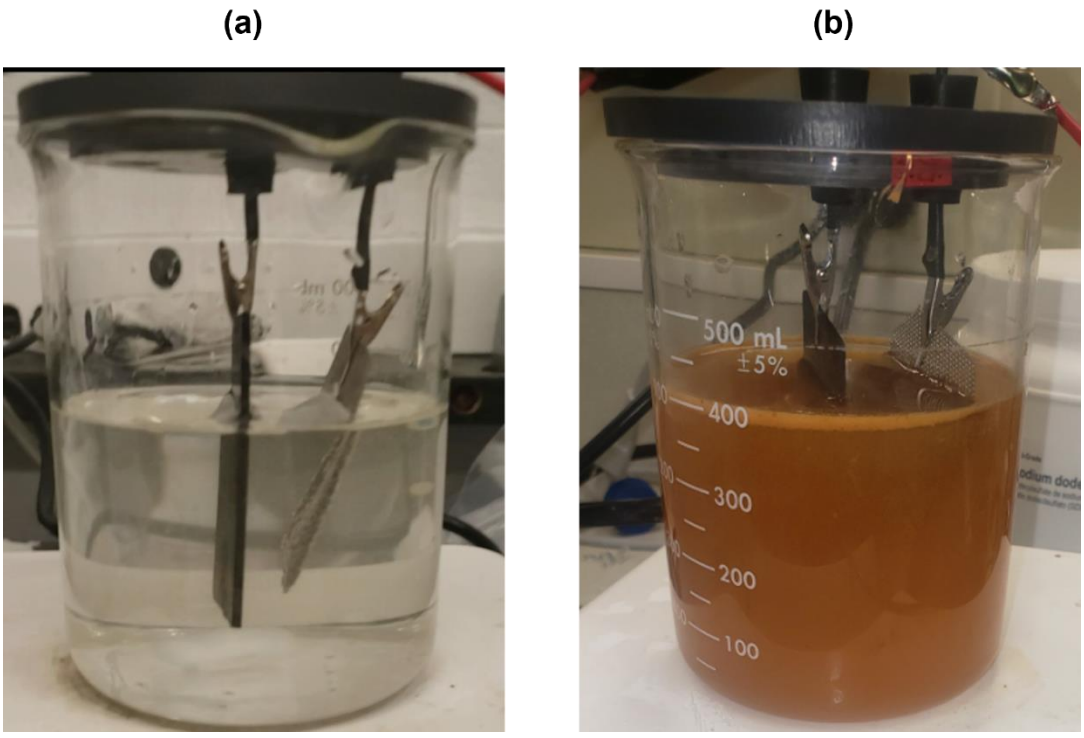

Figure S6. 2: Batch electrochemical cell using stainless steel spacer anode, graphite cathode and 340 ppm $CaSO_4$ electrolyte before (a) and after (b) applying 7V for 1h.

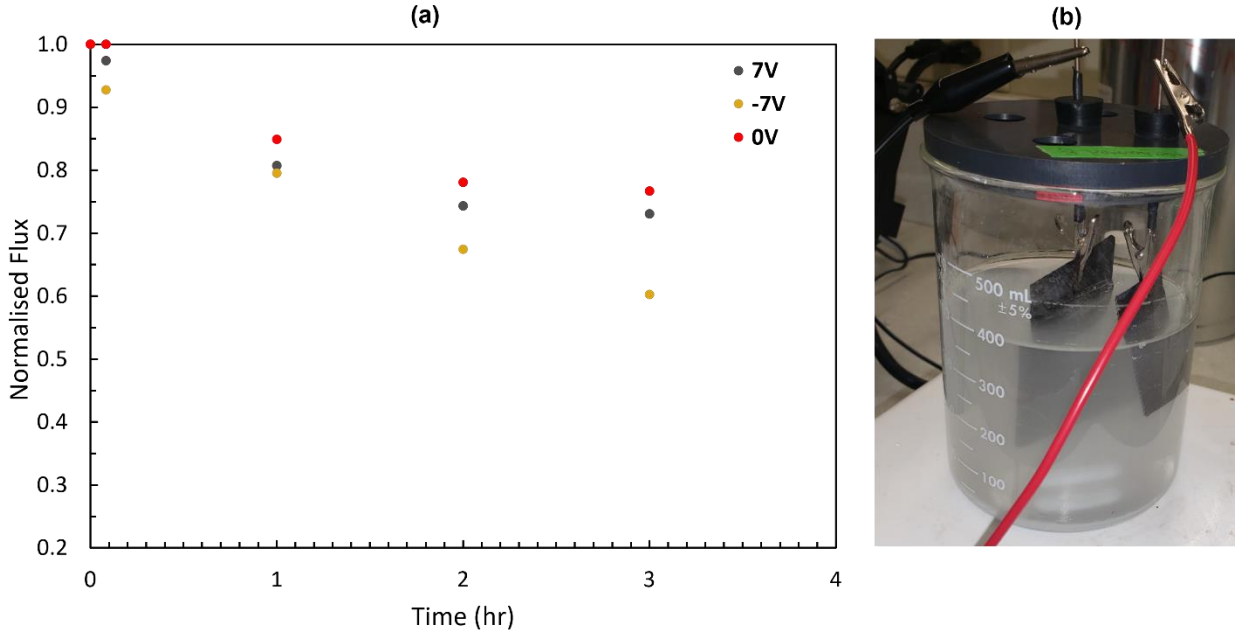

Figure S6. 3: (a) Normalised permeate flux as function of filtration time under different applied potentials between titanium spacer/graphite pair in a cross-flow filtration cell. (b) Batch electrochemical cell using titanium spacer anode, graphite cathode and 340 ppm $CaSO_4$ electrolyte after applying 7V for 1h.

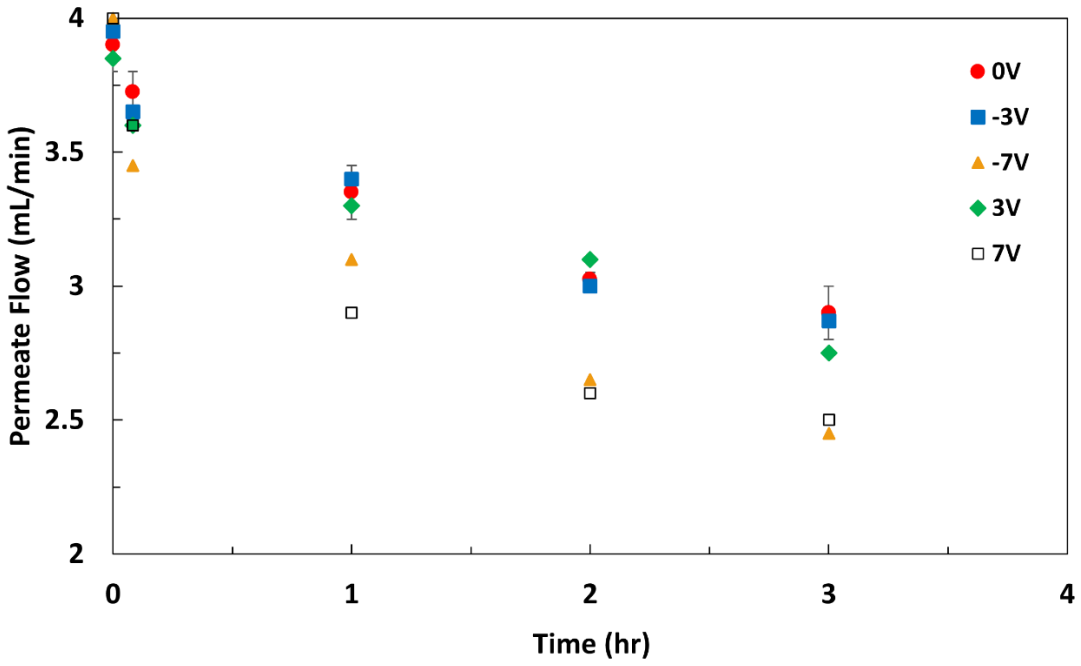

Figure S6. 4: Permeate flow rate as function of filtration time under different applied potentials between stainless-steel spacer/graphite pair in a cross-flow filtration cell.

MATLAB code used for solving the MPB equation for flat plate charged with 1000 mv in 2.5 mM $CaSO_4$ solution

```
% Main Code
clc
clear all
global e0 er k T e_charge c1 c2  z1 z2 kappa NA I  Xsi IR1 IR2 c1max c2max p

c1 = 2.5; % Ca concentration [mol/m^3 or mM]
c2 = 2.5; % SO4 concentration [mol/m^3 or mM]
NA = 6.022140857e23; %Avogadro's number
T = 298; %Temp. [K]
k = 1.381e-23; %Boltzmann's constant
e_charge = 1.602e-19; %Charge of electron
e0 = 8.85e-12; %Permittivity of vacuum
er = 80; %relative permittivity of water
z1=2; %valence of Ca
z2=-2; %valence of SO4
I=0.5*(((z1^2)*c1)+((z2^2)*c2)); %Ionic strength
kappa= sqrt((((e_charge^2))*NA*2*I)/(e0*er*k*T)); 1/debye length [m^-1]
IR1=1*(10^-10); %ionic radius of Ca [m]
IR2=2.58*(10^-10); %ionic radius of sulphate [m]
p=0.64; %packing coefficient
c1max= p/(4*pi*(IR1^3)*NA/3); % maximum Ca concentration [mol/m^3 or mM]
c2max= p/(4*pi*(IR2^3)*NA/3); % maximum SO4 concentration [mol/m^3 or mM]
N = 500; %Number of data points
y = linspace(10^-5,1,N); %Dimensionless distance
phi0 = 1000/1000; % applied potential in v
Xsi = phi0*e_charge/(k*T) % dimensionless applied potential

%Numerically solve the Poisson-Boltzmann equation using BVP4C (Boundary Value Problem)
%-----------------

solinit = bvpinit(y, [10^-8,1]);
sol = bvp4c(@twoode, @twobc, solinit);
phi = deval(sol,y); %assign solution for dimensionless potential as function of distance
phiy = k*T/(e_charge)*phi(1,:); %  potential as function of distance [V]
potenial = phiy*1000; % potential [mV]
x=-1/(kappa*(10^-9))*reallog(y); % distance [nm]
cx1=(c1*exp(-z1*e_charge*phiy/(k*T))./(1+((c1*(1/c1max)*(exp(-z1*e_charge*phiy/(k*T))-
1))+(c2*(1/c2max)*(exp(-z2*e_charge*phiy/(k*T))-1))));  % Ca concentration as function of distance
[mol/m^3 or mM]
cx2=(c2*exp(-z2*e_charge*phiy/(k*T))./(1+((c1*(1/c1max)*(exp(-z1*e_charge*phiy/(k*T))-
1))+(c2*(1/c2max)*(exp(-z2*e_charge*phiy/(k*T))-1))));  % SO4 concentration as function of distance
[mol/m^3 or mM]
```

```
figure(1)
plot((-1/(kappa*(10^-9)))*reallog(y),phiy(1,:)*1000)
title('Potential Distribution')
xlabel('x (nm)')
ylabel('Potential (mV)')
```

```
%Poisson-Boltzman equation function
function dUdy = twoode(y,U)
global e0 er k T e_charge c1 c2 z1 z2 I c1max c2max p
 dUdy = [U(2); ((-1/(2*I*(y^2))*(c1*z1*exp(-1*z1*U(1)) + c2*z2*exp(-
1*z2*U(1))))/(1+((c1*(1/c1max)*(exp(-1*z1*U(1))-1)) + (c2*(1/c2max)*(exp( -1*z2*U(1))-1)))))- U(2)/y];
end
```

```
% Boundary Conditions function
function surf = twobc(dphia, dphib)
global   e0 er k T e_charge c1 c2  z1 z2 c1max c2mac Xsi  p
 surf = [dphia(1); dphib(1)- Xsi];
 end
```